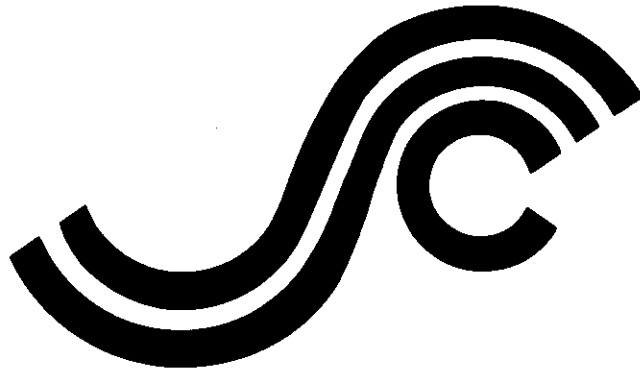


SSC-297

**EVALUATION OF LIQUID
DYNAMIC LOADS IN SLACK LNG
CARGO TANKS**



**This document has been approved
for public release and sale; its
distribution is unlimited.**

SHIP STRUCTURE COMMITTEE

1980

SHIP STRUCTURE COMMITTEE

The SHIP STRUCTURE COMMITTEE is constituted to prosecute a research program to improve the hull structures of ships and other marine structures by an extension of knowledge pertaining to design, materials and methods of construction.

RADM H. H. BELL (Chairman)
Chief, Office of Merchant Marine
Safety
U. S. Coast Guard

Mr. M. PITKIN
Assistant Administrator for
Commercial Development
Maritime Administration

Mr. P. M. PALERMO
Deputy Director,
Hull Group
Naval Sea Systems Command

Mr. R. B. KRAHL
Chief, Branch of Marine Oil
and Gas Operations
U. S. Geological Survey

Mr. W. N. HANNAN
Vice President
American Bureau of Shipping

Mr. C. J. WHITESTONE
Chief Engineer
Military Sealift Command

CDR T. H. ROBINSON, U.S. Coast Guard (Secretary)

SHIP STRUCTURE SUBCOMMITTEE

The SHIP STRUCTURE SUBCOMMITTEE acts for the Ship Structure Committee on technical matters by providing technical coordination for the determination of goals and objectives of the program, and by evaluating and interpreting the results in terms of structural design, construction and operation.

U.S. COAST GUARD

MILITARY SEALIFT COMMAND

CAPT R. L. BROWN
CDR J. C. CARD
CDR J. A. SANIAL, JR.
CDR W. M. SIMPSON, JR.

MR. G. ASHF
MR. T. W. CHAPMAN
MR. A. B. STAVOVY (Chairman)
MR. D. STEIN

NAVAL SEA SYSTEMS COMMAND

U. S. GEOLOGICAL SURVEY

Mr. R. CHIU
Mr. R. JOHNSON
Mr. J. B. O'BRIEN

MR. R. J. GIANGERELLI
MR. J. GREGORY

AMERICAN BUREAU OF SHIPPING

MARITIME ADMINISTRATION

DR. D. LIU
MR. I. L. STERN

MR. N. O. HAMMER
DR. W. MACLEAN
Mr. F. SEIBOLD
Mr. M. TOUMA

NATIONAL ACADEMY OF SCIENCES SHIP RESEARCH COMMITTEE

INTERNATIONAL SHIP STRUCTURES CONGRESS

Mr. O. H. OAKLEY - Liaison
Mr. R. W. RUMKE - Liaison

Mr. S. G. STIANSEN - Liaison

THE SOCIETY OF NAVAL ARCHITECTS & MARINE ENGINEERS

AMERICAN IRON & STEEL INSTITUTE

Mr. N. O. HAMMER - Liaison

Mr. R. H. STERNE - Liaison

WELDING RESEARCH COUNCIL

STATE UNIVERSITY OF NEW YORK MARITIME COLLEGE

Mr. K. H. KOOPMAN - Liaison

Dr. W. R. PORTER - Liaison

U. S. MERCHANT MARINE ACADEMY

U. S. COAST GUARD ACADEMY

Dr. C.-B. KIM - Liaison

CAPT W. C. NOLAN - Liaison

U. S. NAVAL ACADEMY

Dr. R. BHATTACHARYYA - Liaison

Member Agencies:

*United States Coast Guard
Naval Sea Systems Command
Military Sealift Command
Maritime Administration
United States Geological Survey
American Bureau of Shipping*



An Interagency Advisory Committee
Dedicated to Improving the Structure of Ships

Address Correspondence to:

Secretary, Ship Structure Committee
U.S. Coast Guard Headquarters, (G-M/TP 13)
Washington, D.C. 20593

SR-1251

JULY 1980

The liquid slosh-induced loads which impact on the walls of partially filled cargo tanks have caused damages and therefore have been of concern to ship owners and designers for many years. In particular, liquefied natural gas (LNG) carriers have experienced recent problems. Numerous test programs have been conducted using scale models of LNG tanks to investigate slosh loadings. However, not all of these studies have covered the complete range of excitation amplitudes, frequencies, fill depths and tank geometries while obtaining both tank wall pressures and force measurements.

The Ship Structure Committee undertook a project to review and make a uniform presentation of currently available model data, and to perform additional model tests to supplement these data in order to provide a complete picture of slosh loads for both prismatic and spherical tanks.

This report contains the results of that effort.

A handwritten signature in black ink, appearing to read "Henry H. Bell".

Henry H. Bell
Rear Admiral, U.S. Coast Guard
Chairman, Ship Structure Committee

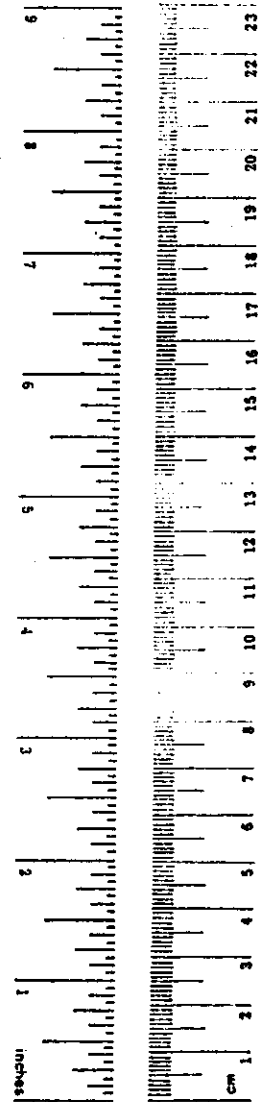
1. Report No. SSC-297		2. Government Accession No.		3. Recipient's Catalog No.	
4. Title and Subtitle EVALUATION OF LIQUID DYNAMIC LOADS IN SLACK LNG CARGO TANKS			5. Report Date May 1980		
			6. Performing Organization Code SR-1251		
7. Author(s) P. A. COX, E. B. BOWLES, AND R. L. BASS			8. Performing Organization Report No. SWRI Project 02-5033		
9. Performing Organization Name and Address SOUTHWEST RESEARCH INSTITUTE P.O. DRAWER 28510, 6220 CULEBRA ROAD SAN ANTONIO, TX 78284			10. Work Unit No. (TRAVIS)		
			11. Contract or Grant No. DOT-CG-71374-A		
12. Sponsoring Agency Name and Address U. S. COAST GUARD OFFICE OF MERCHANT MARINE SAFETY WASHINGTON, D.C. 20593			13. Type of Report and Period Covered FINAL		
			14. Sponsoring Agency Code G-M		
15. Supplementary Notes					
16. Abstract <p>This report provides an evaluation of dynamic sloshing loads in slack LNG cargo tanks. A comprehensive review of worldwide scale model sloshing data is presented. The data are reduced to a common format for the purposes of defining design load coefficients. LNG tank structural details are reviewed with emphasis placed on defining unique design features which must be considered in designing LNG tanks to withstand dynamic sloshing loads. Additional scale model laboratory experiments are conducted to supplement the available model sloshing data. Experiments are conducted in combined degrees of freedom to establish the potential for multi-degree of freedom excitation for augmenting dynamic sloshing loads. Experiments are also conducted to establish the sloshing dynamic pressure-time histories which are necessary for structural response analysis. Experiments are also conducted on representative segments of a full-scale LNG ship tank structure which is loaded with a typical full-scale dynamic sloshing pressure as predicted from the model results. Analytical studies are undertaken to provide techniques for determining wall structural response to dynamic slosh loads. Finally, design methodology is presented for membrane and semi-membrane tanks, gravity tanks, and pressure tanks whereby the design procedure sequences from comparing resonant sloshing periods to ship periods, defining the design loads, and designing the tank structures affected by dynamic slosh loads by delineated procedures which vary with tank type.</p>					
17. Key Words liquefied natural gas sloshing structural response model tests load simulator dynamic loads pressure-time histories			18. Distribution Statement Document is available to the U.S. Public through the National Technical Information Service, Springfield, VA 22161.		
19. Security Classif. (of this report) UNCLASSIFIED		20. Security Classif. (of this page) UNCLASSIFIED		21. No. of Pages 183	22. Price

METRIC CONVERSION FACTORS

Approximate Conversions to Metric Measures

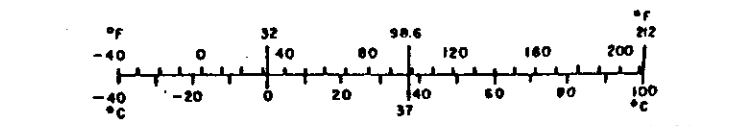
Symbol	When You Know	Multiply by	To Find	Symbol
LENGTH				
in	inches	2.5	centimeters	cm
ft	feet	30	centimeters	cm
yd	yards	0.9	meters	m
mi	miles	1.6	kilometers	km
AREA				
in ²	square inches	6.5	square centimeters	cm ²
ft ²	square feet	0.09	square meters	m ²
yd ²	square yards	0.8	square meters	m ²
mi ²	square miles	2.6	square kilometers	km ²
	acres	0.4	hectares	ha
MASS (weight)				
oz	ounces	28	grams	g
lb	pounds	0.45	kilograms	kg
	short tons (2000 lb)	0.9	tonnes	t
VOLUME				
tsp	teaspoons	5	milliliters	ml
tblsp	tablespoons	15	milliliters	ml
fl oz	fluid ounces	30	milliliters	ml
c	cups	0.24	liters	l
pt	pints	0.47	liters	l
qt	quarts	0.95	liters	l
gal	gallons	3.8	liters	l
ft ³	cubic feet	0.03	cubic meters	m ³
yd ³	cubic yards	0.76	cubic meters	m ³
TEMPERATURE (exact)				
°F	Fahrenheit temperature	5/9 (after subtracting 32)	Celsius temperature	°C

*1 U.S. = 2.54 mm (1 in.). For other exact conversions and more detailed tables, see NBS Misc. Publ. 226, Units of Weights and Measures, Price \$2.25, SD Catalog No. C13.10.286.



Approximate Conversions from Metric Measures

Symbol	When You Know	Multiply by	To Find	Symbol
LENGTH				
mm	millimeters	0.04	inches	in
cm	centimeters	0.4	inches	in
m	meters	3.3	feet	ft
m	meters	1.1	yards	yd
km	kilometers	0.6	miles	mi
AREA				
cm ²	square centimeters	0.16	square inches	in ²
m ²	square meters	1.2	square yards	yd ²
km ²	square kilometers	0.4	square miles	mi ²
ha	hectares (10,000 m ²)	2.5	acres	
MASS (weight)				
g	grams	0.035	ounces	oz
kg	kilograms	2.2	pounds	lb
t	tonnes (1000 kg)	1.1	short tons	
VOLUME				
ml	milliliters	0.03	fluid ounces	fl oz
l	liters	2.1	pints	pt
l	liters	1.06	quarts	qt
l	liters	0.26	gallons	gal
m ³	cubic meters	35	cubic feet	ft ³
m ³	cubic meters	1.3	cubic yards	yd ³
TEMPERATURE (exact)				
°C	Celsius temperature	9/5 (then add 32)	Fahrenheit temperature	°F



C O N T E N T S

I.	INTRODUCTION	1
II.	BACKGROUND	3
	II.1 History of Slosh Problem	3
	II.2 Nature of Liquid Sloshing	7
	II.3 Previous Studies	10
III.	TASK 1 - DATA REVIEW AND EVALUATION	12
	III.1 Scale Model Sloshing Data	13
	III.2 Full Scale Sloshing Data	36
	III.3 Review of Tank Structural Detail	36
IV.	TASK 2 - EXPERIMENTAL STUDIES	47
	IV.1 Experimental Study Objectives	47
	IV.2 Experimental Facilities	47
	IV.3 Combined Degree of Freedom Model Tests	48
	IV.4 Dynamic Pressure-Time Histories	65
	IV.5 Dynamic Load Simulator for Plywood Insulation Box Tests	72
	IV.6 Material Properties Tests	89
V.	TASK 3 - ANALYTICAL STUDIES	95
	V.1 Response Prediction Method	95
	V.2 Design Procedures	96
VI.	TASK 4 - PRESENTATION OF RESULTS - DESIGN METHODOLOGY	111
	VI.1 Current IMCO Requirements and Proposed Changes	111
	VI.2 Design Methodology	113
	VI.3 Example Problem Utilizing Tank Design Methodology	121
	VI.4 Summary	124
VII.	CONCLUSIONS AND RECOMMENDATIONS	125
	VII.1 Summary and Conclusions	125
	VII.2 Recommendations	126
VIII.	REFERENCES	127

C O N T E N T S (CONT'D)

APPENDIX A	SLOSHING FACILITIES FOR	
	o ANGULAR MOTION	
	o SIMULTANEOUS HORIZONTAL AND VERTICAL MOTION	A-1
APPENDIX B	PRESSURE-TIME HISTORY DATA FOR TRANSDUCER LOCATIONS 2 - 13	B-1
APPENDIX C	ONE-DEGREE-OF-FREEDOM EQUIVALENT SYSTEMS	C-1
APPENDIX D	EXAMPLE CALCULATIONS FOR MEMBRANE AND PRISMATIC TANKS	D-1
APPENDIX E	IMCO TANK-TYPE DEFINITIONS	E-1

LIST OF FIGURES

<u>NO.</u>		<u>PAGE NO.</u>
II-1	LNG Carriers: The Current State of the Art	4
II-2	Example LNG Tank Designs	6
II-3	Typical Pressure Waveforms on Tank Walls with Sloshing Liquids	9
III-1	Pressure Definitions	21
III-2	Pressure Histograms for 1000-Cycle and 200-Cycle Resonant Sloshing Tests as Presented in Reference 44	25
III-3	Highest Average Nondimensional Pressure vs Nondimensional Tank Filling Level for All Model Tests Run to Date	26
III-4	Maximum Pressure Coefficient vs Tank Filling Level for ϕ or $(x/l) \leq 0.30$	28
III-5	Pressure Coefficients vs Pitch Amplitude (From Reference 44)	28
III-6	Average Force Coefficient vs Tank Filling Level for ϕ or $(x/l) \leq 0-30$	29
III-7	Average Force Coefficient vs Tank Filling Level (Pitching Motion with $\phi = \pm 0.14$ Rad. or $\pm 8^\circ$)	29
III-8	Resonant Liquid Frequency vs Tank Filling Level for Rectangular or Prismatic Tanks	30
III-9	Slosh Forces on Sphere	32
III-10	Resultant Force on Sphere vs Fill Depth (Reference 44)	32
III-11	Resultant Force on Sphere vs Excitation Period (Reference 44)	33
III-12	Lateral Force on Sphere vs Fill Depth (Reference 44)	33
III-13	Lateral Force on Sphere vs Excitation Period (Reference 44)	33
III-14	Vertical (Dynamic) Force on Sphere vs Fill Depth (Reference 44)	34
III-15	Vertical Static + Dynamic Force on Sphere vs Fill Depth (Reference 44)	34
III-16	Vertical (Dynamic) Force on Sphere vs Excitation Period (Reference 44)	35
III-17	Vertical (Dynamic) Force on Sphere vs Excitation Amplitude (Reference 44)	35

<u>NO.</u>		<u>PAGE NO.</u>
III-18	12-Cell Primary Insulation Box - Gaz Transport System	38
III-19	Arrangement of Insulation Boxes in Gaz Transport System	39
III-20	Section of Cofferdam Bulkhead for Gaz Transport Tanks	40
III-21	Technigaz Membrane System	42
III-22	Typical Horizontal Girder - Conch Tank	43
III-23	Typical Longitudinal Girder	45
III-24	Typical Transverse Frame	46
IV-1	Scale Model Tank Dimensions and Pressure Transducer Locations for 1/50 Scale Prismatic Tank from a 125,000 m ³ Ship	49
IV-2	Test Configuration for Combined Pitch and Heave Test	61
IV-3	Experimental and Theoretical Nondimensional Resonant Slosh Period Versus Tank Filling Level	63
IV-4	Motion Definitions for Surge and Heave	64
IV-5	Typical Pressure-Time History for Slosh-Induced Impact	66
IV-6	Nondimensional Pressure-Time History Values for 200 Resonant Sloshing Cycles at Transducer Location 1 for a 25% Full Tank	69
IV-7	Integrated Nondimensional Pressure Values for 200 Resonant Sloshing Cycles at Transducer Location 1 for a 25% Full Tank	69
IV-8	Nondimensional Pressure vs Impulse Rise Time for 200 Resonant Sloshing Cycles at Transducer Location 1 for a 25% Full Tank	70
IV-9	Nondimensional Pressure vs Impulse Duration for 200 Resonant Sloshing Cycles at Transducer Location 1 for a 25% Full Tank	70
IV-10	Nondimensional Impulse Duration vs Impulse Rise Time for 200 Resonant Sloshing Cycles at Transducer Location 1 for a 25% Full Tank	70
IV-11	Nondimensional Pressure-Time History Values for 200 Resonant Sloshing Cycles at Transducer Location 14 for a 75% Full Tank	70
IV-12	Integrated Nondimensional Pressure Values for 200 Resonant Sloshing Cycles at Transducer Location 14 for a 75% Full Tank	71

IV-13	Nondimensional Pressure vs Impulse Rise Time for 200 Resonant Sloshing Cycles at Transducer Location 14 for a 75% Full Tank.....	71
IV-14	Nondimensional Pressure vs Impulse Duration for 200 Resonant Sloshing Cycles at Transducer Location 14 for a 75% Full Tank	71
IV-15	Nondimensional Impulse Duration vs Impulse Rise time for 200 Resonant Sloshing Cycles at Transducer Location 14 for a 75% Full Tank	71
IV-16	Schematic Diagram of Plywood Insulation Box Dynamic Loader ...	73
IV-17	Typical Pressure-Time Histories for Dynamic Loading Tests on Plywood Insulation Boxes	75
IV-18	Displacement Transducer Locations for Plywood Box Strength Tests	76
IV-19	Cover Deflection vs Pressure for Dynamic and Static Loading of a Standard 12-Cell Box	77
IV-20	Shear Failure of Plywood Insulation Box Cover (Test Box No. 1)	78
IV-21	Bending Failure of Plywood Insulation Box Cover (Test Box No. 8)	79
IV-22	Support Stiffener Failure in a Plywood Insulation Box (Test Box No. 10)	80
IV-23	Plywood Test Specimen Geometry	91
V-1	Sloshing Pressure with Minimum Rise Time and Long Duration for 36 m (118-ft) Long Tank	98
V-2	Dynamic Load Factor for P(T) of Figure V-1	100
V-3	Envelope for Different Rise Times	100
V-4	Effect of Different Load Decay Times, T_3	100
A-1	Slosh Test Facility	A-2
A-2	Slosh Rig Cross-Sectional Dimensions	A-3
A-3	Drive System Block Diagram	A-3
B-1	Nondimensional Pressure-Time History Values for 200 Resonant Sloshing Cycles at Transducer Location 4 for a 25% Full Tank	B-7
B-2	Integrated Nondimensional Pressure Values for 200 Resonant Sloshing Cycles at Transducer Location 4 for a 25% Full Tank	B-7

<u>NO.</u>		<u>PAGE NO.</u>
B-3	Nondimensional Pressure vs Impulse Rise Time for 200 Resonant Sloshing Cycles at Transducer Location 4 for a 25% Full Tank	B-8
B-4	Nondimensional Pressure vs Impulse Duration for 200 Resonant Sloshing Cycles at Transducer Location 4 for a 25% Full Tank	B-8
B-5	Nondimensional Impulse Duration vs Impulse Rise Time for 200 Resonant Sloshing Cycles at Transducer Location 4 for a 25% Full Tank.....	B-8
B-6	Nondimensional Pressure-Time History Values for 200 Resonant Sloshing Cycles at Transducer Location 7 for a 75% Full Tank	B-8
B-7	Integrated Nondimensional Pressure Values for 200 Resonant Sloshing Cycles at Transducer Location 7 for a 75% Full Tank..	B-9
B-8	Nondimensional Pressure vs Impulse Rise Time for 200 Resonant Sloshing Cycles at Transducer Location 7 for a 75% Full Tank..	B-9
B-9	Nondimensional Pressure vs Impulse Duration for 200 Resonant Sloshing Cycles at Transducer Location 7 for a 75% Full Tank..	B-9
B-10	Nondimensional Impulse Duration vs Impulse Rise Time for 200 Resonant Sloshing Cycles at Transducer Location 7 for a 75% Full Tank	B-9
B-11	Nondimensional Pressure-Time History Values for 200 Resonant Sloshing Cycles at Transducer Location 11 for a 75% Full Tank	B-10
B-12	Integrated Nondimensional Pressure Values for 200 Resonant Sloshing Cycles at Transducer Location 11 for a 75% Full Tank	B-10
B-13	Nondimensional Pressure vs Impulse Rise Time for 200 Resonant Sloshing Cycles at Transducer Location 11 for a 75% Full Tank	B-10
B-14	Nondimensional Pressure vs Impulse Duration for 200 Resonant Sloshing Cycles at Transducer Location 11 for a 75% Full Tank	B-10
B-15	Nondimensional Impulse Duration vs Impulse Rise Time For 200 Resonant Sloshing Cycles at Transducer Location 11 for a 75% Full Tank	B-11
B-16	Nondimensional Pressure-Time History Values for 200 Resonant Sloshing Cycles at Transducer Location 13 for a 75% Full Tank.....	B-11
B-17	Integrated Nondimensional Pressure Values for 200 Resonant Sloshing Cycles at Transducer Location 13 for a 75% Full Tank	B-11

<u>NO.</u>		<u>PAGE NO.</u>
B-18	Nondimensional Pressure vs Impulse Rise Time for 200 Resonant Sloshing Cycles at Transducer Location 13 for a 75% Full Tank	B-11
B-19	Nondimensional Pressure vs Impulse Duration for 200 Resonant Sloshing Cycles at Transducer Location 13 for a 75% Full Tank	B-12
B-20	Nondimensional Impulse Duration vs Impulse Rise Time for 200 Resonant Sloshing Cycles at Transducer Location 13 for a 75% Full Tank	B-12
C-1	Deformation Pattern for Simple Beam	C-1
C-2	Equivalent One-DOF System	C-3
C-3	Dynamic Load Factors (DLF) and Time to Maximum Response (t_m) for Different $F(t)$'s ⁽⁹⁶⁾	C-8
C-4	Simply Supported Beam in Equilibrium Under Dynamic Loading..	C-10
D-1	D-3
D-2	D-6
D-3	D-7
D-4	D-10
D-5	D-16

LIST OF TABLES

<u>NO.</u>		<u>PAGE NO.</u>
III-1	Summary of Model Tank LNG Sloshing Experiments	14 - 19
III-2	Equations for Calculating Liquid Natural Periods in Rectangular, Spherical, and Cylindrical Tanks	23
IV-1	Tank Dimensions and Pressure Transducer Locations	50
IV-2	Test Conditions for Combined Motion Laboratory Tests	51
IV-3	Test Pressure Data for Pitching Tank Motion	52
IV-4	Test Pressure Data for Pitching Plus Heaving Tank Motion	53
IV-5	Test Pressure Data for Surging Tank Motion	54
IV-6	Test Pressure Data for Surging Tank Motion	55
IV-7	Test Pressure Data for Surging Plus Heaving Tank Motion	56
IV-8	Average Kp Values For a 1/50 Scale Prismatic Tank From a 125,000 m ³ LNG Carrier	57
IV-9	Maximum Kp Values For a 1/50 Scale Prismatic Tank From a 125,000 m ³ LNG Carrier	58
IV-10	Average Full Scale Pressure Values For a 1/50 Scale Prismatic Tank From a 125,000 m ³ LNG Carrier	59
IV-11	Maximum Full Scale Pressure Values For a 1/50 Scale Prismatic Tank From a 125,000 m ³ LNG Carrier	60
IV-12	Nondimensional Pressure-Time History Values at Transducer Location 1 for a 25% Full Tank	68
IV-13	Nondimensional Pressure-Time History Values at Transducer Location 14 for a 75% Full Tank	68
IV-14	Plywood Cover Deflection Measurements for Test Box Number 1 (Static Loading Test)	81
IV-15	Plywood Cover Deflection Measurements for Test Box Number 2 (Static Loading Test)	81
IV-16	Plywood Cover Deflection Measurements for Test Box Number 3 (Static Loading Test)	82
IV-17	Plywood Cover Deflection Measurements for Test Box Number 6 (Static Loading Test)	83
IV-18	Plywood Cover Deflection Measurements for Test Box Number 7 (Static Loading Test)	83

<u>NO.</u>		<u>PAGE NO.</u>
IV-19	Plywood Cover Deflection Measurements for Test Box Number 8 (Dynamic Loading Test)	84
IV-20	Plywood Cover Deflection Measurements for Test Box Number 10 (Static Loading Test)	84
IV-21	Plywood Cover Deflection Measurements for Test Box Number 11 (Static Loading Test)	84
IV-22	Summary Table of Loading Test Results for the Plywood Insulation Boxes	85 - 88
IV-23	Results of Tests on Specimens from Old Boxes	90
IV-24	Results of Tests on Specimens From New Boxes	92
IV-25	Summary of Plywood Properties (Average Values)	93
IV-26	Range of Plywood Properties	94
V-1	Range of Parameters which Describe Sloshing Pressures In LNG Tanks	97
V-2	Calculation of Envelope of DLF Using Figure C-2(b)	102
V-3	Frequency Coefficients for the Fundamental Mode (Equation V-1)	105
V-4	Values of Constants A', B', C'	106
VI-1	Design Methodology Flow Chart	114 - 116
B-1	Nondimensional Pressure-Time History Values at Transducer Location 2 for a 25% Full Tank	B-1
B-2	Nondimensional Pressure-Time History Values at Transducer Location 3 for a 25% Full Tank	B-2
B-3	Nondimensional Pressure-Time History Values at Transducer Location 4 for a 25% Full Tank	B-2
B-4	Nondimensional Pressure-Time History Values at Transducer Location 5 for a 25% Full Tank	B-3
B-5	Nondimensional Pressure-Time History Values at Transducer Location 6 for a 25% Full Tank	B-3
B-6	Nondimensional Pressure-Time History Values at Transducer Location 7 for a 75% Full Tank	B-4
B-7	Nondimensional Pressure-Time History Values at Transducer Location 8 for a 75% Full Tank	B-4
B-8	Nondimensional Pressure-Time History Values at Transducer Location 9 for a 75% Full Tank	B-5

<u>NO.</u>		<u>PAGE NO.</u>
B-9	Nondimensional Pressure-Time History Values at Transducer Location 10 for a 75% Full Tank	B-5
B-10	Nondimensional Pressure-Time History Values at Transducer Location 11 for a 75% Full Tank	B-6
B-11	Nondimensional Pressure-Time History Values at Transducer Location 12 for a 75% Full Tank	B-6
B-12	Nondimensional Pressure-Time History Values at Transducer Location 13 for a 75% Full Tank	B-7
C-1	Transformation Factors for Beams and One-Way Slabs	C-7
D-1	Plywood Material Properties	D-2
D-2	Material Properties for Balsa, Sweet Birch, and Sugar Maple	D-11

NOMENCLATURE OF IMPORTANT PARAMETERS

A	Cross-sectional area
b	Width
CT	Cryogenic temperature
D	Tank diameter; flexural rigidity of a plate
DLF	Dynamic load factor
dof	Degree of freedom
E	Elastic modulus of a material
EI	Flexural rigidity of a plate-stiffener combination
F	Dynamic force
f	Frequency
G	Shear modulus of a material
g	Acceleration of gravity
GA	Shear rigidity of a material
H	Tank height
h	liquid filling in a tank; plate thickness
I	Second moment of area of stiffener and associated plate; beam section moment of inertia
K	Axial spring constant of a stiffener
K_F	Nondimensional force coefficient
K_L	Dynamic load factor
K_m	Dynamic mass factor
K_p	Nondimensional dynamic pressure coefficient
K'_p	Nondimensional dynamic pressure coefficient corrected for oscillation amplitude effects
K_T	Nondimensional time coefficient
k	Spring constant
KE	Kinetic energy

NOMENCLATURE (Cont.)

l	Tank length; plywood specimen length
LNG	Liquified Natural Gas (Liquid Methane)
LN_2	Liquid nitrogen
LPG	Liquified Petroleum Gas
m	Mass
N	Load applied over a surface
P	Dynamic pressure created by liquid sloshing
R	Resultant dynamic force created by liquid sloshing in a spherical tank
RF	Reduction factor
RT	Room temperature
S	Sectional area of stiffener and associated plate
T	Time; period
T_R	Resonant period
t_r	Rise time
U	Internal strain energy
V	Spherical tank volume; shear reaction
W	Static weight of liquid in a tank; external work
w	Deflection of a beam under loading
x	Translational (horizontal or surge) excitation amplitude of a prismatic or rectangular ship tank
Y	Lateral dynamic force created by liquid sloshing in a spherical tank
y	Translational (vertical or heave) excitation amplitude of a prismatic or rectangular ship tank
Z	Vertical dynamic force created by liquid sloshing in a spherical tank
z	Distance from a ship tank bottom
α	Angle (relative to vertical) of the resultant dynamic force (R) created by liquid sloshing in a ship tank

NOMENCLATURE (Cont.)

γ	Specific weight of a liquid
ϕ	Pitch or roll angle of a ship tank
ρ	Mass density
η	Horizontal excitation amplitude of a spherical ship tank
ψ	See Equation V-9, Pge. 131.
σ	Stress
ν	Poisson's ratio
ω	Circular frequency

I. INTRODUCTION

This report presents all results of Project SR-1251, "Evaluation of Liquid Dynamic Loads in Slack LNG Cargo Tanks." The study was conducted under the direction of the Ship Research Committee of the National Academy of Sciences.

The potential for significant loads resulting from sloshing liquids in slack cargo tanks has been realized by the marine industry for years. In the past decade, with the advent of the supertanker and large LNG ships, sloshing loads have been of even greater concern. In the case of LNG ships, certain operational constraints call for the transport of liquid in slack tanks and, in addition, the absence of tank internals results in no damping of the liquid motions. Also, as ship tanks have grown in size, the probability of resonant sloshing has increased since resonant sloshing periods and ship motions more closely match. In view of this, a significant activity has been undertaken by various agencies throughout the world to establish sloshing loads in LNG cargo tanks. Experimental programs have been conducted using instrumented scale model tanks. These test programs have covered many different ship tank geometries, excitation amplitudes and frequencies, and liquid fill depths. Experiments were necessary because large amplitude sloshing is not amenable to theoretical analysis. To develop usable liquid dynamic load criteria for sloshing requires the combining of current experimental information with new experiments and analysis.

Four project tasks were undertaken to develop dynamic load criteria for slack tanks. In Task 1, all test reports on LNG slosh loads were assembled, and the data reviewed and presented on a uniform basis. The data were summarized with regard to source, test conditions, and types of measurements recorded. To present the data on a uniform basis, nondimensional coefficients were utilized where data from the various reports were presented in the same format. Concurrent with this effort, the structural details of typical LNG tank designs were established, and methods and background information necessary to develop LNG slosh load design methodology were identified.

In Task 2, scale model tanks were utilized to conduct additional sloshing experiments whereby important loads and test conditions not currently covered in the literature were investigated. Scale model LNG ship tanks were utilized whereby dynamic sloshing pressures were measured at resonant sloshing conditions. Both single and combined degree of freedom excitation experiments were conducted to evaluate the ability of single degree of freedom tests to produce maximum impact loads. Significant emphasis was placed on establishing pressure-time histories for resonant sloshing impact loads for use in dynamic tank wall response analysis. Experimental studies were also conducted to reproduce full-scale impulsive impact pressures on representative segments of membrane tank structures and to measure the structural response.

In Task 3, analytical efforts were undertaken to develop methods for predicting LNG tank wall and support structural response to typical slosh

loads. Analytical methods were used to examine the stresses and deformations in typical LNG tank structures and their supports when subjected to dynamic sloshing loads. Design guidelines and design methods were formulated utilizing the analytical studies conducted in this task; the experimental studies from Task 2; and information on past research and analyses, collected and analyzed in Task 1.

Finally, in Task 4, the composite of information generated in the project was utilized to generate simplified design procedures to account for dynamic loads in slack cargo tanks.

II. BACKGROUND

II.1 History of Slosh Problem

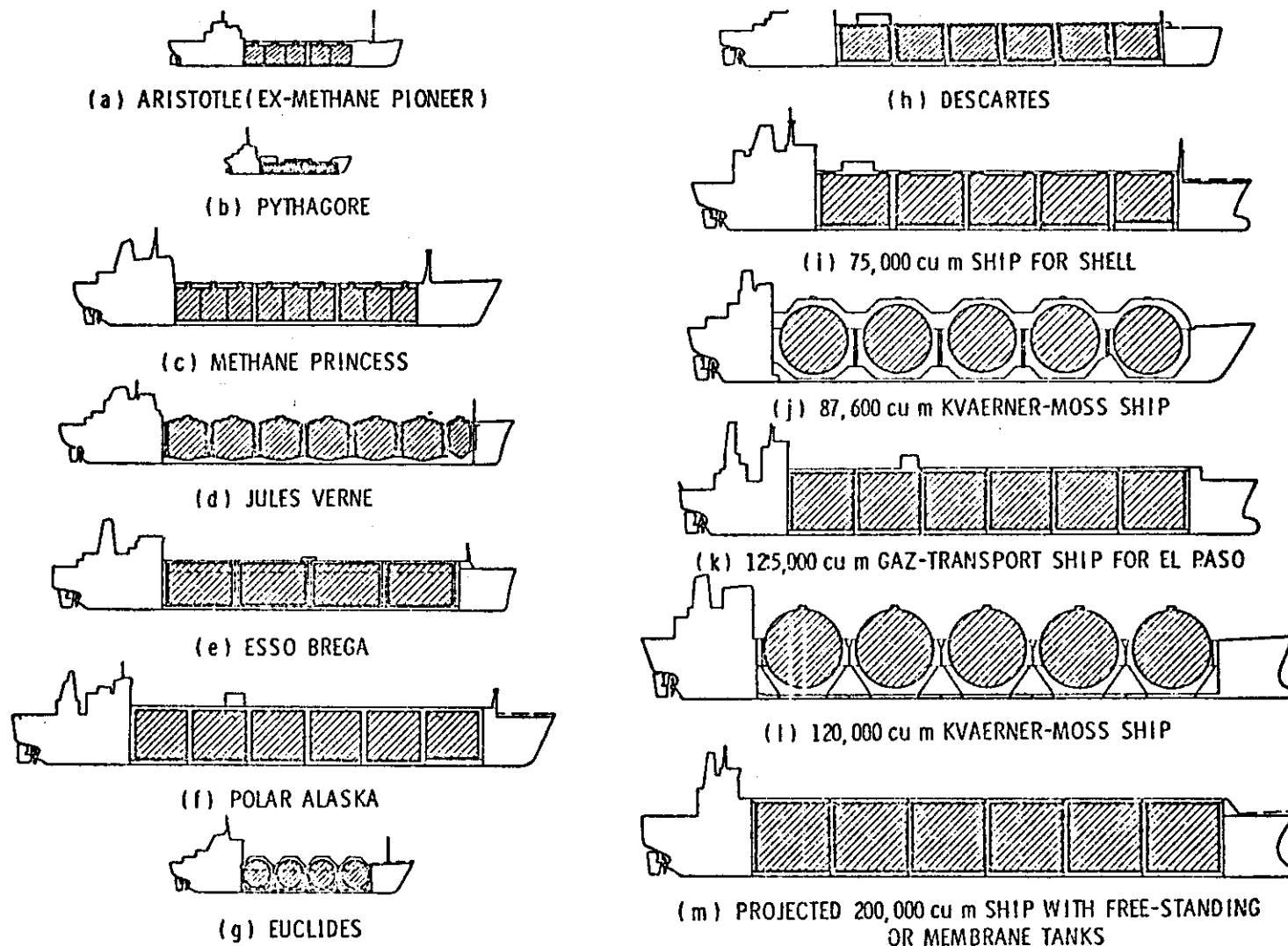
Space Related Activities

The basic problem of determining the dynamic loads which result from the motions ("sloshing") of liquids in partially filled moving containers was studied extensively in the 1950's and 60's in connection with the development of large rocket vehicles for the space program. Liquid sloshing in spherical and cylindrical containers has been studied for space applications, both analytically and experimentally.⁽¹⁾ The nature of slosh loading in these types of tanks and its prediction are probably better understood than for prismatic tanks, but analytical techniques for predicting large amplitude sloshing are still not fully developed, and such loads are extremely important in designing the support structure and internal components of ship tanks. In addition, much of the sloshing technology developed for space applications is not applicable because emphasis was placed on frequencies and total forces as they related to control system requirements, and, therefore, the effects of local peak impact pressure on structural requirements were not studied to any extent. Further, the excitation amplitudes considered in space applications are too small for ship motion simulation.

LNG Ship Related Slosh Problems

Current activity in the design of super tankers as well as ships for liquified gas transport has resulted in renewed consideration of the influence of the contained liquids on cargo tank design,⁽²⁻⁷⁵⁾ especially since the probability of exciting a resonant slosh mode is increased in the larger tanks. In many cases, the transport of liquid cargos in partially filled tanks is prohibited. However, several factors make partial filling either unavoidable or highly attractive. For example, in the case of liquid natural gas (LNG) ships, partially filled conditions are needed because (1) chilled-down liquid is required to maintain cold tanks on return trips, (2) higher specific gravity liquids than LNG are transported in tanks designed for LNG, (3) partial unloading is desirable when multi-port stops are made, and (4) loading or unloading at sea creates significant time periods at undesirable fill depths. For all liquid cargo ships, partial filling in ballast tanks and fuel tanks occurs, and conditions (3) and (4) above for LNG ships also apply. Therefore, the designer of all types of liquid carriers must be aware of the consequences of liquid sloshing and be able to predict the resulting loads.

As the various LNG ship designs have evolved (Figure II-1), several important types of unique ship loads have been considered by the designers. The slosh-generated loads are one of these and have a considerable influence on the tank and support structure design. Several factors make slosh loads more important with regard to LNG ship design. A tank failure in an LNG ship merits special consideration because of (1) the risk of brittle



PROFILES OF TYPICAL LNG SHIPS (CARGO TANKS ARE SHOWN CROSS-HATCHED)

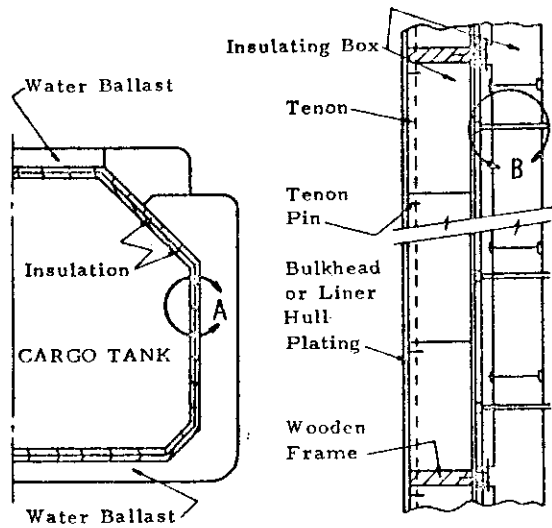
FIGURE II-1. LNG CARRIERS: THE CURRENT STATE OF THE ART

fracture of the primary structure (low-temperature shock), (2) the expensive repair cost of the complicated tank designs (3) the high out-of-service costs, and (4) the potential for large volume vapor release. Also, the complexity of the tank design in LNG carriers is such that at least some LNG tanks are more susceptible to damage from slosh loading than tanks for transporting oil or other petroleum products.

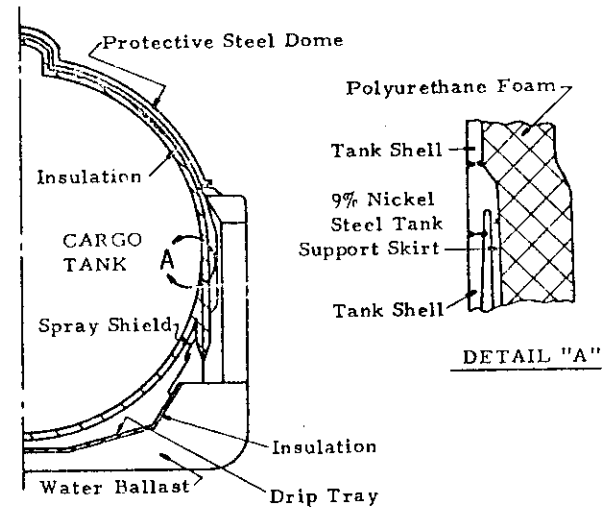
LNG Ship Tank Designs

There are presently over ten designs of LNG tanks that are either currently in use or under major consideration. These tanks generally fall into two categories: namely, freestanding (independent) and non-freestanding (membrane) tanks (Figure II-2). Integral tanks used for LPG transport are not acceptable for LNG since their use is restricted to temperatures greater than -10°C . The freestanding or independent tank is usually of the spherical or cylindrical design, and because of its geometry it is amenable to stress analysis and other conventional analytical techniques. Because the stresses can be calculated, a secondary barrier system is not required as is the case of the non-freestanding tanks. An exception is the prismatic freestanding tank, which does require a secondary barrier. Freestanding tanks are also easier to fabricate, and the insulation is easier to install than on other systems. One drawback to the freestanding design is the disadvantage of requiring a larger ship per given cargo volume. Since freestanding tank walls can be designed to withstand large impact pressures, the primary problem associated with LNG sloshing in freestanding tanks results from the slosh loads on internal components and on the tank support structure.

The second general tank type, the non-freestanding or membrane tank, is essentially built into the ship's hold, making use of the ship's structure for support. The membrane tanks use a thin internal layer of metal to act as a liquid barrier and are directly supported by insulation material. The insulation is applied directly to the hull with no access space, which makes this type of tank difficult to repair after material fracture or other damage. Because of the complex structure, membrane tanks are not amenable to analysis. In addition, because of this and the thinness of the membrane, a complete secondary liquid barrier is required. The primary problem associated with sloshing in membrane tanks is the potential damage to the tank walls from impulsive slosh pressures. Severe impulsive slosh loads in the membrane tank can occur at small fill depths as a result of large-amplitude traveling wave impact, which is not amenable to analysis. Also, severe slosh loads can occur on or near the tank top as a consequence of standing slosh waves in partially filled tanks. Since this type of tank cannot be analyzed to determine its failure strength, special load tests must be performed on representative segments of the structure to determine its load bearing strength. An estimate of the "equivalent" static slosh loads that occur in these types of tanks is then utilized to determine if the structure has the required strength.

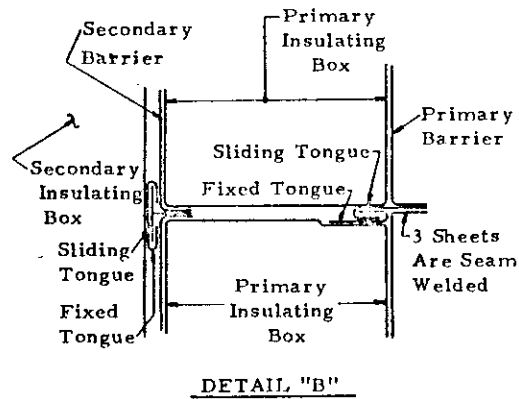


GAZ-TRANSPORT
MEMBRANE TANK



KVAERNER-MOSS
SPHERICAL TANK

(b) Freestanding (Spherical) Tank Design



(a) Non-freestanding (Membrane) Tank Design

FIGURE II-2. EXAMPLE LNG TANK DESIGNS

Recorded LNG Tank Damage from Sloshing

As of 1979, over 80 years of operating experience have been gained with numerous ships of various tank designs. During these years, several structural problems have been recorded which have resulted from slosh loads on LNG cargo tanks.(6) Slosh related loads causing tank damage have occurred on two ships with membrane tanks, the "Polar Alaska" and the "Arctic Tokyo." On the "Polar Alaska," supports of the electric cables supplying the cargo pumps were broken by liquid sloshing loads. This occurred when the tank was approximately 15-20% full. The broken cable supports resulted in damage to the bottom of the membrane tank. On the "Arctic Tokyo," a leak in the number 1 tank was caused from liquid sloshing when the tank was about 20% full. Inspection revealed that the leak was located, along with four deformed points in the membranes, in the aft corners of the transverse and longitudinal bulkheads at about the liquid surface level. Subsequent model tests(15,43) performed on scale models of the damaged "Arctic Tokyo" tank revealed that a 15-30% fill depth with respect to tank length resulted in appreciable impact loads from sloshing. The model tests were not successful, however, in establishing peak impact pressures(7) that could have caused the damage. As a result, additional work(10) was undertaken to investigate more thoroughly all aspects of modeling LNG sloshing and to provide a greater understanding of the slosh generated loads and their implications to tank and ship design. As a result of these studies, operations with partially filled tanks other than nearly full or nearly empty have been prohibited.

In the spring of 1978, the first of the 125,000 m³ membrane tank LNG ships was put into service. On one of the early cargo-laden voyages, the ship experienced heavy seas and the crew heard loud sloshing impact noises in the cargo tanks. After cargo discharge and subsequent inspection of the tanks, damage to the tank structure was noted. Subsequent studies(74,75) concluded that the damage was slosh induced, even though the tanks were approximately 95% full during the voyage. Thus, the designer must also be concerned with slosh loads at near full conditions.

II.2 Nature of Liquid Sloshing

General Conditions

In general, sloshing is affected by liquid fill depth, tank geometry, and tank motion (amplitude and frequency). The liquid motion inside a tank has an infinite number of natural periods, but it is the lowest mode that is most likely to be excited by the motions of a ship. Most studies have, therefore, concentrated on investigating forced harmonic oscillations in the vicinity of the lowest natural period, which is defined as that predicted by linear theory. Nonlinear effects result in the frequency of maximum response being slightly different from the natural frequency and dependent on amplitude. The most significant type of ship tank slosh loads occur with large excitation amplitudes where nonlinear effects are present.

The sloshing phenomena in cargo tanks that are basically rectangular in shape can usually be described by considering only two-dimensional fluid

flow. Sloshing in spherical or cylindrical tanks, however, must usually consider three-dimensional flow effects.

Two-Dimensional Flow

Tanks with two-dimensional flow are divided into two classes: low and high liquid fill depths. The low fill depth case is represented by $h/l < 0.2$, where h is the still liquid depth and l is the tank length in the direction of motion. The low fill depth case is characterized by the formation of hydraulic jumps and traveling waves for excitation periods around resonance. At higher fill depths, large standing waves are usually formed in the resonant frequency range. When hydraulic jumps or traveling waves are present, extremely high impact pressures can occur on the tank walls. Figure II-3a shows typical pressure traces recorded under this sloshing condition. Impact pressures typical of those shown in Figure II-3a can also occur on the tank top when tanks are filled to the higher fill depths. The pressure pulses are similar to those experienced in ship slamming, and the pressure variation is neither harmonic nor periodic since the magnitude and duration of the pressure peaks vary from cycle to cycle even though the tank is experiencing a harmonic oscillation. Figure II-3b shows typical pressure traces that result when small amplitude sloshing is occurring away from resonance at any fill depth.

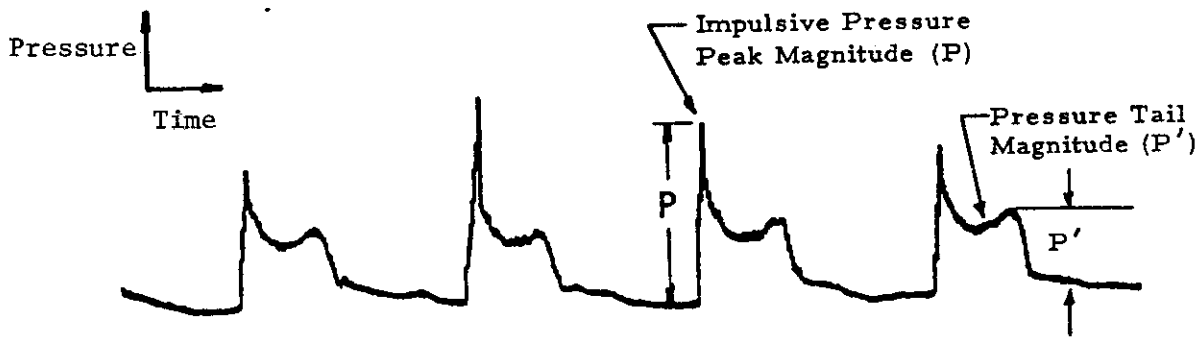
Three-Dimensional Flow

Three-dimensional flow occurs in spherical tanks, usually in the form of a swirl mode.⁽¹⁾ Similar three-dimensional effects can be present in cylindrical or rectangular tanks under certain excitation conditions. The prediction of sloshing forces in the neighborhood of resonance with swirling is extremely difficult, and experimental data obtained with scale model tanks are usually needed to establish pressures and forces with this type of sloshing.

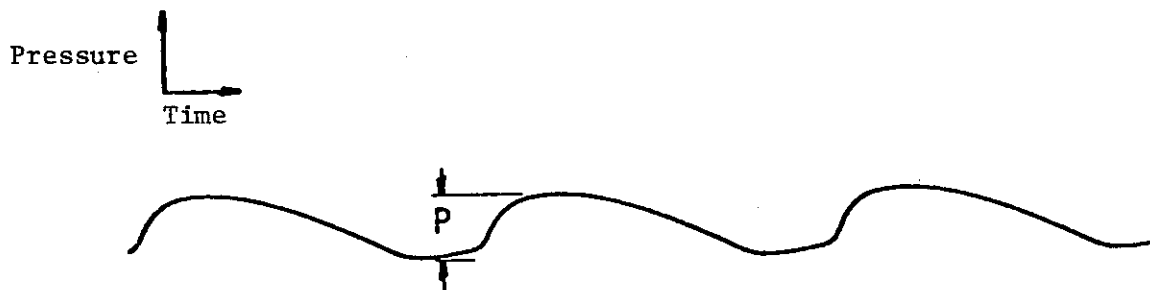
Design Implications

The design of a liquid cargo tank to withstand the dynamic slosh-induced loads requires that the designer be able to predict the resonant slosh periods at different fill depths for the required tank geometry. These periods can then be compared with the expected ship periods to determine the probability of resonant sloshing. An estimate of the maximum dynamic loads to be expected is then made to determine a proper design. Most theoretical analyses are not able to predict slosh pressures and forces in the neighborhood of resonance, especially for the large amplitude excitations typical of a ship cargo tank. However, several theories are available to predict tank loadings at off-resonant, low amplitude sloshing conditions. Depending on the likelihood of resonance and the expected excitation amplitudes, the designer can either use theory or turn to experimental model data to provide the required design information.

Available linear and nonlinear theories are discussed in detail in References 2 and 6. A review of the theoretical efforts reveals that most studies are limited to linear sloshing, which is valid only for small



(a) Impact pressure traces with large amplitude resonant sloshing



(b) Pressure trace for non-resonant sloshing

FIGURE II-3. TYPICAL PRESSURE WAVEFORMS ON TANK WALLS WITH SLOSHING LIQUIDS

amplitudes and frequencies and predicts an infinite response at resonance. Some nonlinear theories are available for specific tank geometries, and these theories allow a prediction of slosh-induced dynamic forces and pressures on tank structures at resonance. However, the nonlinear theories are also limited to small excitation amplitudes and cannot be used for a general tank shape or when certain real sloshing effects are present such as liquid impacting on the tank top. Therefore, emphasis has been placed on utilizing model test data for predicting full scale tank loads for design purposes.

II.3 Previous Studies

A significant number of scale model studies have been conducted to investigate sloshing in LNG cargo tanks. These efforts have been undertaken primarily by three worldwide laboratories:

- o Southwest Research Institute (SwRI)
- o Det norske Veritas (DnV)
- o Bureau Veritas (BV)

These studies are reviewed in detail in Task 1. Nearly all model tests to date have considered the six degrees of ship motion individually and investigated sloshing by varying amplitude and frequency harmonically, usually in heave, surge, pitch, or roll. Also, water has been used almost exclusively as the model liquid. In most studies, the scaling of impact load data to full scale for use in tank design has considered only Froude scaling and thus eliminated any possible effects of fluid properties such as viscosity, compressibility, or vapor pressure (cavitation). Under these assumptions, pressures scale by

$$\left(\frac{P}{\rho g \ell} \right)_p = \left(\frac{P}{\rho g \ell} \right)_m \quad (\text{II-1})$$

where the subscripts m and p are for the model and prototype, respectively. The periods between prototype and model are given by

$$(T \sqrt{g/\ell})_p = (T \sqrt{g/\ell})_m \quad (\text{II-2})$$

In scaling pressure data, a pressure coefficient is defined as

$$K_p = \frac{P}{\rho g \ell \phi} \quad (\text{II-3})$$

where ϕ is the pitch, roll, or yaw angle. For translation, $\ell\phi$ is usually replaced by the translational amplitude, x. (See Figures IV-1 and IV-4 for definitions of ϕ and x, respectively.)

Scaling Effects

The scaling criteria that should be used in predicting full-scale slosh loads from model data are discussed in References 2, 10, 44, and 74. Most model studies have utilized Froude scaling to predict full-scale loads, and no allowance for fluid effects was considered. Depending on the cargo to be carried, some of these fluid properties would appear important. For example, LNG is transported at a tank pressure slightly above its vapor pressure, and, therefore, cavitation and thermodynamic (vapor condensation) effects could be important. Also, LNG has an extremely low viscosity compared to water, and therefore model tests using water could produce nonconservative predictions of full-scale loads if the model tests were overdamped. Also, compressibility of the impacting liquid/vapor could be important in scaling the slosh loads.

SwRI and DnV experimental programs have been conducted to determine the effects of these fluid properties on scaling sloshing loads. The test results indicate that fluid properties will have a minor effect on scaling impact pressures when large amplitude sloshing, typical of a ship cargo tank, is present. To determine the validity of Froude scaling for large amplitude sloshing, full-scale pressure measurements were recorded in a partially water-filled OBO tank under rolling motion (Reference 2). Subsequent model tests in 1/30th scale were conducted with the full-scale roll motions reproduced on the model. Model pressures converted to full-scale using Froude scaling showed excellent agreement for both the magnitudes and distributions of pressures. Since water was used in both model and full-scale tests, the effects of liquid viscosity and vapor condensation were not included. However, an evaluation of these effects in References 10, 44, and 74 indicates they are of small importance to large amplitude slosh scaling. As a result, Froude scaling is appropriate, and Equations II-2 and II-3 are used for scaling periods and loads, respectively.

III. TASK 1 - DATA REVIEW AND EVALUATION

The objective of Task 1 of the project was to review and present currently available slosh test data on a uniform basis, to identify data required to develop design methods, and to outline required experimental and analytical studies. The majority of the research work in LNG sloshing has been done by SwRI, Det norske Veritas, and Bureau Veritas. Numerous model tests have been conducted by these groups and others to study sloshing loads on LNG ship tanks and the effects of these loads on the tanks and on the ship structures. A principal part of Task 1 has been to compile all of this information and present it on a uniform basis.

The initial step in Task 1 was to conduct a thorough literature search to find all information that is presently available on LNG sloshing in ship tanks (including pressures, forces, and tank response) and to obtain information on tank structural details. This search was broken down into three segments: (1) a manual search of appropriate journals and periodicals, (2) a computer search of the pertinent data bases, and (3) written inquiries. Written inquiries were sent to

General Dynamics/Quincy Shipbuilding Division
Avondale Shipyards, Inc.
ABS/Research and Development Division

seeking principally tank structural details and the results of tank analyses for sloshing loads. In search of sloshing data which might not yet appear in the open literature, inquiries were sent to

Mitsui Shipbuilding and Engineering Co., Ltd.
Bureau Veritas
Det norske Veritas

In addition to these written inquiries, personnel at Newport News Shipbuilding, El Paso Marine, and Kaverner-Moss (U.S. office) were contacted for information.

The manual literature search consisted of a survey of all journals and periodicals that might contain information on LNG sloshing in ship tanks or on the structural analysis of ship tanks for slosh-induced loads. The following list consists of all the sources that were reviewed in the search. The majority of the information was listed in the Marine Research Information Service.

Sources Reviewed by the Manual Literature Search

1. Marine Research Information Service
2. Marine Technology
3. Shipping World and Shipbuilder
4. Royal Institute of Naval Architecture
5. The Society of Naval Architects and Marine Engineers

6. Tanker and Bulk Carrier
7. European Shipbuilding
8. Northeast Coast Institute of Engineers and Shipbuilders
9. Ship Structure Committee
10. International Ship Structures Committee
11. United States Coast Guard Report
12. International Shipbuilding Progress
13. Norwegian Maritime Research
14. Marine Engineering Log
15. Naval Engineers Journal
16. The Naval Architect

The computer literature search included searching several data bases to locate articles that contained "key words" that were related to LNG sloshing in ship tanks and structural analysis of ship tanks. Most of the articles that were located by the computer search were also located by the manual search. This fact gives confidence that the search thoroughly investigated the literature that is currently available on this topic. The following list consists of all data bases that were searched by computer.

Sources Reviewed by the Computer Literature Search

1. Computerized Engineering Index
2. Mechanical Engineering Information Service
3. National Technical Information Service
4. Oceanic Abstracts
5. Energy Line

A reference list of all the literature uncovered during this Task I activity is included in Section VIII.

III.1 Scale Model Sloshing Data

The reports identified by the literature search that contain information on model tests of LNG sloshing in ship tanks are summarized in Table III-1. The table includes information on sources of the reports, tank geometries, test conditions, formats of presented results, and general comments and observations. The data contained in these reports were reviewed and analyzed. An attempt was made to reduce all pertinent information from the various reports to a common form for presentation in this report.

A wide range of test conditions is covered by the experimental studies performed to date. Various parameters such as impact pressures, forces, and moments have been measured during these studies. A number of tank geometries, tank motions, and test liquids have also been investigated.

Due to the complexity of the liquid sloshing phenomena and differences in the methods of data acquisition by the various investigators, the data from the model studies contain a significant amount of scatter. For instance, most of the early model experiments recorded data for relatively few sloshing cycles. Later, it was determined (Reference 44) that the small sample sizes of the early experiments ($N < 200$) were not sufficient

TABLE III-1. SUMMARY OF MODEL TANK LNG SLOSHING EXPERIMENTS

Reference	Tank Shape Analyzed	Sloshing Conditions Studied	Loads Measured	Form of Data Presented	Comments
44 (Task A)	Prismatic tank.	Tank filling levels of 0.4 and 0.12 are studied. Sway excitation amplitudes are 0.01 and 0.1 with respect to the tank length in the direction of tank oscillation.	Dynamic pressures and forces are studied by this project. Only inertial forces caused by the fluid in the tank are measured.	Nondimensional pressures and forces are presented. Most values are presented in "% exceedance level."	This study is used to determine the effects of viscosity, cavitation, and compressibility on the sloshing loads in a prismatic tank. Test liquids include water, glycerol, and reginol oil. Several good photographic presentations help illustrate the sloshing phenomena in the tank. A good description of the experimental setup is included in the report.
44 (Task B)	Prismatic tank.	Tank filling levels of 0.05, 0.10, 0.15, 0.20, 0.30, 0.40, 0.50 are studied. Excitation amplitudes of 0.05, 0.10, 0.15, and 0.30 radians are tested.	Dynamic pressures and wall impact velocities are recorded. Only inertial forces caused by the fluid in the tank are measured.	Nondimensional pressures and velocities are presented. Most values are presented in "% exceedance level."	This study investigates the nature and magnitude of impact pressures in a prismatic tank under harmonic roll, harmonic pitch, random pitch, and harmonic roll in a vertical diagonal plane of the tank. Comparisons between predicted data and experimental data are made.
44 (Task C)	Spherical tank.	Tank filling levels of 0.20, 0.30, 0.40, 0.50, 0.60, 0.70, and 0.80. Sway excitation amplitudes are 0.05, 0.01, 0.08 with respect to the tank diameter.	Resultant hydrodynamic forces and impact velocities are studied. Only inertial forces caused by the fluid in the tank are measured.	Nondimensional forces and impact velocities are studied. Maximum average values are presented.	This study looks at the hydrodynamic forces acting on a spherical tank. It also looks at forces acting on and velocities occurring at an internal tower structure.
24	Spherical tank. This tank is a scale model of a tank for an 87,600m ³ LNG-carrier by Moss Rosenberg Verft A/S.	Tank filling levels of 0.29, 0.50, and 0.65 are used. Sway excitation amplitudes of 0.028, 0.056, and 0.167 with respect to the tank diameter are used.	Dynamic wall pressures, resultant forces, and impact velocities are studied. Only the maximum measured values during any one period for a 5-minute test run are presented. No averaged values are given.	Forces are presented in model scale in units of KP. Moments are given, also, in model scale in units of KPM. Velocities are shown in model scale with units of cm/sec. Dynamic pressures are shown in tabular form. Pressure units are KP/m ² , and both impulsive pressures and single amplitude regular pressures are given.	This report inspects the hydrodynamic forces on the tank and the forces and moments caused by liquid sloshing on a pipe tower inside the tank. Wall pressures and impact velocities are also studied. Prediction methods for determining the forces are presented. The effects of a boiling liquid are also discussed. Isopentane and water are used as test fluids. Long-term distributions of data are studied.

TABLE III-1. SUMMARY OF MODEL TANK LNG SLOSHING EXPERIMENTS
(Cont'd)

<u>Reference</u>	<u>Tank Shape Analyzed</u>	<u>Sloshing Conditions Studied</u>	<u>Loads Measured</u>	<u>Form of Data Presented</u>	<u>Comments</u>
10	Rectangular tank. This tank is approximately 1/36 scale of an actual tank.	Tank filling levels of 0.1, 0.15, 0.20, 0.25, 0.30, and 0.40 are used. Pitching excitation amplitude of 8° is used.	Dynamic wall pressures, forces, and moments are studied. Only inertial forces caused by the fluid in the tank are measured.	Pressures, forces, and moments are presented in a nondimensional form. The measured values are maximum average values.	This study considers cavitation, fluid viscosity, and compressibility. Test fluids include methylene chloride, water, glycerin, and hydraulic oil.
7	Prismatic tank. A model of an "Arctic Tokyo" tank is used. The Bureau Veritas tank is 1/52 scale. The Det norske Veritas tank is 1/25 scale.	Tank filling levels of 0.059, 0.05, 0.15, 0.172, and 0.20 are used. Pitching excitation amplitude of 8° is studied.	Dynamic wall pressures are studied.	The pressures are presented in nondimensional form.	This report compares studies done by Det norske Veritas and Bureau Veritas. An explanation of the various nondimensional terms that are important to the analysis is included in this study.
9	Two prismatic tanks are used. The tanks are 1/50 scale. These tanks are models of two tanks in the Methan and Tanker Service Company's 125,000m ³ LNG-carrier.	Tank filling levels of 0.786, 0.849, 0.897, and 1.0 with respect to the tank height are tested. Pitch and roll excitation amplitudes of 4° and 8° are used.	Dynamic wall pressures, forces, and moments are measured. Only inertial forces caused by the fluid in the tank are measured.	Nondimensional pressure, force, and moment values are presented. The measured values are maximum average values.	This report determines the effects of transporting butane, propane, ethane, or ethylene in LNG cargo tanks. Predictions of full-scale forces (in units of pounds) and full-scale pressures (in psi) on the tank wall caused by the various liquids are made.
49	Rectangular tank.	Tank filling levels of 0.05, 0.10, 0.20, 0.30, 0.40, and 0.50 with respect to tank length are studied. The tank is oscillated in a translational mode.	Resonant periods are determined.	Nondimensional frequency and viscosity coefficients are presented.	This study presents a procedure for calculating natural frequencies of viscous liquids in rigid rectangular tanks. Theoretical and experimental results are compared. Water and mineral oil are the test fluids.
11	Rectangular tank. One tank is 1/20 scale and the other tank is 1/32 scale.	Tank filling levels of 0.25, 0.50, 0.60, 0.70, 0.80, and 0.90 with respect to the tank height are studied. Pitching excitation amplitudes of 5°, 7°, 10°, and 13° are examined.	Dynamic wall pressures are measured.	The pressure values are given in the model scale in units of meters of water.	Computer models are compared to experimental data. These models predict wall pressures caused by sloshing.

TABLE III-1. SUMMARY OF MODEL TANK LNG SLOSHING EXPERIMENTS
(Cont'd)

Reference	Tank Shape Analyzed	Sloshing Conditions Studied	Loads Measured	Form of Data Presented	Comments
50	Prismatic tanks.	Tank filling levels of 0.60, 0.70, 0.80, 0.90, and 1.00 with respect to the tank height are tested.	Dynamic pressures and forces on end and swash bulkheads are measured. Regular and transient pitching motions with amplitudes of 0.096, 0.193, and 0.292 are studied.	Nondimensional pressures and forces are presented. Single amplitude and double amplitude pressure values are both used.	This report reviews the work done by Akita. Very little discussion of the experimental setup used to obtain the data is given.
37	Tanks with vertical sides are studied.	Pitch, roll, and translational excitation modes are discussed.	Dynamic wall pressures are predicted.	Pressures are presented in units of meters of water.	This report develops procedures to compute the dynamic pressure heads both for full tanks and for tanks with arbitrary filling.
42	Rectangular tank.	Rolling amplitudes are considered in this study. Several filling heights are observed.	Wall stresses and deflections are measured. The maximum dynamic stress is presented. The maximum mean deflection is presented.	Stresses are presented in units of KP/cm ² and deflections are presented in relative numbers.	This report deals with the problem of dynamic loads due to sloshing in a heavy fuel oil tank on board the T/T "Humboldt." The data were taken on an actual test run of the ship. Long-term distributions of stresses on the wall are predicted.
20	Rectangular tank.	Tank filling height of 0.5 with respect to tank breadth is studied. The excitation amplitudes are 0.1 and 0.2 radians. A rolling motion is studied.	Dynamic pressures are measured. Also, wave amplitudes are examined.	Dynamic pressures are presented in nondimensional form and the wave heights are given in meters.	A nonlinear, inviscid boundary value problem of potential flow is formulated and the steady state solution is found as a power series in $\epsilon^{1/3}$. A comparison between experimental and theoretical results is made.
43	Prismatic tank. The tank scale is 1/25.	Tank filling levels of 0.059 and 0.172 with respect to the tank height are tried. Pitching excitation amplitudes of 5° and 8° are used. Surging excitation amplitudes of 0.157 and 0.303 with respect to the tank length are used.	Liquid velocities and dynamic pressures are measured.	Nondimensional velocities and pressures are presented. The maximum average values for these quantities are given.	Liquid velocities and dynamic pressures are studied in this report. Long-term distributions of liquid velocities and impulsive pressures are predicted. Water is used as the test fluid.

TABLE III-1. SUMMARY OF MODEL TANK LNG SLOSHING EXPERIMENTS
(Cont'd)

Reference	Tank Shape Analyzed	Sloshing Conditions Studied	Loads Measured	Form of Data Presented	Comments
13	Rectangular tanks.	Several tank filling levels are examined. Pitching excitation motions are studied.	Dynamic pressures are measured.	Nondimensional pressures are presented.	Report is in French - <i>damage</i> .
16	Prismatic tank. The tank is 1/50 scale.	Pitch, roll, and surge excitation modes are studied.	Dynamic wall pressures are measured.	Nondimensional pressures are presented.	This report presents pressure measurements due to liquid motion on tops and walls of small scale models of ship tanks. The report is in French.
14	Prismatic tank. This is a model tank of a tank in a 125,000m ³ LNG-carrier owned by El Paso Natural Gas Company. The scale is 1/40.	Tank filling levels of 0.15 and 0.80 with respect to the tank height are used. Angular excitation amplitudes of 5°, 10°, 15°, and 20° are studied.	Dynamic wall pressures are measured. Also, pressures on the top wall are given.	Pressures are presented in nondimensional form. The maximum average and the highest maximum values are given.	This report studies the possibilities of transporting LNG in tanks with less than full fill depths. Only a limited discussion of the experimental setup used to obtain the data is given.
15	Prismatic tank. The tank tested is a model of the number 1 tank in the "Arctic Tokyo." Two models are used. One is 1/52 and the other is 1/47 scale.	Tank filling levels of 0.05, 0.10, 0.15, 0.20, and 0.30 with respect to the tank height are analyzed. Pitching excitation amplitudes are 4° and 8°. Surging excitation is also examined.	Dynamic wall pressures and liquid velocities are measured.	Nondimensional pressures and velocities are presented. Maximum average values and values after impact are given.	This report presents a theoretical treatment of the liquid motion, results of experimental measurements, and estimates of the liquid motion in tank number 1 of the "Arctic Tokyo."

TABLE III-1. SUMMARY OF MODEL TANK LNG SLOSHING EXPERIMENTS
(Cont'd)

Reference	Tank Shape Analyzed	Sloshing Conditions Studied	Loads Measured	Form of Data Presented	Comments
30	Rectangular tanks are analyzed.	Filling levels of 0.4, 0.6, 0.75, and 0.8 are tested. Harmonic and random pitching excitations are observed.	Forces, moments, and impact pressures are determined.	This report gives mostly qualitative results. Some nondimensional pressures are presented.	This study determines the characteristics of loads on tank walls and internal structures such as stringers and web frames.
63	Rectangular, spherical, and cylindrical tanks are studied.	Various filling levels are studied. Sway and roll excitation modes are used.	Forces, pressures, and wave amplitudes are presented.	Nondimensional forces and wave amplitudes are presented.	Experimental and theoretical results are compared for both shallow and non-shallow fill levels.
63	Prismatic tanks are discussed.	Several filling levels are discussed. Sway excitation is studied.	Forces, pressures, and wave amplitudes caused by sloshing are studied.	Some nondimensional wave amplitudes and forces are presented. Also, dynamic pressures for selected sloshing conditions are given.	Short and long term predictions of loads are discussed. Examples of some analysis schemes are presented.
31	Prismatic tank.	Tank filling level of 0.15 is studied. Excitation amplitudes of 0.1 and 0.2 radians are tested.	Dynamic wall pressures are measured.	Nondimensional pressures are presented in "% exceedance level".	This report studies the size of the area over which a large, impulsive pressure acts. The report analyzes the area on the end bulkhead near the still liquid free surface.
21	Prismatic tank.	Tank filling level of 0.75 is studied. Random excitation amplitudes of up to 0.175 radians are tested.	Forces and moments are measured.	Nondimensional resultant forces and moments are presented. Both short and long-term values are determined.	This study investigates the forces and moments acting on a tank during random pitching.

TABLE III-1. SUMMARY OF MODEL TANK LNG SLOSHING EXPERIMENTS
(Concl'd)

Reference	Tank Shape Analyzed	Sloshing Conditions Studied	Loads Measured	Form of Data Presented	Comments
35	Prismatic tank.	The data from several other studies are utilized in an effort to correlate experimental results with the results predicted by the nonlinear sloshing theories. Sway and roll excitation motions are studied.	Surface elevation (wave amplitude), integrated lateral force and moment from slosh induced dynamic pressures are presented.	Nondimensional wave heights, forces, and moments are presented.	This report studies the usefulness of two nonlinear slosh theories. One theory is for shallow liquid depths and the other is for nonshallow liquid depths. The fluid levels where these theories are applicable are determined.
63	Prismatic tanks are analyzed. The model tanks are 1/25 scale.	Filling level of 0.75 is tested. Random pitching is studied.	Moments and forces acting on the deck transverses and bulkheads are measured.	Nondimensional forces and moments are presented.	The forces and moments acting on the deck transverses and bulkheads are studied. The effects of tank lengths are analyzed. Short and long term values for the forces are presented.
63	Spherical tank is tested.	Filling levels of between 0.2 and 0.8 are tested. Sway excitation amplitudes are used in the tests.	Dynamic lateral, vertical, and resultant forces are measured. Also, forces and impact velocities occurring on internal structures are studied.	Nondimensional forces and velocities are presented.	This report discusses test results of a study on a spherical tank. The various forces acting on the tank and on structures inside of the tank are determined. Most of the results given in this report were originally presented in Reference 26.
63	Prismatic tank is studied.	Filling levels of up to 0.5 are tested. Harmonic pitching and rolling are investigated.	Dynamic pressures are studied.	Nondimensional pressures are presented in terms of "% exceedance level".	This study discusses the locations of the tank that experience relatively large impact pressures. Statistical analyses of the data are discussed. Also, the area over which the impact pressures act are investigated.

for accurately predicting worst case sloshing pressures. Therefore, the more recent studies (containing 200 or more cycles of sloshing data) predict worst case sloshing loads that are considerably higher than earlier estimates.

Because of the inappropriateness of some of the model test results, only a select number of references were chosen for the data presented in this report. The predicted worst case sloshing loads from the selected studies provide a more realistic definition of loads than the early model test data. The majority of the summarized data have been extracted from References 9, 10, 44, 64, and 74.

Nondimensional Coefficients

Of principal importance in many tank analyses is the slosh-induced dynamic impact pressure acting on the tank walls. Figure III-1 shows a typical pressure trace and distribution of pressures taken from laboratory test data. There are several formats that can be used to present pressure information. First, there is the average pressure, P_{AVG} . This value is defined in Figure III-1 as the average pressure for a given number of sloshing cycles. Next, there is the maximum (worst case) pressure, P_{MAX} , which is the highest pressure occurring during any one of a given number of sloshing cycles. Finally, there is the "q% exceedance level" pressure, P_q . This is the pressure level which is exceeded by q% of the measured pressures in a given sample size. For example, the median pressure would be the 50% exceedance level. Much of the data presented by Det norske Veritas is presented in this form.

For simplicity and uniformity, the pressure results presented in this report are in nondimensional form. The nondimensional pressure is denoted as K_P . The pressure value used in K_P is either the average pressure (AVG), maximum pressure (MAX), or the "q% exceedance level" pressure (q) as indicated. The pressure has been nondimensionalized using Froude and Euler scaling as discussed in References 44 and 74. The resulting nondimensional pressure is defined by the following relation:

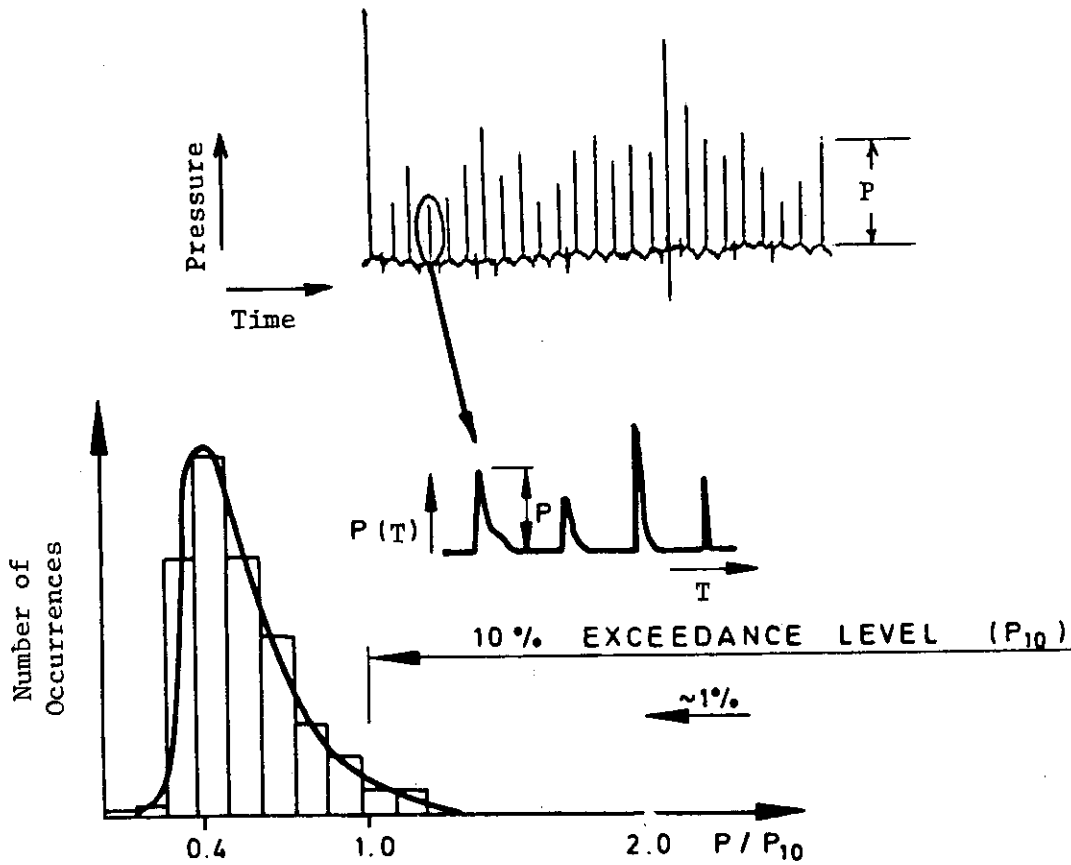
$$K_P = \frac{P}{\rho g \ell \phi} \quad \text{or} \quad \frac{P}{\rho g \ell \left(\frac{x}{\ell}\right)} \quad \text{(III-1)}$$

where P = dynamic wall impact pressure
 ρ = liquid density
 g = acceleration of gravity
 ℓ = tank length in the direction of the tank motion
 ϕ = angular excitation amplitude (in radians)*
 x = translational excitation amplitude (in units of length)

*Single amplitude value

Another important parameter to the design analysis of a tank is the inertial force created by the sloshing of liquid in the tank. A nondimensional force, K_F , similar to the nondimensional pressure has been developed for the presentation of experimental force data. Measured peak sloshing

(a) Typical 25-Cycle Dynamic Pressure Trace



(b) Distribution of Impact Pressure Peaks (P)

P = Peak dynamic pressure during one cycle

$$P_{AVG} = \frac{\sum_{i=1}^n P}{n} \quad \text{where } n = \text{total number of cycles tested}$$

FIGURE III-1. PRESSURE DEFINITIONS

forces do not exhibit the cyclic variations typical of localized impact pressures. As a result, the average peak force (F) measured over a given number of sloshing cycles is representative of the peak force occurring on any given cycle. For a prismatic or rectangular tank geometry, this non-dimensional force is defined as

$$K_F = \frac{F}{\rho g \ell h b \phi} \quad \text{or} \quad \frac{F}{\rho g \ell h b \left(\frac{x}{\ell}\right)} \quad (\text{III-2})$$

where F = dynamic force (only inertial forces caused by the liquid are included)
 h = liquid filling height
 b = tank width transverse to the direction of the tank motion

For a spherical tank, dynamic impact pressures are not of critical importance to tank design.(24,44) However, the tank forces created by the inertia of the sloshing liquid are significant to tank design. The nondimensional force coefficient used for spherical tanks is defined as:

$$K_F = \frac{F}{\rho g V} \quad (\text{III-3})$$

where F = dynamic force (see Figure III-9 for the definitions of the various forces)
 V = tank volume

From Froude scaling, the nondimensional time is defined as:

$$K_T = T \sqrt{g/\ell} \quad (\text{III-4})$$

where T = time.

In addition to resonant sloshing periods, slosh-induced dynamic pressure rise times are normalized by Equation (III-4).

Table III-2 provides equations for calculating the natural period, T_R , of liquid in rectangular, spherical, and cylindrical tanks as a function of fill depth. These equations are derived in Reference 1.

Statistical Analysis of Slosh-Induced Pressures

Because of the random nature of resonant sloshing in an LNG tank, a sufficient sample size must be determined that will give a representative distribution of peak sloshing pressures. References 44 and 64 have both addressed this problem. These two references used somewhat different approaches to obtain similar results.

TABLE III-2. EQUATIONS FOR CALCULATING LIQUID NATURAL PERIODS
IN RECTANGULAR, SPHERICAL, AND CYLINDRICAL TANKS

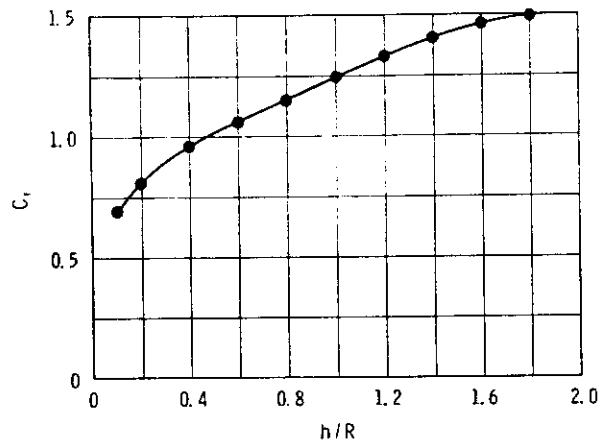
Rectangular:

$$T_R = \frac{2\pi}{\sqrt{\frac{\pi g}{\ell} \tanh\left(\frac{\pi h}{\ell}\right)}}$$

Spherical Tank:

$$T_R = \frac{2\pi}{C_1} \sqrt{\frac{D}{2g}} \sqrt[4]{4\left(\frac{h}{D}\right) - \left(\frac{2h}{D}\right)^2} \quad \text{for} \quad \left(0.05 < \frac{h}{D} < 1.0\right)$$

with the values of C_1 shown on the figure below.



h = liquid filling height
R = tank radius
D = tank diameter

Cylindrical Tank: (Vertical orientation)

$$T_R = \frac{2\pi}{\sqrt{7.664 \left(\frac{g}{D}\right) \tanh\left[7.664 \left(\frac{h}{D}\right)\right]}}$$

Reference 44 recorded 1000 cycles of resonant sloshing pressures. Then, the largest number of consecutive peak pressures less than 85% of the maximum (worst case) pressure was determined. This number varied from 140 to 160 cycles. Based on this information, a sample size of 200 cycles was considered representative. Histograms of the 200-cycle and 1000-cycle test data are pictured in Figure III-2. The distributions are quite similar in shape, indicating good repeatability between a 200-cycle sample and a 1000-cycle sample.

In Reference 64, various sample sizes up to 400 cycles were evaluated. It was determined that 200 cycles were required to give good repeatability of the average pressure for a given sample size. The results of References 44 and 64 show that: (1) 200 cycles are adequate to define the average sloshing pressure (P_{AVG}) and (2) that the worst case pressure (P_{MAX}) will be at least 85% (or greater) of P_{MAX} for 1000 cycles of sloshing.

Reference 44 developed a theoretical pressure distribution for predicting extreme pressure values. This distribution was based on a three-parameter Weibull curve fit. The resulting equation is:

$$Q(P) = \exp - \left(\frac{P - AO}{A - AO} \right)^M \quad (III-5)$$

where $Q(P)$ = the probability that the response variable will be greater than P

P = dynamic pressure

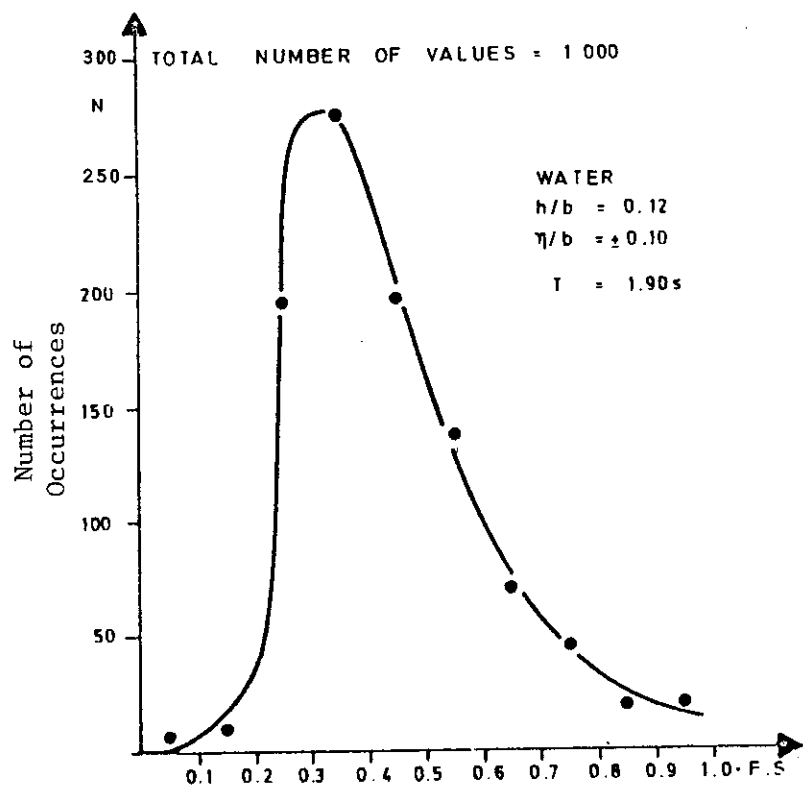
AO, A, M = experimentally determined parameters of the distribution

Utilizing this distribution, Reference 44 presents a procedure for estimating long-term distributions of slosh-induced dynamic impact pressures occurring during the life of a ship. This procedure is based on the statistical analyses of the slosh pressures and the tank excitation motions.

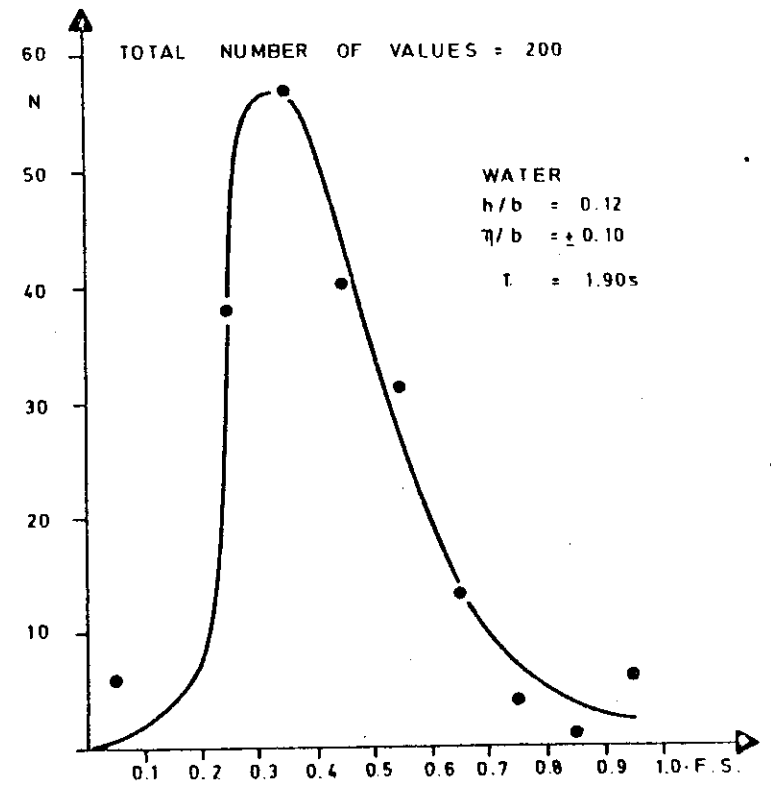
III.1.1 Prismatic Tanks

Model scale data for slosh-induced dynamic wall pressures vary considerably with test conditions. While the general nature of resonant sloshing in prismatic tanks of various geometries is similar, the impact pressures for a given tank can vary significantly with wall location, excitation motion and amplitude, liquid density, and fill level. Since it is impossible to measure all possible combinations of these parameters, the composite of the sloshing pressure data from all sources is presented so that the range of load coefficients can be established for design purposes. Figure III-3 shows the highest (for any measurement location) Kp_{AVG} vs fill level (h/ℓ) for a range of excitation motions and amplitudes, tank geometries (all are prismatic or rectangular), pressure transducer locations, and test liquids. All points on the graph are for resonant sloshing conditions. The Kp_{AVG} ranges between 1 and 25. No distinct relation between Kp_{AVG} and the liquid filling level is noted.

DISTRIBUTION OF PEAK PRESSURES

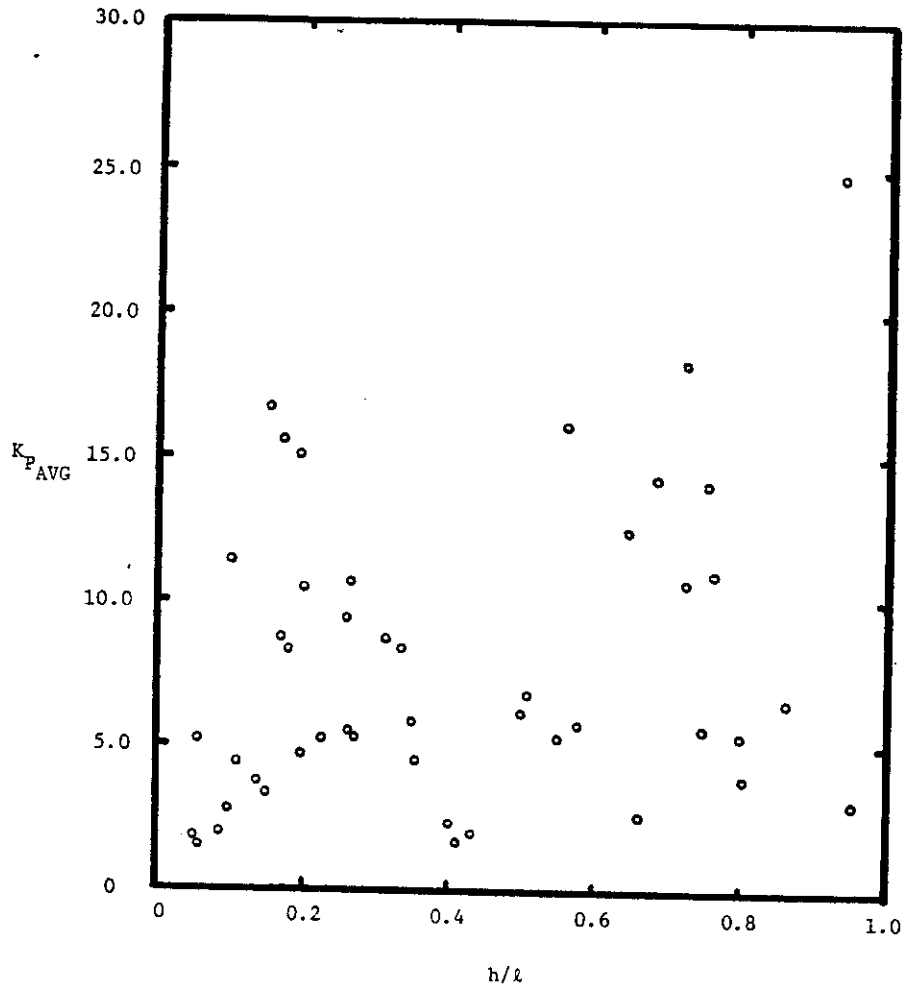


F.S. = 0.252 kp/cm^2 = Full Scale Pressure
 NUMBER OF VALUES EXCEEDING F.S. = 24



F.S. = 0.252 kp/cm^2 = Full Scale Pressure
 NUMBER OF VALUES EXCEEDING F.S. = 4 (≈ 2% $\frac{200}{1000}$)

FIGURE III-2. PRESSURE HISTOGRAMS FOR 1000-CYCLE AND 200-CYCLE RESONANT SLOSHING TESTS AS PRESENTED IN REFERENCE 44



$K_{P_{AVG}}$ = nondimensional pressure coefficient (averaged over many cycles)

h = liquid filling height

l = tank length

NOTE:

Pressures are highest measured values for any test conditions regardless of tank motion, tank geometry, transducer location, and test liquid.

FIGURE III-3. HIGHEST AVERAGE NONDIMENSIONAL PRESSURE VS NONDIMENSIONAL TANK FILLING LEVEL FOR ALL MODEL TESTS RUN TO DATE

Ranges of $K_{p_{MAX}}$ values compiled from the model-scale data are plotted in Figure III-4. These values are for nondimensional excitation amplitudes from 0.05 to 0.30. It should be noted that the data points on this graph are worst case values for at least 200 cycles of resonant sloshing. As the filling level increases, the location of the highest pressure moves from the vertical walls to the tank top. Otherwise, no clearly defined trend of $K_{p_{MAX}}$ with h/ℓ is noted. The location of highest pressures on the vertical walls is usually near the static liquid filling level, while on the tank top the highest pressure occurs near the corners.

Except for one data point, all $K_{p_{MAX}}$ values on Figure III-4 range between 10 and 125. The K_p value of 325 is considered unusual since the other data points represent a wide range of sloshing conditions covering several sources.

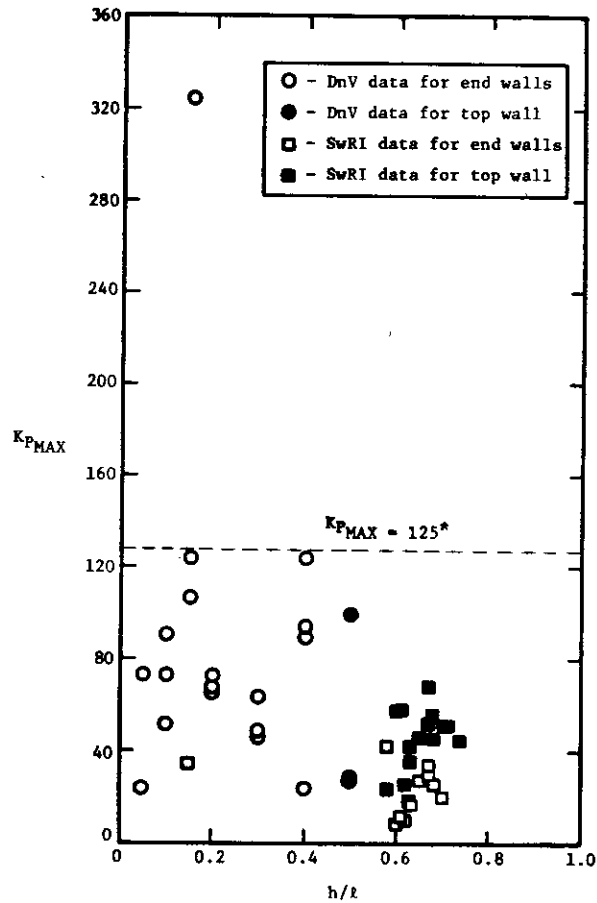
The form of nondimensional pressure coefficient equation, Equation III-1, reveals that the pressure P is assumed to be a linear function of excitation amplitude, ϕ (i.e., $P = K_p \rho g \ell \phi$). In actuality, pressures are only a linear function of ϕ for amplitudes less than ~ 0.1 . Figure III-5 from Reference 44, exhibits pressure vs amplitude data showing this trend. It is evident from Figure III-5 that as ϕ approaches 0.3, the slopes of the $K_{p10} \phi$ vs ϕ curves approach horizontal. This means the influence of the excitation amplitude on the impact pressure diminishes as the amplitude increases. The relation between $K_p \phi$ and ϕ exhibited by Figure III-5 is typical for all areas of the tank that experience slosh-induced impact pressures. Thus, if pressure coefficients obtained at experimental amplitudes less than 0.1 are used to predict pressures at larger amplitudes, the results will be conservative.

Figure III-6 presents sloshing force coefficient data summarized from References 9, 10, and 44 for a range of amplitudes. Figure III-7 shows the same data for a given amplitude ($\pm 8^\circ$). The data indicate that the force coefficients decrease as the filling level increases. However, the actual force will not necessarily decrease with h/ℓ as a result of the definition of K_F (i.e., $F = K_F \rho g \ell^2 (h/\ell) \phi$).

Table III-2 presents an equation that predicts the resonant period of the liquid in a rectangular (or prismatic) tank. Nondimensionalizing the equation from Table III-2, it becomes:

$$\left(T \sqrt{\frac{g}{\ell}} \right)_{\text{RESONANCE}} = \sqrt{4\pi \left[\tanh \left(\frac{\pi h}{\ell} \right) \right]^{-1}} \quad (\text{III-6})$$

A comparison (Figure III-8) of the resonant periods calculated from this equation to measured periods from the model tests for a variety of prismatic tanks indicates that the theoretical values correlate well with the experimental results.



*See discussion in Section VI.2

FIGURE III-4. MAXIMUM PRESSURE COEFFICIENT VS TANK FILLING LEVEL FOR ϕ OR $(x/l) \leq 0.30$

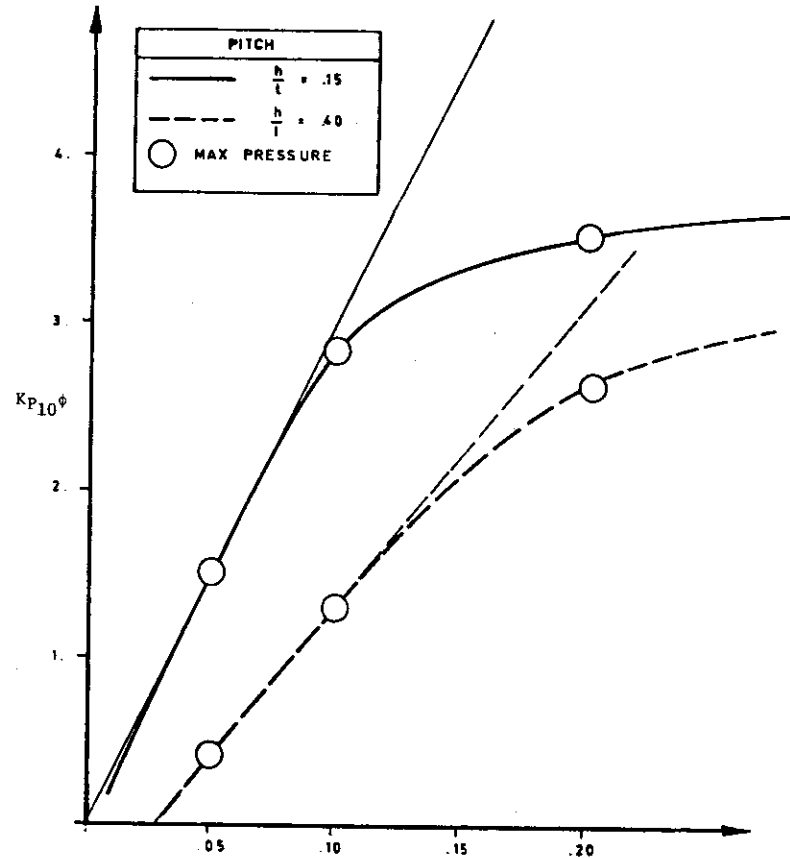


FIGURE III-5. PRESSURE COEFFICIENTS VS PITCH AMPLITUDE (FROM REFERENCE 44)

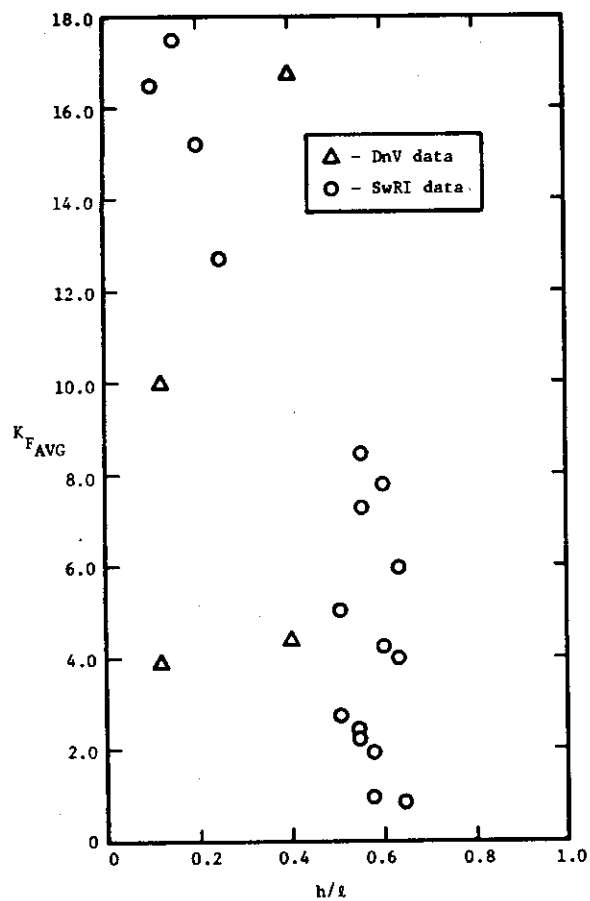


FIGURE III-6. AVERAGE FORCE COEFFICIENT VS TANK FILLING LEVEL FOR ϕ OR $(x/l) \leq 0-30$

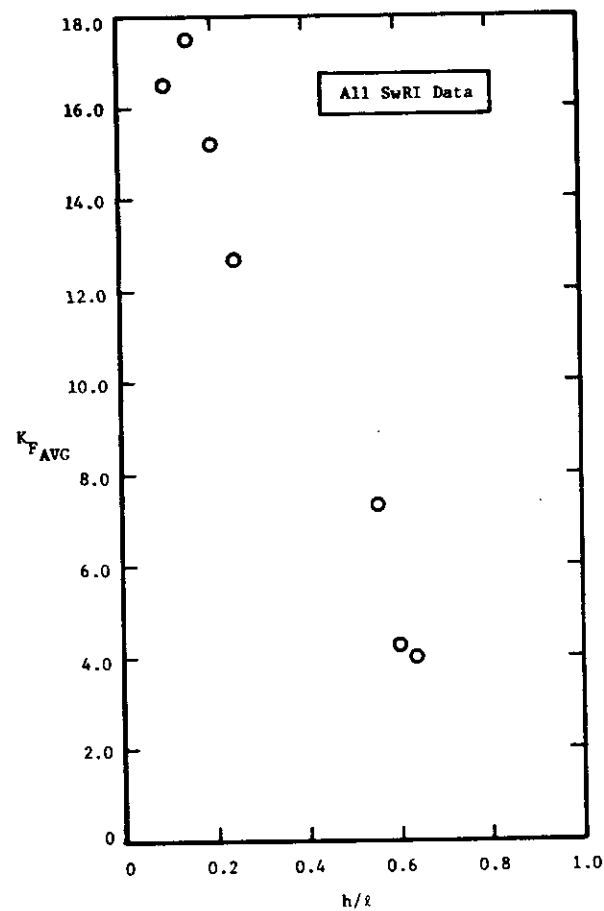


FIGURE III-7. AVERAGE FORCE COEFFICIENT VS TANK FILLING LEVEL (Pitching Motion with $\phi = \pm 0.14$ Rad. or $\pm 80^\circ$)

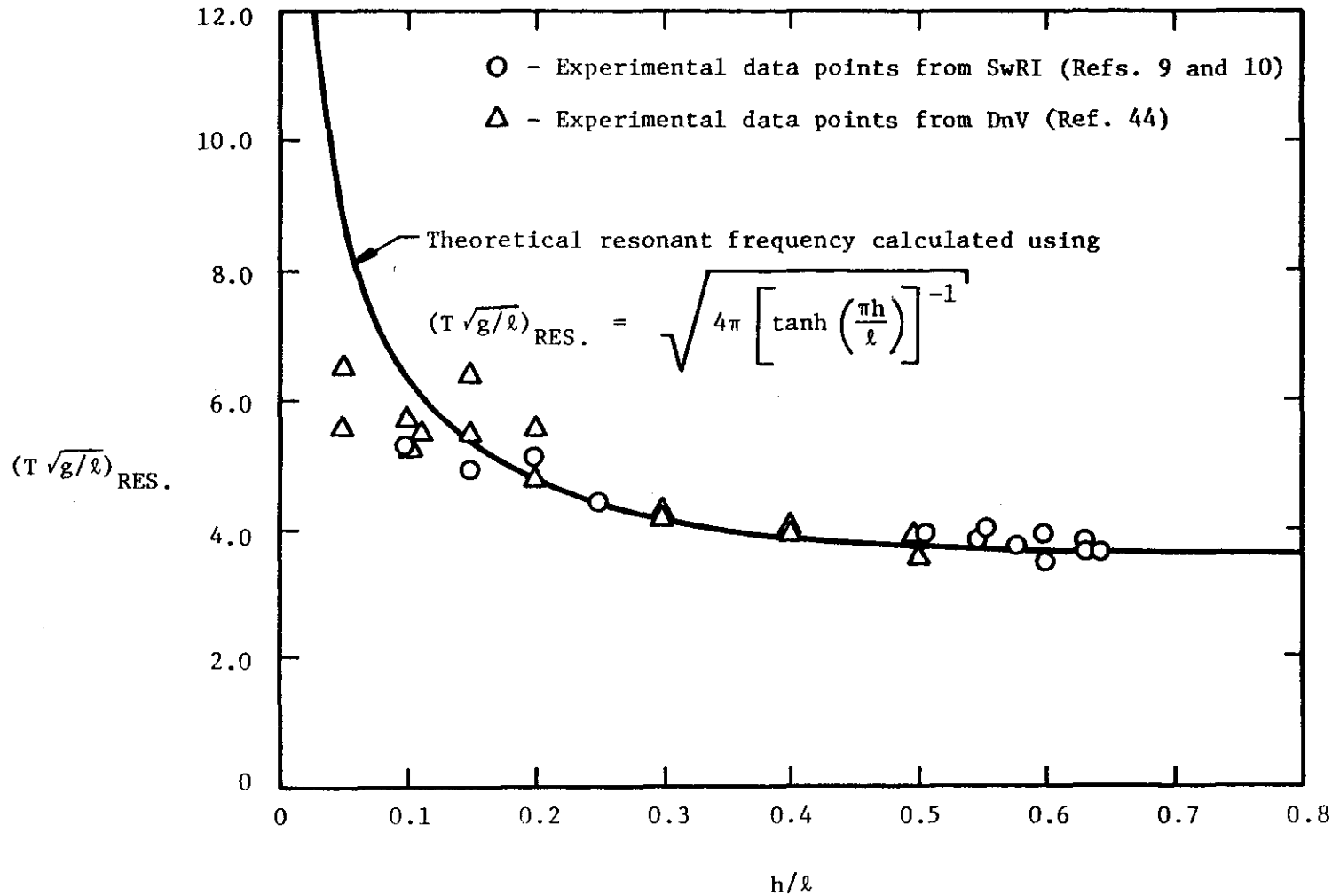


FIGURE III-8. RESONANT LIQUID FREQUENCY VS TANK FILLING LEVEL FOR RECTANGULAR OR PRISMATIC TANKS

The information presented in this section covers the important considerations in the design of a rectangular or prismatic tank. Topics such as scaling criteria for model tests, random excitation motions, statistical analysis of cargo sloshing, and several other problems related to cargo sloshing in LNG tanks have also been addressed by various investigators. Their works are listed in this report in the Reference List of currently available literature.

III.1.2 Spherical Tanks

As previously stated, forces and not impact pressures are of primary concern in the design of a spherical LNG ship tank. References 24 and 44 present a thorough set of data on sloshing forces acting on a spherical tank. The data presented in this section are excerpted from these reports.

The pertinent forces acting on a spherical tank are defined in Figure III-9. Figures III-10 through III-17 show typical force magnitudes for various tank filling levels and excitation amplitudes. All data compiled were obtained using a horizontal tank excitation motion. Reaction forces produced by pitch and roll motions about the tank centerline were not reported. The authors stated that the reaction forces produced by pitch and roll are small relative to those produced by horizontal motions.

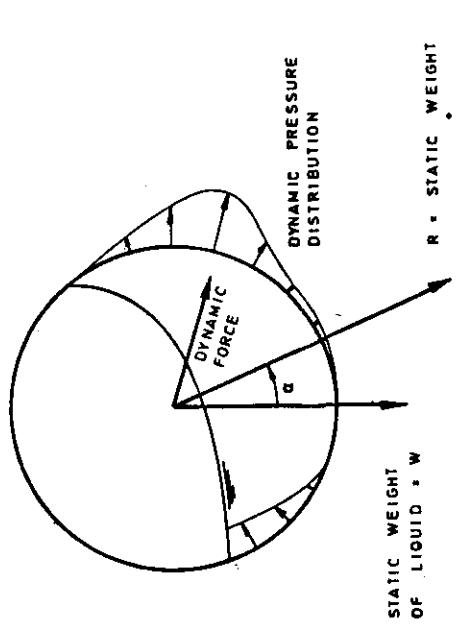
The following general trends were discovered during the analysis of the test data. The maximum lateral force usually occurs under the same conditions as the maximum resultant force. The direction angle, α , of the resultant force is greatest for h/D less than 0.2. The angle decreases as h/D increases from 0.4 to 0.6 and remains about constant for h/D values above 0.6.

The lateral force attains its maximum value when h/D is greater than 0.8 for large amplitude excitation motion (large amplitude being η/D greater than 0.05). The maximum lateral force is about equivalent to the inertial force of a full sphere. For small amplitude excitations (η/D values near 0.01), the maximum lateral force occurs when h/D is about 0.5.

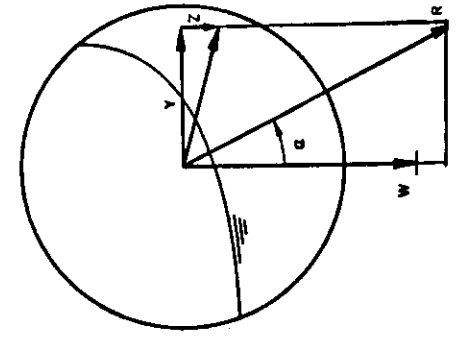
The maximum resultant force is nearly equal to the weight of liquid contained in a full sphere. This maximum occurs during the same conditions that create the maximum lateral force. These maximum resulting and lateral forces occur at relatively high excitation frequencies.

The maximum dynamic vertical force occurs when the filling level of the tank is about 0.4. However, the maximum static plus dynamic vertical force is created when the tank filling level is greater than 0.8. The maximum static plus dynamic force is about equal in magnitude to the maximum resultant force.

The resonant slosh frequencies for the liquid in a spherical tank vary substantially depending on the filling level. High filling levels



R = STATIC WEIGHT DYNAMIC FORCE (VECTORIAL SUM)



Y = LATERAL DYNAMIC FORCE
Z = VERTICAL DYNAMIC FORCE
R = RESULTANT FORCE
alpha = ANGLE OF RESULTANT FORCE RELATIVE TO VERTICAL

NOTE: In Figures III-10 through III-17, η is the horizontal excitation amplitude, γ is the specific weight of the liquid, and D is the tank diameter.

FIGURE III-9. SLOSH FORCES ON SPHERE

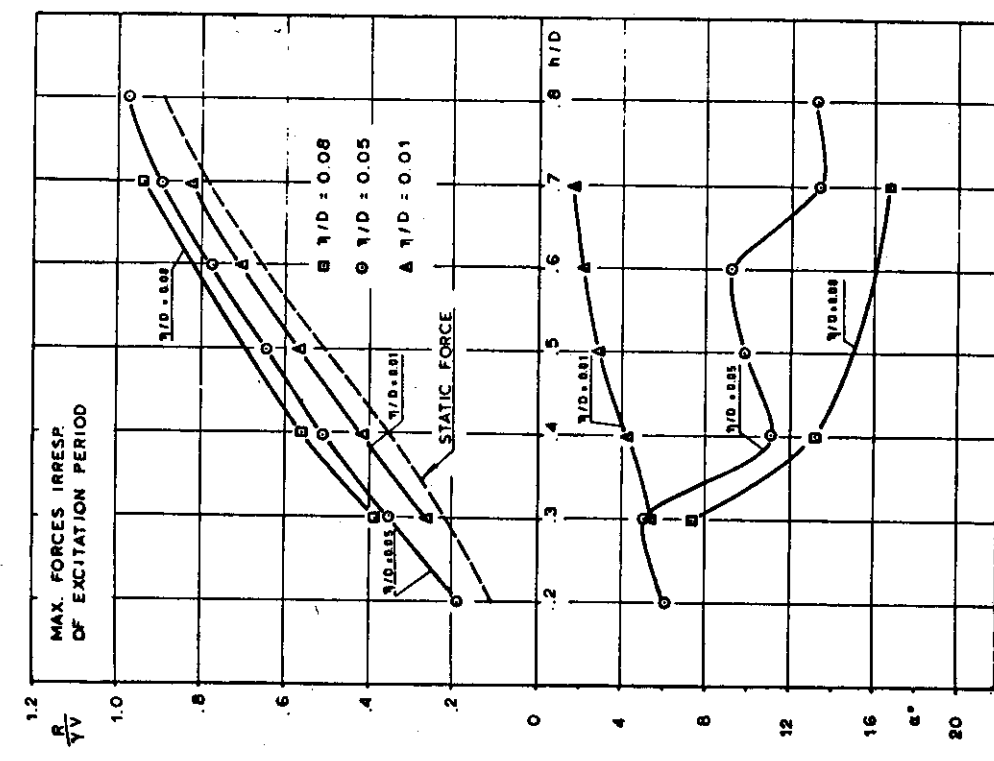


FIGURE III-10. RESULTANT FORCE ON SPHERE VS FILL DEPTH (Reference 44)

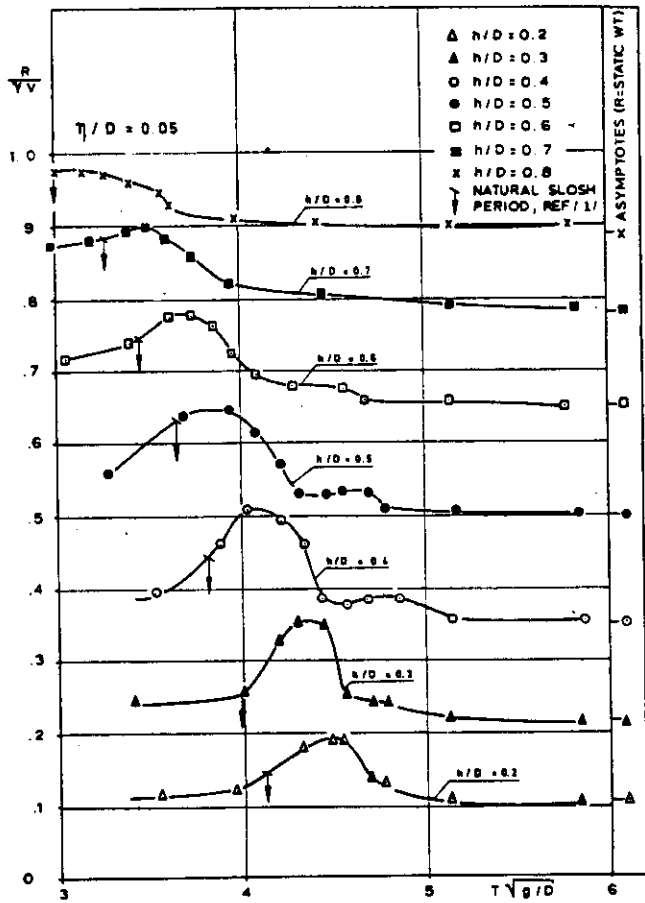


FIGURE III-11. RESULTANT FORCE ON SPHERE VS EXCITATION PERIOD (Reference 44)

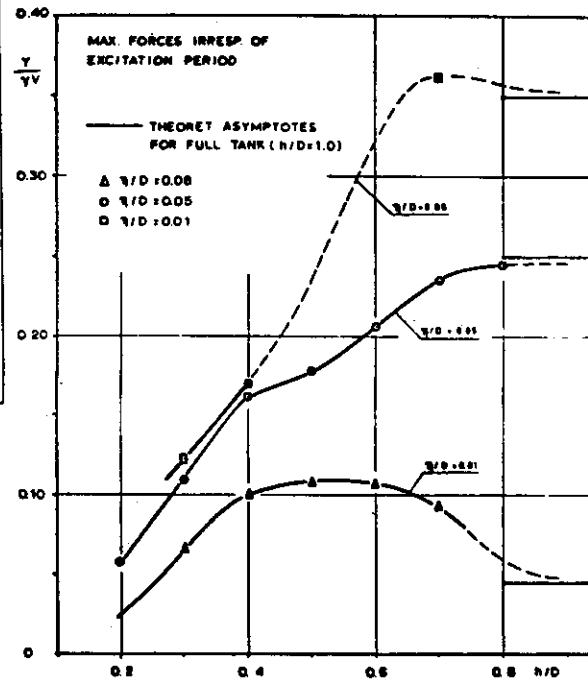


FIGURE III-12. LATERAL FORCE ON SPHERE VS FILL DEPTH (Reference 44)

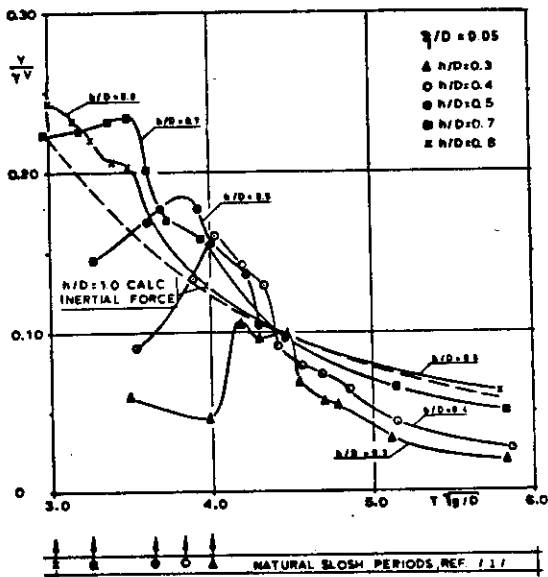


FIGURE III-13. LATERAL FORCE ON SPHERE VS EXCITATION PERIOD (Reference 44)

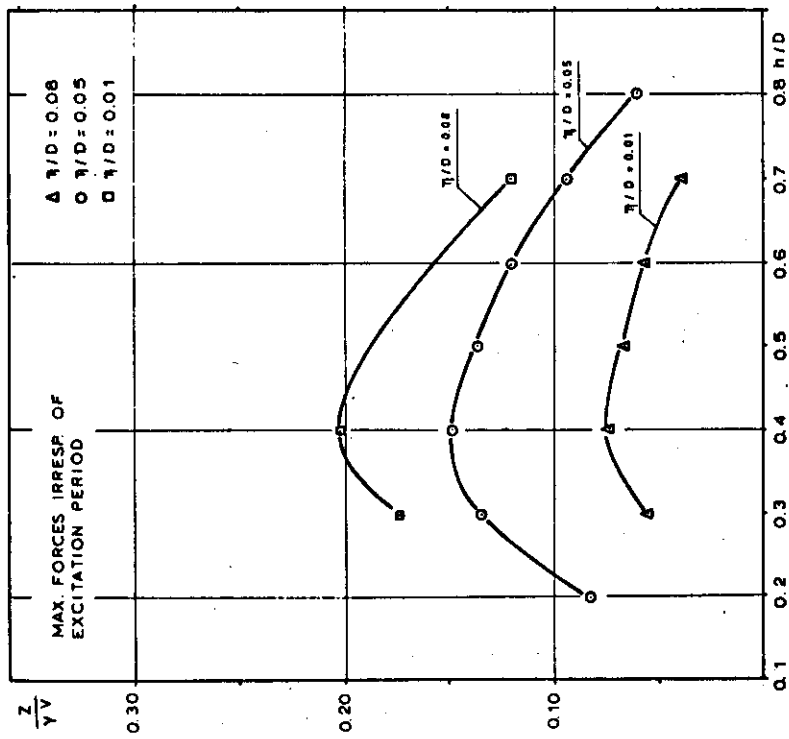


FIGURE III-14. VERTICAL (DYNAMIC) FORCE ON SPHERE VS FILL DEPTH (Reference 44)

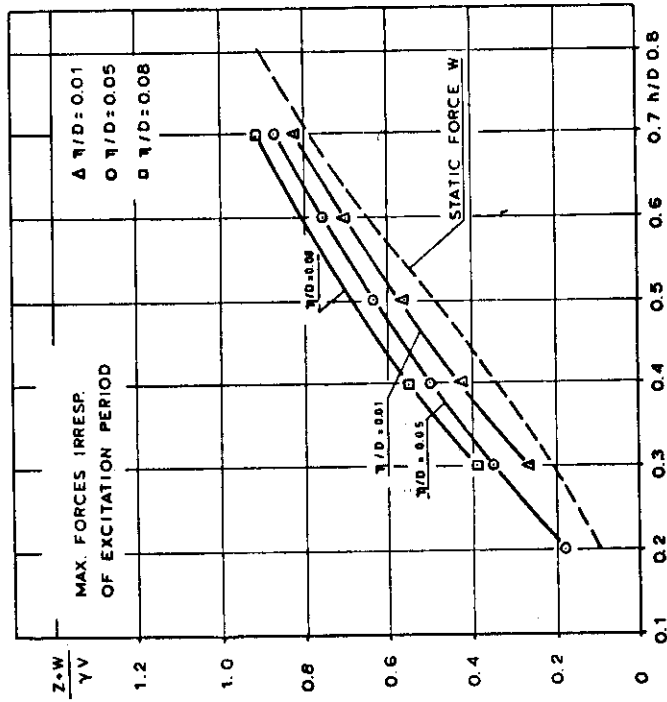


FIGURE III-15. VERTICAL STATIC + DYNAMIC FORCE ON SPHERE VS FILL DEPTH (reference 44)

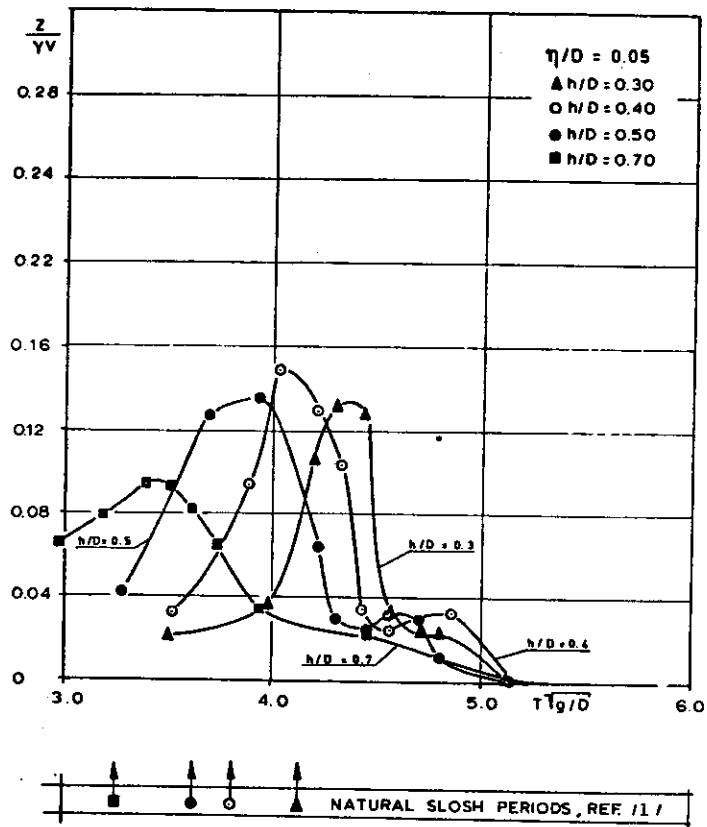


FIGURE III-16. VERTICAL (DYNAMIC) FORCE ON SPHERE VS EXCITATION PERIOD (Reference 44)

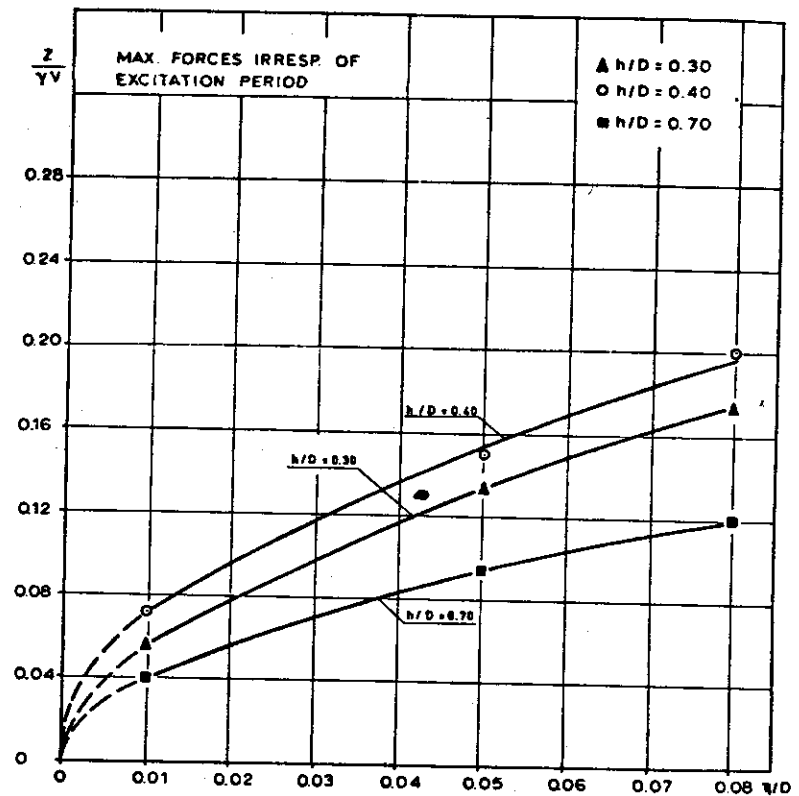


FIGURE III-17. VERTICAL (DYNAMIC) FORCE ON SPHERE VS EXCITATION AMPLITUDE (Reference 44)

have resonant frequencies high enough that the ship motion energy in this frequency range is so low that resonant sloshing is unlikely to occur. For lower filling levels, the liquid response often corresponds with the ship's motion, causing resonant sloshing to occur in the tank.

The resonant sloshing periods predicted by the equation for spherical tanks from Table III-2 are shown in Figures III-11, III-13, and III-16.

III.2 Full-Scale Sloshing Data

Full-scale sloshing data are very scarce. The LNG carrier, the Ben Franklin, has been instrumented for recording slosh-related information, but the ship has yet to go into service. Two El Paso Marine Company carriers, the Sonatrach and the Arzew, have also been instrumented, but no data are available at this time. Full-scale data on the sloshing of fuel oil in a tank with no internal structures are presented in Reference 42; however, this information is only of very limited value to the problem of LNG sloshing in ship tanks. Full-scale impact pressures measured with water sloshing in an OBO tank are compared to model scale pressures in Reference 2. The model data were obtained in a geometrically similar 1/30 scale tank with the recorded full-scale roll motions reproduced on the model. Pressures in model scale were converted to full scale using Froude scaling. A comparison of predicted to actual pressures showed excellent agreement for both the magnitudes and distributions of pressures.

III.3 Review of Tank Structural Detail

A general description of LNG tanks was given in Section II. The importance of sloshing-induced forces in the design of the tank depends largely upon the tank type. For this discussion of tank structural details, it is convenient to divide the tanks into two general categories: pressure tanks and nonpressure tanks. Nonpressure tanks include membrane, semi-membrane, and independent prismatic tanks. These tanks are constructed primarily of plane surfaces and are designed for low vapor pressures. Design for low internal pressures, particularly near the tank top where the liquid head is a minimum, makes these tanks susceptible to localized sloshing pressure in this region. Also, prismatic tanks with plane surfaces are more likely to experience high liquid impact forces during LNG sloshing than, for example, pressure tanks with curved boundaries.

In contrast to nonpressure tanks, pressure tanks are designed for higher internal pressures, approximately 3 to 10 times higher than for nonpressure tanks. In addition, as reported by DnV,⁽²⁴⁾ impulsive sloshing pressures are unlikely to occur in pressure tanks because of their curved boundaries, and the limited measurements which have been made indicate that the pressures are low. Another factor is that pressure tanks which are spherical or cylindrical in geometry will react to the sloshing pressures, even localized ones, primarily with membrane action (as opposed to bending action in tanks with plane surfaces), and thus pressure tanks are less susceptible to damage from local sloshing pressure if they do occur.

Pressure tanks' structural arrangements are much simpler than tanks constructed with plane surfaces. The structure consists principally of a smooth wall sphere or cylinder of relatively heavy gauge (1/2 in.). Attachments to the tank are made only at its support points and at filling locations. A nonstructural insulation is bonded to the outer surface of the tank wall. The most widely used LNG pressure tank is the Moss-Rosenburg system. This system uses an aluminum spherical tank which is attached to the ship by a cylindrical skirt at the equatorial ring (see Figure II-2b). A discussion of design loads for this tank by Glasfeld⁽²³⁾ indicates that sloshing forces influence only the design of the tank support.

As indicated above, nonpressure tanks are more likely than pressure tanks to experience high sloshing pressures and to be damaged by them. Since the structural details of pressure tanks are not unique, only the more complex and unique aspects of LNG prismatic tank structures will be reviewed. The structures of two types of membrane tanks and one independent prismatic tank are described in the following paragraphs. These tanks are representative of the range of designs of nonpressure type tanks which are being built today.

III.3.1 Membrane Tanks

Gaz Transport Design. In the Gaz Transport membrane system, invar membranes are supported from plywood boxes which are filled with Perlite to provide thermal insulation. Two layers of boxes are used, primary and secondary. Primary boxes are on the inside of the tank adjacent to the LNG and support the primary membrane. Primary boxes are separated from the secondary boxes by the secondary membrane. Both secondary and primary boxes are directly attached to the ship's hull, but compression forces on the primary boxes are transferred to the hull through the secondary boxes.

The geometry of a 12-cell box is given in Figure III-18, and the arrangement of the insulation boxes in the tank is shown in Figure III-19. Attachments of the boxes to the hull are not shown. Primary boxes have both a 9-cell and 12-cell construction. Twelve-cell boxes are used in areas where maximum overpressures are expected. All secondary boxes have nine cells. Secondary boxes bear directly against the inner hull of the ship on the bottom and sides of the tank, against transverse bulkheads (cofferdams) at the tank ends, and against the bottom of the trunk deck at the tank top. An example of this type of structure is shown in Figure III-20. It is a section of the cofferdam near the top of the tanks. Local structure between vertical webs is plating stiffened by bulb angles.

Sloshing pressures on the membrane apply loads directly to the covers of the primary boxes. These forces are transferred principally through the longitudinal (parallel to the box axis) stiffeners in the primary box to the transverse stiffeners in the secondary boxes at the stiffener crossing points. This can be seen from Figure III-19. Transverse stiffeners in the secondary boxes transfer the sloshing forces to the ship's hull. As shown in Figure III-20, each stiffener in the cofferdam bulkhead reacts the loading from approximately two box widths. Because the insulation boxes are very stiff (loads are transferred through bending of the covers in the 12-cell

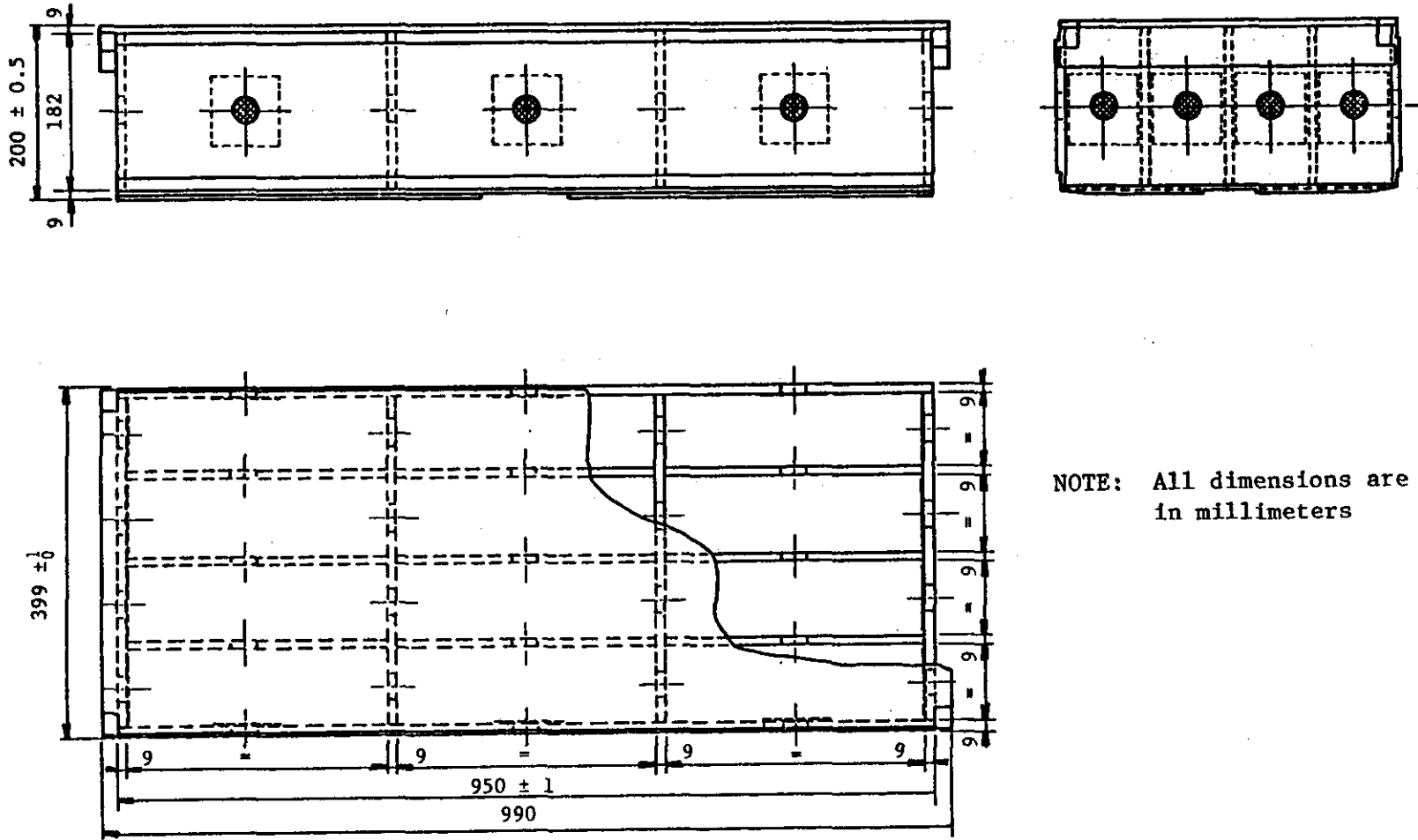
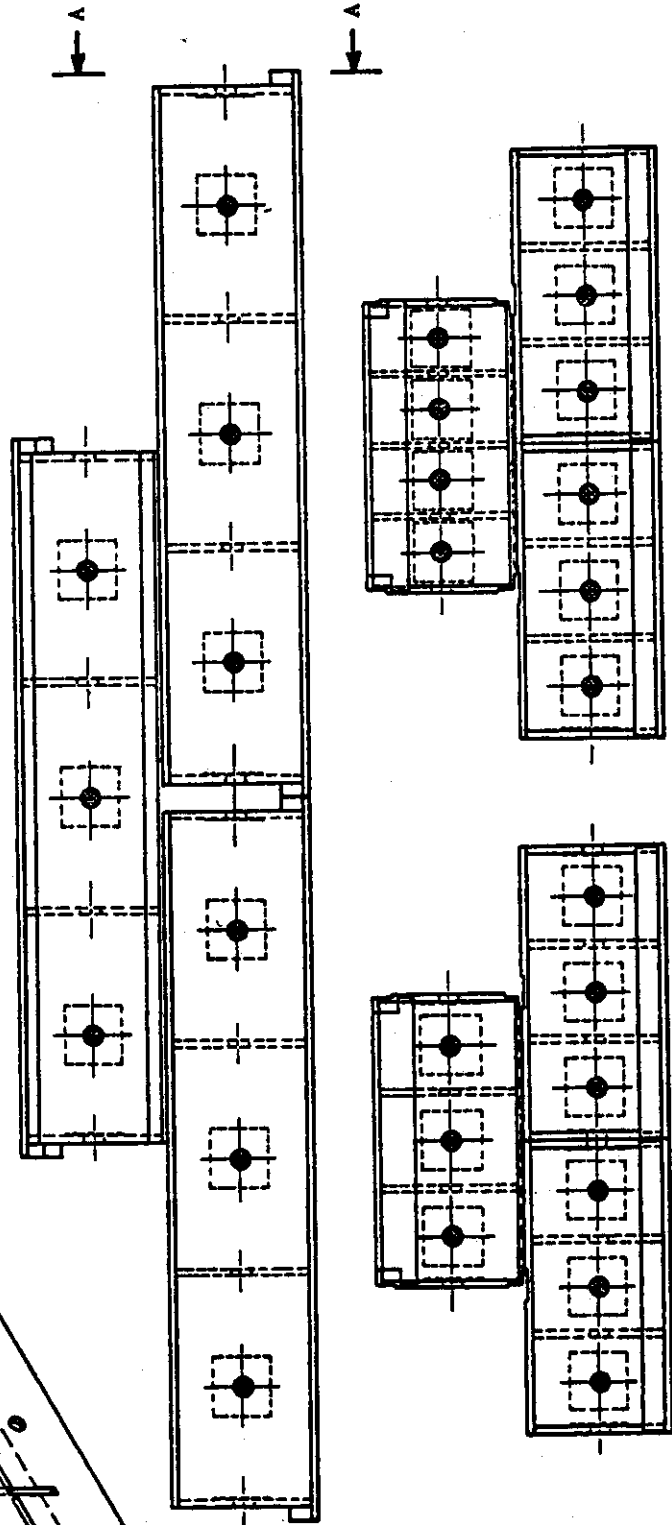
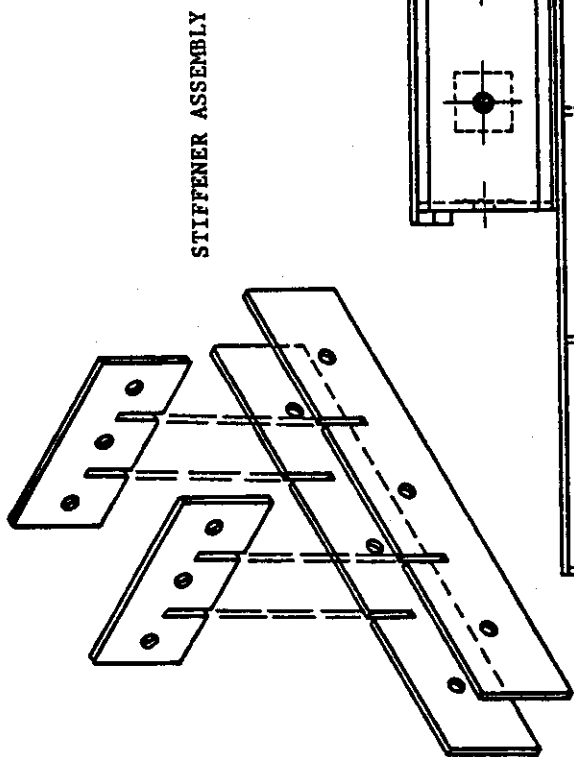


FIGURE III-18. 12-CELL PRIMARY INSULATION BOX - GAZ TRANSPORT SYSTEM



VIEW A-A - 12-CELL PRIMARY BOX

VIEW A-A - 9-CELL PRIMARY BOX

FIGURE III-19. ARRANGEMENT OF INSULATION BOXES IN GAZ TRANSPORT SYSTEM

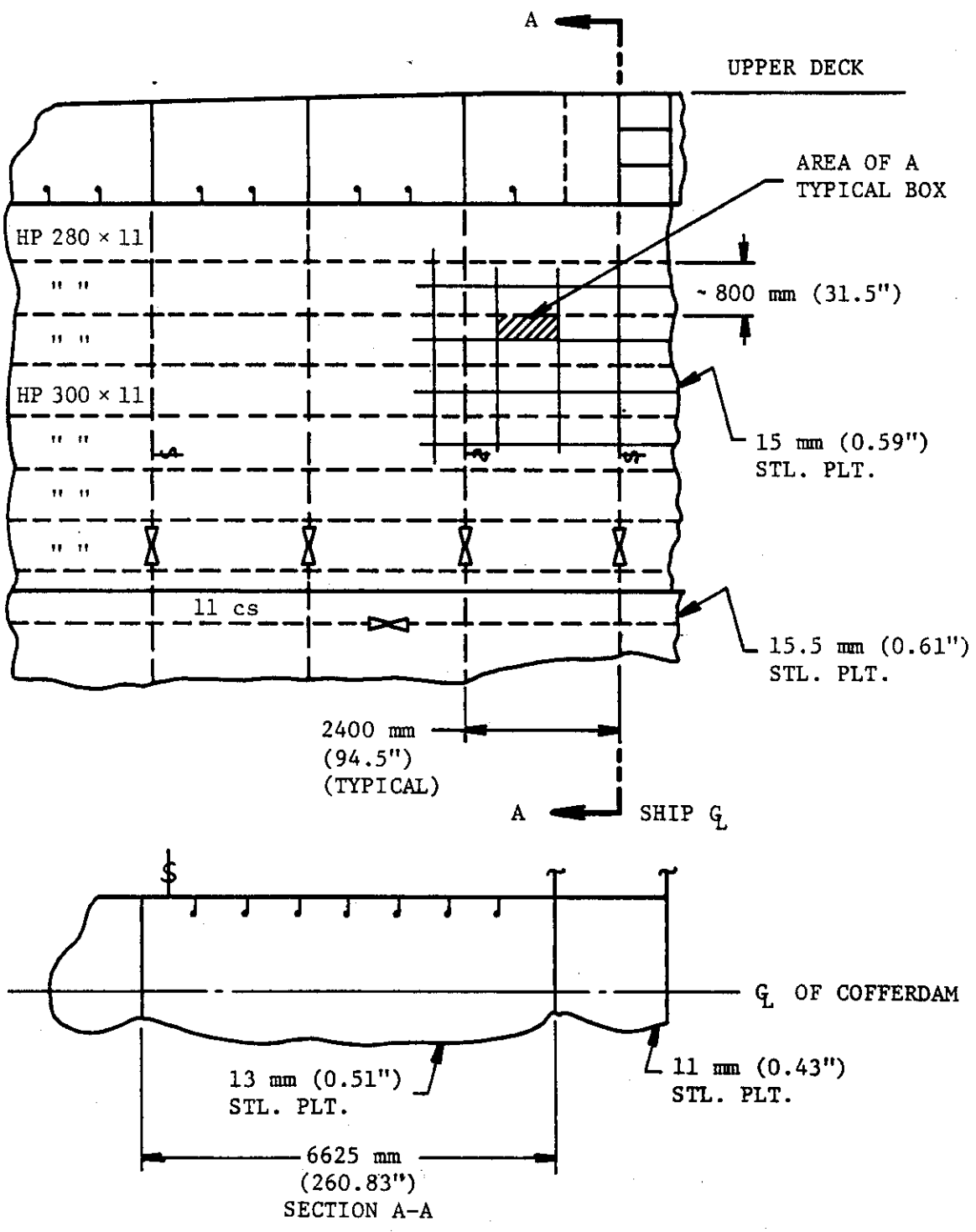


FIGURE III-20. SECTION OF COFFERDAM BULKHEAD FOR GAZ TRANSPORT TANKS

box and through compression of the stiffeners), the sloshing forces will be attenuated very little at the bulkhead. Structures which must be analyzed for sloshing pressures include the primary box covers, stiffeners in the boxes, and local stiffened plates in the hull. Because sloshing pressures are localized, occurring only near the static liquid level, overall bending of the ship's bulkheads is not a problem.

Technigaz Membrane System. As in the Gaz Transport system, a thin metal membrane is attached to an insulation system, which in turn is attached directly to the inner hull of the ship. In the Technigaz system the secondary membrane is a continuous plywood barrier.

A section through the membrane and insulation of the Technigaz System is shown in Figure III-21. The insulation and membrane support in this design consists of:

- (1) An end grain balsa pad which is adjacent to the membrane,
- (2) A thick sandwich panel built with plywood surfaces and balsa core,
- (3) Grounds which are attached to the ship's hull and which support compression from the balsa-plywood panels,
- (4) Glass wool which fills the voids between the sandwich panel and the ship's hull and between the grounds.

Structure in the ship's hull which supports the membrane system is similar to that for the Gaz Transport design.

Sloshing pressures on the membrane bear directly on the balsa pad. These forces are transferred into the balsa-plywood panels, producing bending in the panels between the grounds and shear reactions at the grounds. The grounds transfer the shear reactions in the panels to the ship's hull. Compression in the balsa pad, bending and shear in the panels, and local deformation of the ship's hull must be checked for adequate strength to react to the sloshing pressures.

III.3.2 CONCH Independent Tank

The CONCH LNG tank system is designed to contain the static and dynamic pressures produced by the LNG independent from the ship's hull. It is keyed to the hull to prevent translation and rotation relative to the ship. Glass wool fills the void space between the tank and the ship inner hull (between the supporting blocks). Tanks are subdivided into approximately four equal volumes by centerline and swash bulkheads. Construction of the tanks is similar to that of a ship. Bulkheads and tank walls are constructed of flat plates which are reinforced by stringers and girders. A typical horizontal girder (horizontal section through one of the tanks) is shown in Figure III-22. The weakest parts of the tank appear to be the longitudinal and swash bulkheads, the sides of the tank near the top, and the tank top. These parts of the tank have 0.50-in.-wall thickness and the

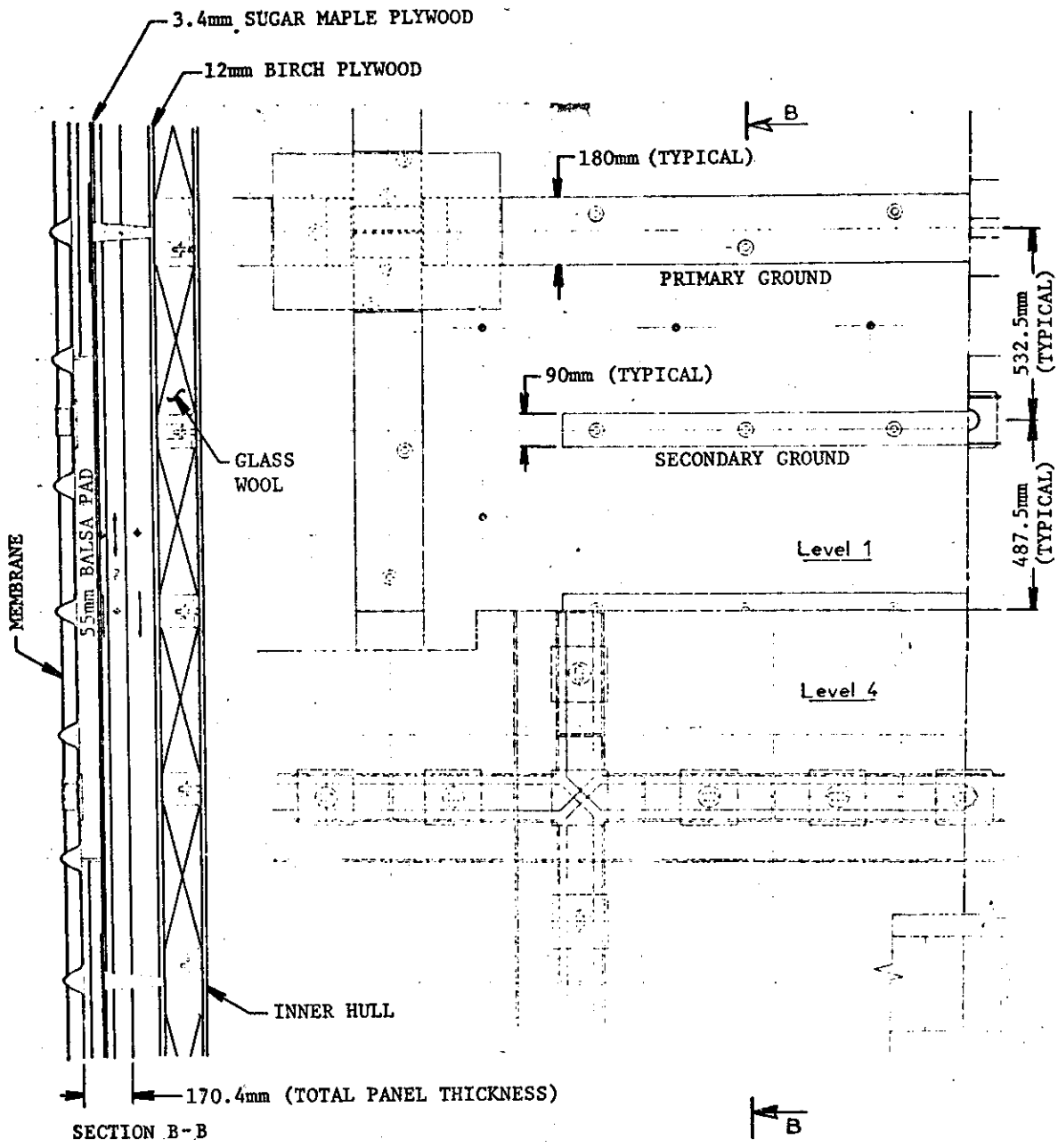


FIGURE III-21. TECHNIGAZ MEMBRANE SYSTEM

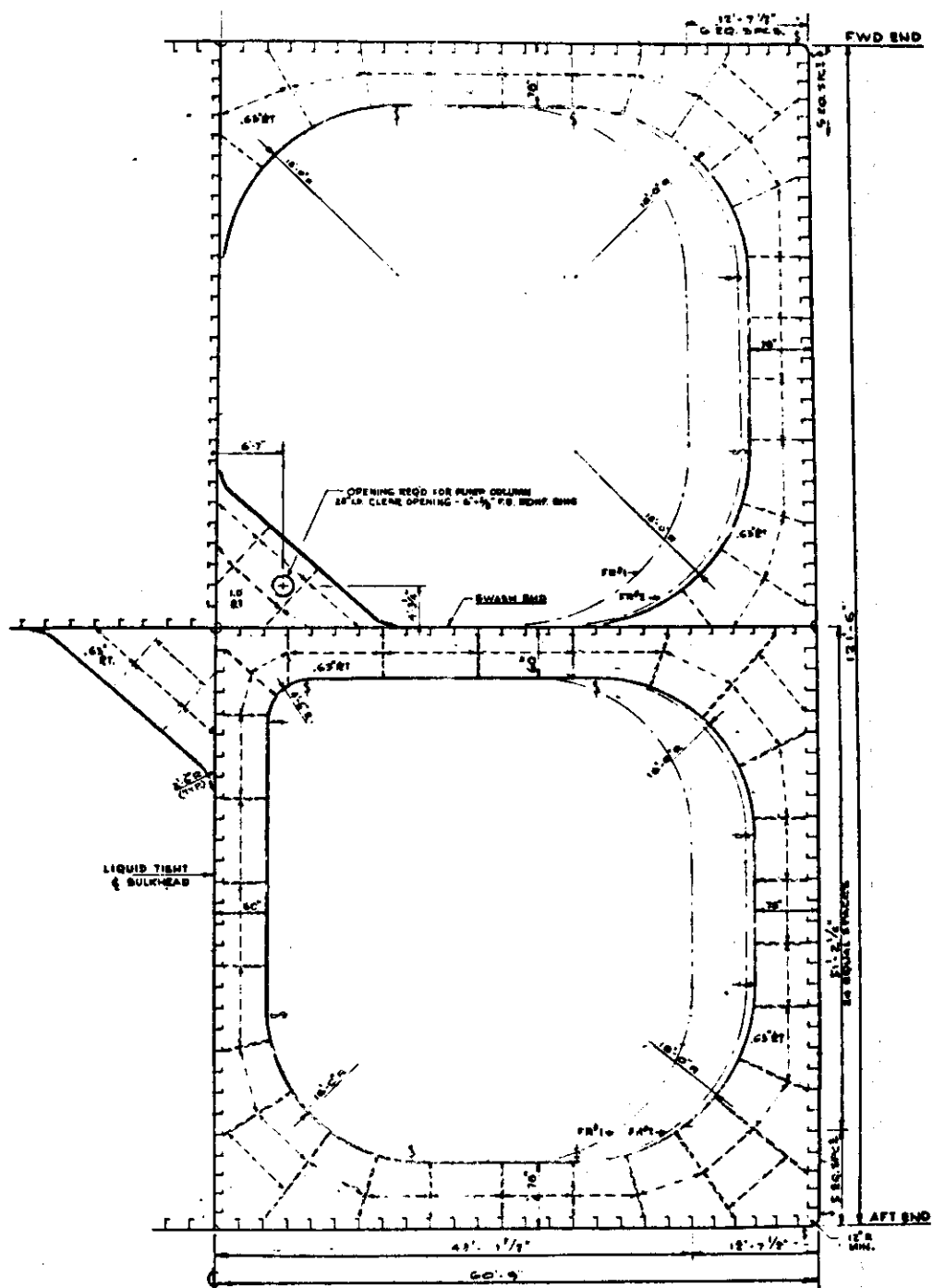


FIGURE III-22. TYPICAL HORIZONTAL GIRDER - CONCH TANK

widest frame spacing. Figures III-23 and III-24 show typical vertical sections taken in the longitudinal and transverse directions, respectively.

Both the frames and stiffened panels between the frames of the tank must be checked for damage to sloshing forces. This is true for the tank walls, bulkheads, and tank top. In addition, tank supports must be analyzed for the reactions produced by the resultant of the sloshing forces.

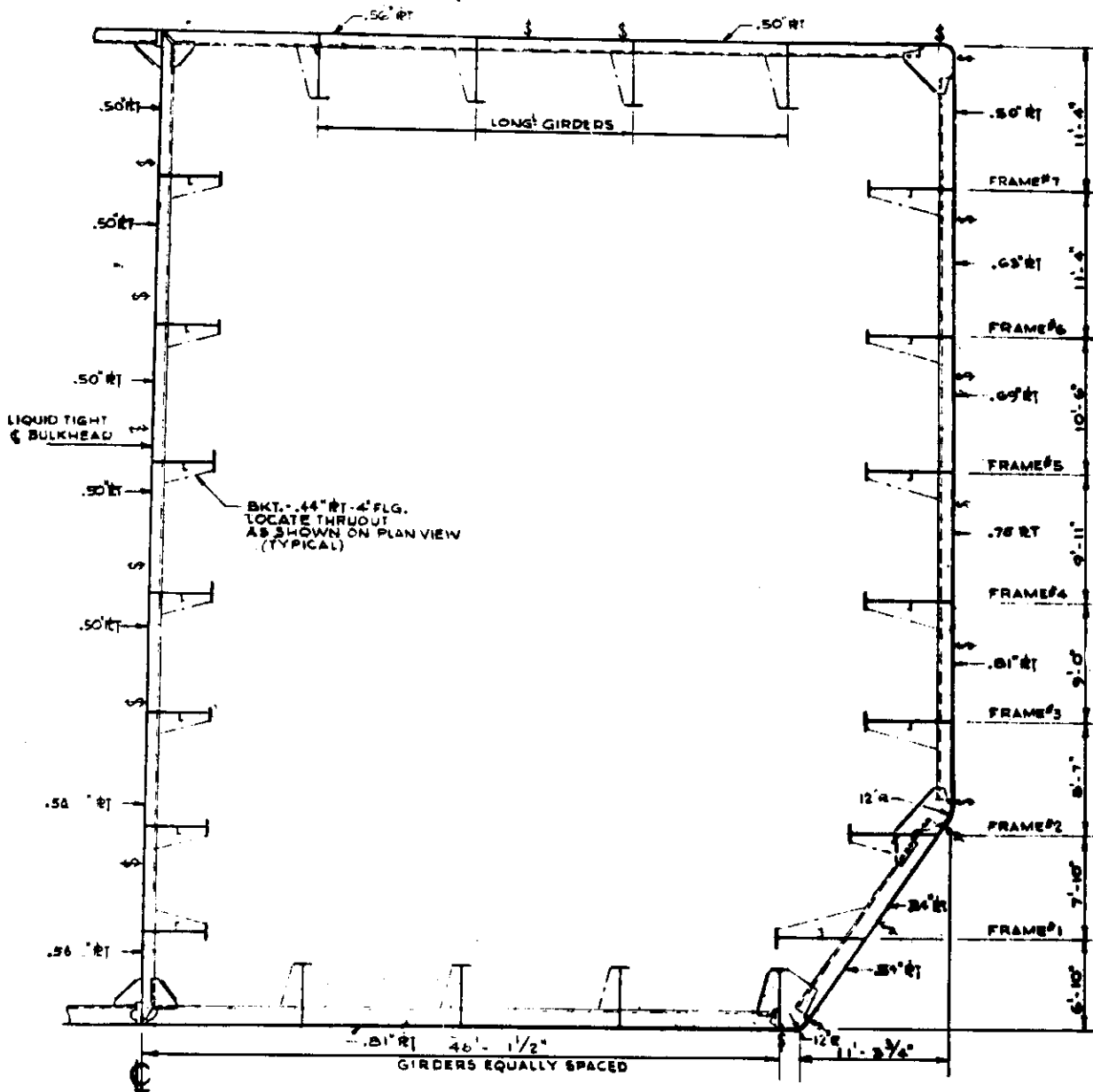


FIGURE III-24. TYPICAL TRANSVERSE FRAME

IV. TASK 2 - EXPERIMENTAL STUDIES

IV.1 Experimental Study Objectives

As a result of the Task 1 review of previous experimental work, the following experiments were performed.

- o Combined degree of freedom excitation (pitch and heave, surge and heave)
- o Impulsive pressure-time history measurements
- o Dynamic loads test on full-scale LNG tank structural segments

Previous studies provide loads data for a wide range of tank geometries, fill depths, and excitation conditions. Previous studies were conducted by exciting the model tank in only one degree of freedom (usually pitch, roll, or surge) and recording loads at resonant sloshing conditions. To determine if combined, simultaneous excitation in more than one degree of freedom would increase the sloshing pressures, additional two degree of freedom experiments were performed.

The impact pressure-time history is of importance to the prismatic tank wall structural design. Previous studies determined peak pressure magnitudes and distributions, but little data were available on pressure-time histories. Additional experiments were performed to establish P(T) vs T characteristics.

To substantiate the analytical procedures developed in this study and to evaluate the response of LNG tank wall structures to dynamic slosh pressures, typical full-scale dynamic pressures (predicted from the model tests) were applied to a representative section of a full-scale LNG membrane tank structure in a set of laboratory tests.

IV.2 Experimental Facilities

IV.2.1 Model Tank Sloshing Apparatus

The laboratory work on this project involved sloshing liquid in scale model ship tanks and measuring slosh-induced dynamic pressures. The laboratory facilities at SwRI include two slosh rigs designed for this purpose. One machine is capable of producing an angular motion (to simulate pitching or rolling), and the other can provide independent and simultaneous horizontal and vertical motions (to simulate surge or sway, and heave). Appendix A provides a detailed description of both these sloshing systems.

IV.2.2 Sloshing Pressure Measurement System

Sloshing dynamic pressures were recorded with Columbia Research Labs' Model 100-P piezoelectric pressure transducers in combination with

Model 4101 amplifiers. These transducer/amplifier combinations have a range of 0.005 to 4000 pounds per square inch, with a frequency response from 0.1 to 10,000 Hz. Transducers were isolated from the walls of the tank by mounting them in a plug of silastic material. The silastic eliminated the possibility of the transducer casing being loaded by flexing of the walls of the model tank.

The pressure signals were input to a light-beam galvanometer-type oscillograph. The oscillograph produced a permanent record of the pressure signals on oscillograph paper. The oscillograph is a Honeywell Model 1858-0790 G Visicorder oscillograph with a frequency response from 0 to 3000 Hz with +0% to -5% error. A Hewlett-Packard Model 9864A digitizer in combination with a Hewlett-Packard Model 9830A computer was used to digitize the pressure signals from the oscillograph traces. The digitized pressure values were stored on magnetic disk files for final data reduction.

IV.2.3 Model Ship Tank

The model tank used for all laboratory tests is a 1/50 scale replica of a prismatic tank from a 125,000 m³ LNG carrier. The tank geometry is typical of most prismatic tanks. The model tank walls are made of plexiglass with sufficient rigidity such that tank wall response was not a factor in the pressure measurements. Figure IV-1 shows the tank and all pressure transducer locations. Table IV-1 lists the model scale and corresponding full-scale tank dimensions. The pitch axes for the 25% and 75% tank filling levels investigated are denoted in Figure IV-1 as z_{p1} and z_{p2} , respectively.

For all tests, the model test liquid was water.

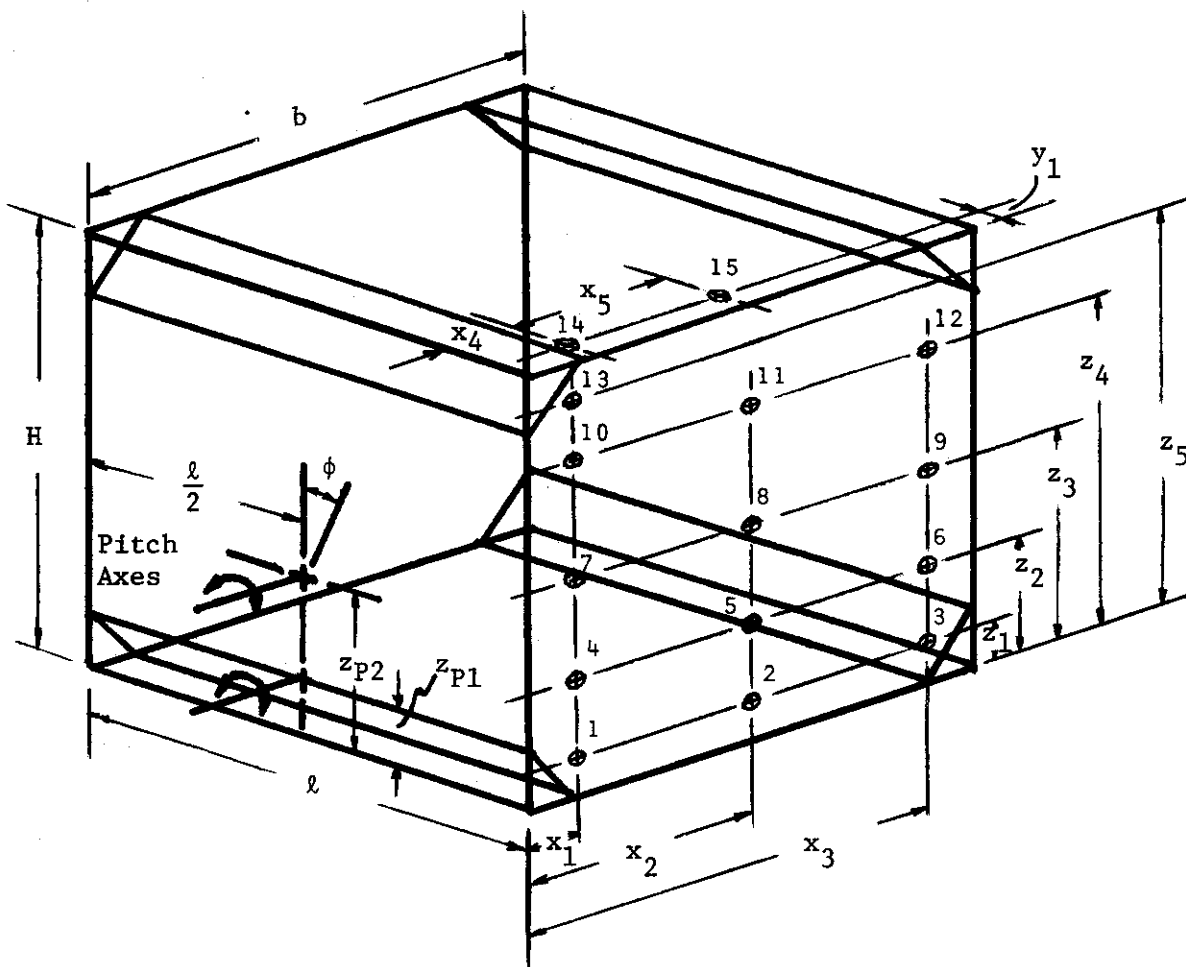
IV.3 Combined Degree of Freedom Model Tests

As part of Task 2, the effects of combined tank motions on slosh pressures were investigated. The purpose of this work was to determine if slosh-induced pressures were augmented by combined motions.

Experimental tank motions included pitching plus heaving and surging plus heaving. The results for these motions were compared to the results for the individual motions of pitching, surging, and heaving. Low (25%) and high (75%) tank filling levels were used for each case. All laboratory test motions are summarized in Table IV-2. The detailed test results are given in Tables IV-3 through IV-7, with the data summarized in Tables IV-8 through IV-11. The excitation amplitudes were chosen to represent typical extreme values that a ship tank might experience while in service. Each test was run for 200 cycles at resonant sloshing conditions, while the tank was undergoing a harmonic excitation motion at resonance.

IV.3.1 Pitching Plus Heaving Test

The angular motion sloshing facility was used to provide the pitching plus heaving motion. The scale model ship tank was placed approximately two tank lengths out from the pitch axis on a cantilevered beam. This location represents the typical placement of the fore or aft tank in an LNG carrier with its pitching axis at the midship. Figure IV-2 shows the location of the model tank with respect to the sloshing rig axis.



○ - Denotes pressure transducer location

FIGURE IV-1. SCALE MODEL TANK DIMENSIONS AND PRESSURE TRANSDUCER LOCATIONS FOR 1/50 SCALE PRISMATIC TANK FROM A 125,000 m³ SHIP

TABLE IV-1. TANK DIMENSIONS AND PRESSURE
TRANSDUCER LOCATIONS

Dimension	Model (ft)	Full Scale (ft)
l	2.23	111.55
b	2.44	122.04
H	1.57	78.51
x_1	0.219	10.94
x_2	1.22	60.94
x_3	2.22	110.94
x_4	0.333	16.67
x_5	0.885	44.27
y_1	0.104	5.21
z_1	0.146	7.29
z_2	0.417	20.83
z_3	0.792	39.58
z_4	1.23	61.46
z_5	1.44	71.88
z_{P1}	0.196	9.81
z_{P2}	0.589	29.44

Conversion Factor: 1 foot = 0.3048 meters.

TABLE IV-2. TEST CONDITIONS FOR COMBINED
MOTION LABORATORY TESTS

Tank Motion	Tank Amplitude	Tank Filling Level	Nondimensional Resonant Slosh Period ($T \sqrt{g/\ell}$)
Pitching	$\phi = +4^\circ$	25%	5.170
Pitching	$\phi = +4^\circ$	75%	3.566
Surging	$\frac{x}{\ell} = 0.019$	25%	4.869
Surging	$\frac{x}{\ell} = 0.019$	75%	3.663
Surging	$\frac{x}{\ell} = 0.038$	25%	4.869
Surging	$\frac{x}{\ell} = 0.038$	75%	3.663
Pitching + Heaving	$\phi = +4^\circ$ and $\frac{y}{H} = 0.417$	25%	4.748
Pitching + Heaving	$\phi = +4^\circ$ and $\frac{y}{H} = 0.417$	75%	7.235 (2nd Harmonic)
Surging + Heaving	$\frac{x}{\ell} = 0.038$ and $\frac{y}{H} = 0.053$	25%	4.869
Surging + Heaving	$\frac{x}{\ell} = 0.038$ and $\frac{y}{H} = 0.053$	75%	3.663

See Figures IV-1 and IV-4 for definitions of x , y , ℓ , H , and ϕ .

TABLE IV-3. TEST PRESSURE DATA FOR PITCHING TANK MOTION

TRNS. LOC.	FILL DEPTH (%)	AVG. KP		MAX. KP		MIN. KP		AVG. KP		MAX. KP		AVG. FULL SCALE (PSI)	MAX. FULL SCALE (PSI)	NONDIM. RESONANT PERIOD	FULL SCALE RES. PER (SEC)
		MODEL	MODEL	MODEL	MODEL	MODEL	MODEL	MODEL	MODEL						
1	25	16.1	37.4	7.5	2.318	2.157	4.999	62.3	26.9	5.17	9.62				
2	25	6.6	15.7	3.2	2.354	2.093	4.925	26.1	11.1	5.17	9.62				
3	25	6.3	17.7	3.9	2.822	1.629	4.598	29.5	10.5	5.17	9.62				
4	25	13.5	31.3	6.0	2.318	2.269	5.259	52.2	22.5	5.17	9.62				
5	25	6.5	16.3	3.0	2.519	2.143	5.400	27.1	10.7	5.17	9.62				
6	25	10.3	31.3	3.3	3.050	3.102	9.461	52.1	17.1	5.17	9.62				
7	75	2.7	5.0	1.7	1.809	1.622	2.933	8.3	4.6	3.57	6.64				
8	75	2.5	3.6	1.7	1.443	1.492	2.153	6.0	4.1	3.57	6.64				
9	75	3.2	4.9	2.1	1.539	1.517	2.334	8.1	5.3	3.57	6.64				
10	75	0.1	1.1	0.0	1.900	1.841	3.498	0.2	0.1	3.57	6.64				
11	75	2.3	3.7	1.5	1.606	1.504	2.415	6.2	3.9	3.57	6.64				
12	75	4.1	8.4	2.7	2.037	1.515	3.086	13.9	6.8	3.57	6.64				
13	75	5.6	16.0	2.5	2.848	2.213	6.303	26.6	9.4	3.57	6.64				
14	75	13.7	33.7	7.2	2.467	1.891	4.666	56.2	22.8	3.57	6.64				

NOTE: See Equation III-1 for definition of KP.

Conversion Factor: 1 psi = 6.895(10)⁻³ N/mm².

TABLE IV-4. TEST PRESSURE DATA FOR PITCHING
PLUS HEAVING TANK MOTION

NO. OF CYCLES PER TEST: 200
OSCILLATION AMPLITUDE: +/-4.0 DEG. &
FLUID: WATER
EXCITATION: PITCH+HEAVE
Y/H=0.417

TRANS. LOC.	FILL DEPTH (%)	AVG. KP MODEL	MAX. KP MODEL	MIN. KP MODEL	MAX. KP ----- AVG. KP	AVG. KP ----- MIN. KP	MAX. KP ----- MIN. KP	MAX. FULL SCALE (PSI)	AVG. FULL SCALE (PSI)	NONDIM RESONANT PERIOD	FULL SCALE RES PER (SEC)
1	25	3.6	22.4	1.4	6.237	2.645	16.495	37.4	6.0	4.75	8.84
2	25	3.8	8.2	1.5	2.180	2.468	5.381	13.7	6.3	4.75	8.84
3	25	3.4	5.5	1.5	1.620	2.212	3.583	9.2	5.7	4.75	8.84
4	25	4.3	21.2	1.1	4.883	3.932	19.198	35.3	7.2	4.75	8.84
5	25	2.7	8.7	1.1	3.250	2.432	7.904	14.5	4.5	4.75	8.82
6	25	2.9	8.4	1.3	2.938	2.246	6.599	14.0	4.8	4.75	8.84
9	25	0.3	3.5	0.0	12.438	0.000	0.000	5.8	0.5	4.75	8.84
7	75	2.8	4.6	1.7	1.652	1.655	2.733	7.7	4.7	7.23	13.47
8	75	2.3	3.1	1.5	1.360	1.469	1.997	5.1	3.8	7.23	13.47
9	75	2.1	2.9	1.3	1.417	1.644	2.330	4.9	3.4	7.23	13.47
10	75	1.1	3.3	0.3	3.046	3.172	9.662	5.5	1.8	7.23	13.47
11	75	0.6	2.1	0.0	3.439	0.000	0.000	3.4	1.0	7.23	13.47
12	75	1.0	2.5	0.0	2.476	0.000	0.000	4.1	1.7	7.23	13.47
13	75	1.6	5.2	0.6	3.144	2.990	9.400	8.6	2.7	7.23	13.47
14	75	7.2	26.9	0.0	3.736	0.000	0.000	44.8	12.0	7.23	13.47

NOTE: See Equation III-1 for definition of KP.

Conversion Factor: 1 psi = $6.895(10)^{-3}$ N/mm².

TABLE IV-5. TEST PRESSURE DATA FOR SURGING TANK MOTION

NO. OF CYCLES PER TEST: 200
 OSCILLATION AMPLITUDE: X/L=0.019
 FLUID: WATER
 EXCITATION: SURGE

TRANS. LOC.	FILL DEPTH (%)	AVG. KP MODEL	MAX. KP MODEL	MIN. KP MODEL	MAX. KP AVG. KP	AVG. KP MIN. KP	MAX. KP MIN. KP	MAX. FULL SCALE (PSI)	AVG. FULL SCALE (PSI)	NONDIM RESONANT PERIOD	FULL SCALE RES PER (SEC)
1	25	8.0	14.2	5.0	1.777	1.595	2.833	6.4	3.6	4.87	9.07
2	25	10.6	16.0	6.9	1.511	1.537	2.323	7.3	4.8	4.87	9.07
3	25	9.8	28.3	4.7	2.887	2.078	5.999	12.8	4.4	4.87	9.07
4	25	6.6	17.0	3.6	2.583	1.806	4.665	7.7	3.0	4.87	9.07
5	25	6.2	36.5	3.0	5.887	2.101	12.367	16.5	2.8	4.87	9.07
6	25	10.2	32.7	5.1	3.198	1.989	6.363	14.8	4.6	4.87	9.07
7	25	2.0	7.5	0.0	3.651	0.000	0.000	3.4	0.9	4.87	9.07
9	25	2.1	11.3	0.0	5.500	0.000	0.000	5.1	0.9	4.87	9.07
7	75	4.7	24.0	1.2	5.066	3.813	19.317	10.9	2.1	3.66	6.82
8	75	3.3	15.5	1.4	4.766	2.308	11.001	7.0	1.5	3.66	6.82
9	75	3.6	11.3	0.5	3.118	7.005	21.842	5.1	1.6	3.66	6.82
10	75	7.4	29.6	1.2	3.978	5.949	23.667	13.4	3.4	3.66	6.82
11	75	4.8	14.2	2.4	2.963	2.021	5.989	6.4	2.2	3.66	6.82
12	75	8.0	27.7	3.0	3.457	2.643	9.137	12.5	3.6	3.66	6.82
13	75	16.8	76.6	1.6	4.564	10.348	47.229	34.7	7.6	3.66	6.82
14	75	13.1	69.3	1.5	5.278	8.901	46.978	31.4	6.0	3.66	6.82
15	75	2.9	26.7	0.0	9.200	0.000	0.000	12.1	1.3	3.66	6.82

NOTE: See Equation III-1 for definition of KP.

Conversion Factor: 1 psi = 6.895(10)⁻³ N/mm².

TABLE IV-6. TEST PRESSURE DATA FOR SURGING TANK MOTION

NO. OF CYCLES PER TEST: 200
 OSCILLATION AMPLITUDE: X/L=0.038
 FLUID: WATER
 EXCITATION: SURGE

TRANS. LOC.	FILL DEPTH (%)	AVG. KP MODEL	MAX. KP MODEL	MIN. KP MODEL	MAX. KP ----- AVG. KP	AVG. KP ----- MIN. KP	MAX. KP ----- MIN. KP	MAX. FULL SCALE (PSI)	AVG. FULL SCALE (PSI)	NONDIM RESONANT PERIOD	FULL SCALE RES PER (SEC)
1	25	6.8	15.0	4.4	2.191	1.564	3.427	13.6	6.2	4.87	9.07
2	25	7.6	10.2	5.4	1.343	1.400	1.880	9.2	6.9	4.87	9.07
3	25	8.4	18.2	4.0	2.153	2.104	4.531	16.5	7.6	4.87	9.07
4	25	6.5	21.9	2.6	3.390	2.451	8.308	19.8	5.9	4.87	9.07
5	25	5.0	10.5	3.1	2.113	1.586	3.352	9.5	4.5	4.87	9.07
6	25	9.5	60.1	0.2	6.333	40.582	256.996	54.5	8.6	4.87	9.07
7	75	2.7	6.0	1.2	2.191	2.206	4.833	5.4	2.5	3.66	6.82
8	75	4.4	11.5	1.9	2.610	2.346	6.124	10.4	4.0	3.66	6.82
9	75	3.6	7.4	1.5	2.052	2.354	4.831	6.7	3.3	3.66	6.82
10	75	5.4	10.8	2.7	1.995	2.003	3.998	9.8	4.9	3.66	6.82
11	75	5.3	9.4	2.8	1.798	1.854	3.333	8.6	4.8	3.66	6.82
12	75	6.7	13.2	1.9	1.970	3.441	6.778	12.0	6.1	3.66	6.82
13	75	6.6	23.5	2.6	3.560	2.506	8.921	21.3	6.0	3.66	6.82
14	75	14.2	43.5	5.2	3.064	2.751	8.429	39.4	12.9	3.66	6.82
15	75	8.1	23.6	0.5	2.906	17.354	50.438	21.4	7.4	3.66	6.82

NOTE: See Equation III-1 for definition of KP.
 Conversion Factor: 1 psi = 6.895(10)⁻³ N/mm².

TABLE IV-7. TEST PRESSURE DATA FOR SURGING
PLUS HEAVING TANK MOTION

NO. OF CYCLES PER TEST: 200
OSCILLATION AMPLITUDE: X/L=0.038 & Y/H=0.053
FLUID: WATER
EXCITATION: SURGE+HEAVE

TRANS. LOC.	FILL DEPTH (%)	AVG. KP MODEL	MAX. KP MODEL	MIN. KP MODEL	MAX. KP ----- AVG. KP	AVG. KP ----- MIN. KP	MAX. KP ----- MIN. KP	MAX. FULL SCALE (PSI)	AVG. FULL SCALE (PSI)	HONDIM RESONANT PERIOD	FULL SCALE RES PER (SEC)
1	25	6.6	11.7	4.2	1.774	1.579	2.000	10.6	6.0	4.87	9.07
2	25	8.0	24.2	5.8	3.030	1.369	4.147	21.9	7.2	4.87	9.07
3	25	8.7	21.7	5.0	2.510	1.745	4.300	19.7	7.8	4.87	9.07
4	25	6.1	16.6	2.6	2.731	2.310	6.308	15.1	5.5	4.87	9.07
5	25	4.7	9.0	2.8	1.903	1.717	3.267	8.2	4.3	4.87	9.07
6	25	10.7	49.1	3.3	4.610	3.254	15.000	44.5	9.7	4.87	9.07
7	25	1.2	12.2	0.0	10.362	0.000	0.000	11.1	1.1	4.87	9.07
9	25	1.2	3.8	0.0	3.319	0.000	0.000	3.5	1.1	4.87	9.07
7	75	3.9	8.9	2.3	2.261	1.728	3.908	8.1	3.6	3.66	6.82
8	75	4.4	23.0	2.1	5.237	2.079	10.890	20.9	4.0	3.66	6.82
9	75	4.0	6.2	2.3	1.540	1.732	2.667	5.6	3.6	3.66	6.82
10	75	4.0	10.2	2.5	2.147	1.902	4.084	9.2	4.3	3.66	6.82
11	75	4.9	14.9	2.4	3.009	2.093	6.298	13.5	4.5	3.66	6.82
12	75	5.8	10.6	3.2	1.816	1.799	3.266	9.6	5.3	3.66	6.82
13	75	5.8	13.0	2.6	2.247	2.190	4.923	11.8	5.2	3.66	6.82
14	75	9.8	28.0	2.9	2.856	3.336	9.528	25.4	8.9	3.66	6.82
15	75	8.3	32.7	2.1	3.958	3.930	15.554	29.7	7.5	3.66	6.82

NOTE: See Equation III-1 for definition of KP.

Conversion Factor: 1 psi = $6.895(10)^{-3}$ N/mm².

TABLE IV-8. AVERAGE K_p VALUES* FOR A 1/50 SCALE PRISMATIC TANK FROM A 125,000 m³ LNG CARRIER

Filling Level	Transducer Location	Average K_p				
		Excitation Motion				
		Pitching $\phi = \pm 4^\circ$	Pitching & Heaving $\phi = \pm 4^\circ$ & $\frac{Y}{H} = 0.417$	Surging $\frac{X}{L} = 0.019$	Surging $\frac{X}{L} = 0.038$	Surging & Heaving $\frac{X}{L} = 0.038$ & $\frac{Y}{H} = 0.053$
25%	1	16.1	3.6	8.0	6.8	6.6
25%	2	6.6	3.8	10.6	7.6	8.0
25%	3	6.3	3.4	9.8	8.4	8.7
25%	4	13.5	4.3	6.6	6.5	6.1
25%	5	6.5	2.7	6.2	5.0	4.7
25%	6	10.3	2.9	10.2	9.5	10.7
25%	7	= 0	= 0	2.0	= 0	1.2
25%	8	= 0	= 0	= 0	= 0	= 0
25%	9	= 0	0.3	2.1	= 0	1.2
75%	7	2.7	2.8	4.7	2.7	3.9
75%	8	2.5	2.3	3.3	4.4	4.4
75%	9	3.2	2.1	3.6	3.6	4.0
75%	10	0.1	1.1	7.4	5.4	4.8
75%	11	2.3	0.6	4.8	5.3	4.9
75%	12	4.1	1.0	8.0	6.7	5.8
75%	13	5.6	1.6	16.3	6.6	5.8
75%	14	13.7	7.2	13.1	14.2	9.8
75%	15	= 0	= 0	2.9	8.1	8.3

* For 200 slosh cycles at resonant sloshing conditions.

TABLE IV-9. MAXIMUM Kp VALUES* FOR A 1/50 SCALE PRISMATIC TANK FROM A 125,000 m³ LNG CARRIER

Filling Level	Transducer Location	Maximum Kp					
		Excitation Motion					
		Pitching $\phi = 4^\circ$	Pitching & Heaving $\phi = 4^\circ$ & $\frac{Y}{H} = 0.417$	Surging $\frac{X}{L} = 0.019$	Surging $\frac{X}{L} = 0.038$	Surging & Heaving $\frac{X}{L} = 0.038$ & $\frac{Y}{H} = 0.053$	
25%	1	37.4	22.4	14.2	15.0	11.7	
25%	2	15.7	8.2	16.0	10.2	24.2	
25%	3	17.7	5.5	28.3	18.2	21.7	
25%	4	31.3	21.2	17.0	21.9	16.6	
25%	5	16.3	8.7	36.5	10.5	9.0	
25%	6	31.3	8.4	32.7	60.1	49.1	
25%	7	= 0	= 0	7.5	= 0	12.2	
25%	8	= 0	= 0	= 0	= 0	0	
25%	9	= 0	3.5	11.3	= 0	3.8	
75%	7	5.0	4.6	24.0	6.0	8.9	
75%	8	3.6	3.1	15.5	11.5	23.0	
75%	9	4.9	2.9	11.3	7.4	6.2	
75%	10	0.1	3.3	29.6	10.8	10.2	
75%	11	3.7	2.1	14.2	9.4	14.9	
75%	12	8.4	2.5	27.7	13.2	10.6	
75%	13	16.0	5.2	76.6	23.5	13.0	
75%	14	33.7	26.9	69.3	43.5	28.0	
75%	15	= 0	= 0	26.7	23.6	32.7	

* For 200 slosh cycles at resonant sloshing conditions.

TABLE IV-10. AVERAGE FULL SCALE PRESSURE VALUES* FOR A
1/50 SCALE PRISMATIC TANK FROM A 125,000 m³ LNG CARRIER

Filling Level	Transducer Location	Average Full-Scale Pressure (psi)					
		Excitation Motion					
		Pitching $\phi = 4.4^\circ$	Pitching & Heaving $\phi = 4.4^\circ$ & $\frac{Y}{H} = 0.417$	Surging $\frac{X}{Z} = 0.019$	Surging $\frac{X}{Z} = 0.038$	Surging & Heaving $\frac{X}{Z} = 0.038$ & $\frac{Y}{H} = 0.053$	
25%	1	26.9	6.0	3.6	6.2	6.0	
25%	2	11.1	6.3	4.8	6.9	7.2	
25%	3	10.5	5.7	4.4	7.6	7.8	
25%	4	22.5	7.2	3.0	5.9	5.5	
25%	5	10.7	4.5	2.8	4.5	4.3	
25%	6	17.1	4.8	4.6	8.6	9.7	
25%	7	* 0	* 0	0.9	* 0	1.1	
25%	8	= 0	= 0	= 0	= 0	= 0	
25%	9	* 0	0.5	0.9	* 0	1.1	
75%	7	4.6	4.7	2.1	2.5	3.6	
75%	8	4.1	3.8	1.5	4.0	4.0	
75%	9	5.3	3.4	1.6	3.3	3.6	
75%	10	0.1	1.8	3.4	4.9	4.3	
75%	11	3.9	1.0	2.2	4.8	4.5	
75%	12	6.8	1.7	3.6	6.1	5.3	
75%	13	9.4	2.7	7.6	6.0	5.2	
75%	14	22.8	12.0	6.0	12.9	8.9	
75%	15	* 0	* 0	1.3	7.4	7.5	

* For 200 slosh cycles at resonant sloshing conditions.

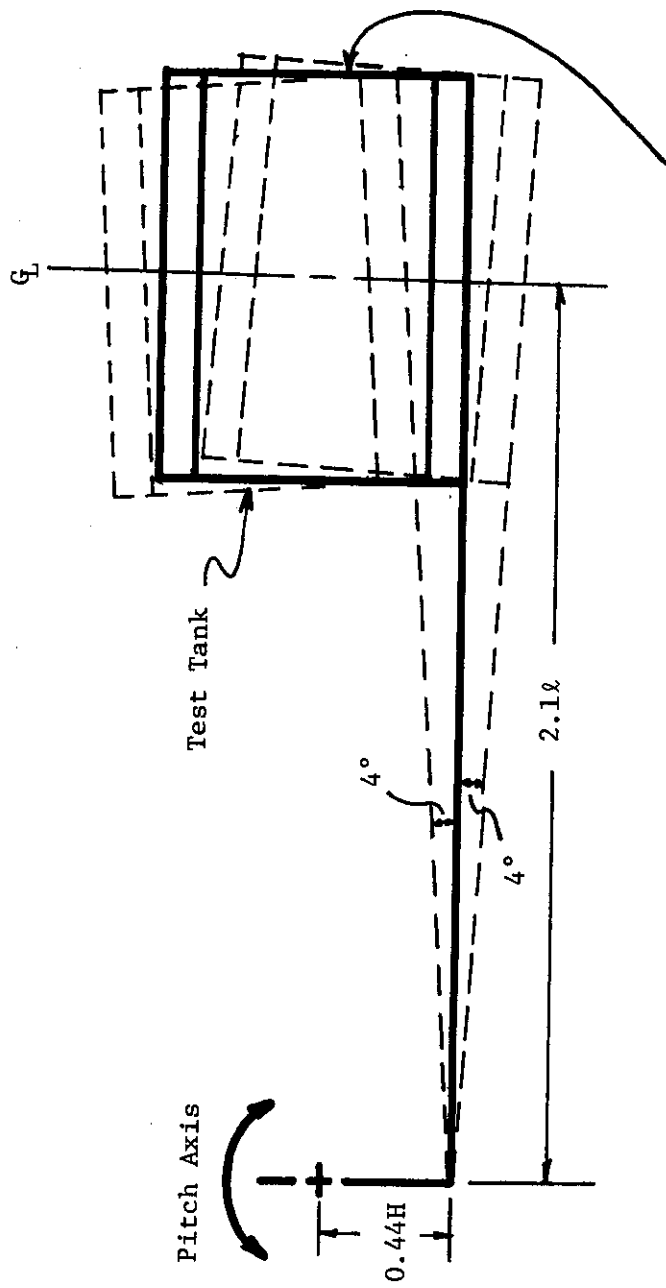
Conversion Factor: 1 psi = 6.895(10)⁻³ N/mm².

TABLE IV-11. MAXIMUM FULL SCALE PRESSURE VALUES* FOR A
1/50 SCALE PRISMATIC TANK FROM A 125,000 m³ LNG CARRIER

Filling Level	Transducer Location	Maximum Full-Scale Pressure (psi)				
		Excitation Motion				
		Pitching $\phi = \pm 4^\circ$	Pitching & Heaving $\phi = \pm 4^\circ$ & $\frac{Y}{H} = 0.417$	Surging $\frac{X}{L} = 0.019$	Surging $\frac{X}{L} = 0.038$	Surging & Heaving $\frac{X}{L} = 0.038$ & $\frac{Y}{H} = 0.053$
25%	1	62.3	37.4	6.4	13.6	10.6
25%	2	26.1	13.7	7.3	9.2	21.9
25%	3	29.5	9.2	12.8	16.5	19.7
25%	4	52.2	35.3	7.7	19.8	15.1
25%	5	27.1	14.5	16.5	9.5	8.2
25%	6	52.1	14.0	14.8	54.5	44.5
25%	7	= 0	= 0	3.4	= 0	11.1
25%	8	= 0	= 0	= 0	= 0	= 0
25%	9	= 0	5.8	5.1	= 0	3.5
75%	7	8.3	7.7	10.9	5.4	8.1
75%	8	6.0	5.1	7.0	10.4	20.9
75%	9	8.1	4.9	5.1	6.7	5.6
75%	10	0.2	5.5	13.4	9.8	9.2
75%	11	6.2	3.4	6.4	8.6	13.5
75%	12	13.9	4.1	12.5	12.0	9.6
75%	13	26.6	8.6	34.7	21.3	11.8
75%	14	56.2	44.8	31.4	39.4	25.4
75%	15	= 0	= 0	12.1	21.4	29.7

*For 200 slosh cycles at resonant sloshing conditions.

Conversion Factor: 1 psi = 6,895(10)⁻³ N/mm².



Pressure transducers
located on this end wall.

Dimensions for H and ℓ are given in Table 1.

FIGURE IV-2. TEST CONFIGURATION FOR COMBINED PITCH AND HEAVE TEST

Due to the design of the test rig, the pitching and heaving motions were simultaneous, but not independent of each other. The two motions were at the same frequency and in phase for these tests. During testing, it was noticed that the fundamental excitation frequency for a 75% full tank undergoing pitching plus heaving did not produce substantial dynamic pressures, so the frequency was increased to the first harmonic. At this frequency, substantial sloshing pressures occurred and were recorded for inclusion in the test results. The theoretical (Equation III-6) and experimental excitation frequencies are shown in Figure IV-3.

The recorded pressure values for pitching plus heaving and only pitching are contained in Tables IV-3 and IV-4. No values are found in the tables for heaving only since the resonant frequency for a heaving motion is twice the natural frequency of the liquid in the tank. The heave resonant frequency is outside the range of interest for ship motions. Therefore, no attempt was made to excite the tank into resonance in heave and record pressures.

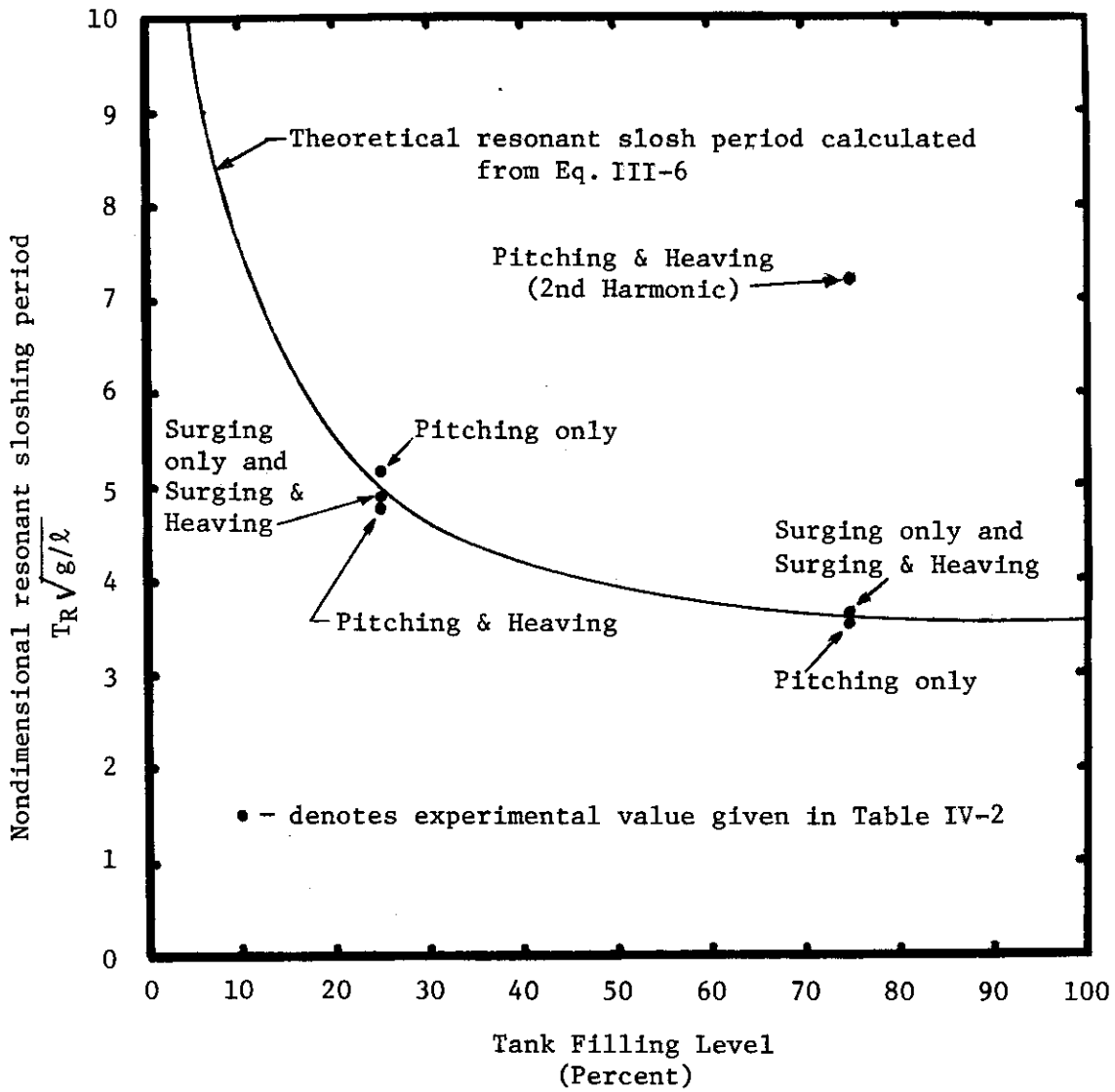
The pressures presented in Tables IV-3 and IV-4 for pitching and pitching plus heaving indicate there was no augmenting of the pressures using the combined motion. In addition, many test pressures were somewhat higher for pitching only motion.

IV.3.2 Surging Plus Heaving Test

The translational motion sloshing facility was utilized for the surging plus heaving tests. As with the pitching plus heaving test, the surging plus heaving test results are compared to the results of the individual excitation motion (surging). Figure IV-4 illustrates the surging and heaving motions.

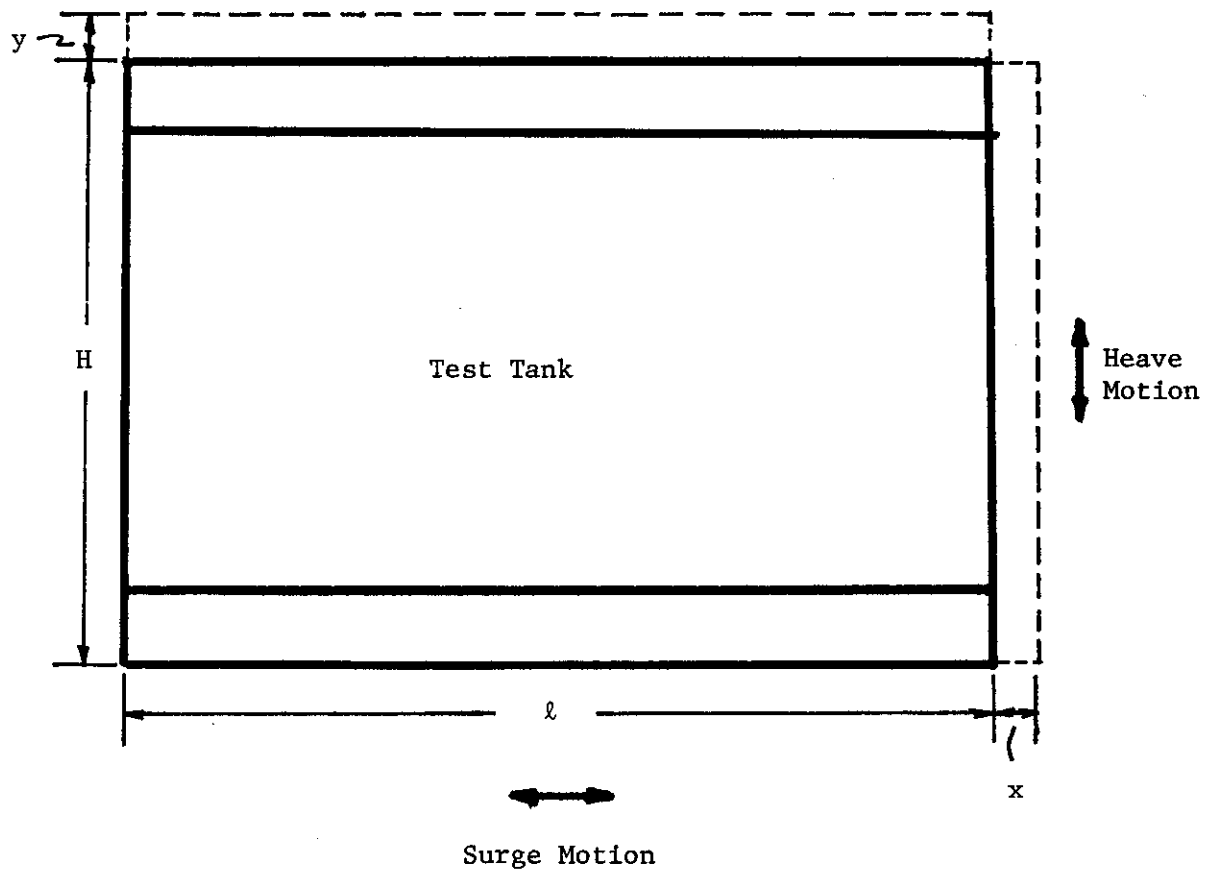
Two surging amplitudes were examined. These are typical extreme values that a full-scale tank might experience during operation. To determine the worst case combined surging plus heaving condition, the tank was oscillated with the surging frequency set at resonance, and the heaving frequency swept through a range of values from 0 to 5 Hz (model scale) or 0 to 0.707 Hz (full scale). Next, the tank was oscillated with the heaving motion set at its theoretical resonant frequency and the surging excitation frequency swept through a range of values [0 to 5 Hz (model scale) or 0 to 0.707 Hz (full scale)]. The worst case was chosen as the one that created the most violent sloshing (by visual observation) and the highest recorded pressures.

The results of these tests indicate that the worst case sloshing occurred when the surging and heaving excitation frequencies were equal to the resonant frequency of the liquid for a surging only motion. The test results were recorded with both the surging and heaving motions at the same frequency and in phase. The tank displacements in the surging and heaving directions were also equal in magnitude ($x = y = 1 \text{ in.} = 2.54 \text{ cm}$), with $(x/L) = 0.038$ and $(y/H) = 0.053$.



T_R = resonant sloshing period
 g = acceleration of gravity
 l = tank length in direction of motion

FIGURE IV-3. EXPERIMENTAL AND THEORETICAL NONDIMENSIONAL RESONANT SLOSH PERIOD VERSUS TANK FILLING LEVEL



- x = surge motion displacement
- y = heave motion displacement
- l = tank length
- H = tank height

FIGURE IV-4. MOTION DEFINITIONS FOR SURGE AND HEAVE.

The test results for surging plus heaving and surging only are found in Tables IV-5, IV-6, and IV-7. The results do not indicate any significant augmenting of the sloshing pressures caused by the combined tank motions of surging plus heaving. Visual observations also suggested that the sloshing for the surging plus heaving was comparable in magnitude to that for only surging.

Based on the results of these laboratory tests, there does not appear to be an increase in the slosh-induced dynamic impact pressures caused by multi-degree of freedom tank motions. However, it is realized that these tests are limited in that simultaneous excitation of all six degrees of freedom could not be investigated. In spite of this limitation, the results do provide insight into the effects of combined degrees of freedom excitation and indicate that worst case loads can be obtained by resonant sloshing in single degree of freedom tests. The excellent full-scale/model-scale pressure agreement for the OBO tank (discussed in Section III-2) where model tests were included in roll only further support this conclusion.

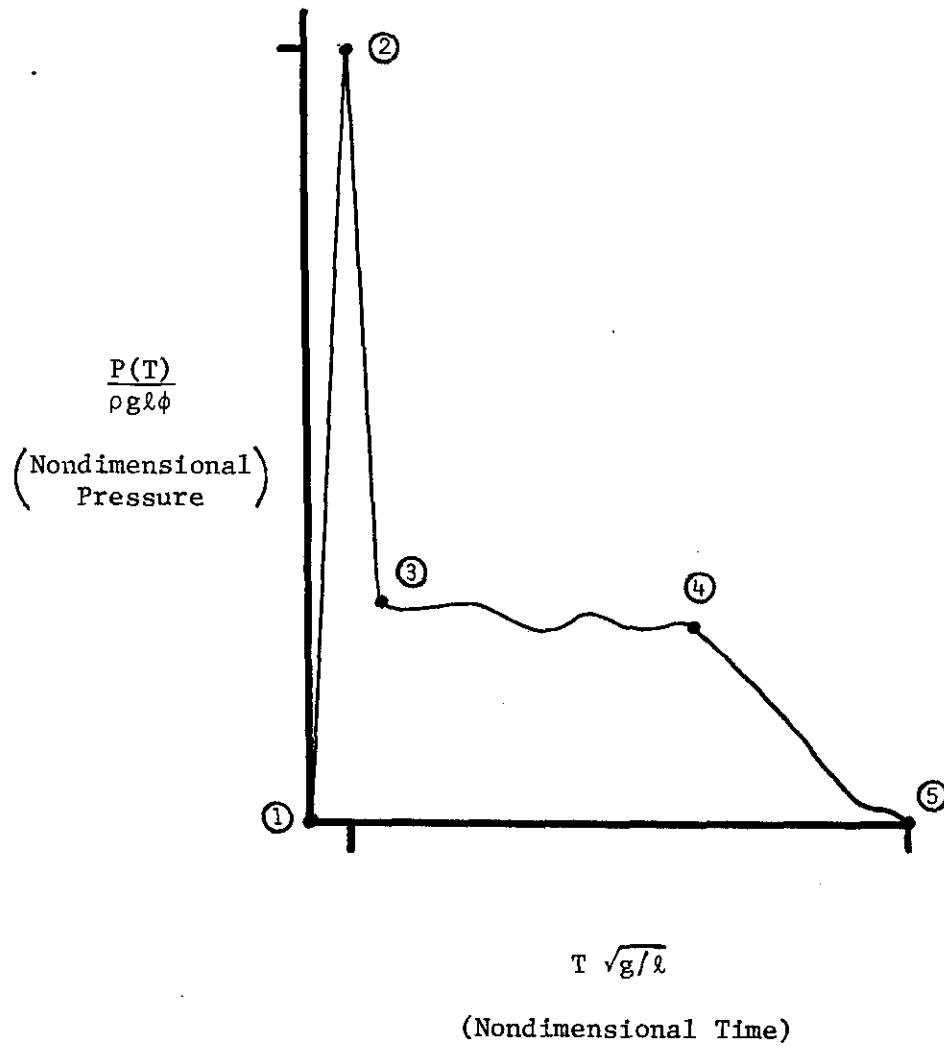
IV.4 Dynamic Pressure-Time Histories

Pressure-time histories were measured in model scale to establish information important to the analysis of the tank's structural response to dynamic loading caused by cargo sloshing.

A typical pressure-time history (nondimensional) is shown in Figure IV-5. For analytical purposes, this pressure trace will be approximated by straight lines connecting points 1, 2, 3, 4, and 5. The most important elements of the pressure trace are (1) the time required to reach the peak pressure (point 2), (2) the magnitude of the peak pressure at point 2, (3) the duration of the pressure spike (point 1 to point 3), (4) the magnitude of the tailing pressure between points 3 and 4, (5) the duration of the tailing pressure between points 3 and 4, and (6) the integrated pressure value over the entire pressure cycle. By knowing these characteristics of the pressure-time history, one can evaluate the structural response of the tank wall to an impact pressure.

Wall impact pressure-time histories for both a 25% and a 75% full tank were recorded. The tank excitation motion was harmonic pitching. Two hundred resonant sloshing cycles were recorded for each test. For the 25% full test, pressures were measured at transducer locations 1 through 9 (Figure IV-1). Pressures at locations 7 through 15 were recorded for the 75% full case.

The test results include two forms of the pressure-time history. First, for each transducer location, there is a composite worst case pressure-time history. This profile includes the shortest pressure rise time (T_2), the longest time durations for T_3 , T_4 , and T_5 , and the highest pressures for all points (P_2 , P_3 , P_4 , and P_5) recorded during any of the 200 sloshing cycles. This trace represents the worst case values (with respect to the loading on a tank wall structure) that the particular transducer location experienced during the 200 cycles of resonant sloshing. In addition, a pressure-time history showing the average values (for 200 resonant



The Trapezoidal Rule using the five numbered points is used to determine the area under the curve (which is the value of the pressure integrated over the entire period).

FIGURE IV-5. TYPICAL PRESSURE-TIME HISTORY FOR SLOSH-INDUCED IMPACT

sloshing cycles) for the points on the curve are plotted. Also, the integrated pressure values versus the pressure duration (T_5) are presented.

An effort was made to determine if any discernible correlations exist between the peak pressure (P_2), the pressure rise time (T_2), and the pressure spike duration (T_3). Plots showing peak pressure versus pressure rise time, peak pressure versus pressure spike duration, and pressure spike duration versus pressure rise time are included in the results.

The nondimensional pressure-time history test results for representative transducer locations 1 and 14 are found in Tables IV-12 and IV-13, and Figures IV-6 through IV-15. Similar data for the other transducer locations are presented in Appendix B. Maximum, average, and minimum pressure and time values are included in the tables. It should be noted that locations 7, 8, and 9 experienced virtually no pressures when the tank was 25% full. Thus, there are no tables for these locations. The same is true of location 15 for the 75% full tank.

The pressure data obtained at transducer locations 1, 4, and 7 are representative results for the test case with the tank 25% full. Dynamic pressures were measured at locations 1 through 6. The pressure-time histories at transducer 1 were similar in magnitude and shape to those at locations 2 and 3. The pressure traces at transducer location 4 were similar to those at locations 5 and 6.

The pressure-time history for location 1 for the 25% full tank is found in Figure IV-6. The integrated pressure value for this transducer is shown in Figure IV-7. Plots exemplifying the relationships between the pressure rise time (T_2), pressure spike duration (T_3), and the peak pressure (P_2) for this location are shown in Figures IV-8 through IV-10. It should be noted that several of the plots have data points clustered in small areas. This was caused by round-off limitations in the computation methodology that was used for data reduction.

A group of data similar to that just described for the test case with a 25% full tank was also compiled for the case with the tank 75% full. Data from pressure transducer locations 7, 11, 13, and 14 were chosen as representative for the 75% full tank. The pressure-time histories at location 7 are similar to those at locations 8 and 9. Likewise, the pressure-time histories at transducer 11 are comparable to those at 10 and 12 (with the exception that the magnitudes at location 10 are somewhat smaller).

Graphs showing pressure-time histories, integrated pressures, and relationships between the pressure rise time, the pressure spike duration, and the peak pressure for transducer 14 are found in Figures IV-11 through IV-15. Locations 7, 8, and 9 were below the static liquid level, and, as a result, these locations did not experience significant dynamic loadings. The pressure rise times were relatively slow and the peak pressure small. Pressures of a more dynamic nature were measured at locations 10 through 14.

TABLE IV-12. NONDIMENSIONAL PRESSURE-TIME HISTORY
VALUES AT TRANSDUCER LOCATION 1 FOR A 25% FULL
TANK

TRANSDUCER LOCATION 1
FLUID: WATER
EXCITATION: PITCH (AMP. = +/- 4.000 DEG.)
NUMBER OF CYCLES PER TEST: 200
PERCENT FILLING: 25

	PT. 2	PT. 3	PT. 4	PT. 5
AVG. KP	16.1333	1.6749	2.7716	0.0282
MAX. KP	37.3927	2.6081	3.4073	0.5775
MIN. KP	7.4799	1.0203	1.0240	0.0000
AVG. TIME	0.1759	0.3302	1.8530	2.6266
MAX. TIME	0.2849	0.5212	2.0395	2.8962
MIN. TIME	0.0740	0.1894	1.6587	2.3738

PT. 1 IS ALWAYS ZERO.

ALL VALUES PRINTED IN THE TABLE ARE NONDIMENSIONAL.

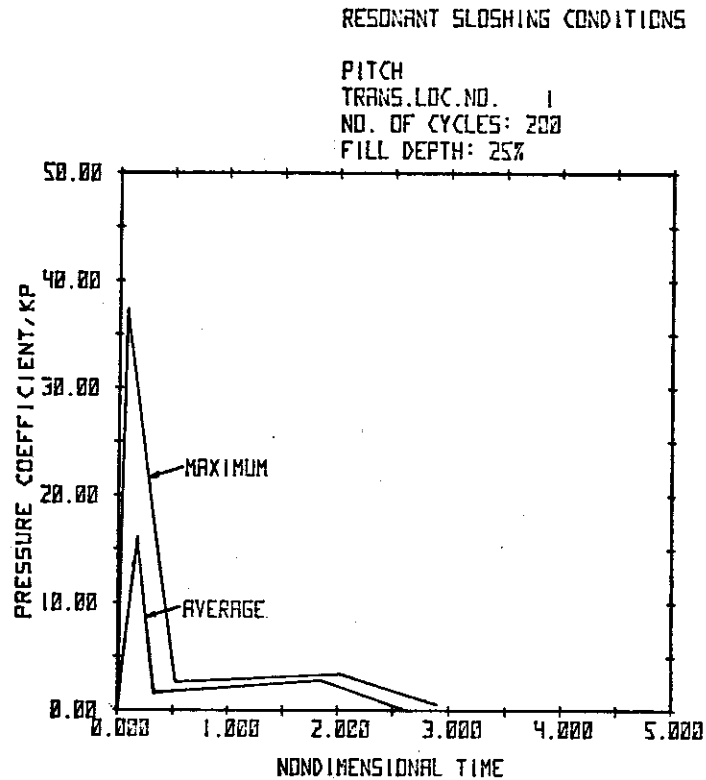
TABLE IV-13. NONDIMENSIONAL PRESSURE-TIME
HISTORY VALUES AT TRANSDUCER LOCATION 14
FOR A 75% FULL TANK

TRANSDUCER LOCATIO 14
FLUID: WATER
EXCITATION: PITCH (AMP. = +/- 4.000 DEG.)
NUMBER OF CYCLES PER TEST: 200
PERCENT FILLING: 75

	PT. 2	PT. 3	PT. 4	PT. 5
AVG. KP	13.6721	0.0000	0.0000	0.0000
MAX. KP	33.7277	0.0000	0.0000	0.0000
MIN. KP	7.2283	0.0000	0.0000	0.0000
AVG. TIME	0.0716	0.3234	0.6457	1.057
MAX. TIME	0.1899	0.5233	0.9983	1.615
MIN. TIME	0.0005	0.1901	0.3808	0.665

PT. 1 IS ALWAYS ZERO.

ALL VALUES PRINTED IN THE TABLE ARE NONDIMENSIONAL.



* THE LINES CONNECTING THE DATA POINTS
ARE ONLY VISUAL AIDS.

FIGURE IV-6. NONDIMENSIONAL PRESSURE-TIME HISTORY VALUES FOR 200 RESONANT SLOSHING CYCLES AT TRANSDUCER LOCATION 1 FOR A 25% FULL TANK

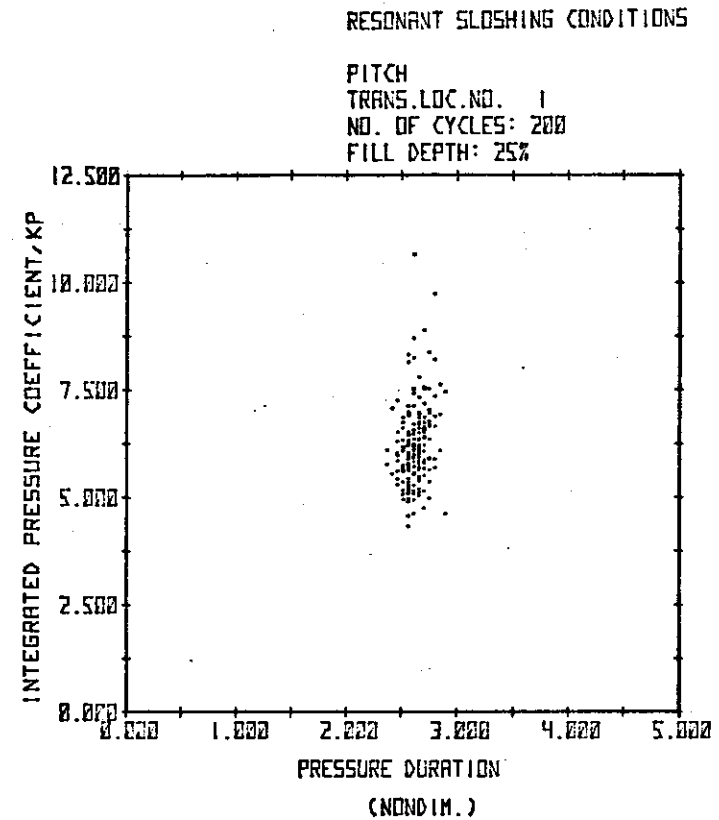


FIGURE IV-7. INTEGRATED NONDIMENSIONAL PRESSURE VALUES FOR 200 RESONANT SLOSHING CYCLES AT TRANSDUCER LOCATION 1 FOR A 25% FULL TANK

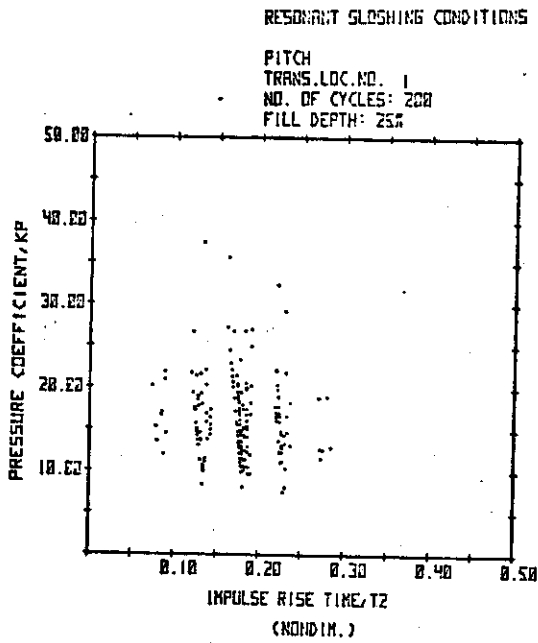


FIGURE IV-8. NONDIMENSIONAL PRESSURE VS IMPULSE RISE TIME FOR 200 RESONANT SLOSHING CYCLES AT TRANSDUCER LOCATION 1 FOR A 25% FULL TANK

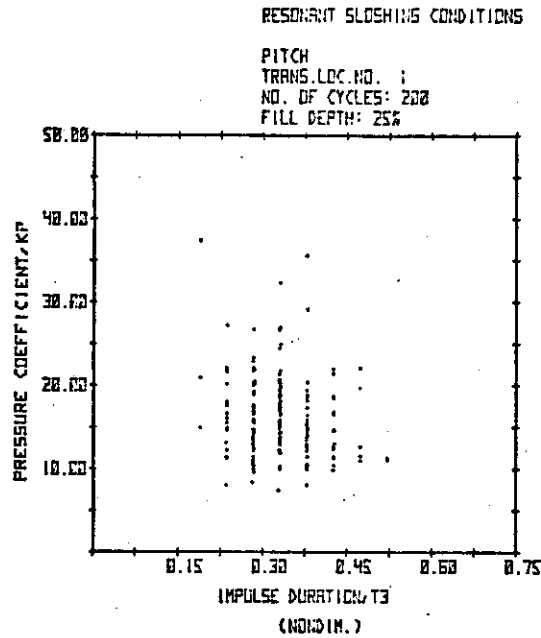


FIGURE IV-9. NONDIMENSIONAL PRESSURE VS IMPULSE DURATION FOR 200 RESONANT SLOSHING CYCLES AT TRANSDUCER LOCATION 1 FOR A 25% FULL TANK

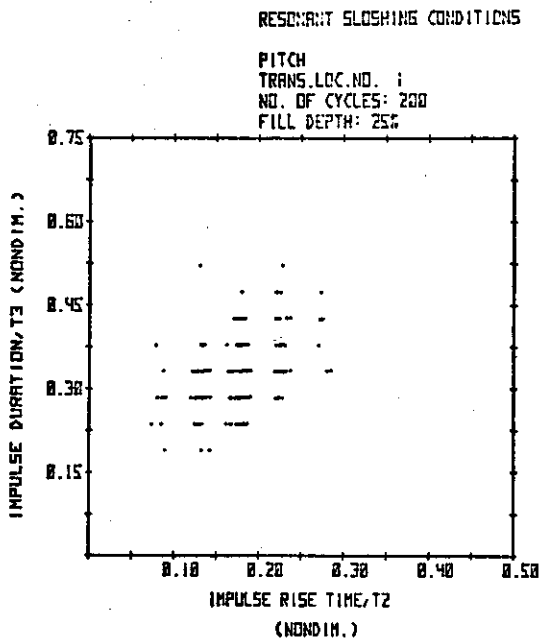
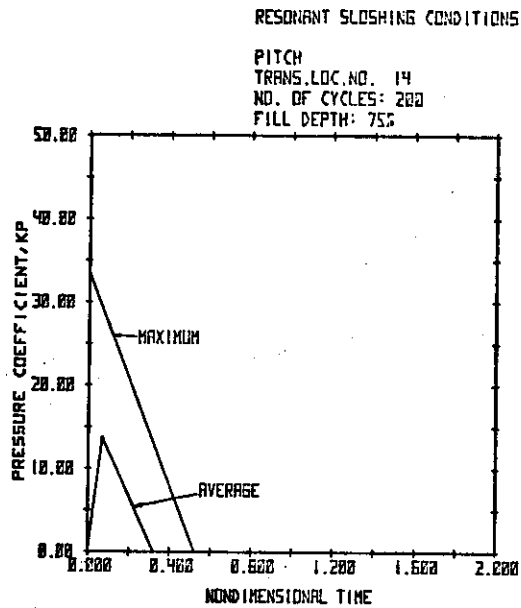


FIGURE IV-10. NONDIMENSIONAL IMPULSE DURATION VS IMPULSE RISE TIME FOR 200 RESONANT SLOSHING CYCLES AT TRANSDUCER LOCATION 1 FOR A 25% FULL TANK



* THE LINES CONNECTING THE DATA POINTS ARE ONLY VISUAL AIDS.

FIGURE IV-11. NONDIMENSIONAL PRESSURE-TIME HISTORY VALUES FOR 200 RESONANT SLOSHING CYCLES AT TRANSDUCER LOCATION 14 FOR A 75% FULL TANK

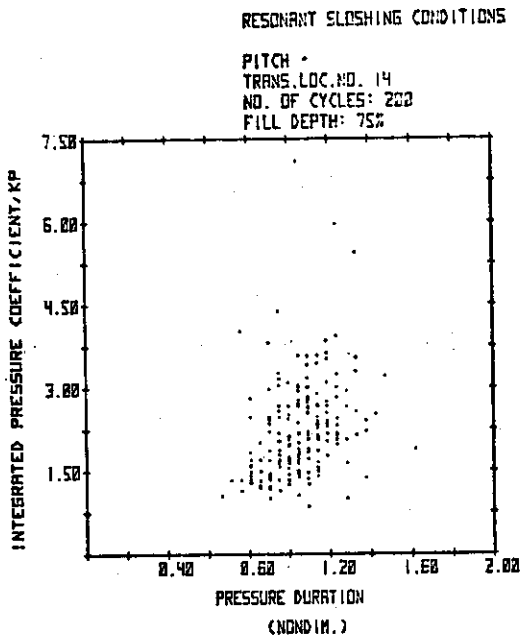


FIGURE IV-12. INTEGRATED NON-DIMENSIONAL PRESSURE VALUES FOR 200 RESONANT SLOSHING CYCLES AT TRANSDUCER LOCATION 14 FOR A 75% FULL TANK

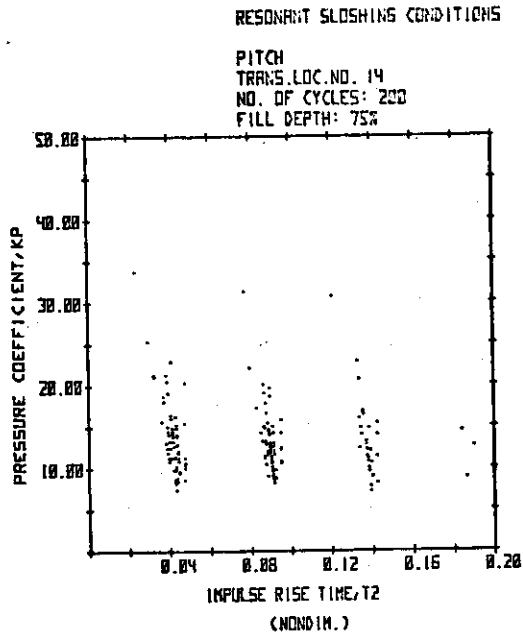


FIGURE IV-13. NONDIMENSIONAL PRESSURE VS IMPULSE RISE TIME FOR 200 RESONANT SLOSHING CYCLES AT TRANSDUCER LOCATION 14 FOR A 75% FULL TANK

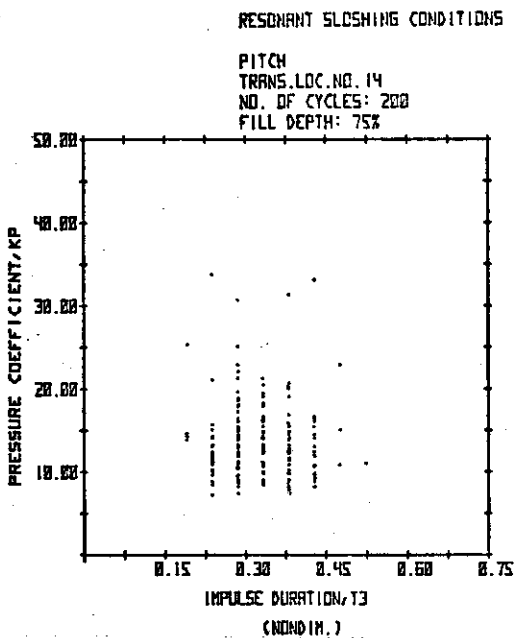


FIGURE IV-14. NONDIMENSIONAL PRESSURE VS IMPULSE DURATION FOR 200 RESONANT SLOSHING CYCLES AT TRANSDUCER LOCATION 14 FOR A 75% FULL TANK

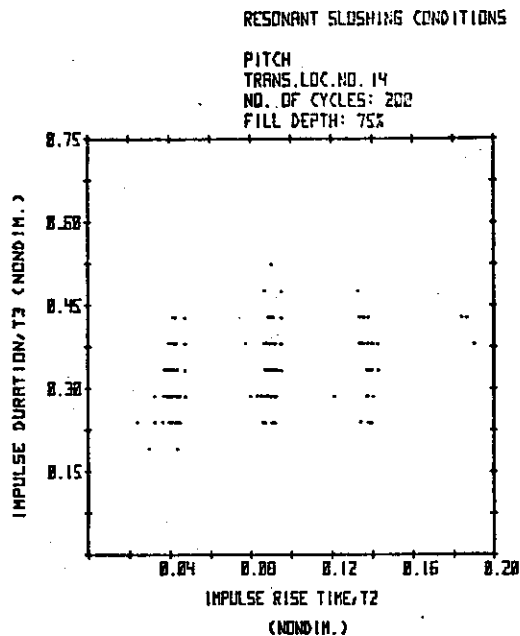


FIGURE IV-15. NONDIMENSIONAL IMPULSE DURATION VS IMPULSE RISE TIME FOR 200 RESONANT SLOSHING CYCLES AT TRANSDUCER LOCATION 14 FOR A 75% FULL TANK

IV.5 Dynamic Load Simulator for Plywood Insulation Box Tests

A series of strength tests were performed on representative plywood insulation boxes (Figure III-18) from a typical membrane tank insulation system. The purpose was to (1) provide structural response data for comparison to analytical predictions, (2) to evaluate the box response to various projected full scale loading conditions, and (3) to determine pressure levels a box could withstand without sustaining damage. The loading conditions were designed to simulate what a structure might encounter in actual operation. Tests included both static and dynamic loadings.

Because of the unusual test conditions, a special test fixture was fabricated. It was necessary to uniformly load the entire cover of the test box. In addition, a typical full-scale pressure-time history (Figure IV-5) had to be produced on the test structure.

The test system consisted of a chamber of water located on top of the box cover with a rubber diaphragm between the two. The box cover was loaded by pressurizing the water chamber. This created a relatively uniform load over the cover since the water deformed to the shape of the cover as it deflected under loading. For the dynamic pressure tests, three fast-opening valves located between the pressure source and the water chamber were used to shape the pressure-time history. A schematic of the test apparatus is presented in Figure IV-16.

The following paragraphs describe the function of each component shown in Figure IV-16. The pressure supply was a tank filled with nitrogen gas. At the exit port to the pressure tank was a hydraulically-operated cock valve. Between the cock valve and the water chamber was a fast-opening, hydraulically operated plunger valve. When this valve and the cock valve were both opened, the high pressure nitrogen gas pressurized the water volume. A solenoid valve located between the cock valve and the plunger valve was used as a relief valve. The pressure-time history for a dynamic pressure test was controlled by the timing of the opening and closing of these three valves. The apparatus was capable of creating dynamic pressure rise times as short as 20 milliseconds. Based on the pressure-time history experiments, this is a typical rise time that a plywood insulation box might experience while in service. Peak dynamic pressures of about 200 psi were attainable. Static pressures on the order of 250 psi were achieved with this particular test rig. These pressures represent worst case pressures that could be encountered in full scale-resonant sloshing.

The supporting structure for the plywood test box (called the primary box) consisted of 1/2-in.-thick, marine-grade fir plywood boxes (called secondary boxes). These boxes simulated the supporting structure of the primary box in the ship tank. Figure III-19 shows the supporting configuration as it is in the tank. The secondary boxes used in the loading tests had stiffener locations similar to those shown in Figure III-19. This allowed the load transfer through the stiffeners of the primary test box to closely approximate the actual full-scale conditions. The secondary boxes in the test apparatus rested on a rigid surface.

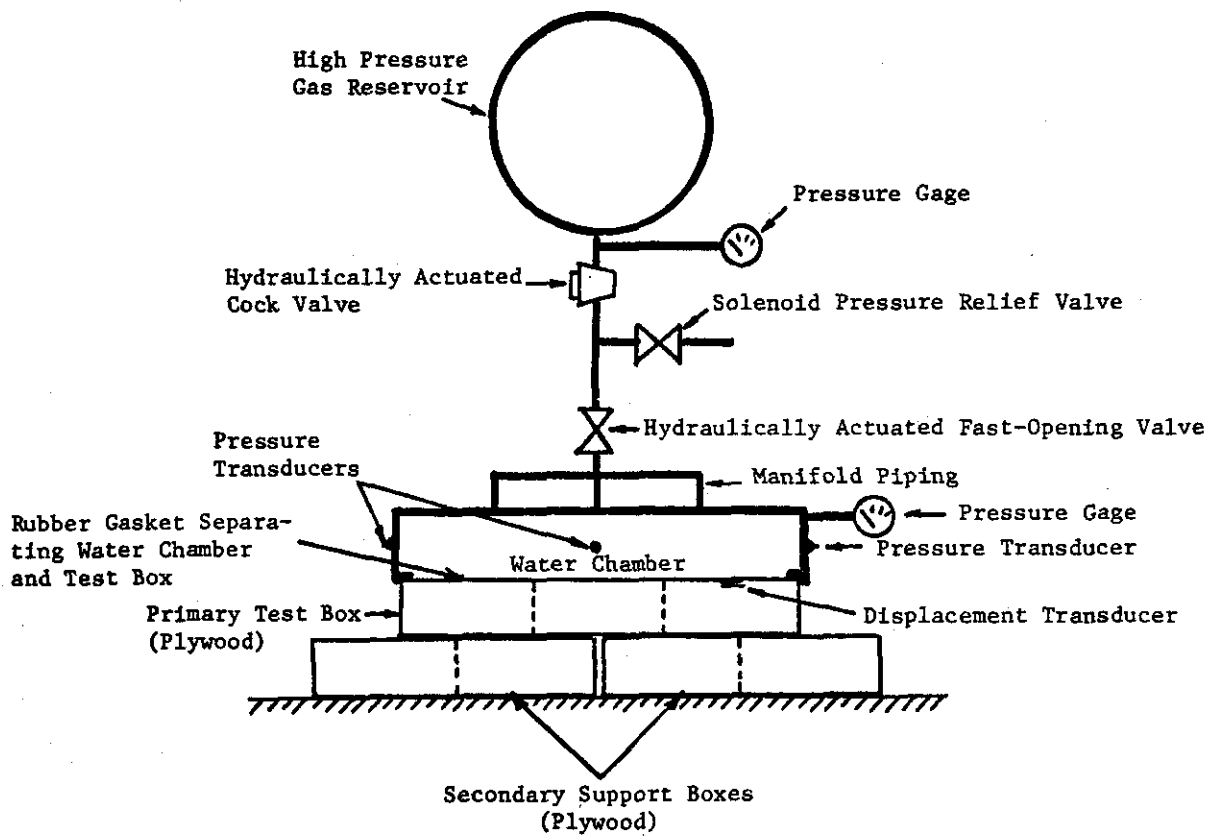


FIGURE IV-16. SCHEMATIC DIAGRAM OF PLYWOOD INSULATION BOX DYNAMIC LOADER

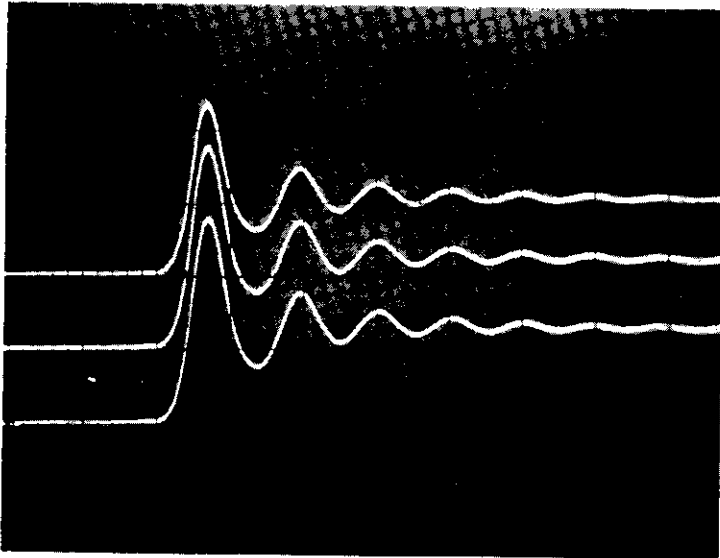
Instrumentation for the loading tests included pressure measuring devices to monitor the pressure on the box cover and displacement transducers to measure the deflection of the cover during loading. For the dynamic loading tests, PCB piezoelectric pressure transducers (Model 102A15) were used to measure the pressures in the water chamber. These transducers have an operating range of 0.01 to 500 psi with a frequency range of 0.5 to 50,000 Hz. Three transducers were used to monitor the uniformity of the pressure in the chamber. Transducers were located at the midpoint of both end walls of the chamber and at the midpoint of one side wall. All three transducers were located approximately 1-1/2 in. above the surface of the test box cover. The general locations of the three pressure transducers and the pressure gage are pictured in Figure IV-16. Figure IV-17 shows typical pressure traces for the three transducers for a dynamic pressure test. The top photograph shows the pressure-time histories for a test that did not experience a box failure. The bottom picture illustrates the pressure waveform when a failure occurred. These pressure signals were recorded on a storage oscilloscope, as were all of the dynamic pressure measurements.

One important aspect of these plywood box tests was the determination of the box cover response during loading. The stiffener configuration divided the boxes into 12 cells. The cover deflections were measured at the centers of the unsupported cell areas. Figure IV-18 shows the cell divisions for a typical 12-celled box and the locations of the displacement measurements. For static loading tests, spring-loaded, linear displacement transducers were utilized for the measurements. For dynamic loadings, a Kaman (Model KD2300-25) inductance-type displacement transducer was used. The performance of the two types of transducers correlated well as evidenced by the results presented in Figure IV-19. This figure shows that the cover response was similar for static and dynamic loading conditions.

The cover deflection measurements are presented in Tables IV-14 through IV-21. In addition to these results, Table IV-22 summarizes the tests and results for all boxes. Some boxes were modified to study the influence of various parameters on box strength.

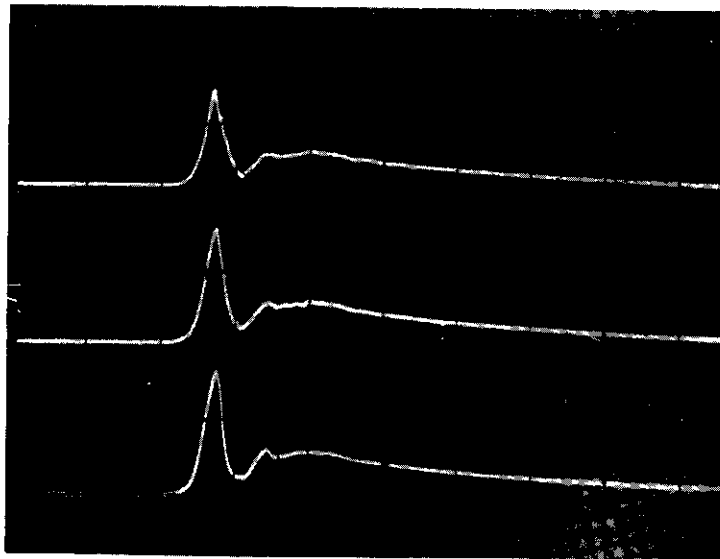
Three types of failures were observed during the box loading tests. First, some covers experienced shear failures. Usually the shear failure would occur at a stiffener support. Second, other covers experienced bending failures along the centerline of the unsupported area of an individual cell. The third type of failure was a buckling failure of a stiffener. This was observed in only one test. Figures IV-20, IV-21, and IV-22 show typical shear, bending, and stiffener failures, respectively.

The test results indicated that the original 12-celled boxes could withstand a pressure of about 120 psi without suffering catastrophic failure. The range of failure pressures was 120 to 158.6 psi for both static and dynamic loading. Also, test results showed no appreciable difference in failure pressures for static or dynamic pressures. A typical dynamic loading is shown in Figure IV-17. The pressure rise time is about 20 ms, the minimum rise time obtainable with the loading device. These observations are



Pressure Scale: 50 psi/div
(0.345 N/mm²/div)
(Typical pressure trace when
box failure does not occur.)

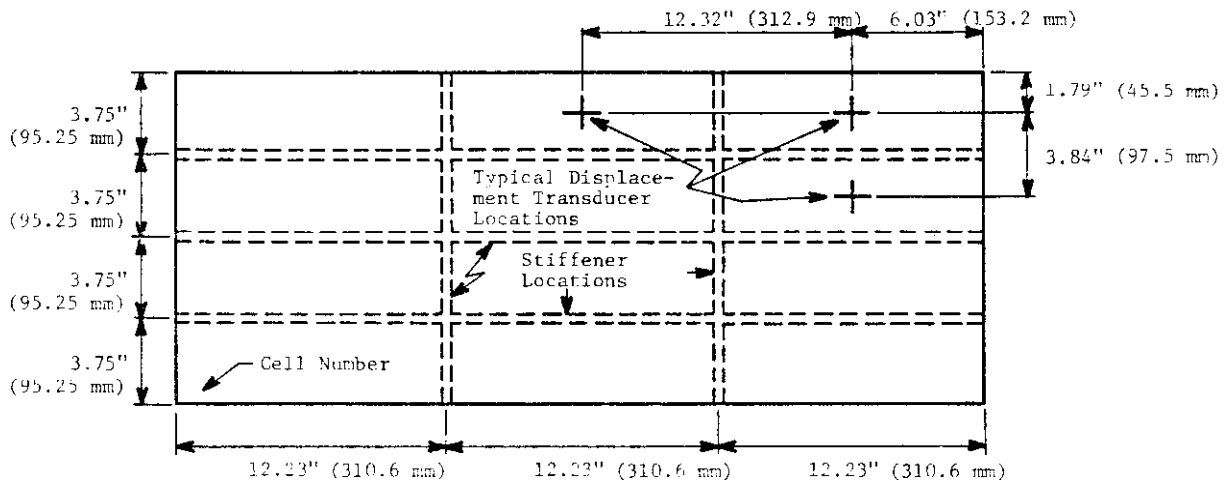
Time Scale: 50 msec/div



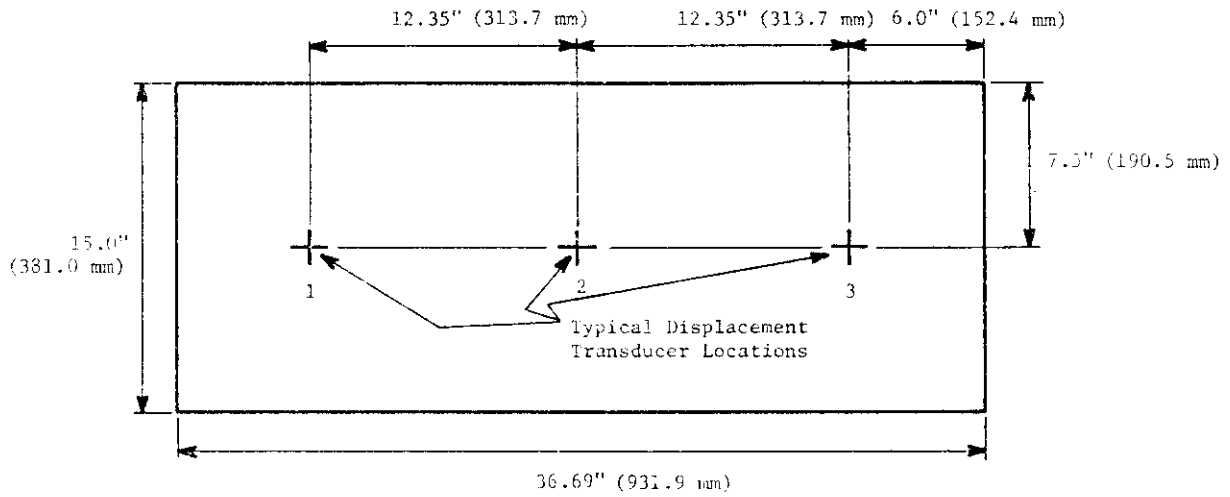
Pressure Scale: 100 psi/div
(0.690 N/mm²/div)
(Typical pressure trace
showing box failure.)

Time Scale: 50 msec/div

FIGURE IV-17. TYPICAL PRESSURE-TIME HISTORIES FOR DYNAMIC LOADING TESTS ON PLYWOOD INSULATION BOXES



(a) Typical Displacement Transducer Locations on 12-Cell Plywood Box Cover



(b) Typical Displacement Transducer Locations for a Plywood Box Cover with All Stiffeners Removed

FIGURE IV-18. DISPLACEMENT TRANSDUCER LOCATIONS FOR PLYWOOD BOX STRENGTH TESTS

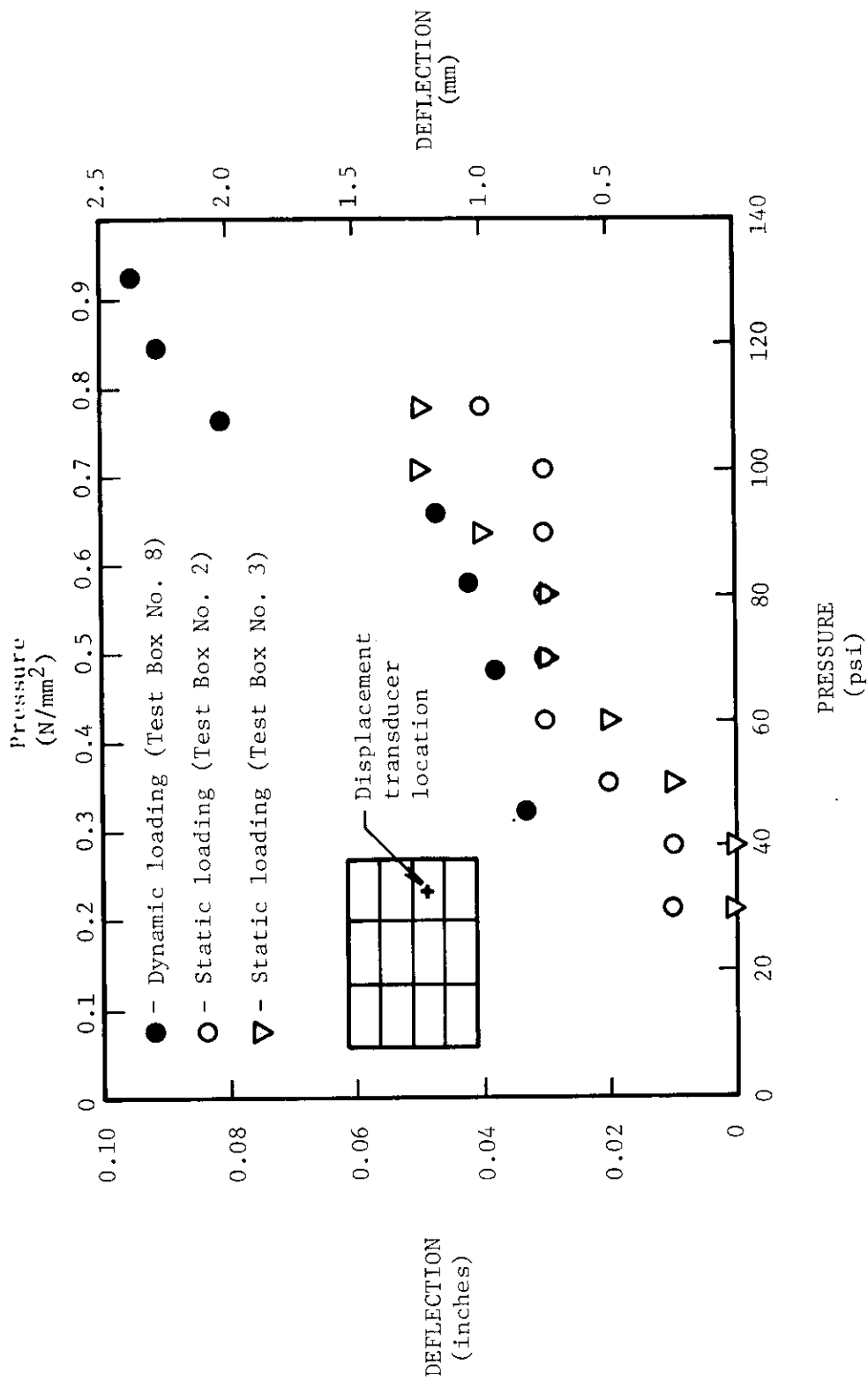


FIGURE IV-19. COVER DEFLECTION VS PRESSURE FOR DYNAMIC AND STATIC LOADING OF A STANDARD 12-CELL BOX

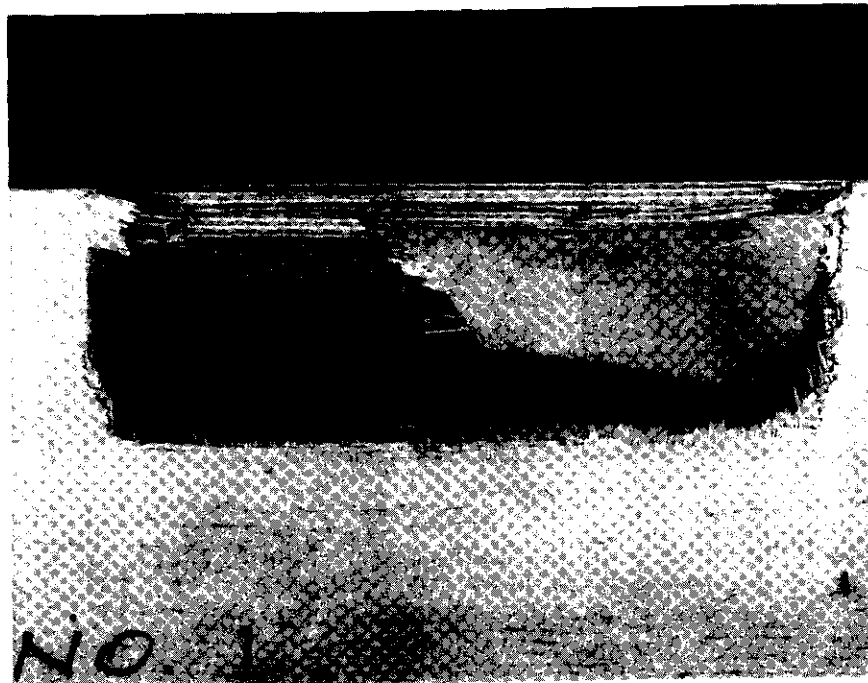
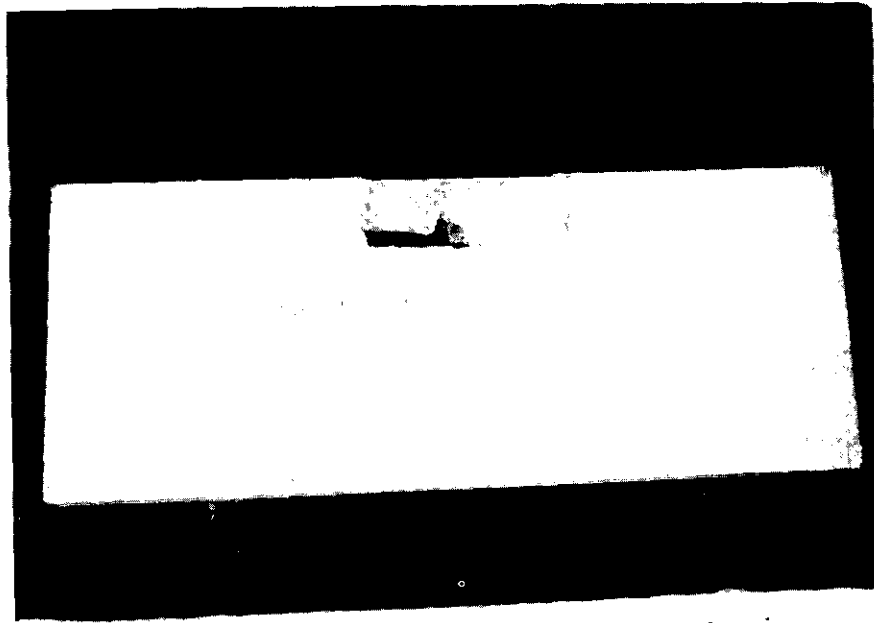


FIGURE IV-20. SHEAR FAILURE OF PLYWOOD INSULATION BOX COVER
(TEST BOX NO. 1)

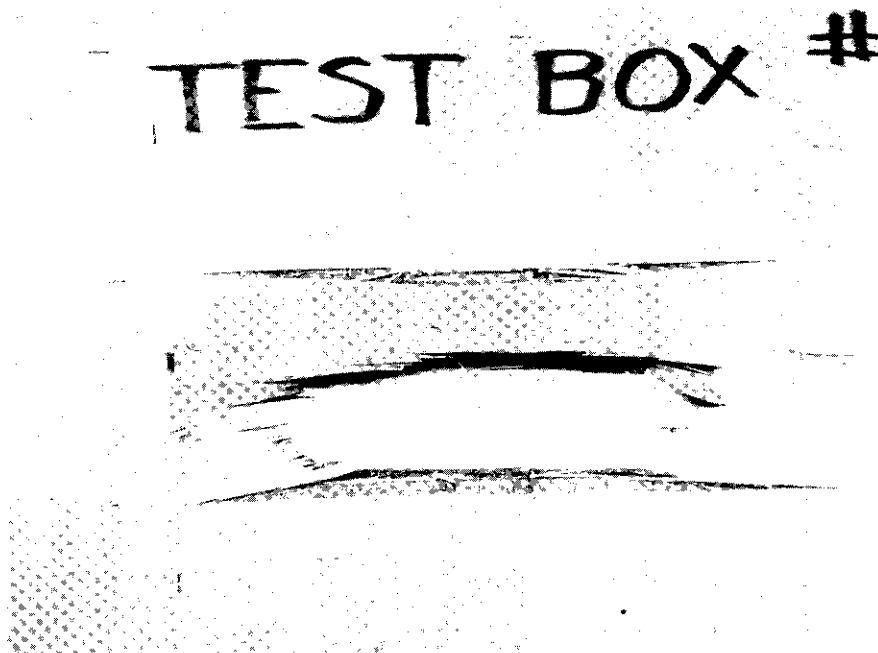
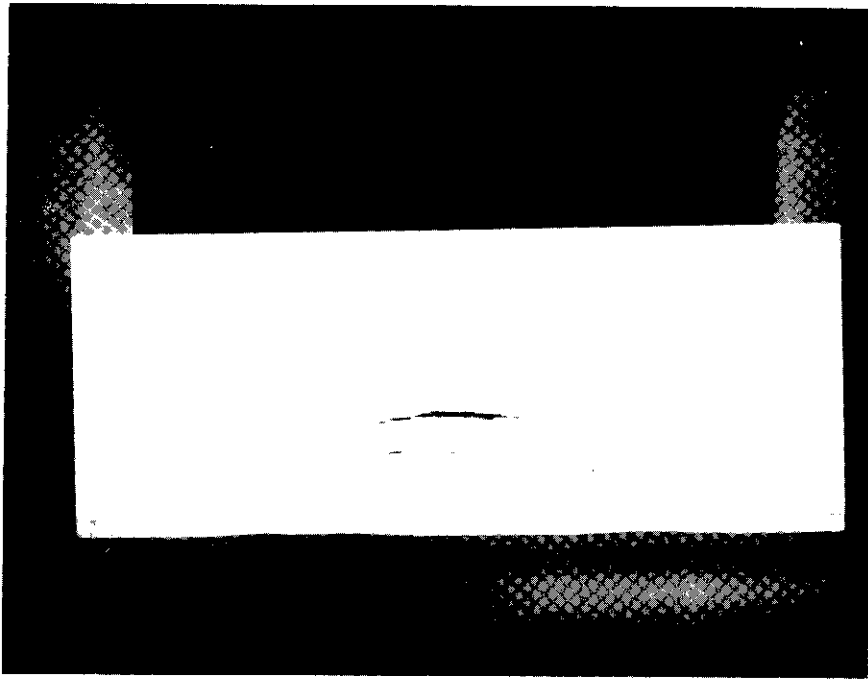


FIGURE IV-21. BENDING FAILURE OF PLYWOOD INSULATION BOX COVER
(TEST BOX NO. 8)

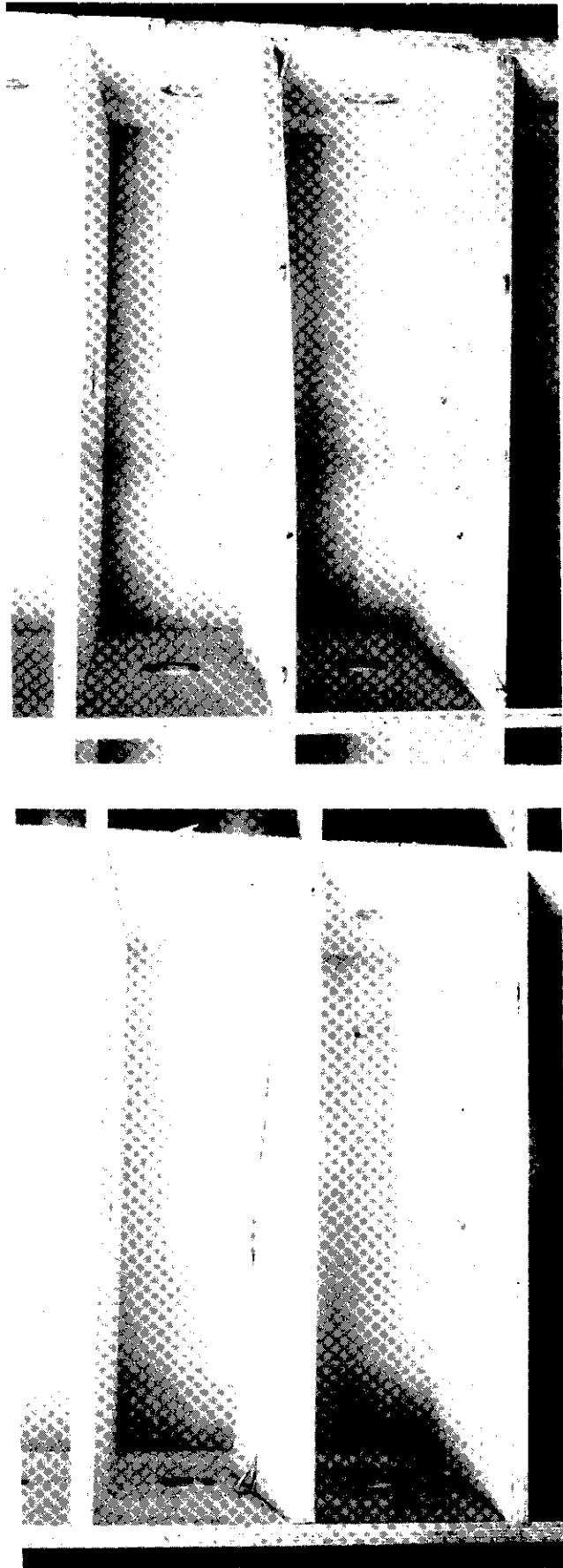
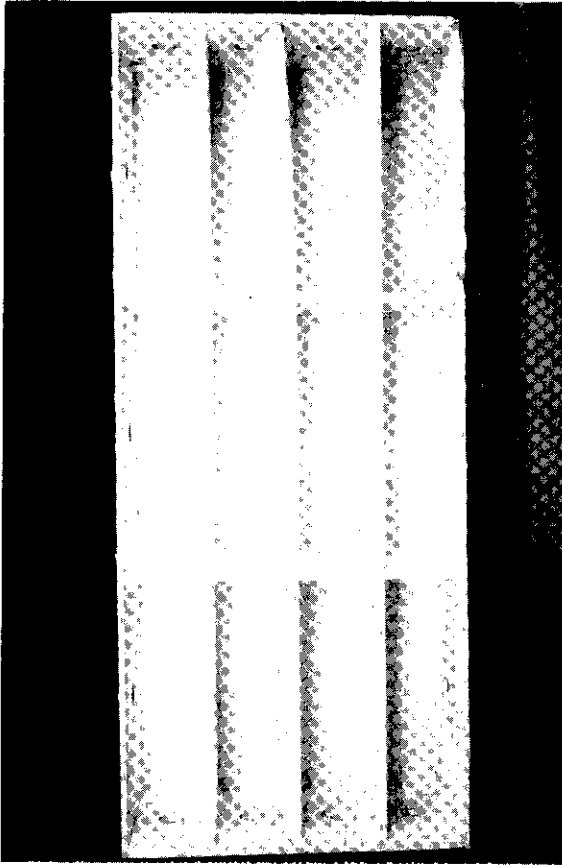


FIGURE IV-22. SUPPORT STIFFENER FAILURE IN A PLYWOOD INSULATION BOX (TEST BOX NO. 10)

TABLE IV-14. PLYWOOD COVER DEFLECTION MEASUREMENTS
FOR TEST BOX NUMBER 1 (Static Loading Test)

Pressure (psi)	Cover Deflection (inches)			
	Cell No. 1	Cell No. 3	Cell No. 10	Cell No. 12
0	0.00	0.00	0.00	0.00
35	0.00	0.00	0.01	0.00
50	0.02	0.00	0.04	0.01
60	0.04	0.00	0.05	0.03
65	0.04	0.00	0.05	0.03
70	0.04	0.00	0.06	0.03
80	0.05	0.00	0.06	0.04
90	0.07	0.05	0.07	0.04
100	0.08	0.08	0.09	0.06
110	0.10	0.08	0.13	0.08
120	0.20	0.16	0.17	0.18

Cell number 11 failed in shear at 130 psi (0.896 N/mm^2).

Conversion Factors: $1 \text{ psi} = 6.895(10)^{-3} \text{ N/mm}^2$

$1 \text{ in.} = 25.4 \text{ mm}$

TABLE IV-15. PLYWOOD COVER DEFLECTION MEASUREMENTS
FOR TEST BOX NUMBER 2 (Static Loading Test)

Pressure (psi)	Cover Deflection (inches)							
	Cell No. 1	Cell No. 2	Cell No. 3	Cell No. 6	Cell No. 9	Cell No. 10	Cell No. 11	Cell No. 12
0	0.00	0.00	0.00	0.00	0.00	0.00	0.00	0.00
30	0.00	0.00	0.00	0.01	0.01	0.03	0.01	0.03
40	0.02	0.00	0.00	0.01	0.01	0.03	0.03	0.05
50	0.04	0.03	0.03	0.02	0.01	0.07	0.04	0.06
60	0.06	0.04	0.05	0.03	0.01	0.08	0.04	0.08
70	0.06	0.05	0.06	0.03	0.01	0.09	0.05	0.08
80	0.07	0.06	0.07	0.03	0.02	0.10	0.08	0.10
90	0.08	0.03	0.08	0.03	0.03	0.10	0.08	0.11
100	0.10	0.05	0.09	0.03	0.03	0.12	0.10	0.16
110	0.11	0.07	0.10	0.04	0.05	0.16	0.10	0.20

Cell number 12 failed in shear at 120 psi (0.827 N/mm^2).

Conversion Factors: $1 \text{ psi} = 6.895(10)^{-3} \text{ N/mm}^2$

$1 \text{ in.} = 25.4 \text{ mm}$

TABLE IV-16. PLYWOOD COVER DEFLECTION MEASUREMENTS
FOR TEST BOX NUMBER 3 (Static Loading Test)

Pressure (psi)	Cover Deflection (inches)						
	Cell No. 1	Cell No. 2	Cell No. 3	Cell No. 6	Cell No. 10	Cell No. 11	Cell No. 12
0	0.00	0.00	0.00	0.00	0.00	0.00	0.00
30	0.01	0.02	0.02	0.00	0.03	0.02	0.02
40	0.02	0.03	0.03	0.00	0.05	0.03	0.05
50	0.03	0.04	0.08	0.01	0.08	0.05	0.07
60	0.04	0.05	0.09	0.02	0.09	0.06	0.08
70	0.05	0.06	0.11	0.03	0.10	0.08	0.09
80	0.07	0.08	0.11	0.03	0.10	0.09	0.10
90	0.08	0.09	0.13	0.04	0.12	0.10	0.10
100	0.10	0.10	0.17	0.05	0.15	0.10	0.11
110	0.11	0.11	0.20	0.05	0.19	0.12	0.11
110*	0.12	0.11	0.22	0.08	0.20	0.14	0.16
110*	0.13	0.11	0.23	0.07	0.20	0.14	0.18
110*	0.13	0.11	0.23	0.08	0.20	0.13	0.17
110*	0.13	0.11	0.23	0.08	0.20	0.14	0.17
90	0.10	0.10	0.20	0.06	0.18	0.12	0.12
110	0.15	0.10	0.23	0.08	0.20	0.16	0.17
30	0.05	0.04	0.10	0.03	0.10	0.08	0.08
0	0.03	0.00	0.02	0.00	0.04	0.02	0.03
110	0.18	0.11	0.28	0.07	0.20	0.16	0.17
0	0.03	0.01	0.03	0.01	0.07	0.03	0.04
120	0.18	0.12	0.30	0.07	0.21	0.18	0.19

Cell number 3 failed in shear at 150 psi (1.03 N/mm²).

* Pressure was reduced to 90 psi (0.621 N/mm²) and then increased back to 110 psi (0.758 N/mm²).

Conversion Factors: 1 psi = 6.895(10)⁻³ N/mm²

1 in. = 25.4 mm

TABLE IV-17. PLYWOOD COVER DEFLECTION MEASUREMENTS
FOR TEST BOX NUMBER 6 (Static Loading Test)

Pressure (psi)	Cover Deflection (inches)			
	Cell No. 1	Cell No. 3	Cell No. 10	Cell No. 12
0	0.00	0.00	0.00	0.00
30	0.02	0.02	0.01	0.00
40	0.03	0.03	0.02	0.00
50	0.03	0.03	0.03	0.01
60	0.04	0.03	0.04	0.03
70	0.05	0.05	0.04	0.03
80	0.06	0.05	0.05	0.04
90	0.06	0.06	0.06	0.04
100	0.09	0.08	0.07	0.05
110	0.10	0.09	0.14	0.09
0	0.05	0.00	0.05	0.01

Cell number 1 failed in shear at 160 psi (1.10 N/mm^2).

Conversion Factors: $1 \text{ psi} = 6.895(10)^{-3} \text{ N/mm}^2$

$1 \text{ in.} = 25.4 \text{ mm}$

TABLE IV-18. PLYWOOD COVER DEFLECTION MEASUREMENTS
FOR TEST BOX NUMBER 7 (Static Loading Test)

Pressure (psi)	Cover Deflection (inches)			
	Cell No. 1	Cell No. 3	Cell No. 10	Cell No. 12
0	0.00	0.00	0.00	0.00
60	0.02	0.02	0.03	0.02
70	0.03	0.03	0.03	0.02
80	0.03	0.03	0.04	0.03
90	0.04	0.04	0.05	0.03
100	0.05	0.05	0.07	0.04
110	0.06	0.07	0.08	0.05
120	0.08	0.08	0.09	0.06

Cell number 1 failed in shear at 240 psi (1.65 N/mm^2).

Conversion Factors: $1 \text{ psi} = 6.895(10)^{-3} \text{ N/mm}^2$

$1 \text{ in.} = 25.4 \text{ mm}$

TABLE IV-19. PLYWOOD COVER DEFLECTION MEASUREMENTS FOR TEST BOX NUMBER 8 (Dynamic Loading Test)

Pressure (psi)	Cover Deflection (inches)	
	Cell No. 6	
0	0.000	
45.5	0.033	
68.1	0.038	
81.8	0.042	
93.2	0.047	
107.8	0.081	
119.3	0.091	
130.7	0.095	

Cell number 5 failed in bending at 142.1 psi (0.980 N/mm²).

Conversion Factors: 1 psi = 6.895(10)⁻³ N/mm²

1 in. = 25.4 mm

TABLE IV-20. PLYWOOD COVER DEFLECTION MEASUREMENTS FOR TEST BOX NUMBER 1 (Static Loading Test)

Pressure (psi)	Cover Deflection (inches)		
	Cell No. 1	Cell No. 3	Cell No. 10
0	0.00	0.00	0.00
30	0.00	0.00	0.00
40	0.00	0.00	0.00
50	0.02	0.00	0.00
60	0.02	0.01	0.00
70	0.03	0.02	0.01
80	0.04	0.02	0.01
90	0.05	0.03	0.02
100	0.05	0.03	0.03
110	0.06	0.03	0.03
120	0.06	0.04	0.05

The center longitudinal stiffener buckled between cells 4 and 7 and 6 and 9 at a pressure between 150 and 180 psi (1.03 and 1.24 N/mm²).

Conversion Factors: 1 psi = 6.895(10)⁻³ N/mm²

1 in. = 25.4 mm

TABLE IV-21. PLYWOOD COVER DEFLECTION MEASUREMENTS FOR TEST BOX NUMBER 11 (Static Loading Test)

Pressure (psi)	Cover Deflection (inches)		
	Location No. 1	Location No. 2	Location No. 3
0	0.00	0.00	0.00
5.0	0.10	0.15	0.10
7.5	0.14	0.23	0.13
10.0	0.22	0.32	0.20
12.5	0.28	0.42	0.23
15.0	0.30	--	0.28
17.5	0.37	--	0.33

The cover cracked (bending failure) at the 20 psi (0.138 N/mm²) pressure level.

Conversion Factors: 1 psi = 6.895(10)⁻³ N/mm²

1 in. = 25.4 mm

TABLE IV-22. SUMMARY TABLE OF LOADING TEST RESULTS
FOR THE PLYWOOD INSULATION BOXES

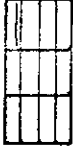
Box Number	Box Description	Static or Dynamic Test	Peak Pressure At Failure (psi)	Peak Pressure Rise Time (msec)	Type of Failure	Location of Failure	Comments
1	Standard 12 cell box.	Static	130 (0.896 N/mm ²)	--	Shear	At stiffener supports in cells 1, 10, and 11. 	Total failure in cell 11.
2	Standard 12 cell box.	Static	120 (0.827 N/mm ²)	--	Shear	At stiffener support in cell 12. 	Total failure in cell 12.
3	Standard 12 cell box.	Static	150 (1.03 N/mm ²)	--	Shear	At stiffener support in cell 3. 	Total failure in cell 3.
4	Standard 12 cell box.	Dynamic	158.6 (1.09 N/mm ²)	20	Bending	At the center of the unsupported area in cell 12. 	

TABLE IV-22. SUMMARY TABLE OF LOADING TEST RESULTS
FOR THE PLYWOOD INSULATION BOXES (Cont'd)

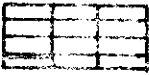
Box Number	Box Description	Static or Dynamic Test	Peak Pressure At Failure (psi)	Peak Pressure Rise Time (msec)	Type of Failure	Location of Failure	Comments
5	Standard 12 cell box.	Dynamic	120.4 (0.830 N/mm ²)	50	Bending	At the center of the unsupported area in cell 12. 	
6	Modified 12 cell box. The 9 mm cover was turned 90° so that the grain on the exterior ply was oriented in the transverse direction.	Static	240 (1.65 N/mm ²)	--	Shear	At the center of the unsupported area in cell 1. 	Cells 2, 5, 8, and 11 were not tested. Cell 10 experienced a partial shear failure.
7	Modified 12 cell box. The 9 mm cover was replaced with a 3/4" thick, marine grade fir plywood with the grain direction of the outer ply being transverse.	Static	240 (1.65 N/mm ²)	—	Shear	At the stiffener support in cell 1. 	The bottom side of the cover showed signs of partial shear failure at other stiffener supports.

TABLE IV-22. SUMMARY TABLE OF LOADING TEST RESULTS
FOR THE PLYWOOD INSULATION BOXES (Cont'd)

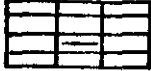
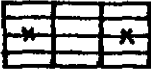
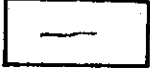
Box Number	Box Description	Static or Dynamic Test	Peak Pressure At Failure (psi)	Peak Pressure Rise Time (msec)	Type of Failure	Location of Failure	Comments
8	Standard 12 cell box.	Dynamic	142.1 (0.980 N/mm ²)	20	Bending	At the center of the unsupported area in cell 5. 	The box experienced 25 pressure cycles before failure.
9	Standard 12 cell box.	Dynamic	144.3 (0.995 N/mm ²)	20	Bending	At the center of the unsupported area in cell 2. 	A partial shear failure at the stiffener support in cell 1 was also observed.
10	Modified 12 cell box. A 3/4" thick marine grade fir plywood cover was nailed over the top of the original cover. The grain of the outer ply of the 3/4" cover ran longitudinally.	Static	150-180 (1.03 to 1.24 N/mm ²)	—	Buckling of the center stiffener.	The center stiffener in cells 4 and 7 and 6 and 9 buckled near the end walls of the box. The grain of the exterior ply of failed stiffener runs longitudinally. 	Loud cracking began at about 150 psi and continued until the 180 psi level was reached. The test was then terminated at the 180 psi level.

TABLE IV-22. SUMMARY TABLE OF LOADING TEST RESULTS
FOR THE PLYWOOD INSULATION BOXES (Concl'd)

Box Number	Box Description	Static or Dynamic Test	Peak Pressure At Failure (psi)	Peak Pressure Rise Time (msec)	Type of Failure	Location of Failure	Comments
11	Modified 12-cell box. All internal stiffeners were removed and the original cover was replaced with a 1/2" thick, marine grade fir plywood with the grain of the outer ply oriented in the longitudinal direction.	Static	20 (0.138 N/mm ²)	--	Bending	At the center of the unsupported area. 	The crack was in the longitudinal direction.
12	Same as box 11.	Static	19.2 (0.132 N/mm ²)	--	Bending	Near the center of the unsupported area. 	The crack was in the transverse direction.
13	Same as box 11.	Dynamic	15.2 (0.105 N/mm ²)	50	Bending	Near the center of the unsupported area. 	The crack was in the transverse direction.

consistent with analytical calculations of dynamic response presented in Section V, which show that rise times must be about 1-2 ms to produce dynamic amplification of the loading.

By modifying the test boxes, loading pressures up to 240 psi could be obtained before box failure occurred. It was observed that the box covers could withstand approximately 0.2-in. deflections at the centers of the unsupported cell areas before failure of the cover was observed. Permanent deformations of the cover (not total failure) were witnessed when pressure levels reached 80-90 psi. These deformations could be described as "scalloping" of the unsupported cell areas with the magnitudes of these deformations in the range of 0.05- to 0.10-in. maximum.

IV.6 Material Properties Tests

A series of tests on plywood specimens taken from the Gaz Transport boxes were conducted. The purpose of these tests was to provide material property data for the analysis of the plywood box and to aid in the interpretation of tests to measure box strengths. These tests were necessary because data from tests by Mitsui⁽⁷⁶⁾ and by Gaz Transport^(77,78) gave widely varying results for plywood strength and stiffness.

All plywood tests were conducted with simple beams in 3-point bending. As shown in Figure IV-23, the specimens were approximately 50mm wide, and support spacing was either 121mm, 88mm, or 50mm. Spacings of 121mm and 88mm match the widths of the cells in the 9-cell and 12-cell boxes, respectively. The spacing of 50mm was used to check the effect of very short spans. All specimens were cut transverse (perpendicular) to the grain.* This is the weakest direction and also the direction across the narrow dimension of the cells in the plywood boxes. Principal bending in the actual boxes will occur in the cross-grain direction.

Specimens were cut from the covers of boxes which had been in service ("old" boxes) and from new boxes which had never been exposed to cryogenic temperatures. Tests on the specimens from the old boxes were performed at two loading rates. A slow rate of 2.54 mm/min represents a static test, and the fast loading rate of 508 mm/min is the limit of the test machine. Tests with specimens from the new boxes were conducted at both room temperature (RT) and at cryogenic temperature (CT). All tests were performed at the slow loading rate.

Results for the old plywood are presented in Table IV-23. Considerable variation in the stiffness and stress values are evident. Stress values range from a low of 20.9 N/mm² to a high of 65.5 N/mm², a factor greater than 3. Average values of σ and E for the two different loading rates and overall are:

	σ , N/mm ² (psi)	E, N/mm ² (psi)
Fast Loading	40.1 (5,816)	2144 (310,987)
Slow Loading	49.4 (7,165)	3797 (550,755)
Overall	44.2 (6,411)	2941 (426,592)

*Grain direction of the exterior ply.

TABLE IV-23. RESULTS OF TESTS ON SPECIMENS FROM OLD BOXES

Specimen No.	Test Temp.	Loading* Rate	l_g (mm)	b (mm)	h (mm)	P_c (N)	P_e (N)	Y_e (mm)	E (N/mm ²)	σ (N/mm ²)
1	RT	S	88	50.5	9.1	1890.0	889.6	1.08	3753	60.0
2		S	88	50.4	9.1	878.6	667.2	1.08	2819	31.1
3		S	88	49.5	9.1	1334.4	889.6	1.32	3131	43.2
4		F	88	49.9	9.0	2001.6	--	--	--	65.5
5		F	88	50.1	9.0	845.1	667.2	2.03	1559	27.6
6		F	88	50.0	9.1	1579.0	889.6	2.49	1643	50.6
7		F	121	50.4	9.1	480.4	444.8	1.63	3182	20.9
8		F	121	50.1	9.1	822.9	667.2	3.57	2192	36.0
9		S	121	50.5	9.2	1490.0	889.2	1.93	5246	63.3

*F = Fast = 508 mm/min.

S = Slow = 2.54 mm/min

P_c = Failure Load

P_e = Load at Yielding

Y_e = Deflection at Yielding

$$E = P_e l_g^3 / 4 Y_e b h^3$$

$$\sigma = 3 P_c l / 2 b h^3$$

Conversion Factors: 1 psi = 6.895(10)⁻³ N/mm²

1 in. = 25.4 mm

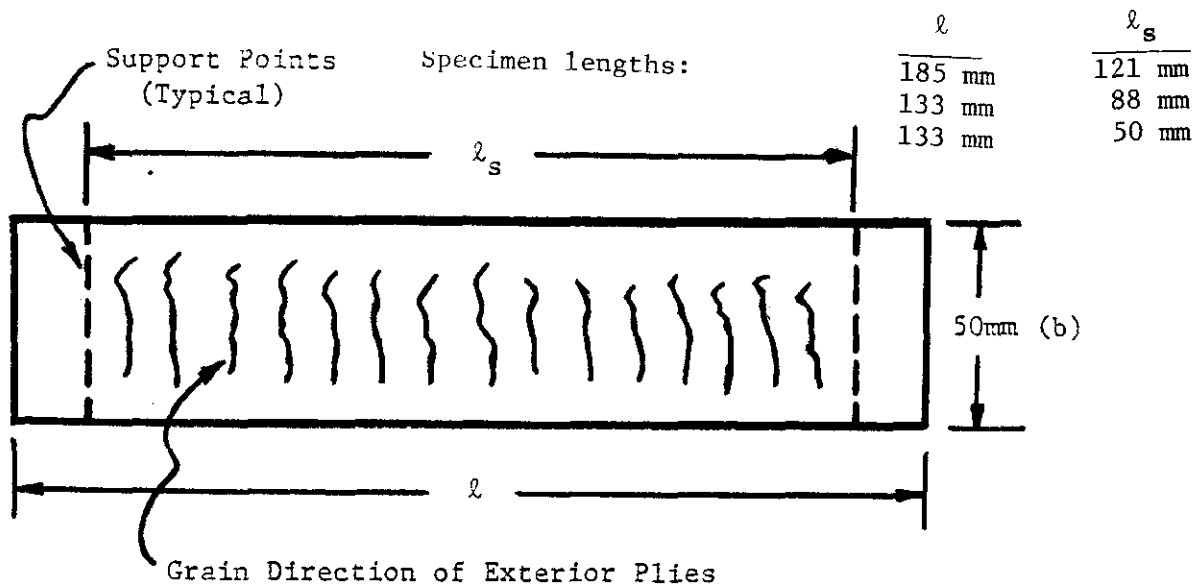


FIGURE IV-23. PLYWOOD TEST SPECIMEN GEOMETRY

Although σ and E for the fast loading rate are lower than for the slow rate, this difference was disregarded for three reasons. First, the maximum and minimum values for stress occurred at the fast loading rate, which indicates that there is no consistent trend. Second, even the fast loading rate used in the tests* is slow by several orders of magnitude compared to the expected response rate of the plywood covers in the insulation boxes. Third, drop tests conducted by Mitsui,⁽⁷⁶⁾ which give faster loading rates, showed no difference in results from static tests. For these reasons, the average values from all tests were taken as representative of plywood properties from the old boxes. The spread in the results for different specimens implies that there is considerable variation in the plywood even for a single box cover.**

Results for the new plywood boxes are given in Table IV-24. Tests were performed at both cryogenic and room temperatures. Plywood strength at cryogenic temperatures is consistently higher than at room temperature. Also, scatter is somewhat less in the strength results for the new boxes. In the room temperature tests, for example, the values differ by a factor of 2.45 as opposed to 3.13 for the old boxes, and this is based on about twice as many tests for the new plywood.

Plywood data for all tests, conducted by Mitsui, Gaz Transport and SwRI, are summarized in Table IV-25. These data include one test on the new box material which is compressive parallel to the grain of the exterior plies. This test was to give some indication of the basic strength of the vertical stiffeners in the boxes.

*Fast loading rate used in these tests was the highest rate obtainable with the test device.

**All specimens from the old boxes were cut from a single box cover.

TABLE IV-24. RESULTS OF TESTS ON SPECIMENS FROM NEW BOXES

Specimen No.	Test Temp.	Loading Rate	l_s (mm)	b (mm)	h (mm)	P_c (N)	P_e (N)	Y_e (mm)	F (N/mm ²)	σ (N/mm ²)
1-3*	RT	S	50	53.9	9.1	3158	2224	1.04	1662	53.5
2-1				50.4	9.0	2913	2224	1.14	1673	58.4
2-2				50.0	9.1	3025	2224	1.14	1591	54.3
2-3				51.8	9.1	2558	2224	1.42	1256	44.8
3-1				50.7	9.0	3158	2224	1.21	1573	58.0
3-2				50.1	9.0	2958	2224	1.27	1503	54.8
3-3				59.2	8.9	2002	1334	0.81	1213	31.7
1-4			121	50.7	9.0	1535	896	3.49	3053	67.5
1-5				50.7	9.0	1757	896	3.43	3140	77.8
1-6				50.5	9.0	1557	896	3.68	2887	68.4
1-7				50.7	9.0	1535	896	1.73	6161	67.6
2-4				54.6	9.0	1245	896	2.21	4491	50.9
2-5				56.6	9.1	1334	896	2.60	3590	51.7
2-6				53.9	9.1	845	445	1.58	3114	34.6
2-7				53.9	9.2	1334	896	2.60	3655	53.2
3-4				50.4	9.0	1268	896	2.60	4196	56.7
3-5				50.8	8.8	1490	896	2.32	4873	68.2
3-6				51.3	9.0	1223	896	2.64	4035	53.5
3-7				50.2	9.1	1334	896	2.44	4664	57.7
1-8	CT**			50.3	9.0	1334	1334	4.45	3601	59.2
1-9				49.3	9.1	2068	2068	4.70	5266	92.2
2-8				50.5	9.1	2224	2224	5.53	4700	96.7
2-9				50.5	9.0	2180	2180	5.46	4818	96.9
3-8				50.5	9.0	2331	2331	5.25	5364	103.7
3-9				50.4	9.1	1979	1979	4.70	4958	86.6

*Specimens are Identified by Box

**Submerged in Liquid Nitrogen @ -321°F

Conversion Factors: 1 psi = 6.895(10)⁻³ N/mm²

1 in. = 25.4 mm

TABLE IV-25. SUMMARY OF PLYWOOD PROPERTIES (AVERAGE VALUES)

SUMMARY OF EXPERIMENTS WITH PLYWOOD TO DETERMINE MATERIAL PROPERTIES											
SOURCE	KIND OF TEST	SPECIMEN				TEST CONDITIONS			σ N/mm ²	E N/mm ²	
		l mm	b mm	h mm	Bound.	Direct.	Temp.				
Mitsui	Droptest on Simply Supported Beams	40	23	9	SS-SS	CG*	RT	75.5			
		40	23	9	SS-SS	CG	CT	75.5			
Gaz Transport	Droptest on Simply Supported Beams	275	50	9	SS-SS	CG	CT	42.8			
	Static Loading of Simply Supported Beams	275	50	9	SS-SS	CG	RT		5000		
	Static Loading of Part of a Box Structure	133	100	9	C-C	CG	RT	50	4500		
Southwest Research Institute	Static Loading on Simply Supported Beams of OLD Plywood	88 121	50	9	SS-SS	CG	RT	49.4	3737		
	Fast Loading on Simply Supported Beams of OLD Plywood	88 121	50	9	SS-SS	CG	RT	40.1	2144		
	Static Loading on Simply Supported Beams of NEW Plywood	50 121 121	50 50 50	9 9 9	SS-SS SS-SS SS-SS	CG CG CG	RT RT CT	50.8 59.0 89.2	3988 4785		
	Static Loading in Axial Compression of NEW Plywood		63.5	9		PG	RT	39.0			

*CG - Cross Grain
 PG - Parallel Grain
 Conversion Factors: 1 psi = 6.895(10)⁻³ N/mm²
 1 in. = 25.4 mm

As noted, considerable scatter was found in tests on the specimens from the old box cover. This cover had sustained localized visible damage, but specimens were cut from areas which appeared to be undamaged. However, the large scatter may indicate that some unnoticed damage was present in some of the specimens tested. Thus, plywood properties for in-service boxes were established from tests on both the old and new boxes. Tests on the new boxes were used to establish the minimum, average, and maximum values for both cryogenic temperature (CT) and room temperature (RT). These values, taken from Table IV-24, are listed in Table IV-26.

TABLE IV-26. RANGE OF PLYWOOD PROPERTIES

Birch Plywood, New Properties Perpendicular to Exterior Plywood	Minimum		Average		Maximum	
	RT	CT	RT	CT	RT	CT
σ , N/mm ² (psi)	31.17 (4,598)	59.20 (8,587)	55.96 (8,117)	89.05 (12,916)	77.80 (11,285)	103.70 (15,042)
E, N/mm ² (psi)	1213 (175,946)	3601 (522,325)	3070 (445,304)	4785 (693,992)	6161 (893,653)	5364 (778,048)

A reduction factor, RF, for in-service conditions was established by the ratio of average RT values for the old and new plywood. From Tables IV-23 and IV-24, these average RT values are:

$$\begin{aligned} \text{Old plywood: } \sigma_{AVG} &= 44.20 \text{ N/mm}^2 \quad (4,411 \text{ psi}) \\ &E_{AVG} = 2941 \text{ N/mm}^2 \quad (426,592 \text{ psi}) \\ \text{New Plywood: } \sigma_{AVG} &= 55.96 \text{ N/mm}^2 \quad (8,117 \text{ psi}) \\ &E_{AVG} = 3070 \text{ N/mm}^2 \quad (445,304 \text{ psi}) \end{aligned}$$

For "in-service" conditions, the reduction factors become:

$$\text{For } \sigma: \quad RF = \frac{44.20}{55.96} = 0.79$$

$$\text{For } E: \quad RF = \frac{2941}{3070} = 0.96$$

V. TASK 3 - ANALYTICAL STUDIES

V.1 Response Prediction Method

Analytical studies were performed to develop wall-response prediction methods for prismatic tanks. The methods were developed for and applied to the two specific tank designs (membrane and prismatic) for which structural details were available. Example calculations for these two tank types are given in Appendix D. Also in this appendix, predicted wall response was compared to the experimental response data presented in Section IV.5, to evaluate the validity of the analytical methodology. Pressure type tanks were not analyzed since impulsive sloshing pressures on the walls of spherical and cylindrical tanks are low and are not significant in the wall design. Sloshing forces are created on cylindrical and spherical tanks, but only the resultant forces are of interest. Methods of predicting these forces are presented in Section III.2, and design for these forces is discussed in Section VI.

The response of structures to dynamic loads can be quite complicated; however, simplifying assumptions can be made which make the response calculation tractable and suitable for design purposes. One approach is to assume or prescribe a deformation pattern for the structure. When the deformation pattern is prescribed, then the displacements at all points in the structure are known when the displacement at only one point in the structure has been determined. This is also true of velocity and acceleration; thus, the transient response of the structure can be described by one degree of freedom (dof). To apply this approach, an equivalent one-dof system must be developed. Properties of the equivalent one-dof system are computed from energy principles as explained in Appendix C. This explanation is centered around the work by Biggs,(79) but the basic principles are the same for all similar approaches.

This method of calculating the response of structures to dynamic loading is used widely for design purposes (see References 80 through 83) because of its simplicity and ease of use. Comparisons between calculated and measured behavior have been made by Westine and Baker,(84) Westine and Cox,(85) and Westine, Cox and Esparza;(86) and the one degree of freedom approximation has been shown to give good results. Although much work of this nature has been for elastic-plastic behavior, for the design of ship tanks only elastic behavior is required. Our approach in this work is to assume that the structure will be designed for elastic behavior, even for the worst case loadings. This is certainly a necessity for structures made of plywood which exhibit brittle behavior at cryogenic temperatures. In other materials some plastic behavior could perhaps be tolerated, but it is not treated here.

As explained in Appendix C, methods for computing equivalent one-dof systems usually prescribe the static deformed shape as the deformation pattern; however, it was also shown that for symmetrical structures with uniform loading, the fundamental mode shape gives almost identical results. Three other important points are made in Appendix C.

- (1) Solutions for elastic behavior can be based upon a dynamic load factor (DLF) which is a function of the load-time history and of the fundamental period of the structure.
- (2) The dynamic load factor, when multiplied by the peak force which occurs in $F(t)$, gives an equivalent static force for design purposes.
- (3) For elastic behavior of structures which are subjected to loads of long duration, relative to the structure's fundamental period, the equivalent static force gives good estimates of maximum shear reactions in the structures.

Locally, sloshing pressures are uniform, so that the assumption of the fundamental mode of vibration as the deformation pattern is valid for structural components in the tank. Thus, the approach used for the analysis of ship tanks will be to compute a dynamic load factor (DLF) for structural elements, which is based upon the fundamental period of the structure and the worst case pressure-time history. A static analysis of the structure is then performed using the peak load multiplied by DLF.

To apply this approach, one must be able to compute the fundamental frequency of the component being analyzed, establish the maximum DLF to be expected from the sloshing pressures (using the fundamental period), determine the peak value of the sloshing pressure or load, and perform a static analysis of the structural component for the design loading, i.e., (Peak sloshing pressure) x DLF. Procedures for computing structural frequencies and establishing the DLF are given in the next section. Guidelines are also given for the analysis of the structure.

V.2 Design Procedures

V.2.1 Dynamic Load Factors

Measurements of rise and decay times for sloshing pressure, as reported in Section IV.4, showed no consistent relationship between the rise time, decay time, and peak pressure. Thus, it was not possible to establish correlations which might show that maximum sloshing pressures are associated with the minimum rise times or that the opposite is true. Likewise, no relationship could be established between peak pressure and decay time or between rise time and decay time. Thus, a complete range of values must be considered if the worst case loading for any particular structure is to be obtained.

The wave form for typical sloshing pressures is shown in Figure IV-5, Section IV.4, and the ranges of values for pressure and time are given in Tables IV-12 and IV-13 and in Appendix B. These values are in nondimensional form. To better understand the range of pressures and times, maximum, minimum, and average values were extracted from Tables IV-12 and IV-13 and B-13 through B-24. These values are given in Table V-1, both in nondimensional form and for an LNG tank which is 36 m (118 ft) long. This length is typical of prismatic tanks in today's LNG ships.

TABLE V-1. RANGE OF PARAMETERS WHICH DESCRIBE
SLOSHING PRESSURES IN LNG TANKS

Slosh Wave Parameters (See Fig. IV-5)	Nondimensional			36 m (118-ft) Ship Tank		
	Min.	Avg.	Max.	Min.	Avg.	Max.
T ₂ [*]	0.0005	0.1677	0.7583	0.0010	0.3213	1.4523
P ₂ ^{**}	0.0297	7.0008	33.7277	0.0700	16.4660	79.3280
T ₃	0.0350	0.3139	0.9489	0.0670	0.6012	1.8173
P ₃	0.0000	0.5989	2.2346	0	1.4090	5.2560
T ₄	0.0548	0.8491	1.4716	0.1050	1.6262	2.8184
P ₄	0.0000	0.2719	1.5348	0	0.6400	3.6100
T ₅	0.1642	1.3582	2.0900	0.3145	2.6012	4.0028
P ₅	0.0000	0.0006	0.3310	0	0.0010	0.7790

* Nondimensional times are $T\sqrt{g/l}$; dimensional times are in seconds.

** Nondimensional pressures are $P/\rho g l \phi$. For the 36 m (118-ft) tank, pressures are in psi per 0.1 radian of excitation amplitude ϕ . Multiply by 0.006895 to obtain pressure in MPa (N/mm^2).

In the discussions which follow, scaled times for the "typical" 36 m (118-ft) LNG tank will be used. For different tank sizes, the times will scale by the square root of the tank length ratio, increasing for larger tanks and decreasing for smaller tanks. These discussions lead to a method for determining the dynamic load factors which is applicable to tanks of any size.

Note from Table V-1 that the rise times, T_2 , vary from a minimum of 0.001 sec to a maximum of 1.4523 sec and that the decay times, T_3 , for the pressure spike vary from 0.601 to 1.817 sec. Also, the "trailing pressure" (P_3 and P_4) is usually much lower than the pressure spike and lasts for several seconds. Typical structures in LNG tanks have fundamental periods of less than 50 ms; thus, they will be excited by the pressure spike. The trailing pressure will act as a static load and, having a much lower magnitude than the pressure spike, will be a much less severe load. Thus, the trailing pressure is neglected in the analysis.

Generally, the worst case sloshing load for a structural component is one which has the following properties:

- (1) highest pressure
- (2) shortest rise time
- (3) longest duration

For example, if the rise time is zero and the duration is long relative to the fundamental period of the structure, then the loading will closely approximate a step function which gives a dynamic load factor of 2.0. This is seen in Figure C-2 (Appendix C) for the constant load with finite rise time (when the rise time goes to zero) and for the square and triangular force pulses (with zero rise time) when their duration is long.

A good approximation for the worst case loading is then to combine the shortest rise time with the longest decay time. Figure V-1 shows such an approximation for the pressure spike at resonant sloshing. The rise time of 1.0 ms is based on the shortest nondimensional value from laboratory tests, and the time to decay of 1000 ms is a reasonable worst case value. Longer durations were recorded but most were shorter, and, for structural components with fundamental periods of 50 ms and less, the differences in structural responses for decay times of 250, 500, or 1000 ms are insignificant. This will be demonstrated.

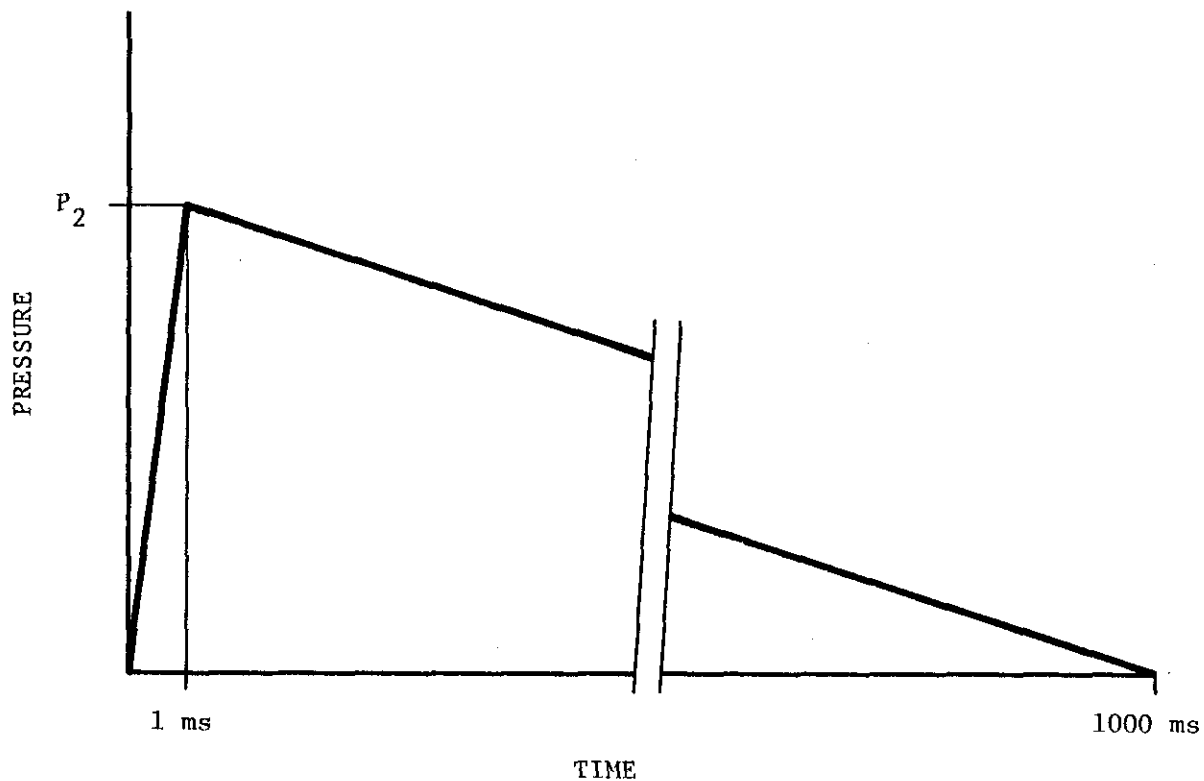


FIGURE V-1. SLOSHING PRESSURE WITH MINIMUM RISE TIME AND LONG DURATION FOR 36 m (118-ft) LONG TANK

For the pressure-time history of Figure V-1, the DLF computed for a one-dof system is given in Figure V-2. This dynamic load factor was found by computing the maximum transient response of a one-dof system to a force produced by the $P(T)$ in Figure V-1. The maximum transient deformation, divided by the deformation produced by the same force applied statically, gives the DLF. Stiffness of the spring-mass system was varied to vary the periods. It covers fundamental periods of vibration from 0.5 ms to 28 ms. Note that the DLF has a maximum value of about 2.0 (1.97) and drops to 1.0 (no dynamic effect) at 1.0 ms and 0.50 ms. These periods are whole multiples of the rise time, and the structure responds as though the load were applied statically.

Because the rise times vary in every sloshing cycle, multiple rise times must be considered to obtain the worst case for each frequency (each structural component); that is, a structure with a fundamental period of 1.0 ms would not be designed for a DLF of 1.0 because a slightly longer or shorter rise time would produce greater response. If the DLF is computed for several different rise times, the envelope of Figure V-3 is obtained. Curves for two different rise times are shown for illustration. The straight lines connecting the tops of the curves for all different rise times greater than 1.0 ms form the top of the envelope. These intersect the DLF curve for $t_r = 1.0$ ms because it was the minimum rise time considered.

The effect of shorter decay times is shown in Figure V-4. All curves were calculated for a rise time of 1 ms. The curve for a decay time of 1000 ms is repeated from Figure V-2 and compared with decay times of 250 ms and 500 ms. Maximum amplification occurs for the longest rise times as expected, but differences are small. Thus, by using the envelope of Figure V-3 for fundamental periods of less than or equal to 1.2 ms and the curves of Figure V-2 for periods greater than 1.2 ms, the DLF is found for the worst case combination of rise and decay times. Of course, the peak pressure is obtained from data presented in Section III.

The above results are strictly correct only for a tank which is 36 m (118 ft) long. For longer tanks, the values of DLF will be slightly conservative because the rise time will not be as short and decay times greater than 1000 ms will have very little effect on the DLF for structural periods of 50 ms and below. For smaller tanks, the results could be unconservative because the rise times will be shorter.

The envelope of the DLF, corresponding to Figures V-2 and V-3, can be reproduced for any tank size using the data in Appendix C if the approximation is made that the decay time of the sloshing pressures is infinite. Because the maximum decay times are long relative to the structural period of interest in LNG tankers, this assumption is very reasonable and gives a slightly conservative result.

To establish the envelope of DLF for a tank of a particular size, Figure C-3(b), Appendix C, is used. This graph gives $(DLF)_{max}$ as a function of the rise time, t_r , and the structural period, T . A three-step procedure is required:

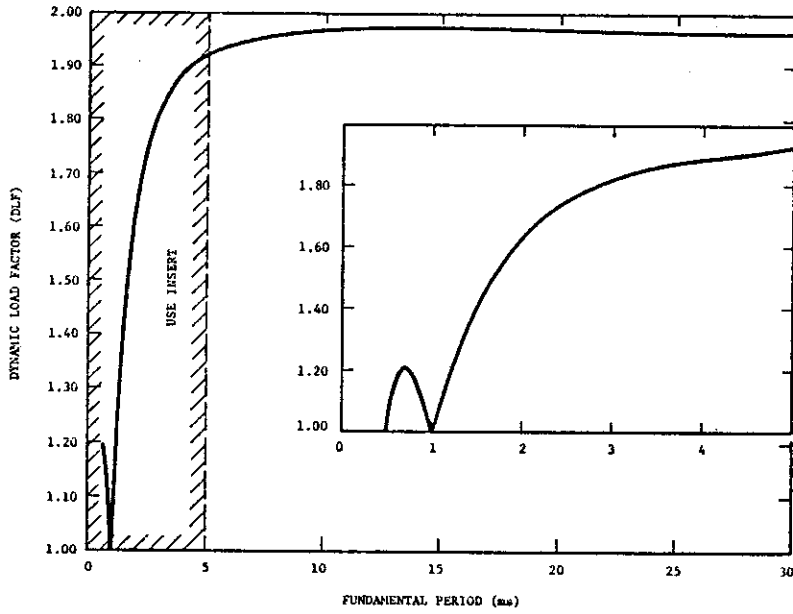


FIGURE V-2. DYNAMIC LOAD FACTOR FOR P(T) OF FIGURE V-1

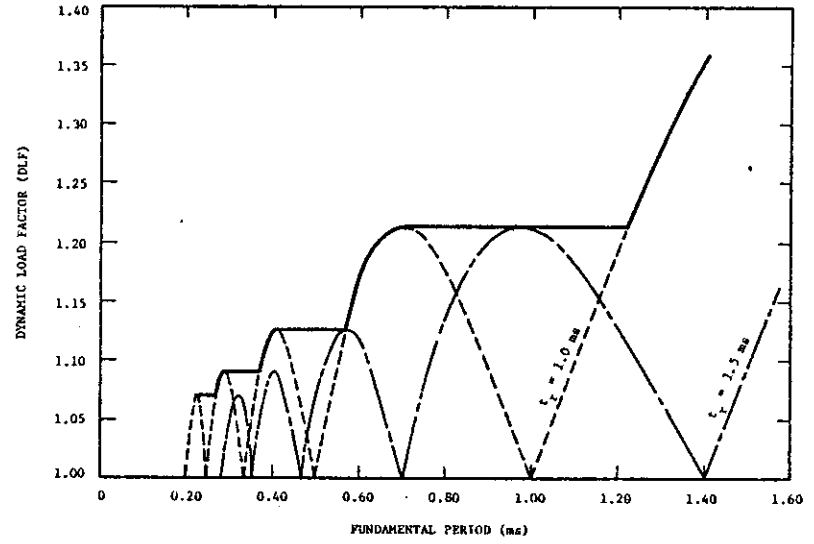


FIGURE V-3. ENVELOPE FOR DIFFERENT RISE TIMES

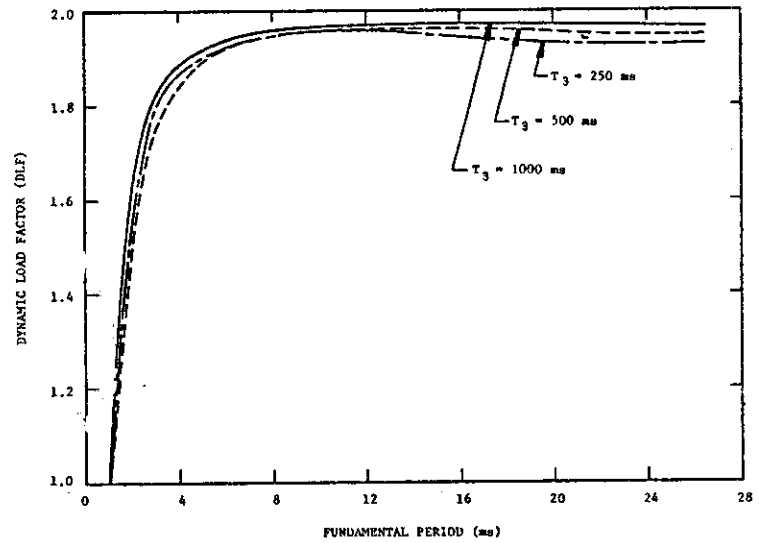


FIGURE V-4. EFFECT OF DIFFERENT LOAD DECAY TIMES, T_3

- (1) Determine the minimum rise time, t_r , using the minimum value of the nondimensional time $T_2 \sqrt{g/l}$ in Table V-1 and the tank length.
- (2) Establish a range of values of T depending upon the range of structural periods of interest, e.g., $0.5 \text{ ms} \leq T \leq 30 \text{ ms}$ as in Figure V-2.
- (3) Determine the value of $(DLF)_{\max}$ for each value of T by entering Figure C-2(b) for the corresponding values of t_r/T and taking the maximum value of $(DLF)_{\max}$ for all t_r/T greater than or equal to the value used to enter the figure.

Table V-2 illustrates this procedure for the 36-m (118-ft) tank. Note that closely spaced periods, T , are used in some regions to better define the curve. The values of DLF in Table V-2 are very nearly the same as those given by Figures V-2 and V-3.

It is not necessary to establish the envelope of DLF for each tank type. For each structural component analyzed, the appropriate value of DLF can be read directly from Figure C-2(b) for the value of t_r calculated for the tank size and T calculated for the structural component. As for Step 3 in the determination of the envelope, the maximum value of DLF is selected for all $t_r/T \geq$ the calculated value. The maximum DLF is selected for all $t_r/T \geq$ (the value used to enter the figure) to account for the fact that rise times can be greater, but not smaller, than the minimum value used to enter the figure.

V.2.2 Frequency Calculations

From the review of LNG tank structural details in Section III.3, it is clear that several different types of structural elements are subjected to sloshing pressures. These include:

- o beams
- plates
 - isotropic
 - orthotropic
- o stiffened panels
 - uniaxial stiffening
 - biaxial stiffening
- o compression members

In addition, the elements are often submerged in liquid on one side, and added mass effects of the liquid will alter natural frequencies. Also, non-structural material, such as insulation, is often attached to the wall of a tank, and this mass must be included in frequency calculations.

TABLE V-2. CALCULATION OF ENVELOPE OF DLF
USING FIGURE C-2(b)

t_r/T^*	T (ms)	DLF from Figure C-2(b)
0.0625	16.00	1.990
0.1250	8.00	1.970
0.2500	4.00	1.900
0.5000	2.00	1.640
0.7500	1.33	1.300
0.8100	1.23	1.215
1.0000	1.00	1.215
1.2500	0.800	1.215
1.4000	0.710	1.215
1.5000	0.670	1.210
1.7500	0.570	1.130
2.0000	0.500	1.130
2.2500	0.440	1.130
2.4500	0.410	1.130
2.6500	0.380	1.100
2.7000	0.370	1.090
3.0000	0.330	1.090
3.2500	0.310	1.090
3.5000	0.290	1.090

* Minimum T_2 (t_r) for 36 m (118-ft) tank is

$$T_2 = t_r = 0.0005 \sqrt{\frac{118}{32.17}} = 0.000958 \approx 0.001 \text{ sec}$$

Frequency formulas for uniform beams in bending and for axial members are common in textbooks on structural vibrations and will not be included here. Formulas for orthotropic plates and stiffened panels are less readily available, and methods for computing frequencies of these elements are given in the following paragraphs. The equation for orthotropic plates reduces to that for isotropic plates when isotropic material properties are used. In addition to the plate-panel formulas, a formula for beams in which shear is significant is included. Plates with stiffeners can often be analyzed as a beam which includes one of the stiffeners and part of the stiffened plate.

The formulas presented for stiffened panels are for uniform spacing of uniform stiffeners. For non-uniform panels and girders, more general numerical procedures are needed. Finite-element methods are very well adapted to the analysis of complicated geometries. Many other methods have also been developed specifically for stiffened panels and grillages. See, for example, the work of Smith,⁽⁸⁷⁾ Madsen,⁽⁸⁸⁾ Chang,⁽⁸⁹⁾ Chang and Michelson,⁽⁹⁰⁾ and Chang and Pilkey.⁽⁹¹⁾

V.2.2.1 Orthotropic Plates (Reference 92)

Frequency equation:

$$f = \frac{1}{2\pi} \sqrt{\frac{1}{\rho h} \left(\frac{A^4 D_x}{a^4} + \frac{B^4 D_y}{b^4} + \frac{2CD_{xy}}{a^2 b^2} \right)}, \text{ HZ} \quad (\text{V-1})$$

where ρ = plate material density
 a = long dimension of the plate (x-direction)
 b = short dimension of the plate (y-direction)

$$D_x = \frac{E_x h^3}{12(1 - \nu_x \nu_y)} \quad (\text{V-2a})$$

$$D_y = \frac{E_y h^3}{12(1 - \nu_x \nu_y)} \quad (\text{V-2b})$$

$$D_{xy} = D_x \nu_y + \frac{Gh^3}{6} \quad (\text{V-2c})$$

where

- h = plate thickness
- ν = Poisson's ratio
- E_x, E_y = elastic moduli parallel to x and y axes, respectively
- G = shear modulus

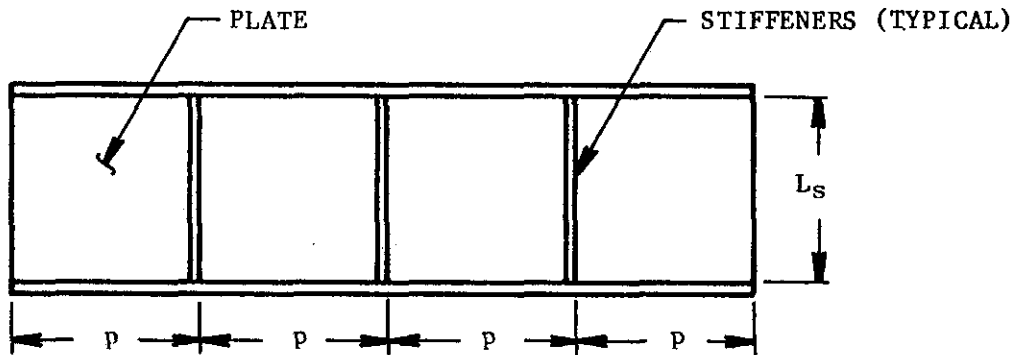
The constants A, B, and C are given in Table V-3 for different boundary conditions.

V.2.2.2 Panels Stiffened in One Direction (Reference 93)

Frequency equation:

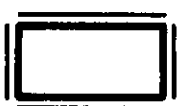
$$f = \frac{A'}{L_s^2} \sqrt{\frac{E}{\rho} \left(B' \frac{I}{S} + C' \frac{L_s h^2}{n_s p} \right)} \text{ HZ} \quad (V-3)$$

Panel geometry and definition of terms:



- E = material elastic modulus
- ρ = material density
- h = plate thickness
- I = second moment of area of stiffener and associated plate
- S = sectional area of stiffener and associated plate = $A_s + p h$
- A_s = sectional area of stiffener
- n_s = number of stiffeners

TABLE V-3. FREQUENCY COEFFICIENTS FOR THE FUNDAMENTAL MODE (EQUATION V-1)

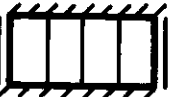
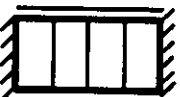
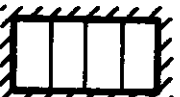
CASE NO.	BOUNDARY CONDITIONS*	A	B	C
1		4.730	4.730	151.300
2		4.730	3.927	141.379
3		4.730	π	121.396
4		3.927	3.927	132.118
5		3.927	π	113.444
6		π	π	97.409

*  FIXED BOUNDARY

 SIMPLY SUPPORTED BOUNDARY

The constants A' , B' , C' are defined in Table V-4.

TABLE V-4. VALUES OF CONSTANTS A' , B' , C'

CASE NO.	BOUNDARY CONDITIONS	A'	B'	C'
1		1.5764	1.00	0.0833
2		1.5764	2.25	0.0833
3		1.5764	1.00	0.1875
4		1.5764	4.85	0.0833
5		1.5764	1.00	0.4042
6		3.4642	1.00	0.0833

The effect of submergence is described in Section V.2.2.5. To account for uniformly distributed added mass, such as insulation bonded to the panel, adjust the density ρ as follows.

$$\rho' = \rho \cdot \frac{W_A + W_P}{W_P} \quad (V-4)$$

where W_P = total mass or weight of the panel

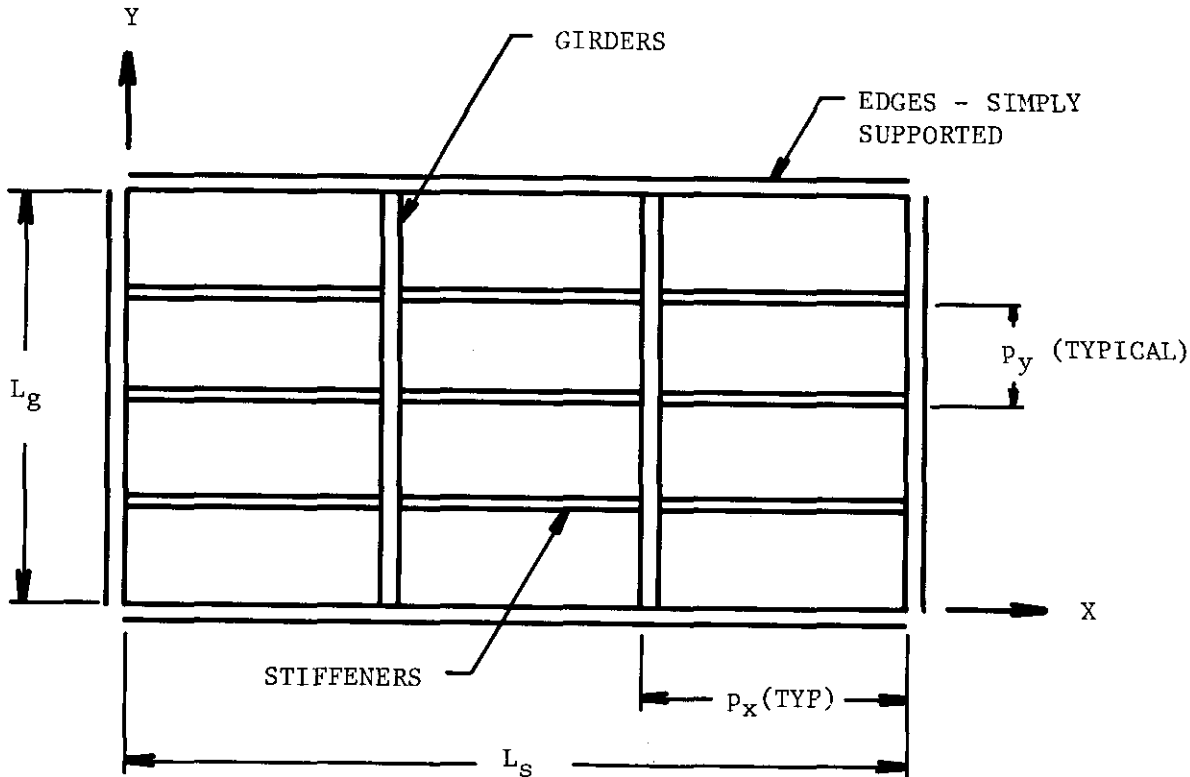
W_A = total mass or weight, in excess of the panel structure, but which moves with the panel during vibration

V.2.2.3 Panels Stiffened in Both Directions (Reference 93)

Frequency equation:

$$f = 1.5764 \sqrt{\frac{E}{\rho} \left(\frac{I_g}{L_g^4 S_g} + \frac{I_s}{L_s^4 S_s} \right)}, \text{ Hz} \quad (V-5)$$

Geometry and definition of terms:



- n_s = number of stiffeners (parallel to the x-direction)
 m_s = number of girders (parallel to the y-direction)
 h = plate thickness
 I_s, I_g = second moment of area of stiffeners and girders, respectively, plus the associated plating
 A_s, A_g = cross-sectional area of stiffeners and girders, respectively

$$S_s = A_s + p_x h + \frac{p_x \cdot h}{m_s} \quad (\text{V-6a})$$

$$S_g = A_g + p_y h + \frac{p_y \cdot h}{n_s} \quad (\text{V-6b})$$

Corrections for added mass effects associated with submersion in a fluid are given in Section V.2.2.5. Account for a uniformly distributed mass, such as insulation which is attached to the panel, by adjusting the panel thickness e in the equation for S_s and S_g .

V.2.2.4 Beam Formula for Plate Stiffener (Reference 87)

Frequency formula for the fundamental mode (assumes simple support of the stiffener):

$$f = \frac{\pi}{2L^2} \sqrt{\frac{EI}{m_B \left(1 + \frac{\pi^2 EI}{L^2 GA} \right)}}, \text{ HZ} \quad (\text{V-7})$$

where EI = flexural rigidity of the plate-stiffener combination

GA = shear rigidity of the plate-stiffener combination

L = beam length

m_a = mass per unit length of the stiffener and associated plating

V.2.2.5 Effect of Submergence (Reference 93)

To obtain the frequency, f_a , of a plate with one side exposed to air and the other side exposed to a liquid, modify the frequency calculated in air, f_a , by the following formula:

$$f_{\ell} = f_a \cdot \psi \quad (V-8)$$

$$\text{where } \psi = \sqrt{\frac{K}{K + \rho_{\ell}/\rho_p}} \quad (V-9)$$

$$K = \pi h \sqrt{\frac{1}{a^2} + \frac{1}{b^2}} \quad (V-10)$$

ρ_{ℓ} = density of the liquid

ρ_p = density of the plate

a = plate length

b = plate breadth

h = plate thickness

With both sides of the plate submerged, ψ becomes

$$\psi = \sqrt{\frac{K}{K + 2\rho_{\ell}/\rho_p}}$$

V.2.3 Response Calculations

In Section V.2.2, methods are presented for calculating the fundamental frequencies of typical structural components in the walls of LNG tanks. These components include beams, plates, and stiffened panels. Based upon the fundamental frequency and the minimum rise time of the sloshing forces, a method is given in Section V.2.1 for determining the maximum dynamic load factor (DLF) of the structural components. The DLF plus the maximum value of the sloshing forces (sloshing pressure multiplied by the appropriate area over which it acts) gives an equivalent static load for which the structural component must be designed to withstand the worst case sloshing forces. These analyses will be performed for structural elements such as beams, plates, and stiffened panels.

No particular guidance is necessary for the analysis of these components; however, coupling between structural components can and does occur in complex structures such as the wall of an LNG tank. For these cases, the analyst must decide whether or not the various components of the tank wall can be analyzed individually or should be analyzed as a multi-degree of freedom system. If each component in the tank structure is to be analyzed individually, then it is usually conservative to assume rigid support for each element (neglecting flexibility in the supporting structure) and that the sloshing forces are transferred, undistorted, from one member to the next. Often the response is attenuated by coupling, but it can be increased as well.

To resolve such questions which arise when applying simple analytical procedures, a multi-degree of freedom solution is required. These can be obtained by finite-element method or by similar procedures. If a transient response calculation is made, then the actual $F(t)$ produced by the sloshing pressure is applied to the structure. To be certain that the maximum response is obtained, the calculation must be performed with the minimum rise time and with several rise times of longer duration. Such an analysis procedure can be quite costly to perform, if many dynamic dof's are included in the calculation.

An alternate approach, which avoids a dynamic transient solution is to perform an approximate modal analysis using the dynamic load factor determined for a one-dof system (as already described). This method is possible because in a modal superposition analysis, each normal mode responds to the loading independently as a single degree of freedom system. The general procedure is as follows:

- (1) Calculate the mode shapes and frequencies of the multi-degree of freedom model of the structure.
- (2) Calculate the modal displacements and stresses for the peak sloshing force (statically applied).
- (3) Find the dynamic load factors for each mode (each modal frequency) for the minimum rise time. Figure C-2(b) is used and the values of DLF are read at the corresponding values of t_r/T_i for $i = 1$ through N modes. Note that these are not the envelope values described in Section V.2.1.
- (4) Multiply the modal displacement and stresses by their respective DLF's.
- (5) To find the absolute maximum displacement, sum the modal contributions. To find the most probable response, take the square root of the sum of the squares of the modal contributions.

This procedure should be repeated for several longer rise times to be certain that the worst case loading is used. Alternately, a conservative value can be obtained if in Step (3) values of DLF for each mode are read from an envelope of DLF established for the tank.

This approximate procedure for calculating the response of a structure to dynamic loading without performing a transient solution is commonly used in the nuclear industry⁽⁹⁴⁾ for earthquake excitation. A more detailed explanation of the method is given by Biggs.⁽⁷⁹⁾

VI. TASK 4 - PRESENTATION OF RESULTS - DESIGN METHODOLOGY

This chapter presents the methodology for designing LNG ship tanks to withstand slosh loads. The procedures are based on the experimental and analytical studies described in Chapters III - V.

VI.1 Current IMCO Requirements and Proposed Changes

VI.1.1 General

Unified Rules for Gas Tankers: Cargo Containment, as published by IMCO, uses the following classification for LNG tanks:

- Integral
- Membrane (see Figure II-2(a))
- Semi-membrane
- Independent

Type A

Type B

Type C (pressure tanks) (see Figure II-2(b))

Appendix E includes definitions for all of the above mentioned task classifications. With the exception of Type C independent tanks, all tanks must be analyzed for local sloshing pressures as defined in Section VI.2.2.2. For integral, membrane and semi-membrane tanks, the local sloshing forces must be accounted for in the design of the insulation, and the ship supporting structure must be checked for adequate strength. Local sloshing pressures are produced on the longitudinal bulkheads, transverse bulkheads, and on the tank top. Areas of the tank which must be checked for sloshing pressures will depend upon permissible filling depths. In addition to the localized sloshing pressures, the support attachments for all independent tanks must be checked for the resultant of the sloshing forces. Dynamic effects of these forces must be accounted for.

Where tanks or the ship's hull has been designed in accordance with the rules and formulas of the classification societies, then the resulting scantlings must be checked for the slosh-induced forces and increased as necessary. This is true for integral, membrane, semi-membrane, and Type A independent tanks. In Type B independent tanks, which are analyzed by refined analytical methods, the slosh-induced forces must be included in these analyses, as described in Section V.

Inadequate information is available to determine the phasing of the slosh-induced force with other dynamic forces. Thus, stresses produced by sloshing are assumed to be independent of other dynamic loads and so are combined with them, taking the square root of the sum of the squares. It

should be noted that stresses produced by sloshing forces add directly to stresses produced by vapor pressure, stationary thermal loads, and other static loads which affect the tank, but they are not combined with them.

VI.1.2 Specific Requirements

Specific requirements for the design of LNG tanks to resist sloshing forces are offered which fit within the framework of the IMCO rules. The following revisions and/or additions to the rules are suggested.

IMCO Para. 4.3.5 Sloshing Loads: Revise Paragraph (a) to read: The risk of significant loads due to sloshing induced by any of the ship motions mentioned in 2.4.6 must be considered for all filling levels less than 100% full.

IMCO Para. 4.4.1 Integral Tanks: Add Paragraph (b): If significant sloshing induced forces are found to occur in the tanks according to 4.3.5, then ship hull scantlings in the transverse and longitudinal bulkheads and in the tank top must be checked for the slosh-induced forces and the scantlings increased as necessary. Dynamic effects of the sloshing forces are to be considered.

IMCO Para. 4.4.2 Membrane Tanks: Revise (d) to read: Special attention is to be paid to the possible collapse of the membrane and the insulation due to an over-pressure in the interbarrier space, to a possible vacuum in the cargo tank, to the sloshing effects, and to hull vibration effects.

Add Paragraph (f): Special consideration must be given to the effect of sloshing forces on the ship hull as in 4.4.1.

IMCO Para. 4.4.4 Independent Tanks Type A: Add Paragraph (c): If significant slosh-induced forces are found to occur in the tank according to 4.3.5, then ship hull scantlings in the tank walls, roof, and intermediate bulkheads must be checked for the slosh-induced forces and the scantlings increased as necessary. Dynamic effects of the sloshing forces are to be considered.

IMCO Para. 4.6 Supports: Add Paragraph 4.6.8: Supports for independent tanks must be analyzed for the resultant forces produced by sloshing motions in the tank. Stresses produced by the dynamic sloshing forces should be combined with the wave-induced loads of 4.6.3 according to 4.5.1 for independent dynamic stresses.

The IMCO paragraphs referenced above are from the IMCO rules dated 1976.

VI.2 Design Methodology

A design methodology is presented in flow-chart format in Table VI.1. The design procedure is shown to vary with tank type, i.e., independent pressure tanks (IMCO type C), independent gravity tanks (IMCO types A & B), and membranes and semi-membrane tanks. For all tanks, the design sequence proceeds from (1) comparing ship periods to predicted resonant slosh periods to (2) establishing loads based on sloshing pressure and force coefficients to (3) designing structures by specific delineated methods which vary with tank type.

Each important block in the design sequence is coded on Table VI.1. A description of the procedures for each coded block is given below.

VI.2.1 Loads Prediction Methodology

Resonant Slosh Periods - TR

Resonant sloshing periods, which are a function of tank geometry and fill depth, are determined by the appropriate equation given in Table III-2. If partial filling is allowed, then T_r should be determined for fill depths between 10% and 98%. Slosh periods considering both the tank length (l) and breadth (b) must be determined for this range of fill depths. If partial filling is prohibited, resonant periods should be determined for fill depths from 90 to 98%. It is important that these fill depths be considered even when partial filling is prohibited since boil-off results in LNG typically being carried in this filling range.

Ship Periods - TS

Using standard practices, ship periods in roll, pitch, and surge should be determined for comparison with the resonant sloshing periods. In the event of overlap between ship periods and resonant sloshing periods, either partial filling (less than about 98% full) must be prohibited or the tank must be designed to withstand slosh loads.

Design Pressure Coefficients - KP

Several methods exist for establishing design pressure coefficients. Based on the results given in this report, the maximum pressure coefficient is $K_{p_{MAX}} = 125$. The average pressure coefficient is $K_{p_{AVG}} = 25$. A conservative approach would be to assume $K_{p_{MAX}}$ and base all subsequent design analysis on this worst case pressure. An alternate approach would be to adopt the techniques presented in Reference 44. In this reference, a probabilistic procedure, involving the response of the liquid in the tank at different conditions and the probability of these operating conditions occurring, is undertaken. Although there is insufficient detail in Reference 44 to include a complete example of how peak sloshing pressures are computed using the probabilistic procedure, the major steps can be identified.

The procedure utilizes a statistical distribution of pressures obtained from scale model experiments and couples this statistical definition

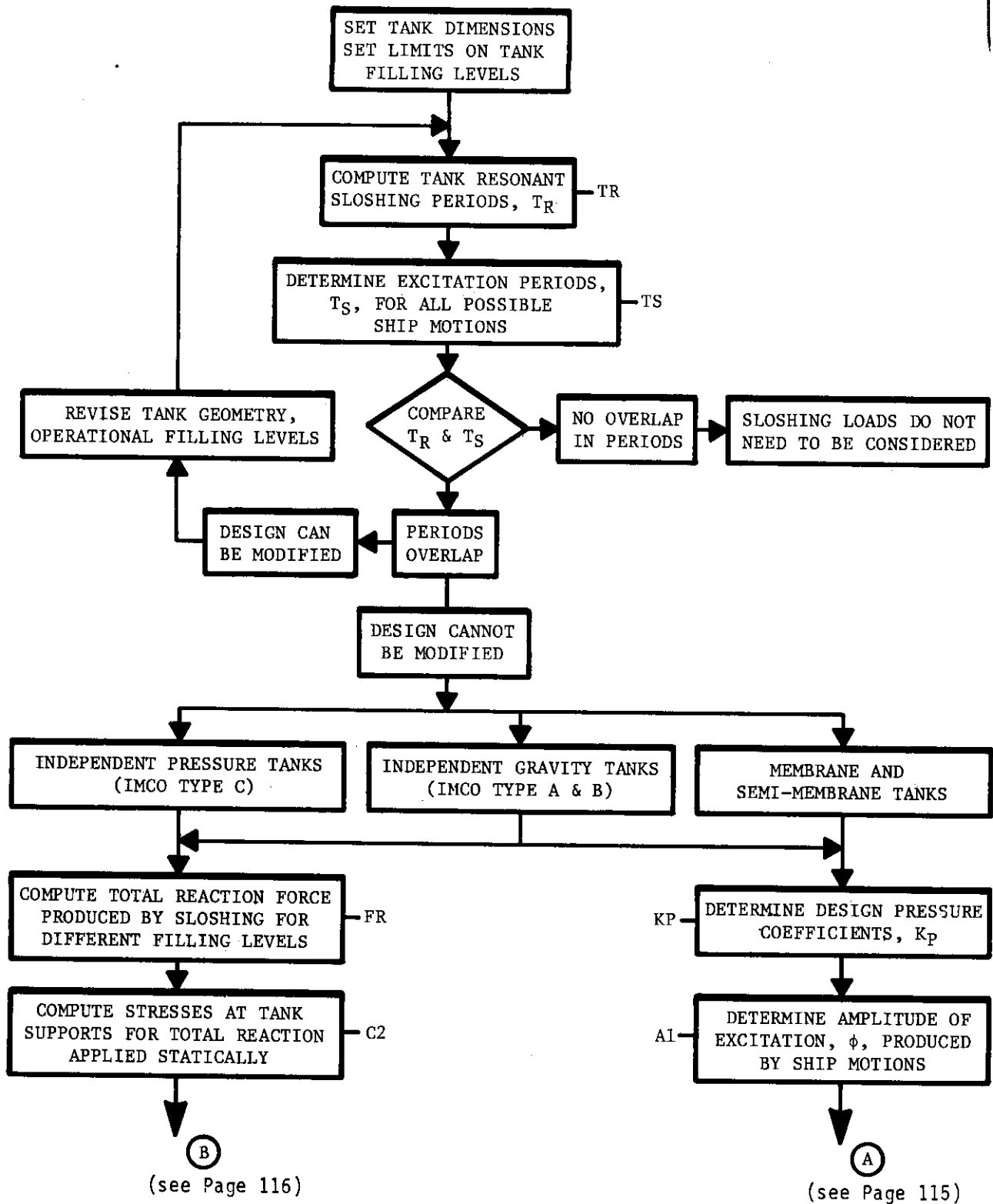


TABLE VI-1 DESIGN METHODOLOGY FLOW CHART

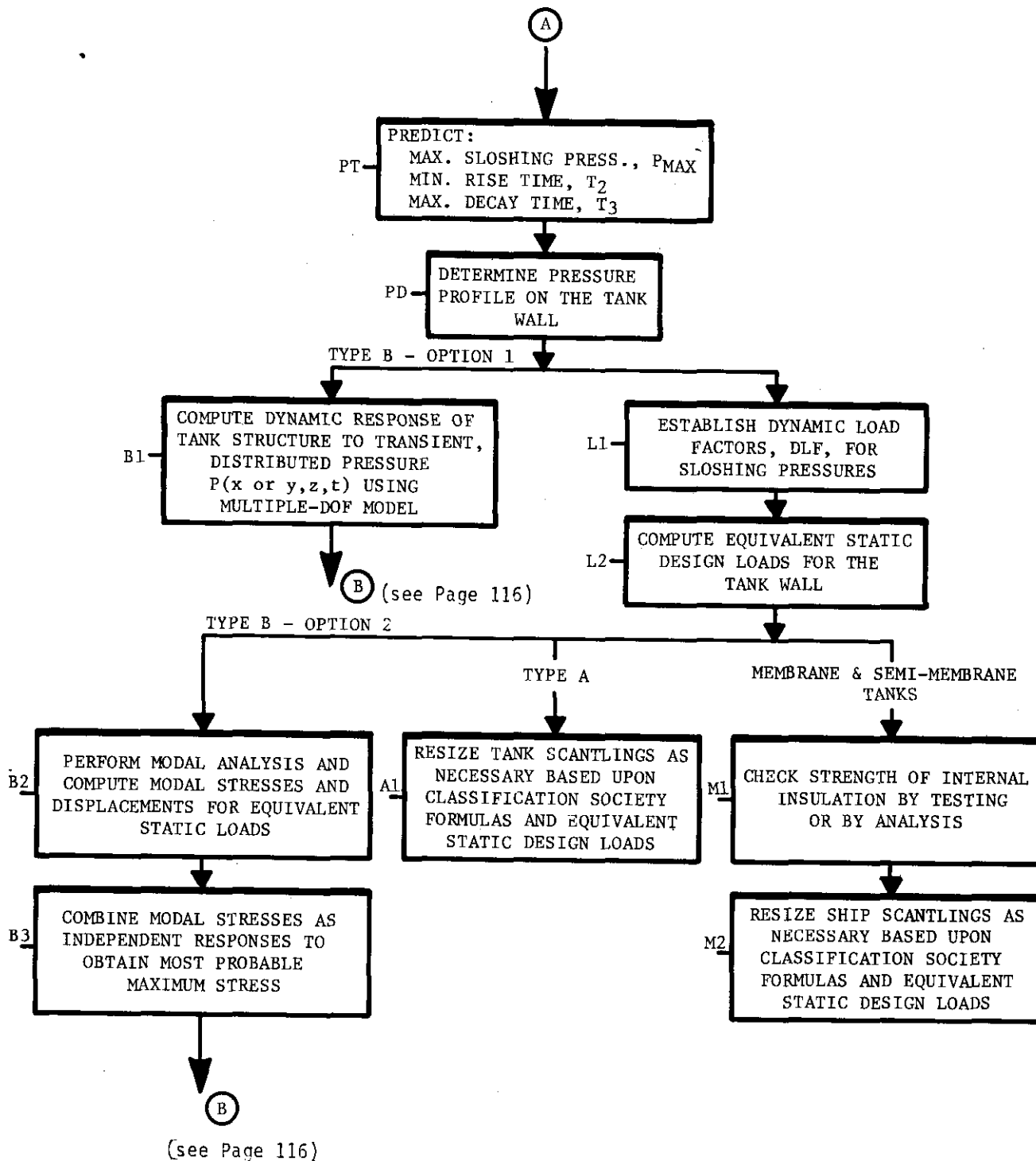


TABLE VI-1 DESIGN METHODOLOGY FLOW CHART (CONTD.)

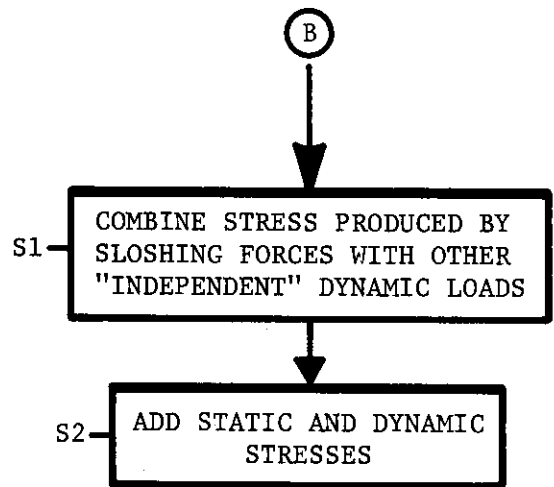


TABLE VI-1 DESIGN METHODOLOGY FLOW CHART (CONTD.)

of pressure distributions with information on ship motion spectral density in the frequency ranges around the resonant slosh frequencies. Using statistical techniques, this procedure then determines the worst case sloshing loads that are likely to occur in a 20-year operational period. Pressure coefficients greater or less than $K_p = 125$ may be predicted statistically depending on the actual conditions encountered. Based on the results reported herein, it is recommended that tank designers use a K_p equal to 125 or the statistical approach of Reference 44. A $K_{p_{MAX}} = 125$ is believed to be a highly conservative number, and its use would preclude the use of a more complicated procedure which is based on probabilistic conditions.

Ship Motion Amplitude - A1

To determine pressure magnitudes, the amplitudes in each of the important degrees of freedom must be established. Maximum amplitudes will result in setting maximum anticipated pressures for design purposes. Maximum amplitudes should be considered for roll, pitch, and surge.

Sloshing Pressures - PT

Sloshing pressures are determined from the pressure coefficient and amplitude information established above. Pressures should be predicted for each of the appropriate tank walls, whereby the appropriate length dimension, l or b , is utilized. The following values of the pressure coefficients should be used depending on the amplitude.

$$K'_p = K_p \quad x/l \text{ or } \phi < 0.1 \quad (\text{VI-1})$$

$$K'_p = K_p \left(0.075 + \frac{0.0925}{\phi} \right) \quad x/l \text{ or } \phi > 0.1 \quad (\text{VI-2})$$

At low amplitude sloshing, the pressures are shown to be linear with amplitude, while at amplitudes greater than 0.1 the pressures do not increase linearly. (See Figure III-5.) Equation VI-2 uses currently available data which give the effect of amplitude on pressure coefficients and provide a more realistic definition of K_p at high amplitudes.

To determine a characteristic range of rise and decay times of the dynamic sloshing pressures, the following coefficients should be utilized. These values are taken from Table V-1.

$$\text{Minimum pressure rise time: } K_{T_2} = 0.0005$$

$$\text{Maximum pressure spike duration: } K_{T_3} = 0.9489$$

Thus, both maximum and minimum times are established for subsequent structural response calculations. Both length and breadth dimensions of the tank must be utilized for the characteristic length dimension in these equations.

Tank Wall Pressure Distribution - PD

The pressure distributions over the tank walls are important in determining the walls' responses to slosh-induced loads. The following idealized pressure distributions are for (1) vertical tank walls and (2) the tank top. The following pressure distributions have been compiled using the currently available data. Because the distributions are affected by a great many variables, these idealized distributions should be considered as conservative estimates.

For the vertical tank walls, the pressure may be considered constant in the horizontal direction. In the vertical direction, the pressure variation is described by the following cosine function. The maximum pressure occurs at the static liquid filling level and decays to zero at levels 20% above and below the static liquid level.

$$K_{P_z} = \frac{1}{2} K_{P_{MAX}} \left[1 + \cos \left(\frac{5\pi (z - h)}{H} \right) \right] \quad (VI-3)$$

where K_{P_z} = pressure coefficient at level z

$K_{P_{MAX}}$ = maximum pressure coefficient

z = distance from the tank bottom

h = liquid filling height

H = tank height

and with limits:

$$h - \frac{H}{5} \leq z \leq h + \frac{H}{5}$$

For localized areas of 4 m^2 ($2 \text{ m} \times 2 \text{ m}$) or less, the pressure can be assumed to act uniformly over the area.

For the tank top, the pressure may be assumed to be constant (the maximum value) on the corner areas. These areas should extend in from the port and starboard walls one-third of the width of the tank and from the fore and aft walls one-third of the length of the tank. The remaining top areas should be designed to withstand sloshing pressure based on $K_{P_{AVG}}$.

Total Sloshing Forces - FR

The total forces exerted on the tank bulkheads by the sloshing liquid can be determined from Figure III-6 for prismatic tanks and from Figures III-10 - III-17 for spherical tanks. It is noted that for prismatic tanks these forces represent the inertia forces that occur on the tank wall due

to resonant liquid sloshing. They do not include the forces exerted on the structure by the inertia of tank structural components. For spherical tanks, both the resultant forces (Figures III-10 and III-11) and the sloshing components (Figures III-12 through III-17) are given. The resultant forces represent the combination of static weight and inertial sloshing loads.

VI.2.2 Tank Design Methodology

Tank Support Stress - C2

The sloshing reaction force is the integral of the sloshing pressures over the tank wall area. It is produced by the motion of the liquid in the tanks and does not include the inertia of the tank structure or the weight of the liquid. As noted in block FR, some results are given for spherical tanks which include the weight of the liquid. Rise times and durations are not given, but it is safe to assume that the reaction is quasi-static for the response of the tank on its supports, and so the supports should be analyzed for the peak sloshing reaction force, statically applied. This reaction produces stress both in the tank and in the supporting structure. The structural arrangements for tank support can be very complicated, and complex multi-dof analysis procedures are often required to accurately compute the resulting stresses.

Dynamic Tank Structure Response - B1

Independent tanks, Type B, are analyzed using refined analytical techniques such as the finite-element method. One approach (Option 1) for calculating the stresses in the tank produced by sloshing pressures is to perform a dynamic transient solution for the actual pressure-time or force-time history. This calculation procedure is discussed in Section V.2.3. An analysis of this type should provide the most accurate solution to the behavior of the tank for sloshing pressures, but it can be very expensive in terms of computation time. Multiple analyses, with different loading conditions (different rise times for the sloshing pressure) are usually required to determine the worst case loading, making this approach even more costly. Thus, a more practical approach is the approximate modal analysis suggested as Option 2. (see Section V.2.3).

Dynamic Load Factors - L1

Once the minimum rise time and maximum decay time of the sloshing pressures have been determined, the dynamic load factors for a range of frequencies of the tank structure can be established. The dynamic load factors depend only upon the rise and decay times of the loading and the structural vibration periods. They are independent of the pressure magnitude. This procedure is described in detail in Section V.2.1.

Equivalent Static Design Loads - L2

From the dynamic load factors (DLF's) and the peak value of the sloshing pressures, equivalent static design loads can be determined for the tank

structure. Design static pressures are simply the peak pressure multiplied by DLF. Design forces are the design static pressures integrated over the appropriate wall area of the tank.

Modal Stress Computation - B2

An alternate approach to a dynamic transient solution for the computation of stresses in the Type B independent tank is to perform an approximate modal solution. This approach, Option 2, is based upon a multi-dof solution for modal frequencies and modal stresses produced by the peak value of the sloshing pressure, applied statically (see Section V.2.3). Frequencies, mode shapes, and static stress are less costly to obtain than a dynamic transient solution described as Option 1 and, once obtained, the solutions for stresses under different loading conditions (different rise times) are easy to obtain.

Combined Modal Stresses - B3

Once modal frequencies have been calculated, the dynamic load factors, DLF's, for each mode can be determined. Static modal stresses multiplied by the modal DLF gives the modal stress for the dynamic loading. The most probable maximum stress in the structure is then obtained by combining modal stresses by the "square root" method. This method of combining stresses assumes that modal stresses are independent. An upper limit on stress is obtained by simply adding modal values.

Set Tank Scantlings (Type A) - A1

Scantlings for Type A independent tanks are sized according to formulas of the classification society. Once the equivalent static sloshing pressures have been determined for the tank, these same formulas can be used to size or resize the scantling for the sloshing forces. Alternate methods, such as those suggested for Type B independent tanks or for the membrane insulation, are also applicable to Type A tanks. Approval to use alternate methods must be granted by the classification society.

Internal Insulation Strength - M1

Strength of the insulation which supports the membrane must be adequate for the sloshing pressures. As demonstrated in Appendix D, strength of insulation system can be well approximated by fairly simple classical methods and/or laboratory tests at the equivalent static design pressure. A combination of testing and analysis is recommended because of uncertainties in the material properties of some insulation systems. Of course, more refined analytical methods can be used, but these are recommended only if material properties of construction materials are well defined.

Set Tank Scantlings (Membranes) - M2

As for Type A independent tanks, the scantlings of the ship's inner hull are determined using formulas of the ship classification society. Once

the equivalent static sloshing pressures have been determined for the tanks, these same formulas can be used to size or resize scantlings for the sloshing forces. Alternate methods, such as those suggested for Type B independent tanks or for the membrane insulation are also applicable for Type A tanks. Approval must be granted by the society to use these alternate methods.

Combined Stresses from Sloshing and Other Dynamic Loads - S1

Insufficient information exists to determine the phasing of the slosh loads with other dynamic loads which act on the tank; thus, the resulting stresses are treated as independent with respect to stresses produced by other dynamic loads. Combination of these independent stresses to produce the most probable maximum dynamic stress is by the square-root method, which is the square root of the sum of the square of the independent values. When combining stress produced by localized sloshing pressure with other dynamic stresses, stress produced by the dynamic liquid head is omitted. Measured sloshing pressures include the dynamic liquid head. Also, because sloshing pressures occur very near the static liquid level, or above as in the case of sloshing pressure on the tank top, the liquid head is very small where sloshing pressures are highest.

Combined Static and Dynamic Stress - S2

The resulting dynamic stress is added directly to stresses produced by static loads such as thermal loads, still-water loads, vapor pressure loads, etc., to find the maximum stress for the condition being investigated.

VI.3 Example Problem Utilizing Tank Design Methodology

The following example problem illustrates the use of the tank design method presented in Table VI-1. The example analyzes a prismatic membrane tank with the Gaz Transport membrane system (plywood insulation boxes). Tank dimensions are arbitrarily set at

$$l = 36 \text{ m (118 ft)}$$

$$b = 36 \text{ m (118 ft)}$$

$$H = 24.4 \text{ m (80 ft)}$$

and tank motion amplitudes (A1) are assumed to be:

$$\phi_{\text{PitchMAX}} = \pm 5^\circ \text{ (0.087 rad.)}$$

$$\phi_{\text{RollMAX}} = \pm 10^\circ \text{ (0.175 rad.)}$$

$$\frac{x}{l} \text{ SurgeMAX} = \pm 0.1$$

Tank filling levels during operation are placed at 90 to 98%. Current regulations limit most LNG tanks to maximum operational filling levels of 97-98%, with partial filling prohibited. From Table VI-1, the initial design steps are to calculate (TR) the resonant periods of the liquid in the tank, to establish (TS) ship motion periods, and to determine if the tank resonant periods coincide with ship motion periods. For purposes of this example, the ship motion periods are assumed to be in the range of 6 to 12 seconds.

The resonant periods of the liquid in the tank are calculated using Equation III-6 for prismatic tanks. For filling levels between 90 and 98%, the resonant pitch and roll sloshing periods are:

$$6.89 \text{ sec} \leq T_R \leq 6.94 \text{ sec}$$

$$0.9 \leq h/H \leq 0.98$$

Thus, the tank excitation periods overlap the resonant periods of the tank liquid so there is the potential for resonant sloshing.

At this point, the designer can decide to modify the tank size or geometry to change the resonant periods of the liquid in the tank. In this example, the tank will remain unchanged, so it must be designed to withstand resonant sloshing conditions.

For design purposes, the maximum nondimensional pressure coefficient (KP) is 125. Equations VI-1 and VI-2 are then used to correct this coefficient for tank excitation amplitude effects. As previously mentioned, the amplitudes for this example are assumed values. The corrected coefficients for pitching, rolling, and surging motions (PT) are:

$$\text{for pitching } (\phi = \pm 5^\circ \text{ or } 0.087 \text{ rad.}): K_{P_{MAX}}' = 125.0$$

$$\text{for rolling } (\phi = \pm 10^\circ \text{ or } 0.175 \text{ rad.}): K_{P_{MAX}}' = 75.4$$

$$\text{for surging } \left(\frac{x}{\lambda} = \pm 0.1 \right): K_{P_{MAX}}' = 125.0$$

At this point, it is necessary to choose the pressure rise and duration time values (K_{T_2} and K_{T_3}) associated with the pressure-time history of the dynamic impact pressure. Using Table V-1, the minimum nondimensional rise time (K_{T_2}) is 0.0005. The maximum spike duration (K_{T_3}) is 0.9489.

Now that the nondimensional design pressures and times have been established, full scale pressures and times can be calculated. Pressures can be determined using Equation III.4. For this example, the liquid density is 493.19 kg/m^3 (30.79 lbm/ft^3). The design pressures are found to be:

$$\text{for pitching: } P_{MAX} = 1.892 \text{ N/(mm)}^2 \text{ (274.4 psi)}$$

$$\text{for rolling: } P_{MAX} = 2.295 \text{ N/(mm)}^2 \text{ (332.9 psi)}$$

for surging: $P_{MAX} = 2.175 \text{ N/(mm)}^2$ (315.4 psi)

Full-scale times are determined using Equation II-2. The minimum pressure rise time is 1.0 millisecond, and the maximum pressure spike duration is 1.82 seconds.

To compute design loads for structural components of the tank (block L1 of Table VI-1), the dynamic load factors, corresponding to the rise and decay times of the sloshing pressures, are determined for a range of structural frequencies. This was done for a tank which is 36 m (118 ft) long (or wide) in Section V.2, and the results, expressed as the envelope of the dynamic load factors (DLF), are plotted in Figures V-2 and V-3.

To determine the equivalent static design load for structural components of the tank (block L2), the fundamental vibration period of the component must be calculated. With the fundamental period known, the DLF is read directly from Figures V-2 or V-3. These steps were performed for the Gaz Transport insulation boxes and are described in detail in Appendix D, part D.1. Two components of the box were analyzed in the example: the box cover and the longitudinal stiffener of a primary box. Results for these steps are:

	Fundamental Period, T	DLF
Box Cover (12-cell box):	0.93 ms	1.22
Longitudinal Stiffeners:	1.96 ms	1.63

Equivalent static design pressures for the cover and stiffener are obtained by multiplying the peak sloshing pressures from block PT by the DLF. Using the maximum pressure, P_{MAX} , which occurs in roll for this example, the design static pressures are:

$$\begin{aligned} \text{Cover: } P_{des} &= 1.22 (2.295) = 2.80 \text{ N/mm}^2 \text{ (406 psi)} \\ \text{Stiffener: } P_{des} &= 1.63 (2.295) = 3.74 \text{ N/mm}^2 \text{ (543 psi)} \end{aligned}$$

Strength of the insulation boxes (block M1) was established in Appendix D and expressed in terms of the peak allowable sloshing pressure, P_a . This allowable pressure is the static pressure which the box component will withstand divided by DLF. The allowable pressure, P_a , would be compared with the maximum sloshing pressure, P_{MAX} , rather than the design pressure, P_{des} . To obtain a pressure for comparison with P_{des} , P_a from Appendix D is simply multiplied by DLF. From Appendix D we have

$$\begin{aligned} \text{Cover: } P_a &= 0.853 \text{ N/mm}^2 \text{ (124 psi)} \\ P_{des}^s &= 1.22 (0.853) = 1.04 \text{ N/mm}^2 \text{ (151 psi)} \end{aligned}$$

$$\text{Stiffener: } P_a = 0.778 - 0.937 \text{ N/mm}^2 \text{ (113 - 136 psi)}$$

$$P_{des}^s = 1.63 (0.770 - 0.937) = 1.268 - 1.527 \text{ N/mm}^2 \\ \text{(184 - 222 psi)}$$

where P_{des}^s denotes the design static strength of the component. Comparing these values to P_{des} computed in block L2, we find

$$\text{Cover: } P_{des}^s = 1.04 \text{ N/mm}^2 \text{ (151 psi)} < P_{des} = 2.80 \text{ N/mm}^2 \text{ (407 psi)}$$

$$\text{Stiffener: } P_{des}^s = 1.268 - 1.527 \text{ N/mm}^2 \text{ (184 - 222 psi)} < P_{des} = \\ 3.74 \text{ N/mm}^2 \text{ (543 psi)}$$

Thus, for this example, the design strength of the insulation is inadequate. In this example, only the primary insulation box was analyzed for the sloshing pressures. Of course, in practice the designer would need to check the strength of the secondary box as well.

The final step (block M2) in evaluating membrane tanks for sloshing pressures is to check the strength of the ship's inner hull which supports the membrane system. Scantlings of the hull are checked using formulas of the classification societies and the equivalent static design load. In this example we did not apply classification society formulas to check hull strength; however, alternate methods of analysis are applicable, but approval of the classification society must be obtained before alternate procedures can be applied. As an example of alternate methods, see the analysis of the CONCH independent tank in part D.3 of Appendix D.

VI.4 Summary

The design methodology presented in this chapter is based on a thorough review of the literature supplemented by additional experiments and analytical studies. Since information required for many of the steps in this procedure is limited, the procedures developed herein have been based on utilizing conservative approaches. For example, pressure coefficients are based on the worst case pressure coefficients determined from a wide range of data available from the literature. Likewise, analytical methods which are based on simplified one degree of freedom analysis have been developed with conservatism imposed. Thus, utilizing these techniques, a conservative design could occur. It is believed that the major steps in the proposed design methodology are appropriate, and it is left to the individual designer to substitute more realistic loads when he believes it is appropriate. As an example, sloshing loads could be more realistically established from scale model tests on replica models of interest. Scaled ship motions could be imposed on the models at fill depths of interest and the resulting loads and load distributions determined. This would provide more accurate data relative to a specific design. However, if resonant sloshing for all filling levels were investigated, it is likely that a $K_{p_{MAX}}$, nearing the 125 value established herein, would be approached.

VII CONCLUSIONS AND RECOMMENDATIONS

As a result of the study reported herein the following conclusions and recommendations are presented.

VII.1 Summary and Conclusions

- o A significant amount of scale model sloshing data for both prismatic and spherical tanks and covering a wide range of fill depths, excitation frequencies and amplitudes, tank wall pressure measurement locations and total force measurements is available in the literature.
- o A compilation of this data and presentation in a common format has been accomplished to provide design pressure and force coefficients.
- o Because the complexity of resonant large amplitude sloshing causes a wide variation in the impact pressure magnitude on each successive sloshing cycle, both worst case and average pressure coefficients have been defined for design purposes. These pressures are assumed to potentially occur at any location on the tank wall if partial filling is allowed.
- o Pressure-time histories have been established for sloshing dynamic impact pressures. No correlation was found to exist between impact pressure magnitude and duration. A representative range of impact pressure rise times and durations were established.
- o Dynamic loads test, where predicted full-scale pressure/time histories were reproduced on representative segments of a LNG membrane tank structure, established structural response and failure characteristics. It is noted that failure occurred at simulated loads that could occur during "worst case" resonant sloshing.
- o Combined-degree-of-freedom resonant sloshing test (pitch and heave, surge and heave) produced impact pressures no greater than the corresponding pressures measured in single-degree-of-freedom resonant sloshing (at the same amplitudes).
- o Materials properties measured on plywood used in some LNG membrane structures showed considerable variation. This data is valuable in the design of tank wall structures using such materials.
- o Analytical methods were developed to predict structural response to dynamic slosh loads. Localized areas of the tank structure are treated as equivalent one degree-of-freedom systems and a dynamic load factor (DLF) is established based on the fundamental

period of the structure and a worst case pressure-time history. Examples for typical structural elements are given and show that some typical structures are not designed to withstand worst case impact loads.

- o Design methods are presented for independent pressure and gravity tanks and membrane and semi-membrane tanks. The design sequence proceeds from 1) comparing ship periods to predicted resonant slosh periods to 2) establishing loads based on loads coefficients to 3) designing structures by specific delineated methods which vary with tank type.

VII.2 Recommendations

- o Additional literature review and experiments are required to evaluate loads on liquid bulk carriers with significant tank internal structures (i.e., typical crude and chemical carriers). Emphasis should be placed on localized loads on web frames, pump columns and swash bulkheads. Total forces should also be established.
- o Full scale LNG sloshing data currently being obtained should be analyzed in light of the results reported herein. Simulated full scale ship motion conditions on scale models should be undertaken with model sloshing loads compared to full scale.
- o Additional model experiments should be conducted to further establish effects of excitation amplitude on measured pressure coefficients. Also end wall pressure distributions for a complete range of prismatic tank fill levels should be established.
- o Analytical methods and design procedures presented herein should be further refined after the above recommended work is accomplished and feedback from industry is obtained.

ACKNOWLEDGEMENTS

Many individuals and organizations assisted in the conduct of this program. Special thanks are extended to El Paso Marine Company for providing the full-scale LNG membrane tank wall segments and support information needed for this project. In addition, our sincere appreciation is expressed to the American Bureau of Shipping, Newport News Shipbuilding and Drydocking Company, General Dynamics-Quincy Division, and Avondale Shipyards for furnishing information on tank structural details and design procedures. Additional thanks are extended to Det norske Veritas, Bureau Veritas, and The Swedish Ship Research Foundation for their comments and LNG sloshing model data which were reviewed in this report.

Special thanks are extended to Mr. A. C. Rogers for his help in the design of the dynamic load simulator and to Messrs. C. M. Wood and J. R. Winfield for their work in conducting the experimental studies. Finally, this report could not have been produced without the skillful typing and figure productions of Mrs. Cathy Dean, Mrs. Adeline Raeke, and Mr. Victor Hernandez. Special thanks are extended to these individuals.

VIII. REFERENCES

1. Abramson, H. N., The Dynamic Behavior of Liquids in Moving Containers, NASA SP-106, 1966.
2. Abramson, H. N., Bass, R. L., Faltinsen, O., and Olsen, H. A., "Liquid Slosh in LNG Carriers," 10th Symposium of Naval Hydrodynamics, M.I.T., Boston, Massachusetts, June 25, 1974.
3. Baitis, A. E., et. al., "Prediction of Lifetime Extreme Accelerations for Design of LNG Cargo Tanks," Naval Ship Research and Development Center, Mar. 1974.
4. Baitis, A. E., "Summary of Development for LNG Tank Design Acceleration Rules," David W. Taylor Naval Ship Research and Development Center, Bethesda, Maryland, Dec. 1976.
5. Baitis, A. E., Bales, S. L., and Meyers, W. G., "Design Acceleration and Ship Motions for LNG Cargo Tanks," David Taylor Research and Development Center, Bethesda, Maryland.
6. Bass, R. L., "Dynamic Slosh Induced Loads on Liquid Cargo Tank Bulkheads," Society of Naval Architects and Marine Engineers, Report R-19, Aug. 1975.
7. Bass, R. L., "Liquid Impact Loads in LNG Carriers," Tech. Report No. 1, Aug. 1972, El Paso Natural Gas Co., Southwest Research Institute.
8. Bass, R. L., Hokanson, J. C., and Cox, P. A., "A Study to Obtain Verification of Liquid Natural Gas (LNG) Tank Loading Criteria," Final Technical Report SSC-258, Naval Sea Systems Command Project SR-218, May 1976.
9. Bass, R. L., and Oldham, G. A., "Liquid Impact Loads in Partially Filled Tanks of a 125,000 m³ LNG Carrier," Final Technical Report, Feb. 1975, Methane Tanker Service Co., Southwest Research Institute.
10. Bass, R. L., and Ransleben, G. E., "Scaling Criteria for Large Amplitude Sloshing in LNG Ship Cargo Tanks," Technical Report No. 2, Oct. 1974, Methane Tanker Service Co., Southwest Research Institute.
11. Blixell, A., "Calculation of Wall Pressures in a Smooth Rectangular Tank due to Movement of Liquids," Research and Technical Advisory Services Report No. 5108, Lloyd's Register of Shipping, March 1972.
12. Brathu, M. C., Huther, M., and Planeix, J. M., "Computer Calculations of Liquid Motions in Tanks," Shipping World and Shipbuilder, Dec. 1972.
13. Bureau Veritas, "Étude des Replissages Partiels dans les Cales des Navires," N.I. 171 BM.1, May 1976.

14. Bureau Veritas, "Motions of Liquids in a Short LNG Carrier Tank," BM.1-Ht/nc, Sept. 4, 1972, Gaz Transport Study AT 47, Bureau Veritas.
15. Bureau Veritas, "Motions of Liquid in a LNG Carrier Tank with Low Filling," BM.1-HT/Plx/nc, Gaz Transport Study AT 27, Bureau Veritas (Confidential Report).
16. Campus, P., and DuBois, M., "Mesure sur Modules des Sollicitations des Parois et des Plafonds de Citernes de Navires dues au Mouvement des Cargaisons Liquides," 1974, Bureau Veritas.
17. Chan, A. S. L., and Trbojevic, V. M., "Thin Shell Finite Element by the Mixed Method Formulation-Part 1."
18. Conners, Thomas G., "Update: Domestic LNG Vessel Construction," Marine Technology, Vol. 15, No. 1, Jan. 1978, pp 1-13.
19. Drake, Elizabeth and Reid, Robert C., "The Importation of Liquefied Natural Gas," Scientific American, Vol. 236, No. 4, April 1977.
20. Faltinsen, O., "A Nonlinear Theory of Sloshing in Rectangular Tanks," Journal of Ship Research, Vol. 18, No. 4, Dec. 1974.
21. Filstead, C. G., Jr., "The Design and Operation of LNG Ships with Regard to Safety," Shipping World and Shipbuilder, Vol. 165, No. 3866, pp. 259-262, Feb. 1972.
22. Gastech 76, International LNG/LPG Conference New York 1976, "For LNG-A Concrete Answer," Extracts from papers read at this important assembly.
23. Glasfeld, R. D., "Design of Spherical Shipborne LNG Cargo Tanks," presented at the Marine Technology Symposium, San Diego, Calif., 1976.
24. Hansen, R., and Rimeid, B. E., "Moss Rosenberg Verft A/S 87, 600 m³ LNG-Carrier Prediction of Loads due to Sloshing in Tanks," Report No. 72-45-C, May 19, 1972, Moss Rosenberg Verft A/S, Det norske Veritas.
25. Hansen, Hans R., "Some Aspects concerning the Design of LNG Carriers," Classification and Registry of Shipping, Information No. 10, Nov. 1972.
26. Hori, Tohru, et. al., "Observations on an Experimental LNG Carrier at Sea (Part 2)," Hitachi Shipbuilding and Engineering Co., Ltd.
27. Howard, J. L., Kvamsdal, R. S., and Naesheim, K., "Building and Operating Experience of Spherical-Tank LNG Carriers," Marine Technology, Vol. 14, No. 2, April 1977, pp. 158-174.
28. Howard, J. L., "LNG Marine Carrier Construction," Marine Technology, Vol. 9, No. 3, pp. 281-291, July 1972

29. Huther, M., Dubois, M., and Planeix, J. M., "Model Studies on the Movement of Liquid in Tanks," Marine Engineers Review, Jan. 1973.
30. Huther, M.; Olsen, H., and Thomsson, O., "Liquid Sloshing in Tanks with Internal Structures," S.S.F. project 5609 Summary Report, April 1977.
31. Hysing, Thor, and Harald Olsen, "A Mini-Study of the Spatial Distribution of Slosh Impact Pressures," Report No. 75-18-S, Det norske Veritas, Sept. 1, 1975.
32. Iino, Nobu, Kenji Sakano, Takeshi Vemura, and Yorimitsu Kobayashi, "Method of Safety Assessment on Structures Under Repeated Loading," Engineering Review, Vol. 9, No. 1, Jan. 1976,
33. Jackson, R. G., and Kotcharian, M., "Testing and Technology of Models of Integrated Tanks for LNG Carriers," First International Conference on LNG, Chicago, Ill., 1968.
34. Johnsen, K. R., and Harald Olsen, "Nonlinear Sloshing in a Rectangular Container," Vol. 2, Report No. 74-72-S, Det norske Veritas, July 24, 1975.
35. Johnsen, K. R., and Harald Olsen, "Nonlinear Sloshing in a Rectangular Container," User's Manual to the Computer Routine NVSLOSH, Report No. 74-72-S, Det norske Veritas, Jan. 22, 1975.
36. Kvamsdal, R., Ramstad, H., Bognaes, R., and Frank, H. J., "The Design of an 88,000 m³ LNG Carrier with Spherical Cargo Tanks and No Secondary Barrier," Det norske Veritas and Moss-Rosenberg Verft.
37. Lydersen, N., "Dynamic Liquid Pressure in Tanks," Report No. 69-44-S, Jan. 23, 1970, Det norske Veritas.
38. Marine Media Management, Ltd., "Sener-Crinavia LNG Carrier Production," Marine Engineers Review.
39. Mathisen, J., "Sloshing Loads due to Random Pitch Motion," Vol. 4, No. 3, Norwegian Maritime Research, 1976, Det norske Veritas.
40. Mitsui Shipbuilding and Engineering Co., Ltd., "Sloshing Test Program for Liquid Cargo Tanks," Ship Research and Development Department, Sept. 12, 1972.
41. Odland, J. R., "A Simplified Calculation of the Interaction Forces Between Hull and Tank System for a Moss Rosenberg Type LNG Carrier," No. 1, Vol. 3, Norwegian Maritime Research, 1975, Det norske Veritas.
42. Olsen, H. A., "Dynamic Stresses in Bulkhead Plating and Load on Fuel Tank Bulkhead due to Sloshing," Report No. 70-120-0, Dec. 1970, Akergruppen, Oslo, Det norske Veritas.

43. Olsen, H. A., "Slack LNG Tank Study--3 Dimensional Model. Liquid Responses Caused by Surge and Pitch Motions," Report No. 71-35-0, May 10, 1971, Kockums Mekaniska Verkstads, Det norske Veritas.
44. Olsen, H. A., and Hysing, T., "A Study of Dynamic Loads Caused by Liquid Sloshing in LNG Tanks," Report No. 74-276-C, Dec. 1974, Maritime Administration, Det norske Veritas.
45. Ordin, P. M., "Bibliography on Liquified Natural Gas Safety," Lewis Research Center, Cleveland, Ohio, April 1976.
46. Pederson, "Buckling of Spherical Cargo Tanks for Liquid Natural Gas," Transcript of RINA, 1975.
47. Pederson, "Correlation Between Experimental Buckling Loads and Theoretical Predictions for Spherical Cargo Tanks for LNG," Report No. 100, Technical University of Denmark.
48. Planeix, J-M, Huther, M., and Latché, M., "Dynamic and Stochastic Aspects in the Structural Analysis of VLCC's and ULCC's," March 4, 1974, Bureau Veritas.
49. Scarsi, Giulio, "Natural Frequencies of Viscous Liquids in Rectangular Tanks."
50. 6th International Ship Structures Congress, "Liquid Cargo Sloshing Problems," Report of Committee II.3, 1976, pp. 31-40.
51. Swenson, Erich D. and Marcelo D. Arcos, "Dynamic Loading and Fatigue Testing on LNG Carriers," Shipbuilding and Shipping Record, Jan. 29, 1971.
52. Tenge, P., "Fracture Mechanics in the Design of Large Spherical Tanks for Ship Transport of LNG," Norwegian Maritime Research, Vol. 1, No. 1, Feb. 1973.
53. Tenge, P., and Solli, O., "9 percent Nickel Steel in Large Spherical Tanks for Moss-Rosenberg 87,000 m³ LNG-Carrier," European Shipbuilding, No. 1, 1972, pp. 9-25.
54. Terai, K., and Susei, "Applied Fracture Mechanics for Designing Aluminum Alloy 5083-0 Large Spherical Tank for LNG Carriers," Proceedings of the Japan-U.S. Seminar on the Significance of Defects in Welded Structures, Tokyo, 1973.
55. Thomas, W. du Barry, and Schwendtner, A. H., "LNG Carriers: The Current State of the Art," Trans. SNAME, Vol. 79, 1971.
56. Thomas, W. D., "Whither the LNG Ship?", Royal Institute of Naval Architects, Oct. 21, 1974.

57. Tonnessen, Arne, "Spherical LNG Tanks on Continuous Cylindrical Skirts. A Shipbuilder and Licensor's Experience," Sept. 1977, Moss Rosenberg Verft. a.s., Moss, Norway.
58. Vilbo, O. R., "Dynamic Loads Upon Watertight and Swash Bulkhead in Partly Filled Tanks. A Study Made on a Set of Published Data," Report No. 72-17-S, Feb. 26, 1973, Det norske Veritas.
59. Vinje, Tor, "On Calculation of the Characteristic Frequencies of Fluid-Filled Spherical Shells," Norwegian Maritime Research, Vol. L, No. 1, Feb. 1973.
60. Yajima, H., "On the Brittle Fracture Initiation Characteristics of 9% Ni Steel for Spherical LNG Tank," Proceedings of the Japan-U.S. Seminar on the Significance of Defects in Welded Structures, Tokyo, 1973.
61. "Current Developments in Liquified Natural Gas presented at International Conference," Industrial Heating, Nov. 1977.
62. "Hassi R'Mel Algerian Owned LNG Ship," Shipping World and Shipbuilder, Vol. 165, No. 3869, pp. 571-574, May 1972.
63. "Papers from the Seminar on Liquid Sloshing," Sponsored by Det norske Veritas, May 20-21, 1976.
64. Bowles, E. B., Jr. and R. L. Bass, III, "Evaluation of Near Full Sloshing Loads in El Paso Marine Company's 125,000 m³ LNG Ship Tanks," Tech. Report No. 1, June 1978, El Paso Natural Gas Co., Southwest Research Institute (Confidential).
65. Ochi, Yoshio and Nobuyuki Kobayachi, "Sloshing Experiment of a Cylindrical Storage Tank," IHI Engineering Review, Vol. 11, No. 2, April 1978.
66. Faltinsen, O. M., "A Numerical Nonlinear Method of Sloshing in Tanks with Two-Dimensional Flow," Report No. 77-014, Jan. 12, 1977, The Royal Norwegian Council for Scientific and Industrial Research, Det norske Veritas.
67. Hagiwara, K., "On Secondary Loads on Ship Structure, Part II," June 1976, Mitsubishi Heavy Ind., Ltd., Nagasaki Tech. Inst., Japan.
68. Sawayangi, M., and Matsumoto, Y., "Experimental Study on the Sloshing Pressure of Rectangular Tanks," Mitsui Eng. and Shipbuilding Co., Ltd., Chiba Laboratory.
69. Verhagen, J., and van Wijngaarden, "Nonlinear Oscillations of Fluid in a Container," Journal of Fluid Mechanics, Vol. 22, Part 4, pp. 737-751, 1965.

70. Huther, M., H. Olsen, and O. Thomsson, "Liquid Sloshing in Tanks with Internal Structures," S.S.F. Project 5609, Main Report, April 1977.
71. Whitman, A. M., and M. C. Pancione, "A Similitude Relation for Flat Plate Hydrodynamic Impact," Journal of Ship Research, Vol. 17, No. 1, 1973.
72. Ochi, Yoshio, Osamu Asai, and Kiyoshi Naito, "Coupled Vibration of Liquid and a Cylindrical Tank," IHI Engineering Review, Vol. 11, No. 3, July 1978.
73. Asan, Seiichi, et al., "Observations on an Experimental LNG Carrier at Sea (Part 1)," Hitachi Shipbuilding and Engineering Co., Ltd.
74. Bowles, E. B., R. L. Bass, and F. T. Dodge, "Evaluation of Scaling Criteria for Scale Model Sloshing Simulations of El Paso Marine Company's 125,000 m³ LNG Ship Tanks," Technical Report No. 2, December 1978, El Paso Marine Co., Southwest Research Institute (Confidential).
75. Bowles, E. B., R. L. Bass, and P. A. Cox, "Evaluation of Near Full Sloshing Loads and Structural Response in El Paso Marine Company's 125,000 m³ LNG Ship Tanks," Technical Report No. 3, in preparation, El Paso Marine Co., Southwest Research Institute (Confidential).
76. "Dynamic Test on Plywood," Mchiba Laboratory, Technical Division, Mitsui Shipbuilding & Engineering Co., Ltd., 20 Nov. 1972.
77. "Relevés de Flexion sur Eprouvettes en Contreplaqué de Bouleau (Tranches de Ceissons)," Gaz Transport, Essai N^o 70.7, 22 May 1970.
78. "Investigation sur le Comportement au Choc des Contreplaqués a' la Température Ambiante et a' la Temperature de L'azote Liquide (-196°C)," Gaz Transport, 17 Fevrier 72, Doc. Int. N^o 101.
79. Biggs, J. M., Introduction to Structural Dynamics, McGraw-Hill Book Co., New York, 1964.
80. Army Manual TM5-1300, "Structures to Resist the Effects of Accidental Explosions," June 1969.
81. "The Air Force Manual for Design and Analysis of Hardened Structures," AFWL-TR-74-102, October 1974.
82. "Shelter Design and Analysis, Volume 4: Protective Construction for Shelters," TR-20, Review Draft, dated July 1972.
83. "Suppressive Shields Structural Design and Analysis Handbook," U.S. Army Corps of Engineers, Huntsville Division, Publication HNDM-1110-1-2, November 1977.

84. Westine, P. S., and W. E. Baker, "Energy Solutions for Predicting Deformations in Blast-Loaded Structures," Edgewood Arsenal Contractor Report EM-CR-76027, Report No. 6, November 1975.
85. Westine, P. S., and P. A. Cox, "Additional Energy Solutions for Predicting Structural Deformations," Edgewood Arsenal Contract Report EM-CR-76031, Report No. 4, Contract DAAA15-75-C-0083, SwRI, San Antonio, Texas, 1975.
86. Westine, P. S., P. A. Cox, and E. D. Esparza, "Structural Analysis Emphasizing Energy Methods: Some Comparisons with Suppressive Shield Experiments," Minutes of the 17th Explosives Safety Seminar, Denver, Colorado, September 1976.
87. Smith, C. S., "Bending, Building and Vibration of Orthotropic Plate-Beam Structures," Journal of Ship Research, December 1968, pp 249-268.
88. Madsen, N. F., "Vibration of Orthogonally Stiffened Panels," Journal of Ship Research, Vol. 22, No. 2, June 1978, pp 100-109.
89. Chang, Pin-Yu, "A Simple Method for Elastic Analysis of Grillages," Journal of Ship Research, June 1968, pp 153-159.
90. Chang, Pin-Yu, and F. C. Michelsen, "A Vibration Analysis of Grillage Beams," Journal of Ship Research, March 1969, pp 32-39.
91. Chang, Pin-Yu, and W. O. Pilkey, "An Efficient, General Method for the Analysis of Grillages," Journal of Ship Research, June 1971, pp 153-171.
92. Leissa, A. W., "Vibration of Plates," NASA SP-160, 1969.
93. Bureau Veritas, "Recommendations Designed to Limit the Effects of Vibrations On-Board Ships," Guidance Note N.I. 138 BM.3.E, May 1971.
94. Nuclear Regulatory Commission, Regulation Guide 1.92.
95. Den Hartog, Mechanical Vibrations, 4th Edition, McGraw-Hill Book Co., Inc., New York, 1956.
96. U. S. Army Corps of Engineers, "Design of Structures to Resist the Effects of Atomic Weapons," Manual EM 1110-345-415, 1957.
97. Wood Handbook: Wood as an engineering material, by Forest Products Laboratory, Forest Service, U.S. Department of Agriculture, Agriculture Handbook No. 72, Revised August 1974, Library of Congress Catalog Card No. 73-600335.
98. Plywood Design Specification, Published by the American Plywood Association, 1924.

99. S. Timoshenko and S. Woinowsky-Krieger, Theory of Plates and Shells, McGraw-Hill Book Co., New York, 1959.
100. R.F.S. Hermon, "The Frequency of Flexural Vibration of Rectangular Orthotropic Plates with Clamped or Supported Edges," Journal of Applied Mechanics, Dec. 1959, pp 537-540.
101. R.J. Roark and W.C. Young, Formulas for Stress and Strain, 5th Ed., McGraw-Hill Book Company, New York, 1975.

SLOSHING FACILITIES FOR ANGULAR MOTION AND SIMULTANEOUS HORIZONTAL AND VERTICAL MOTIONA.1 Angular Motion Slosh Rig

The angular motion slosh test facility (see Figure A.1) consists of a trunnion-mounted "picture frame" weldment made from 8-inch square steel tubing. The trunnions are pivoted in pillow blocks mounted on top of structural steel pedestals attached to a base frame, which is anchored to a concrete floor. An adjustable crank attachment is fastened to one of the vertical legs of the "picture frame". A hydraulic actuator piston rod is connected to this crank, while the cylinder is anchored to the pedestal, to provide the excitation.

Dynamometers attached to the upper and lower horizontal members of the "picture frame" carry a vertical support near each side. The model support frame is attached to these vertical supports at a height determined by the desired model vertical location relative to the pitch (roll) axis. Thus, all loads are transmitted into the "picture frame" through the dynamometers.

An overall view of the facility is shown in the photograph of Figure A-1 and clearance dimensions within the support system and picture frame are shown on Figure A.2. The maximum possible angular travel is about $\pm 15^\circ$, provided the actuator force capacity is not exceeded.

The maximum model tank width and height are fixed by the clearances shown in Figure A.2. Models which do not span the width of the support frame must be mounted on rails attached to either the top or bottom of the support frame. The actual size of the model tank, however, must be such that the dynamometers and actuators are not overloaded. The determining factors in selection of model size are: (1) The total mass of the tank plus liquid; (2) The combination of excitation frequency, excitation amplitude, vertical offset of the model (tank plus liquid), center of gravity from the pitch (roll) axis, and the horizontal offset of model from the pitch axis which results in the greatest inertia moment about the pitch axis. These variations determine the greatest force reactions on the dynamometers. (3) The combination of the above parameters which result in the highest reaction force on the actuator. This combination may not be the same as that which results in the greatest dynamometer reactions.

A maximum model size cannot, therefore, be determined until the entire range of test parameters has been defined. Reactions on the dynamometers and actuator must be investigated for every combination of test parameters.

Excitation of the system is provided by a linear hydraulic actuator connected to a crank on the "picture frame". The actuator has a maximum force output of about 10,000 pounds at its highest velocity, and up to 14,000 pounds at very low velocities (low frequency and low amplitude). A self-contained servo-valve and feedback transducer within the actuator are used in conjunction with an external controller to control the actuator.

The controller has provisions for centering the actuator at any point within its stroke (at the center of the stroke for normal testing), and

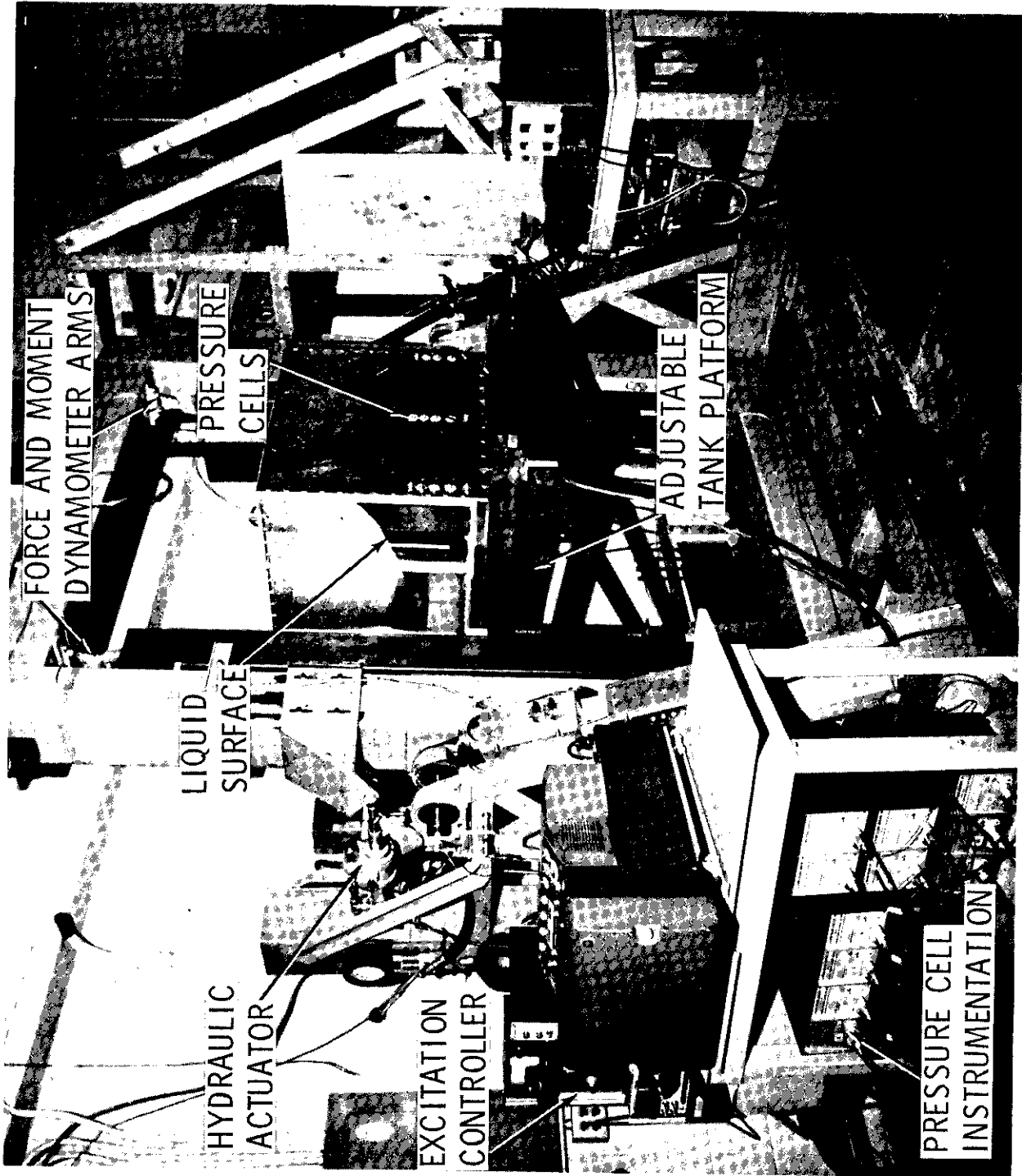
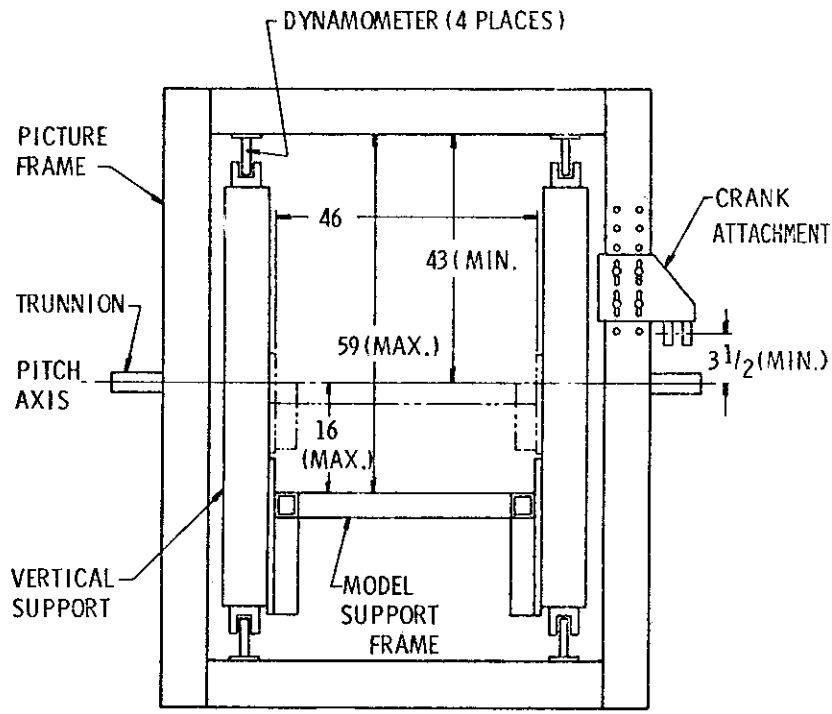


FIGURE A. 1. SLOSH TEST FACILITY



All dimensions in inches

FIGURE A.2. SLOSH RIG CROSS-SECTIONAL DIMENSIONS

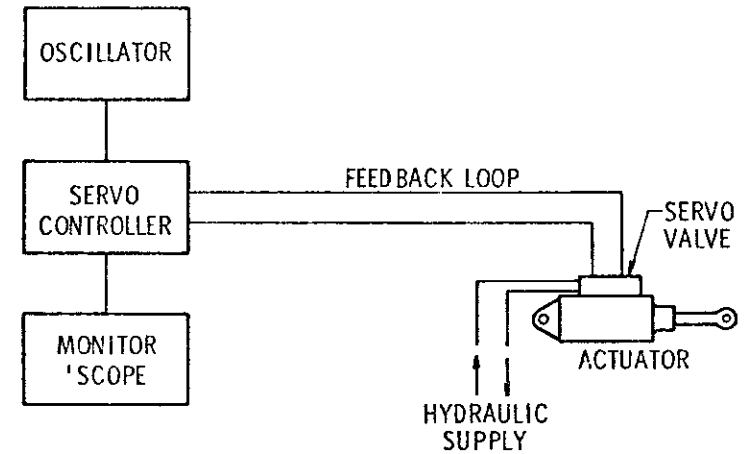


FIGURE A.3. DRIVE SYSTEM BLOCK DIAGRAM

for setting the excitation amplitude. Excitation waveform and frequency are determined externally to the controller input. A function generator connected to the input can excite sinusoidal, square, triangular, or sawtooth motions of the actuator at any discrete frequency.

A tape input can be used to excite random motions with various spectral contents, or any other specified motion (such as typical ship motions) within the limitations of the actuator.

The actuator is limited to total useful stroke of about 2.2 inches peak-to-peak and a maximum linear velocity (restricted by the servo-valve) of about 8 inches per second. The limits of the actuator are determined by the maximum stroke for an excitation frequency up to 1.2 Hz, then by the maximum velocity up to the frequency where the reaction force on the actuator rod exceeds the maximum actuator force. A block diagram of the drive system is shown on Figure A.3.

A.2 Translational Motion Slosh Rig

The translational motion slosh rig operates on a system very similar to the angular motion rig. The translational machine consists of a 5 foot by 5 foot mounting table that can be excited with simultaneous vertical and horizontal motion that is independent along each axis. Maximum table payload capacity is 6000 pounds dead weight. As with the angular motion unit, the translational table drive mechanisms are servo-controlled electrohydraulic actuators, and have the following capabilities:

	<u>Horizontal</u>	<u>Vertical</u>
Frequency Range	0-200 Hz	0-100 Hz
Force Capacity	10,000 lb	20,000 lb
Maximum Stroke	8.0 in.	6.6 in.
Maximum Velocity	45 in./sec	22 in./sec
Maximum Acceleration*	16 g	10 g

*(At zero payload)

The excitation signals are provided by function generators or analog tape signals. Table displacement is accurately controlled by automatic feedback to respond to an arbitrary voltage signal.

APPENDIX B

PRESSURE-TIME HISTORY DATA FOR TRANSDUCER LOCATIONS 2 - 13

TABLE B-1. NONDIMENSIONAL PRESSURE-TIME HISTORY VALUES
AT TRANSDUCER LOCATION 2 FOR A 25% FULL TANK

TRANSDUCER LOCATION 2
FLUID: WATER
EXCITATION: PITCH (AMP. = +/- 4.000 DEG.)
NUMBER OF CYCLES PER TEST: 200
PERCENT FILLING: 25

	PT.2	PT.3	PT.4	PT.5
AVG.KP	6.6493	1.0960	1.0303	0.0435
MAX.KP	15.6515	2.1194	1.8873	0.9474
MIN.KP	3.1777	0.2357	0.3548	0.0027
AVG.TIME	0.1804	0.3225	1.4294	1.9184
MAX.TIME	0.3777	0.5694	1.6614	2.2314
MIN.TIME	0.0398	0.1889	1.1393	1.6617

PT.1 IS ALWAYS ZERO.

ALL VALUES PRINTED IN THE TABLE ARE NONDIMENSIONAL.

NOTE: See Figure IV-5 for definitions.

TABLE B-2. NONDIMENSIONAL PRESSURE-TIME HISTORY
VALUES AT TRANSDUCER LOCATION 3 FOR A 25% FULL
TANK

TRANSDUCER LOCATION 3
FLUID: WATER
EXCITATION: PITCH (AMP. = +/- 4.000 DEG.)
NUMBER OF CYCLES PER TEST: 200
PERCENT FILLING: 25

	PT.2	PT.3	PT.4	PT.5
AVG. KP	6.2818	1.7825	1.6325	0.0121
MAX. KP	17.7300	2.5701	2.3261	0.7836
MIN. KP	3.8564	1.2851	0.7827	0.0064
AVG. TIME	0.1104	0.2160	1.2747	2.0386
MAX. TIME	0.1890	0.3321	1.6138	2.2319
MIN. TIME	0.0426	0.0944	1.0914	1.7565

PT.1 IS ALWAYS ZERO.

ALL VALUES PRINTED IN THE TABLE ARE NONDIMENSIONAL.

NOTE: See Figure IV-5 for definitions.

TABLE B-3. NONDIMENSIONAL PRESSURE-TIME HISTORY
VALUES AT TRANSDUCER LOCATION 4 FOR A 25% FULL
TANK

TRANSDUCER LOCATION 4
FLUID: WATER
EXCITATION: PITCH (AMP. = +/- 4.000 DEG.)
NUMBER OF CYCLES PER TEST: 200
PERCENT FILLING: 25

	PT.2	PT.3	PT.4	PT.5
AVG. KP	13.5162	0.5957	0.3471	0.0017
MAX. KP	31.3328	1.2143	0.7741	0.3310
MIN. KP	5.9576	0.1106	0.0014	0.0000
AVG. TIME	0.0356	0.1647	1.1812	1.9619
MAX. TIME	0.1311	0.2391	1.4716	2.0900
MIN. TIME	0.0005	0.0933	0.4748	1.1869

PT.1 IS ALWAYS ZERO.

ALL VALUES PRINTED IN THE TABLE ARE NONDIMENSIONAL.

NOTE: See Figure IV-5 for definitions.

TABLE B-4. NONDIMENSIONAL PRESSURE-TIME HISTORY
VALUES AT TRANSDUCER LOCATION 5 FOR A 25% FULL
TANK

TRANSDUCER LOCATION 5
FLUID: WATER
EXCITATION: PITCH (AMP. = +/- 4.000 DEG.)
NUMBER OF CYCLES PER TEST: 200
PERCENT FILLING: 25

	PT. 2	PT. 3	PT. 4	PT. 5
AVG. KP	6.4545	1.0630	0.1265	0.0032
MAX. KP	16.2614	1.6066	0.6066	0.2042
MIN. KP	3.0115	0.4019	0.0000	0.0000
AVG. TIME	0.0539	0.1657	0.5915	1.2973
MAX. TIME	0.1880	0.2845	1.2342	1.5199
MIN. TIME	0.0378	0.0461	0.3319	0.9022

PT. 1 IS ALWAYS ZERO.

ALL VALUES PRINTED IN THE TABLE ARE NONDIMENSIONAL.

NOTE: See Figure IV-5 for definitions.

TABLE B-5. NONDIMENSIONAL PRESSURE-TIME HISTORY
VALUES AT TRANSDUCER LOCATION 6 FOR A 25% FULL
TANK

TRANSDUCER LOCATION 6
FLUID: WATER
EXCITATION: PITCH (AMP. = +/- 4.000 DEG.)
NUMBER OF CYCLES PER TEST: 200
PERCENT FILLING: 25

	PT. 2	PT. 3	PT. 4	PT. 5
AVG. KP	10.2661	0.7052	0.3370	0.0000
MAX. KP	31.3111	1.9103	0.7689	0.0000
MIN. KP	3.3095	0.1282	0.0013	0.0000
AVG. TIME	0.0612	0.1774	1.0488	1.5943
MAX. TIME	0.1394	0.2845	1.3290	1.7577
MIN. TIME	0.0346	0.0941	0.8071	1.4718

PT. 1 IS ALWAYS ZERO.

ALL VALUES PRINTED IN THE TABLE ARE NONDIMENSIONAL.

NOTE: See Figure IV-5 for definitions.

TABLE B-6. NONDIMENSIONAL PRESSURE-TIME HISTORY
VALUES AT TRANSDUCER LOCATION 7 FOR A 75% FULL
TANK

TRANSDUCER LOCATION 7
FLUID: WATER
EXCITATION: PITCH (AMP. = +/- 4.000 DEG.)
NUMBER OF CYCLES PER TEST: 200
PERCENT FILLING: 75

	PT. 2	PT. 3	PT. 4	PT. 5
AVG. KP	2.7409	1.1194	1.0022	0.0179
MAX. KP	4.9585	1.9186	1.8103	0.4596
MIN. KP	1.6903	0.5640	0.3448	0.0028
AVG. TIME	0.5652	0.7688	1.6501	2.0353
MAX. TIME	0.8060	1.0910	1.8988	2.4220
MIN. TIME	0.2812	0.3783	1.1867	1.6143

PT. 1 IS ALWAYS ZERO.

ALL VALUES PRINTED IN THE TABLE ARE NONDIMENSIONAL.

NOTE: See Figure IV-5 for definitions.

TABLE B-7. NON DIMENSIONAL PRESSURE-TIME HISTORY
VALUES AT TRANSDUCER LOCATION 8 FOR A 75% FULL
TANK

TRANSDUCER LOCATION 8
FLUID: WATER
EXCITATION: PITCH (AMP. = +/- 4.000 DEG.)
NUMBER OF CYCLES PER TEST: 200
PERCENT FILLING: 75

	PT. 2	PT. 3	PT. 4	PT. 5
AVG. KP	2.4869	1.1233	0.9063	0.0086
MAX. KP	3.5876	2.1765	1.8002	0.5222
MIN. KP	1.6666	0.3884	0.1309	0.0035
AVG. TIME	0.9539	1.1417	1.9190	2.2043
MAX. TIME	1.3276	1.6136	2.3736	2.6119
MIN. TIME	0.2845	0.5220	1.5191	1.9466

PT. 1 IS ALWAYS ZERO.

ALL VALUES PRINTED IN THE TABLE ARE NONDIMENSIONAL.

NOTE: See Figure IV-5 for definitions.

TABLE B-8. NONDIMENSIONAL PRESSURE-TIME HISTORY
VALUES AT TRANSDUCER LOCATION 9 FOR A 75% FULL
TANK

TRANSDUCER LOCATION 9
FLUID: WATER
EXCITATION: PITCH (AMP. = +/- 4.000 DEG.)
NUMBER OF CYCLES PER TEST: 200
PERCENT FILLING: 75

	PT.2	PT.3	PT.4	PT.5
AVG.KP	3.1801	1.8189	1.3260	0.0215
MAX.KP	4.8943	2.6620	2.1103	0.5788
MIN.KP	2.0967	0.5611	0.4247	0.0069
AVG.TIME	0.6364	0.8232	1.6586	2.1718
MAX.TIME	0.8529	1.1371	2.1359	2.6115
MIN.TIME	0.3779	0.4744	1.0917	1.4246

PT.1 IS ALWAYS ZERO.

ALL VALUES PRINTED IN THE TABLE ARE NONDIMENSIONAL.

NOTE: See Figure IV-5 for definitions.

TABLE B-9. NONDIMENSIONAL PRESSURE-TIME HISTORY
VALUES AT TRANSDUCER LOCATION 10 FOR A 75% FULL
TANK

TRANSDUCER LOCATION 10
FLUID: WATER
EXCITATION: PITCH (AMP. = +/- 4.000 DEG.)
NUMBER OF CYCLES PER TEST: 200
PERCENT FILLING: 75

	PT.2	PT.3	PT.4	PT.5
AVG.KP	0.0547	0.0085	0.0051	0.0000
MAX.KP	0.1039	0.0282	0.0179	0.0031
MIN.KP	0.0297	0.0000	0.0000	0.0000
AVG.TIME	0.0357	0.0555	0.1315	0.1841
MAX.TIME	0.0499	0.0697	0.1593	0.2090
MIN.TIME	0.0196	0.0350	0.0548	0.1642

PT.1 IS ALWAYS ZERO.

ALL VALUES PRINTED IN THE TABLE ARE NONDIMENSIONAL.

NOTE: See Figure IV-5 for definitions.

TABLE B-10. NONDIMENSIONAL PRESSURE-TIME HISTORY
VALUES AT TRANSDUCER LOCATION 11 FOR A 75% FULL
TANK

TRANSDUCER LOCATION 11
FLUID: WATER
EXCITATION: PITCH (AMP. = +/- 4.000 DEG.)
NUMBER OF CYCLES PER TEST: 200
PERCENT FILLING: 75

	PT. 2	PT. 3	PT. 4	PT. 5
AVG. KP	2.3220	0.9793	0.4631	0.0000
MAX. KP	3.7282	1.6734	1.1602	0.0000
MIN. KP	1.5435	0.2592	0.0043	0.0000
AVG. TIME	0.5554	0.6799	1.1487	1.5606
MAX. TIME	0.7583	0.9489	1.4238	1.9519
MIN. TIME	0.2840	0.4275	0.9019	1.3284

PT. 1 IS ALWAYS ZERO.

ALL VALUES PRINTED IN THE TABLE ARE NONDIMENSIONAL.

NOTE: See Figure IV-5 for definitions.

TABLE B-11. NONDIMENSIONAL PRESSURE-TIME HISTORY
VALUES AT TRANSDUCER LOCATION 12 FOR A 75% FULL
TANK

TRANSDUCER LOCATION 12
FLUID: WATER
EXCITATION: PITCH (AMP. = +/- 4.000 DEG.)
NUMBER OF CYCLES PER TEST: 200
PERCENT FILLING: 75

	PT. 2	PT. 3	PT. 4	PT. 5
AVG. KP	4.1034	1.4486	0.8963	0.0000
MAX. KP	8.3567	2.2346	1.5348	0.0000
MIN. KP	2.7081	0.9401	0.3578	0.0000
AVG. TIME	0.3603	0.5383	1.1181	1.7276
MAX. TIME	0.5203	0.7587	1.3289	1.9000
MIN. TIME	0.2345	0.3788	0.9487	1.4721

PT. 1 IS ALWAYS ZERO.

ALL VALUES PRINTED IN THE TABLE ARE NONDIMENSIONAL.

NOTE: See Figure IV-5 for definitions.

TABLE B-12. NONDIMENSIONAL PRESSURE-TIME HISTORY
VALUES AT TRANSDUCER LOCATION 13 FOR A 75% FULL TANK

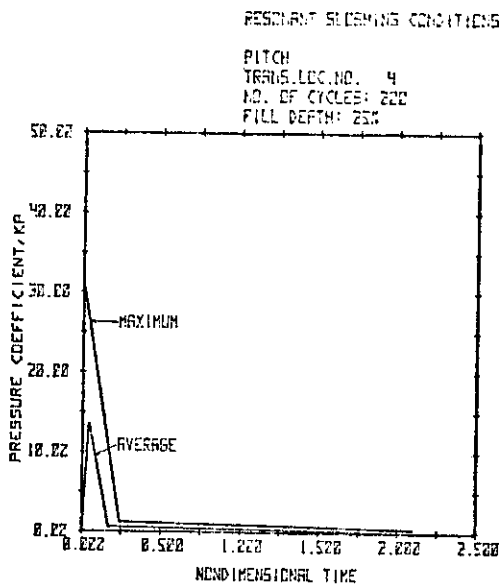
TRANSDUCER LOCATION 13
FLUID: WATER
EXCITATION: PITCH (AMP. = +/- 4.000 DEG.)
NUMBER OF CYCLES PER TEST: 200
PERCENT FILLING: 75

	PT. 2	PT. 3	PT. 4	PT. 5
AVG. KP	5.6172	0.0000	0.0000	0.0000
MAX. KP	15.9974	0.0013	0.0000	0.0000
MIN. KP	2.5381	0.0000	0.0000	0.0000
AVG. TIME	0.1676	0.4066	0.9276	1.4816
MAX. TIME	0.3303	0.6182	1.1879	1.8528
MIN. TIME	0.0358	0.2842	0.7128	1.1405

PT. 1 IS ALWAYS ZERO.

ALL VALUES PRINTED IN THE TABLE ARE NONDIMENSIONAL.

NOTE: See Figure IV-5 for definitions.



* THE LINES CONNECTING THE DATA POINTS
ARE ONLY VISUAL AIDS.

FIGURE B-1. NONDIMENSIONAL PRESSURE-TIME HISTORY VALUES FOR 200 RESONANT SLOSHING CYCLES AT TRANSDUCER LOCATION 4 FOR A 25% FULL TANK

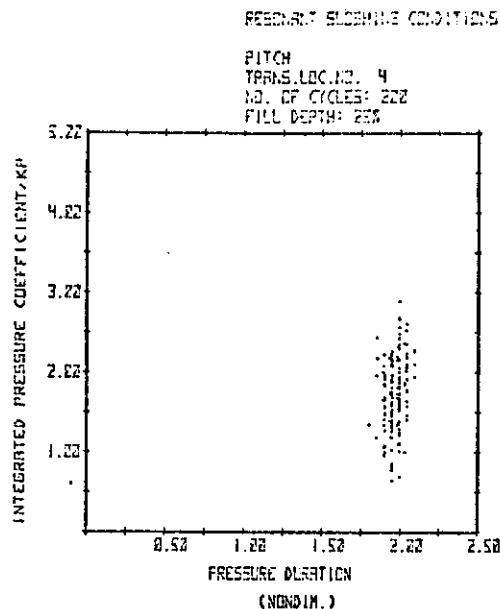


FIGURE B-2. INTEGRATED NONDIMENSIONAL PRESSURE VALUES FOR 200 RESONANT SLOSHING CYCLES AT TRANSDUCER LOCATION 4 FOR A 25% FULL TANK

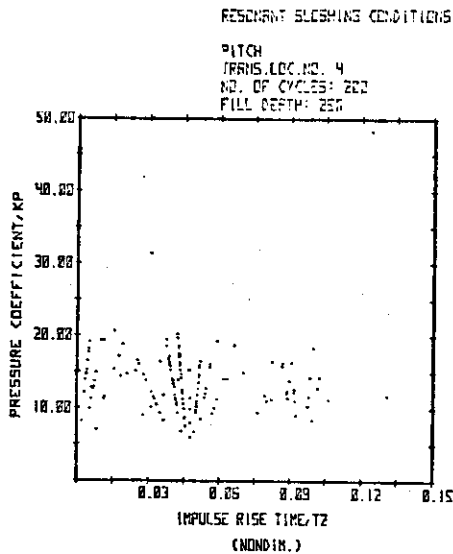


FIGURE B-3. NONDIMENSIONAL PRESSURE VS IMPULSE RISE TIME FOR 200 RESONANT SLOSHING CYCLES AT TRANSDUCER LOCATION 4 FOR A 25% FULL TANK

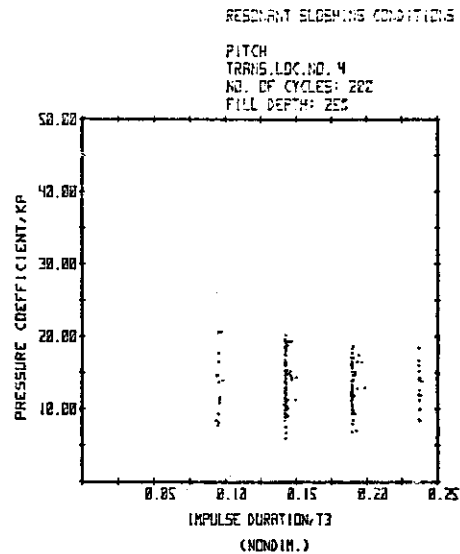


FIGURE B-4. NONDIMENSIONAL PRESSURE VS IMPULSE DURATION FOR 200 RESONANT SLOSHING CYCLES AT TRANSDUCER LOCATION 4 FOR A 25% FULL TANK

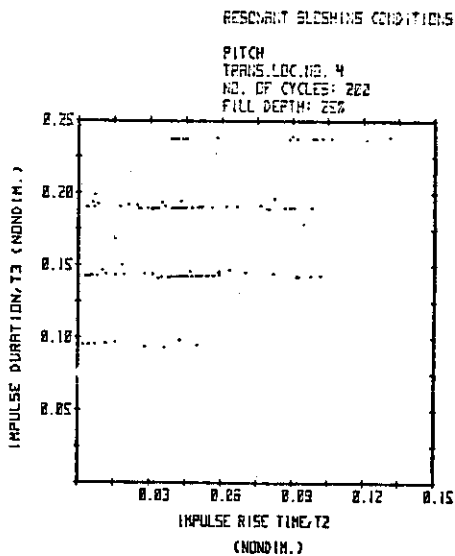
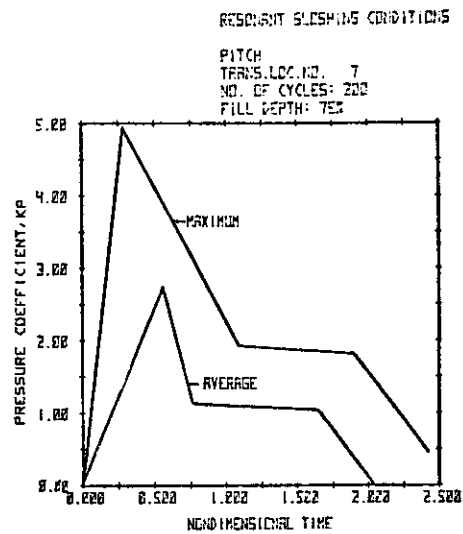


FIGURE B-5. NONDIMENSIONAL IMPULSE DURATION VS IMPULSE RISE TIME FOR 200 RESONANT SLOSHING CYCLES AT TRANSDUCER LOCATION 4 FOR A 25% FULL TANK



* THE LINES CONNECTING THE DATA POINTS ARE ONLY VISUAL AIDS.

FIGURE B-6. NONDIMENSIONAL PRESSURE-TIME HISTORY VALUES FOR 200 RESONANT SLOSHING CYCLES AT TRANSDUCER LOCATION 7 FOR A 75% FULL TANK

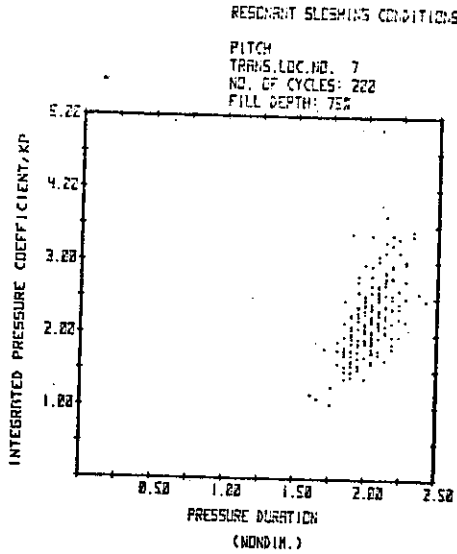


FIGURE B-7. INTEGRATED NON-DIMENSIONAL PRESSURE VALUES FOR 200 RESONANT SLOSHING CYCLES AT TRANSDUCER LOCATION 7 FOR A 75% FULL TANK

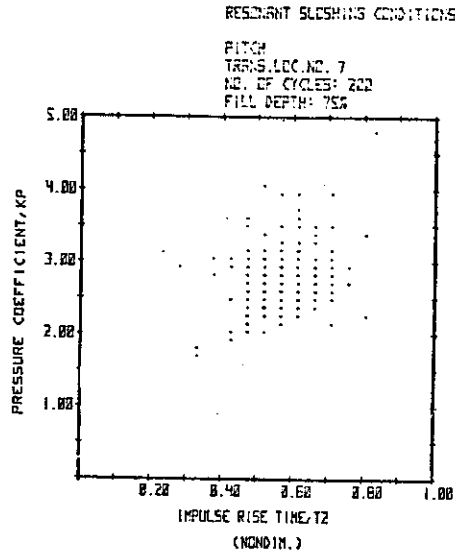


FIGURE B-8. NONDIMENSIONAL PRESSURE VS IMPULSE RISE TIME FOR 200 RESONANT SLOSHING CYCLES AT TRANSDUCER LOCATION 7 FOR A 75% FULL TANK

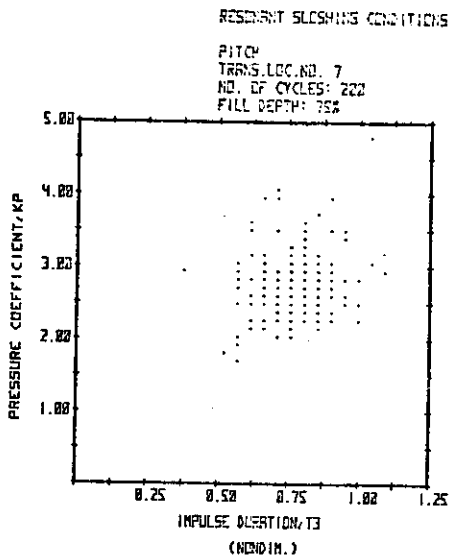


FIGURE B-9. NONDIMENSIONAL PRESSURE VS IMPULSE DURATION FOR 200 RESONANT SLOSHING CYCLES AT TRANSDUCER LOCATION 7 FOR A 75% FULL TANK

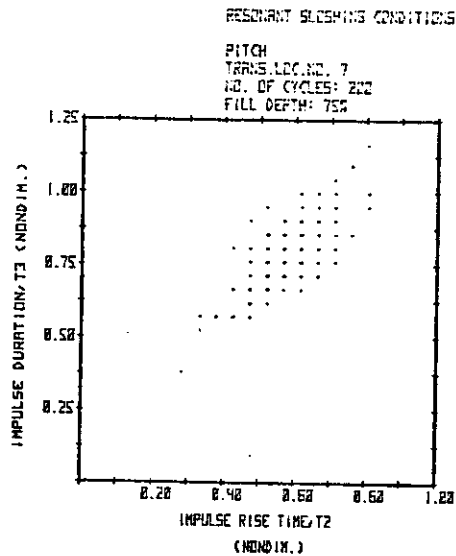
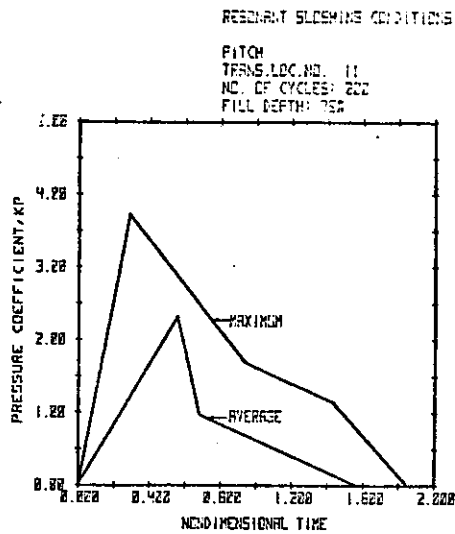


FIGURE B-10. NONDIMENSIONAL IMPULSE DURATION VS IMPULSE RISE TIME FOR 200 RESONANT SLOSHING CYCLES AT TRANSDUCER LOCATION 7 FOR A 75% FULL TANK



* THE LINES CONNECTING THE DATA POINTS
ARE ONLY VISUAL AIDS.

FIGURE B-11. NONDIMENSIONAL
PRESSURE-TIME HISTORY VALUES
FOR 200 RESONANT SLOSHING
CYCLES AT TRANSDUCER
LOCATION 11 FOR A 75% FULL
TANK

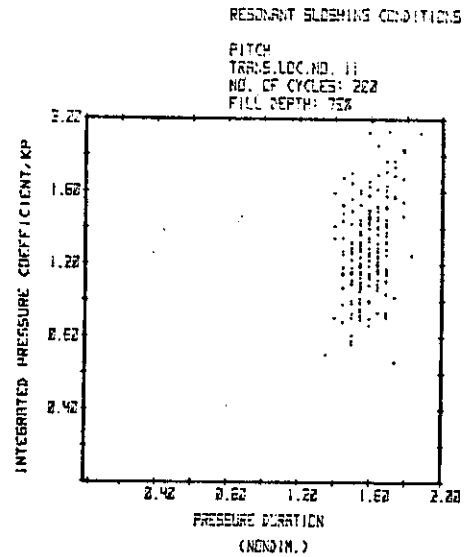


FIGURE B-12. INTEGRATED NON-
DIMENSIONAL PRESSURE VALUES
FOR 200 RESONANT SLOSHING
CYCLES AT TRANSDUCER LOCATION
11 FOR A 75% FULL TANK

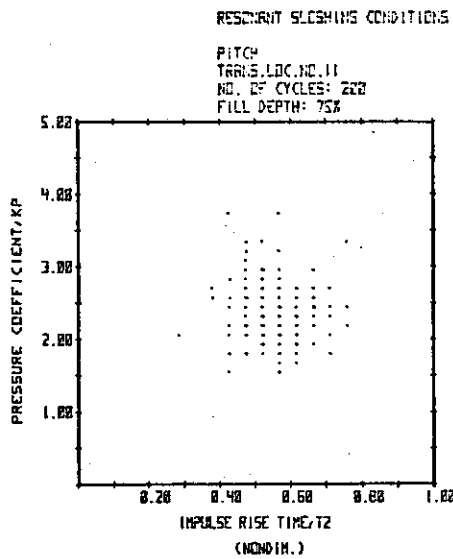


FIGURE B-13. NONDIMENSIONAL
PRESSURE VS IMPULSE RISE
TIME FOR 200 RESONANT
SLOSHING CYCLES AT TRANS-
DUCER LOCATION 11 FOR A
75% FULL TANK

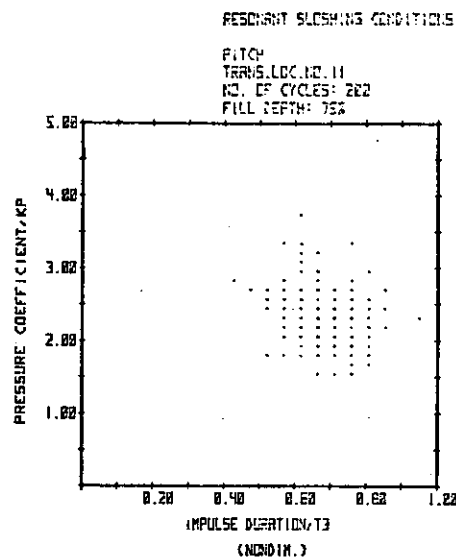


FIGURE B-14. NONDIMENSIONAL
PRESSURE VS IMPULSE DURATION
FOR 200 RESONANT SLOSHING
CYCLES AT TRANSDUCER
LOCATION 11 FOR A 75% FULL
TANK

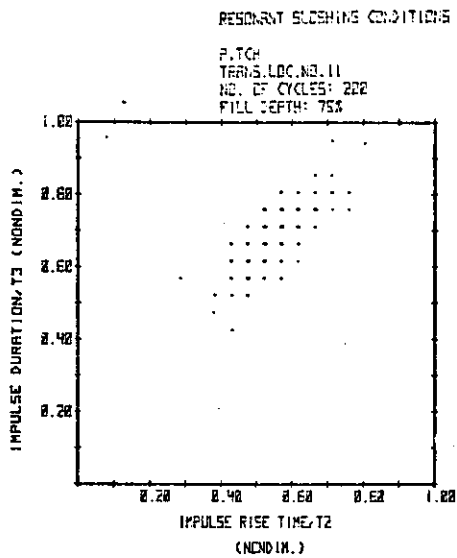


FIGURE B-15. NONDIMENSIONAL IMPULSE DURATION VS IMPULSE RISE TIME FOR 200 RESONANT SLOSHING CYCLES AT TRANSDUCER LOCATION 11 FOR A 75% FULL TANK

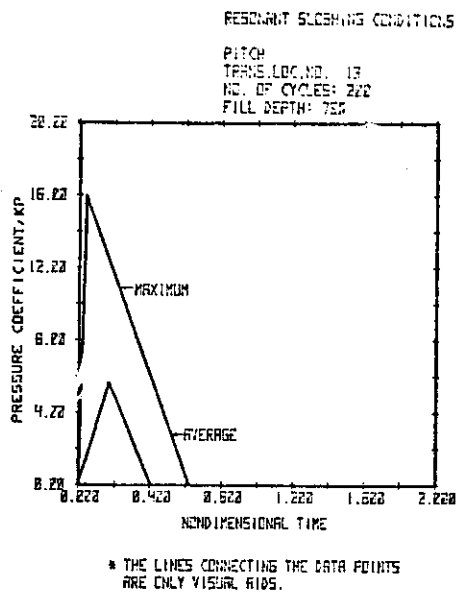


FIGURE B-16. NONDIMENSIONAL PRESSURE-TIME HISTORY VALUES FOR 200 RESONANT SLOSHING CYCLES AT TRANSDUCER LOCATION 13 FOR A 75% FULL TANK

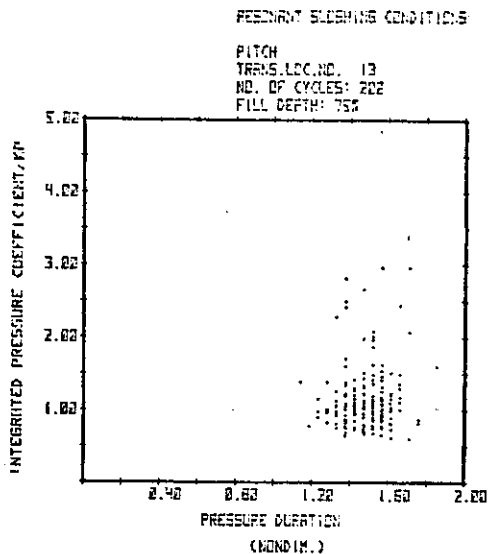


FIGURE B-17. INTEGRATED NON-DIMENSIONAL PRESSURE VALUES FOR 200 RESONANT SLOSHING CYCLES AT TRANSDUCER LOCATION 13 FOR A 75% FULL TANK

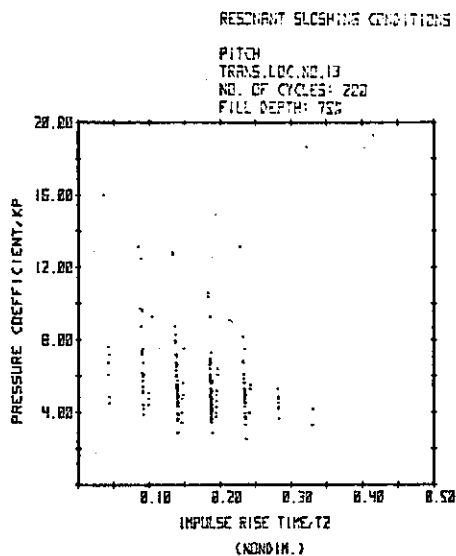


FIGURE B-18. NONDIMENSIONAL PRESSURE VS IMPULSE RISE TIME FOR 200 RESONANT SLOSHING CYCLES AT TRANSDUCER LOCATION 13 FOR A 75% FULL TANK

RESONANT SLOSHING CONDITIONS

PITCH
 TRANS. LOC. NO. 13
 NO. OF CYCLES: 200
 FILL DEPTH: 75%

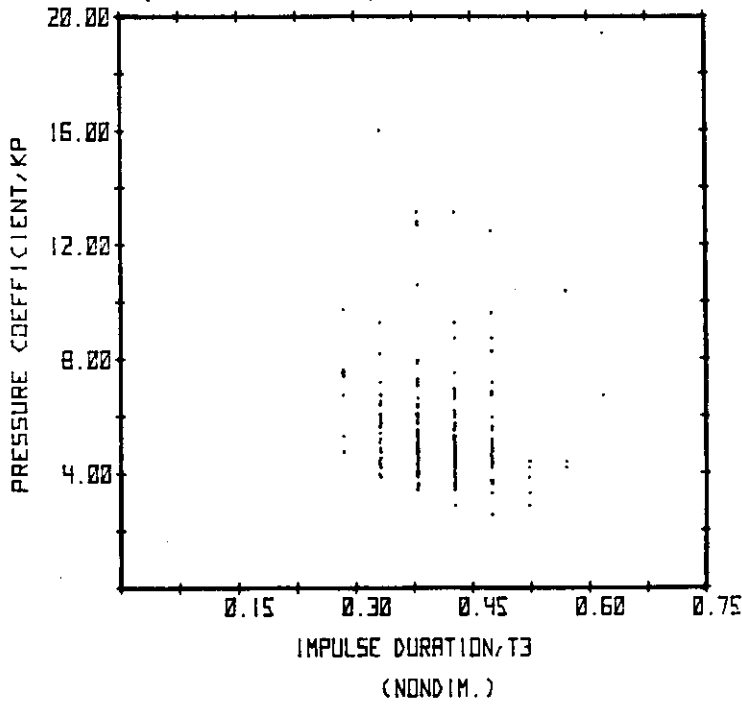


FIGURE B-19. NONDIMENSIONAL PRESSURE VS. IMPULSE DURATION FOR 200 RESONANT SLOSHING CYCLES AT TRANSDUCER LOCATION 13 FOR A 75% FULL TANK

RESONANT SLOSHING CONDITIONS

PITCH
 TRANS. LOC. NO. 13
 NO. OF CYCLES: 200
 FILL DEPTH: 75%

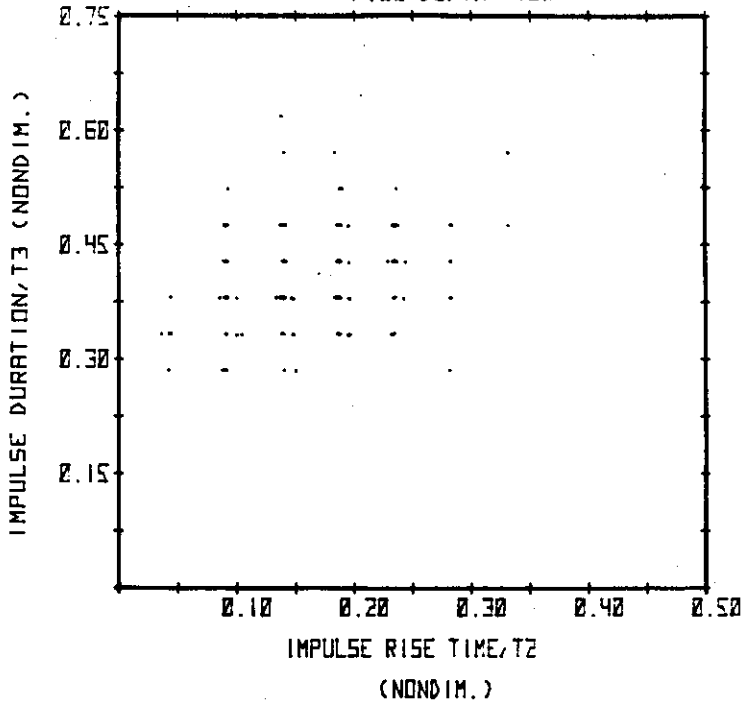


FIGURE B-20. NONDIMENSIONAL IMPULSE DURATION VS. IMPULSE RISE TIME FOR 200 RESONANT SLOSHING CYCLES AT TRANSDUCER LOCATION 13 FOR A 75% FULL TANK

APPENDIX C

ONE-DEGREE-OF-FREEDOM EQUIVALENT SYSTEMS

To derive one-degree-of-freedom (one dof) "equivalent" systems for what are normally regarded as multi-dof structural elements requires that some assumptions be made about the behavior of the structure. The basic assumption is a deformation pattern which defines displacements of the total element in terms of a single displacement at some point in the structure.

As an example, consider the simply supported beam of Figure C-1. If the displacement along the beam can be described in terms of a single variable, for example, the center displacement, w_0 , then the motions are reduced to a single dof. This is accomplished by assuming a deformation pattern for the beam which is some function of w_0 . Various choices can be made, e.g., the fundamental mode shape, the static deformed shape for the load distribution of the dynamic loading, or simply some approximate shape which resembles the fundamental mode or static deformed shape and matches the appropriate boundary conditions. For elastic behavior, Biggs⁽⁷⁹⁾ chooses the static deformed shape of the structure. For the simply supported beam, uniformly loaded by the distributed load $N \cdot g(t)$, $[g(t)]$ is the time function for the load; the static deformed shape for elastic behavior is given in Figure C-1.

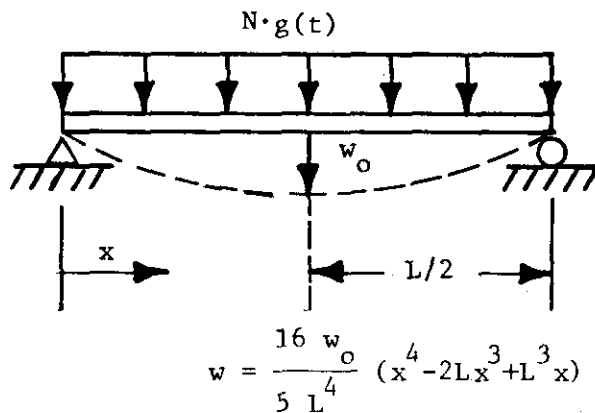


FIGURE C-1. DEFORMATION PATTERN FOR SIMPLE BEAM

Reducing displacements to a single dof does not guarantee similarity between the computed response of a one-dof system and the structural element. One way that similarity can be obtained is to equate the energies of the distributed and single-dof systems. At any time, the internal strain energy and the system kinetic energy must equal the external work as shown by Equation C-1.

$$W = U + KE \tag{C-1}$$

W = external work

U = internal strain energy

KE = kinetic energy

If kinematic similarity (equal displacements and velocities in this case) is maintained between the distributed and single-dof systems, then equating energies of the two systems will assure similarity of the computed behavior. This is true for elastic or elastic-plastic behavior, but in ship tanks only elastic behavior will be considered.

As a first example, we chose the fundamental mode of the simply supported beam as the deformed shape. This choice will permit a check on frequency with the exact solution to demonstrate kinematic equivalence of the distributed and equivalent systems. The deformed shape for the fundamental mode is

$$w(x) = w_o \sin \frac{\pi x}{L} \quad (C-2)$$

Evaluating W, U, and KE for this deformation pattern gives

$$W = \int_0^L N \cdot g(t) w(x) dx = \frac{2}{\pi} N \cdot g(t) w_o L \quad (C-3a)$$

$$U = \frac{EI}{2} \int_0^L \left(\frac{d^2 w(x)}{dx^2} \right)^2 dx = \frac{\pi^4 EI w_o^2}{4L^3} \quad (C-3b)$$

$$KE = \frac{1}{2} \int_0^L \left[\dot{w}(x) \right]^2 \rho A dx = \frac{1}{4} \rho A L \dot{w}_o^2 \quad (C-3c)$$

where

E = material modulus

I = beam section moment of inertia

A = beam cross-sectional area

ρ = material density

w_o = the beam center displacement and is some function of time.

These same energies, evaluated for the single-dof system of Figure C-2, are

$$W = F_e \cdot g(t) w_o \quad (C-4a)$$

$$U = \frac{1}{2} k_e w_o^2 \quad (C-4b)$$

$$KE = \frac{1}{2} m_e \dot{w}_o^2 \quad (C-4c)$$

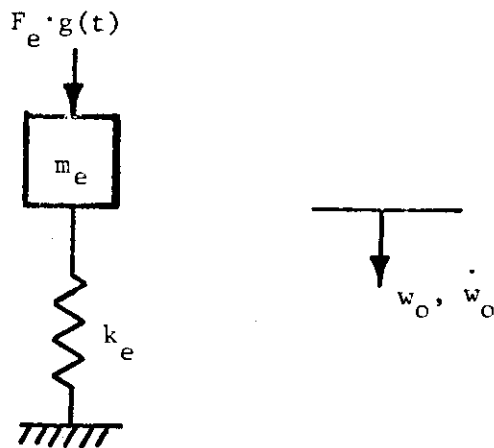


FIGURE C-2. EQUIVALENT ONE-DOF SYSTEM

Equating equations C-3 and C-4 and recognizing that

$$\rho AL = m, \text{ total beam mass}$$

$$NL = F, \text{ total beam static load}$$

the following relationships are obtained

$$K_L = \frac{F_e}{F} = 0.6366 \quad (C-5a)$$

$$k_e = \frac{\pi^4 EI}{2L^3} = 0.634 k \quad (C-5b)$$

$$K_m = \frac{m_e}{m} = 0.500 \quad (C-5c)$$

where

k = spring constant for the simply supported beam
($N \cdot L$ divided by static center deflection)

K_L = load factor

K_m = mass factor

Notice that the equivalent spring constant is very nearly equal to the static spring constant multiplied by the load factor.

Because these relationships were developed on the basis of kinematic equivalence of the displacement w_0 , it is instructive to compare the frequency given by the equivalent mass and spring constants with the exact solution for a simply supported beam. The exact solution for the fundamental mode is given by Den Hartog⁽⁹⁵⁾ as

$$\omega = \pi^2 \sqrt{\frac{EI}{mL^3}} \quad (C-6)$$

where

m = total beam mass = ρAL

For the equivalent system,

$$\begin{aligned} \omega &= \sqrt{\frac{k_e}{m_e}} = \sqrt{\frac{\pi^4 EI}{2L^3 (0.5m)}} \\ &= \pi^2 \sqrt{\frac{EI}{mL^3}} \end{aligned} \quad (C-7)$$

As expected, the assumption of the fundamental mode for the deformed shape gives a frequency which is exactly equal to the beam's fundamental frequency.

Now, K_L , K_m , and k_e will be determined for the static deformed shape of the beam for comparison with the results of Biggs⁽⁷⁹⁾. The static deformed shape is given in Figure C-1, and for this case the energies of the distributed system are:

$$W = N \cdot g(t) \frac{16 w_o L}{25} \quad (C-8a)$$

$$U = \frac{3072 EI w_o^2}{125L^3} \quad (C-8b)$$

$$KE = \frac{1984}{7875} \rho AL \dot{w}_o^2 \quad (C-8c)$$

Equating to equations (C-4), as before, we obtain

$$K_L = \frac{F_e}{F} = 0.64 \quad (C-9a)$$

$$k_e = \frac{6144 EI}{125L^3} = 0.64 k \quad (C-9b)$$

$$K_m = \frac{m_e}{m} = 0.5026 = 0.50 \quad (C-9c)$$

These values of stiffness and mass of the equivalent system give a frequency of

$$\omega = 9.889 \sqrt{\frac{EI}{mL^3}} \quad (C-10)$$

which is within 0.2% of the fundamental mode of the beam [Equation (C-6)]. Because the static deformed shape is made up of many normal modes, in addition to the first, some difference in frequency is to be expected. If the beam truly deforms dynamically with the static deformed shape, then it would respond with the equivalent system frequency.

Several observations can be made as a result of these calculations for elastic behavior:

1. A rational method is available for deriving an equivalent one-dof system for a distributed structure.
2. Kinematic equivalency is maintained if the assumed deformation pattern exactly matches the behavior of the distributed system.
3. The values of K_L , K_m , and k_e match those given by Biggs⁽⁷⁹⁾ and others for the static deformed shape. Table C-1 gives these values for simply supported beams.
4. For the static-deformed shape, the equivalent stiffness, k_e , can be computed from the static stiffness of the distributed system and the load factor.
5. The fundamental mode shape and the static deformed shape give very similar results for a uniform loading. Using the static deformed shape should give the best results for other than uniform loading or uniform structures because the deflected shape will not match the fundamental mode so closely.

Transformation factors as in Table C-1 have been developed by Biggs⁽⁷⁹⁾ and others for many different structural elements and different loading conditions for each element. For example, Biggs gives values for

- o simply-supported beams
- o clamped beams
- o propped cantilevers
- o one- and two-way slabs with edge supports
- o two-way slabs with interior supports

C.1 Displacements of the Equivalent Systems

Displacements of these equivalent one-degree-of-freedom systems can be computed using simple numerical methods or closed form solutions. A convenient way to present the solution for elastic behavior is in terms of a dynamic load factor (DLF). The dynamic load factor is simply the maximum displacement produced by the dynamic load, divided by the displacement produced by the peak load applied statically. Thus, the DLF can be either smaller or greater than one depending upon the nature of the loading and vibration period of the responding structure.

Plots of dynamic load factors for different types of loading functions are given in Figure C-3. Note from these figures that the maximum DLF is 2.0, whereas the minimum approaches zero for certain types of loads of very short duration.

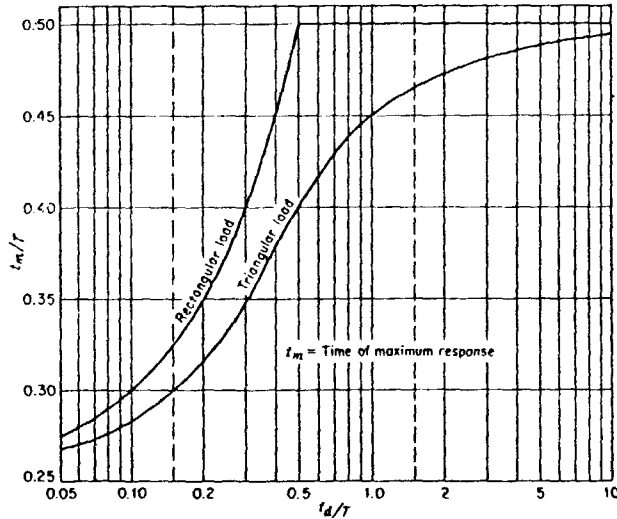
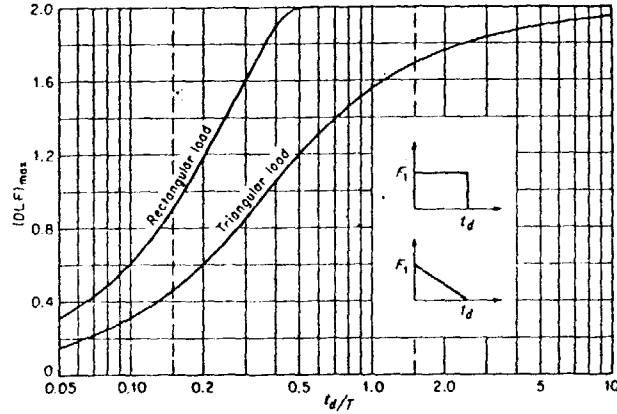
TABLE C-1. TRANSFORMATION FACTORS FOR BEAMS AND ONE-WAY SLABS



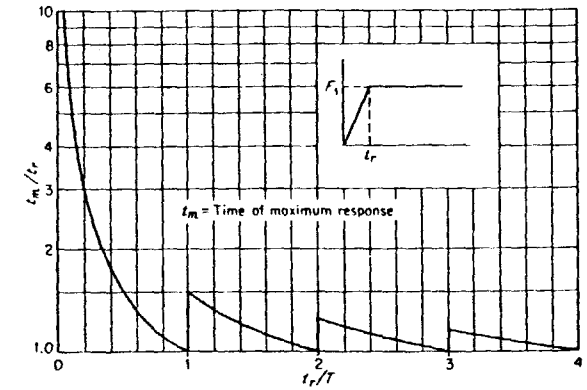
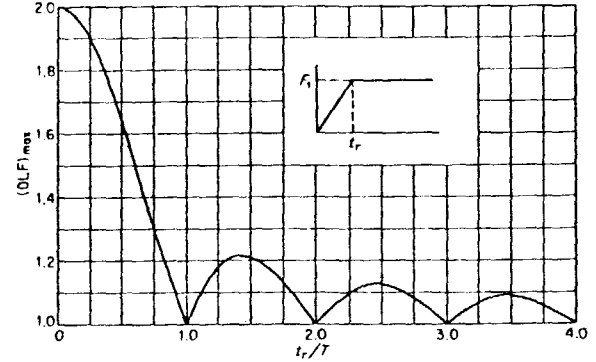
Loading diagram	Strain range	Load factor K_L	Mass factor K_M		Load-mass factor K_{LM}		Maximum resistance R_m	Spring constant k	Dynamic reaction V
			Concentrated mass*	Uniform mass	Concentrated mass*	Uniform mass			
	Elastic	0.64	0.50	0.50	0.78	$\frac{83R_p}{L}$	$\frac{384EI}{5L^3}$	$0.39R + 0.11P$	
	Plastic	0.50	0.33	0.33	0.66	$\frac{83R_p}{L}$	0	$0.38R_m + 0.12P$	
	Elastic	1.0	1.0	1.0	0.49	$\frac{43R_p}{L}$	$\frac{48EI}{L^3}$	$0.78R - 0.28P$	
	Plastic	1.0	1.0	1.0	0.33	$\frac{43R_p}{L}$	0	$0.75R_m - 0.25P$	
	Elastic	0.87	0.76	0.76	0.60	$\frac{63R_p}{L}$	$\frac{50.4EI}{L^3}$	$0.525R - 0.025P$	
	Plastic	1.0	1.0	1.0	0.56	$\frac{63R_p}{L}$	0	$0.52R_m - 0.02P$	

* Equal parts of the concentrated mass are lumped at each concentrated load.

Source: U. S. Army Corps of Engineers



(a) Triangular and rectangular force pulses with zero rise time



(b) Constant force with finite rise time

FIGURE C-3. DYNAMIC LOAD FACTORS (DLF) AND TIME TO MAXIMUM RESPONSE (t_m) FOR DIFFERENT $F(t)$'s (96)

C.2 Shear in the Equivalent System

As Biggs⁽⁷⁹⁾ states,

"It is important to recognize that the dynamic reactions of the real structural element have no direct counterpart in the equivalent one-degree system, i.e., the spring force, is not the same as the real reaction. This is true because the simplified system was deliberately selected so as to have the same dynamic deflection as the real element, rather than the same force or stress characteristics."

These comments are particularly true for elastic-plastic behavior, where the maximum resistance is limited by permitting plastic deformation to occur in the structure. For this case the maximum resistance is not a good indication of the maximum shear which has occurred in the structural element. When only elastic behavior occurs, the maximum resistance of the member, the applied load multiplied by DLF, gives a good indication of the peak shear in the member. Here, only elastic behavior will be treated in keeping with the philosophy that only elastic behavior will be tolerated in ship tanks.

To determine the dynamic reaction, V , of Table C-1, a free-body diagram of the element, including inertia effects, must be used. For the uniformly-loaded, simply-supported beam of Figure C-1, such a free-body diagram is given in Figure C-4. Inertia forces are distributed according to the assumed deformation pattern and are opposed to the motion. Only the period of time up to the maximum response, t_m , is considered.

From the free-body diagram of one-half of the beam, an expression for $V(t)$ is obtained by taking moments at $x = a$, the line of action of the resulting inertia forces.

$$V(a) - M_{x=L/2} - F(t) a - \frac{L}{4} = 0 \quad (C-11)$$

For elastic behavior, locations of the resultant of the inertia forces and the mid-span moment are determined from the static deformed shape. They are

$$a = \frac{61}{192} L$$

$$M_{x=L/2} = \frac{48EI}{5L^2} w_0$$

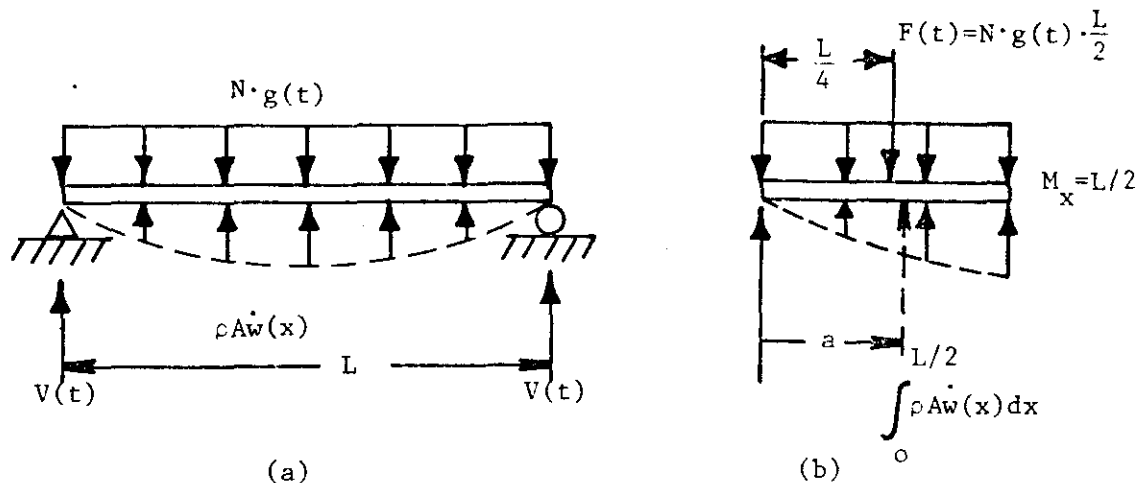


FIGURE C-4. SIMPLY SUPPORTED BEAM IN EQUILIBRIUM UNDER DYNAMIC LOADING

Substituting into Equation (C-11), the dynamic reaction at the beam end for elastic behavior is

$$V = \frac{30.216EI}{L^3} w_0 + 0.1066 F(t) \quad (C-12)$$

where $F(t)$ is the total dynamic load on the beam [$N \cdot g(t) \cdot L$] and w_0 is understood to be a function of time. Thus, the shear reaction is a function of the loading as well as the elastic resistance in the member. Notice in Equation C-12 that the maximum reaction may occur when w_0 is a maximum, when $F(t)$ is a maximum or somewhere in between.

For elastic behavior only, it is worthwhile to compare the shear reactions predicted by Equation C-12 or the equation in Table C-1 with that obtained from the equivalent static loading. This can be easily done for a simply supported beam, uniformly loaded by a triangular force with zero rise time. This loading most closely approximates the worst case sloshing load because the rise time is only about 1.0 ms and is very short relative to the decay time.

The shear equation from Table C-1 is

$$V = .39R + .11F(t) \quad (C-13)$$

For elastic behavior the resistance at the time of maximum response, t_m , will equal the dynamic load factor, DLF, multiplied by the peak applied load F_1 . This gives

$$V = .39 \cdot DLF \cdot F_1 + .11 F(t) \quad (C-14)$$

Also, for a triangular pulse of duration t_d , $F(t)$ can be expressed in terms of the peak load F_1 as

$$F(t) = F_1 \frac{(t_d - t)}{t_d} \quad \text{for } 0 \leq t \leq t_d \quad (C-15)$$

Now

$$\begin{aligned} V &= .39 \cdot DLF \cdot F_1 + .11 F_1 \frac{t_d - t}{t_d} \\ &= F_1 [.39 DLF + .11(t_d - t)/t_d] \end{aligned} \quad (C-16)$$

At $t = 0$, the second term in brackets is maximum but the first is zero (the system has not displaced). The first term in the brackets corresponds to the maximum resistance and occurs at $t = t_m$. Because sloshing pressures are of long duration, the shear will most likely peak at $t = t_m$. Thus,

$$\frac{V}{F_1} = .39 \cdot DLF + .11(t_d - t_m)/t_d \quad (C-17)$$

This expression is compared to

$$V' = 0.5(F_1 \cdot DLF) \quad (C-18)$$

which is the maximum shear in a simply supported beam acted on by a uniform static load $F_1 \cdot DLF$. In non-dimensional form

$$\frac{V'}{F_1} = 0.5 \cdot DLF \quad (C-19)$$

Equating equation (C-19) to equation (C-17) and setting the second term in equation (C-17) to its maximum value of 0.11 we find

$$.5DLF = .39 \cdot DLF + .11 \quad (C-20)$$

The sides are only equal when DLF is 1.0 (static loading). When DLF is larger than 1.0, the left side is greater because the term 0.11 is not multiplied by DLF. For $DLF < 1.0$ the right side can be greater, depending upon

the contribution of the second term for which 0.11 is the maximum value. Because sloshing pressures have short rise times and long duration (relative to the structural periods of interest), the DLF will always be greater than 1.0 for LNG sloshing forces in ship tanks.

APPENDIX D

EXAMPLE CALCULATIONS FOR MEMBRANE AND PRISMATIC TANKS

Calculations were performed for typical LNG tank structures to illustrate the methods of computing structural frequencies and the dynamic load factors. In addition, calculations of structural strength have been made and are expressed in terms of allowable sloshing pressures which the structural components can withstand. Allowable sloshing pressures for the Gaz Transport insulation boxes are compared with results from laboratory tests conducted on the boxes. Results of the laboratory tests, in which both static and dynamic pressure loads were applied to the cover of the boxes, are summarized in Section IV.5. It should be noted that the structural strength calculations are only examples of how such analyses may be performed. Certainly, more rigorous methods are available, as discussed in Section V.2.3, and might be preferred; however, for these cases the one dof analysis is a good approximation to actual structural behavior and should give conservative results.

D.1 Plywood Insulation Boxes

In this example, the strength of the cover and longitudinal stiffener in the 12-cell box will be determined. These are the primary load-carrying members in the primary boxes and failures were produced in these members during laboratory testing. Dynamic load factors for the boxes are based on a tank which is 36m (118 ft) long. Tank length sets the time constants for the sloshing pressures and determines the dynamic amplification as shown in Section V.2.1.

Material Properties

The insulation boxes are constructed of 7-ply birch plywood. Flexural strength and stiffness were measured in 3-point bending tests both at room and at LN₂ temperatures. Exterior plies were oriented perpendicular (cross-grain) to the direction of the bending stress; this orientation corresponds to the principal loading direction of the box covers. Results from these tests are summarized in Section IV.4.

Material properties used in the analysis are given in Table D-1. Values for the elastic modulus and rupture stress in the perpendicular (\perp) direction are taken from Section IV.6. The elastic modulus parallel (\parallel) to the grain was calculated using properties for white birch from the Wood Handbook⁽⁹⁷⁾ and procedures outlined in the Plywood Design Guide⁽⁹⁸⁾. Plywood density was measured on box material and Poisson's ratios parallel and perpendicular to the grain of the exterior ply were estimated using values for birch from Reference 97.

Cover Strength

The corner cells are the weakest part of the box covers because, for uniform pressure loadings, the boundaries over the stiffeners are treated as clamped and the edges along the side and end of the box are treated as simply supported. All other cells have three clamped edges. Dimensions and boundary conditions of the corner cell are:

TABLE D-1. PLYWOOD MATERIAL PROPERTIES

	<u>New Plywood - Average Properties - RT</u>	
	<u>Direction With Respect to Grain of Exterior Ply</u>	
	<u>Perpendicular (y)</u>	<u>Parallel (x)</u>
σ_r N/mm ² (psi)	55.96 (8,117)	108.4 (15,727)
E_b N/mm ² (psi)	3070 (445,304)	7149 (1,037,000)
ν	.206	.268
ρ kg/mm ³ ($\frac{\text{lb sec}^2}{\text{in.}^4}$)	55.36 x 10 ⁻⁸ (5.18 x 10 ⁻⁵)	
E_a N/mm ² (psi)	464 (67,260)	618 (89,680)

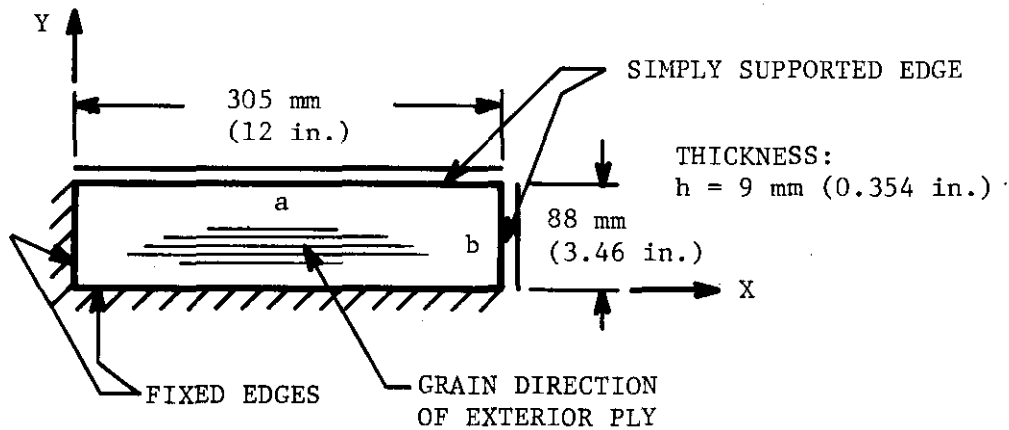


FIGURE D-1

Static Pressure

Timoshenko and Woinowsky-Krieger (99) give a solution for bending stresses in a plate with these boundary conditions. The maximum moment occurs near the center of side b and is given by

$$M_y = 0.1180 P b^2 \quad \text{for } a/b = 2 \quad (\text{D-1})$$

For the corner cell

$$a/b = 3.47,$$

but the magnitude of the moment changes very little for $b/a > 2$ so the value given is close to the true value. The stress produced by this moment is

$$\sigma = \frac{6M_y}{h^3} \quad (\text{D-2})$$

Substituting Equation (D-1) for M_y and the rupture stress σ_r for σ , an expression for the allowable static pressure p_a , can be obtained.

$$p_a = \frac{\sigma_r h^2}{.708b^2} \quad (\text{D-3})$$

For $\sigma_r = 55.96 \text{ N/mm}^2$ (8117 psi)
 $h = 9 \text{ mm}$ (.354 in.)
 $b = 88 \text{ mm}$ (3.46 in.)

Equation (D-3) gives

$$P_a = 0.827 \text{ N/mm}^2 \text{ (120 psi)}$$

Thus, 0.827 N/mm^2 (120 psi) is the allowable static pressure of new boxes at room temperature based upon average values. This gives a 50% probability of failure if the properties have a normal distribution.

Test results on three new 12-cell boxes produced failures at static pressures of 120 psi, 130 psi and 150 psi. Table IV-22 in Section IV.5 shows the damage and describes the failure. In three tests failures occurred in the corner cells. In one test, the outer cell in the center of the long cell also failed. This is the second weakest cell in the box cover. The damage is cited as shear failure because the cover was completely severed at the stiffener. Shear properties were not measured for the covers and these failures were not predicted. Rough estimates indicate that the cover has about equal shear and bending strength, and the resulting failure is some combination of shear, bending, and local compression. Compression tends to cut through the inner ply; tension tends to crack the outer ply. These together weaken the plywood in shear.

Dynamic Pressure

To determine the permissible dynamic or sloshing pressure, rise and decay times of the loading must be known. These times are a function of tank length and were determined in Section V.2.1 for a tank 36 m (118 ft) long. From these times, the envelope of the dynamic load factor (DLF) was also determined and is given in Figures V-2 and V-3. Thus, these calculations will be for a tank which is 36m long so that the DLF already calculated can be used.

To read the value of DLF from Figure V-2 and V-3, the fundamental frequency of the structural component must be computed. Equations (V-1) and (V-2) of Section V.2.2.1 will be used. Substituting plywood properties from Table D-1 and the plywood thickness from Figure D-1, we have

$$D_x = \frac{E_x h^3}{12(1-\nu_x \nu_y)} = 458,426 \text{ N}\cdot\text{mm (4058 lb in.)}$$

$$D_y = \frac{E_y h^3}{12(1-\nu_x \nu_y)} = 196,837 \text{ N}\cdot\text{mm (1742 lb in.)}$$

$$D_{xy} = D_x \nu_y + \frac{Gh^3}{6} \approx D_x / 4.8^* = 95,505 \text{ N}\cdot\text{mm (845 lb in.)}$$

The frequency equation is

$$f = \frac{1}{2\pi} \sqrt{\frac{1}{\rho h} \left(\frac{A^4 D_x}{a^4} + \frac{B^4 D_y}{b^4} + \frac{2CD_{xy}}{a^2 b^2} \right)} \text{ Hz}$$

From Table V.1 A = B = 3.927
 C = 132.118

* Measured by Herman (100) on five-ply maple plywood.

Substituting the known parameters, the fundamental frequency and period of the corner cell in the cover are found to be

$$f = 2058 \text{ Hz}; T = \frac{1}{f} = 0.485 \text{ ms}$$

These values are for the box cover vibrating in air, whereas in the tank it is exposed to LNG on one side (even though separated by the membrane). The effect of the membrane on the added mass of the liquid is uncertain; however, including the effect of the liquid on the frequency will increase the period and produce a higher DLF (see Figure V-3), a conservative effect. Thus, the added mass will be included. Section V.2.2.5 gives approximate formulas which account for submergence. The frequency in air, f_a , is multiplied by a parameter ψ to find the frequency, f_ℓ , in the liquid. ψ is given by

$$\psi = \sqrt{\frac{K}{K_x \rho_\ell / \rho_p}}$$

where

$$K = \pi h \sqrt{\frac{1}{a^2} + \frac{1}{b^2}}$$

For LNG

$$\rho_\ell = .48 \rho_{H_2O} = .48 \times 10^{-6} \frac{\text{kg}}{\text{mm}^3} \left(4.63 \times 10^{-5} \frac{\text{lb-sec}^2}{\text{in.}^4} \right)$$

Substituting for ρ_ℓ and the panel dimensions from Figure D-1 we have:

$$\begin{aligned} K &= .3346 & f_e &= \psi f_a = 1076 \text{ Hz} \\ \psi &= .523 & T &= 1/f_e = 0.928 \text{ ms} \end{aligned}$$

From Figure V-3 the dynamic load factor is found to be

$$\text{DLF} = 1.22$$

To predict the allowable sloshing pressure for the box cover, the allowable static pressure is divided by this factor; however, to be representative of in-service conditions, the allowable static pressure of $.827 \text{ N/mm}^2$ (120 psi), previously calculated, should be adjusted to account for LNG

temperatures and in-service effects. The average strength of the plywood at LNG temperatures is increased as shown in Table IV-26 from 55.96 N/mm² (8117 psi) to 89.05 N/mm² (12,916 psi). Section IV-4 also gives the degradation of strength for in-service conditions as 79%. Accounting for the three effects of dynamic loading, LNG temperatures and in-service conditions, the allowable sloshing pressure for the cover is

$$P_a = \frac{.827}{1.22} \frac{\text{N}}{\text{mm}^2} \left(\frac{89.05}{55.96} \right) (0.79) = .853 \text{ N/mm}^2 (124 \text{ psi})$$

Average rather than minimum properties have been used in these calculations, so there is a 50% probability of a bending failure at this pressure for a normal distribution of plywood properties.

Strength of Longitudinal Stiffener

From the analysis of the corner cell in the box cover, it is apparent that the majority of the pressure loading on the cover is transferred to the long edges of the cell. These edges are supported by the sides of the box or by the longitudinal stiffeners. The longitudinal stiffener picks up load from two adjacent cells and so is more highly loaded than the box sides. Figure III-19 shows the arrangement of the stiffeners in the box and their support points on the transverse stiffeners of the secondary boxes.

Figure D-2 shows the longitudinal stiffener at one end of the primary box. A uniform loading N is applied to the top of the stiffener from the

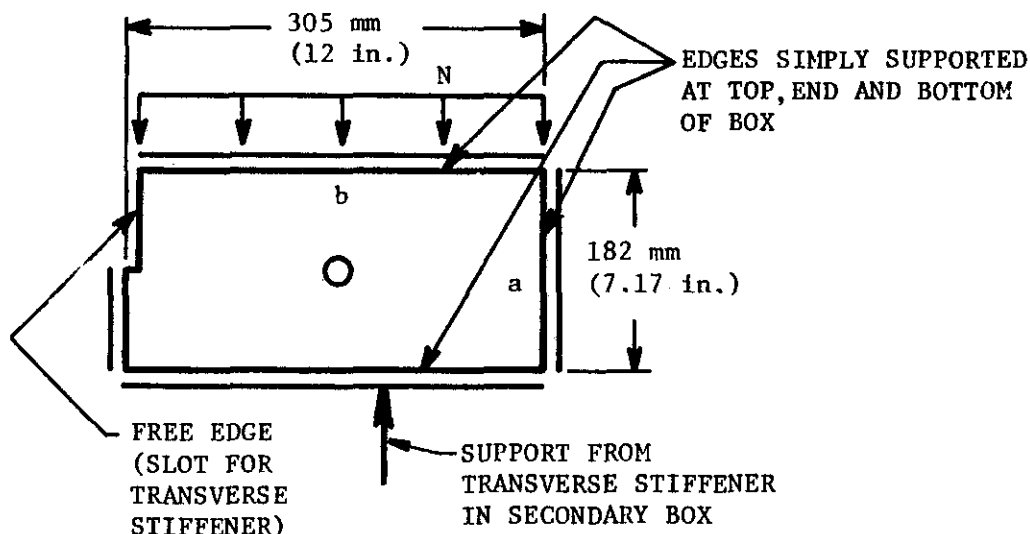


FIGURE D-2

cover and the bottom is assumed to be supported only at the transverse stiffener in the secondary box. Simple solutions do not exist for this

combination of geometry, support conditions and loading. A rather complex multidegree-of-freedom analysis, such as with finite elements, would be required for a good representation of these conditions; however, some approximations can be made to bound the buckling strength of the stiffener and this approach will be followed here.

Static Pressure

Two approximations to the actual conditions were checked. They are shown schematically in Figure D-3.

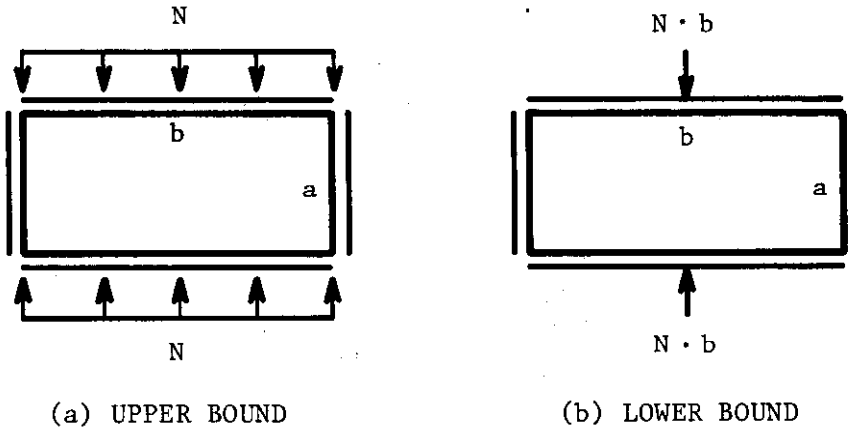


FIGURE D-3

Solutions for these cases are given by Roark and Young (101). Noting that the load N is equal to the pressure applied to the box cover multiplied by the width of a cell ($N = 88\text{mm} \cdot P$) we can express the allowable buckling load directly in terms of the pressure on the box cover. Material properties for the load perpendicular to the grain of the exterior ply (the weakest direction) have been used.

$$\text{Case (a)} \quad N = (88\text{mm})P_a = 4.27 \frac{E}{1-\nu^2} \left(\frac{h}{b}\right)^2 \cdot h \quad (\text{D-4})$$

For the load perpendicular to grain of exterior ply

$$P_a = 9 \cdot \frac{4.27}{88} \frac{(3070)}{1-(.206)^2} \left(\frac{9}{305}\right)^2 = 1.22 \text{ N/mm}^2 \text{ (177 psi)}$$

$$\text{Case (b)} \quad N \cdot b = (88\text{mm}) P_a \cdot b = \frac{\pi}{3} \frac{E h^3}{(1-\nu^2)b} \quad (\text{D-5})$$

Again for loading perpendicular to the grain of the exterior ply the

allowable pressure is

$$P_a = .30 \text{ N/mm}^2 \text{ (43 psi)}$$

These two cases should give reasonable bounds for the buckling strength of the longitudinal stiffeners, expressed in terms of a uniform static pressure applied to the box cover. Of course, average properties have been used and the grain of the stiffener is assumed to be parallel to the box axis and perpendicular to the load direction.

In laboratory tests on the boxes (refer to Table IV-22), buckling of the longitudinal stiffener in the end cell was observed at a static pressure of 1.03-1.24 N/mm² (150-180 psi). The exterior grain of the stiffener was parallel to the box axis, corresponding to the direction in the predictions above. Thus, the upper bound estimate, Case (a) appears to offer a reasonable approximation to the behavior of the stiffener. It is interesting to note in Table IV-22 that on Test No. 7 the static pressure reached 1.65 N/mm² (240 psi) without stiffener failure. Stiffeners for the box used in this test were oriented with the exterior grain perpendicular to the box axis (the strong direction). The predicted buckling pressure for this orientation would increase by the ratio of the elastic modulus in the two directions or would be approximately doubled.

Dynamic Pressure

Under dynamic conditions, the response of the cover was increased by a factor of 1.22. Depending upon the frequency of the stiffener in compression, similar amplification may occur. To estimate the frequency of the stiffener for compressive loads, use a spring mass model as in the sketch below. Den Hartog (95) gives the frequency equation for this case as

$$f = \frac{1}{2} \sqrt{\frac{K}{\left(M + \frac{1}{3} m\right)}}$$

$$M = M_c + M_e$$

M_c = mass of cover

M_e = added mass of the liquid

m = mass of stiffener

K = axial spring constant of the stiffener

For a unit width of the stiffener and cover the values are:

$$M_c = (88\text{mm})(1)(9\text{mm})(55.36 \times 10^{-8}) = 4.385 \times 10^{-4} \text{ kg} \\ (2.498 \times 10^{-6} \frac{\text{lb-sec}^2}{\text{in.}})$$

$$M_l^* = \frac{1}{2} \cdot \frac{\pi(88)^2}{4} \cdot (1)(49.48 \times 10^{-8}) = 1.51 \times 10^{-3} \text{ kg} \\ (8.572 \times 10^{-6} \frac{\text{lb-sec}^2}{\text{in.}})$$

$$m = (1)(182)(9)(55.36 \times 10^{-8}) = 9.068 \times 10^{-4} \text{ kg} \\ (5.17 \times 10^{-6} \frac{\text{lb-sec}^2}{\text{in.}})$$

$$K = AE/L = (9)(1)(464)/182 = 22.94 \text{ N/mm (131 lb/in.)}$$

Substituting into the frequency equation gives

$$f = 509 \text{ Hz; } T = 1/f = 1.96 \text{ ms}$$

This period is approximately twice that of the cover. Generally, for this condition (a large spread in the stiffnesses of a coupled system) the load transferred to the supporting system will be attenuated; however, for this approximation it was assumed that the load is unaltered. From Figure V-2 the dynamic load factor for this frequency is

$$\text{DLF} = 1.63$$

As for the cover, to predict the allowable buckling load produced by sloshing pressures, the increase in stiffness which occurs at reduced temperatures and the reduction in strength for in-service conditions should also be accounted for. From Section IV.6, Table IV-26, we find

$$\frac{E_{CT}}{E_{RT}} = \frac{4785}{3070}$$

and the in-service reduction is 79% as before. Combining these factors, the allowable sloshing pressure for dynamic buckling (using measured buckling load from Test 10 in Table IV-22) is

$$P_a = \frac{(1.03 - 1.24 \text{ N/mm}^2)}{1.63} \left(\frac{4785}{3070} \right) (0.79) \\ = .778 - .937 \text{ N/mm}^2 (113 - 136 \text{ psi})$$

* M_l is taken as the mass per unit length of a liquid which is contained within a half cylinder which lies above one cell of the box cover.

This allowable sloshing pressure for buckling of the longitudinal stiffener is based upon one measured value of the static buckling load; however, the experiment did correlate well with the upper bound on buckling strength computed for the stiffener using average material properties. As for the cover, the material is assumed to be oriented in its weakest direction, and this condition does exist in the boxes tested.

D.2 Technigaz Membrane Support System

The Technigaz membrane system is described in Section III.3.1 and shown in Figure III.3.4. Structural support for the membrane is provided by a composite panel formed from plywood sheets with a balsa core. The panel is separated from the membrane by an "end grain" balsa pad and supported from the inner hull by grounds. Sloshing pressures on the membrane produce bending and shear stresses in the composite panel between the grounds. The allowable sloshing pressures will be based upon these stresses.

A section of the composite panel between the secondary grounds is shown in Figure D-4.

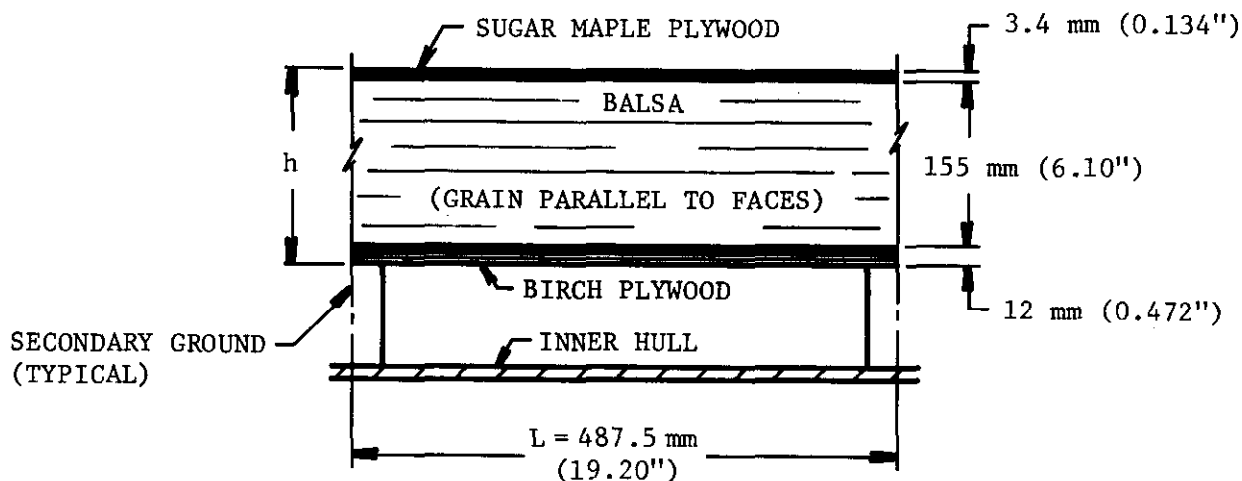


FIGURE D-4

Material properties for balsa, sweet birch and sweet sugar maple were taken from Reference 97. Pertinent properties are given in Table D-2. Details of the plywood construction were unknown so the following assumptions were made:

- (1) Birch plywood is 7 ply with grain of exterior plies parallel to the grounds (weakest orientation).
- (2) Maple plywood is 5 ply with grain of exterior plies parallel to the grounds.

TABLE D-2. MATERIAL PROPERTIES FOR BALSA,
SWEET BIRCH, AND SUGAR MAPLE

	<u>Balsa</u>	<u>Sweet Birch</u>	<u>Sugar Maple</u>
Specific gravity	.17	.65	.63
Elastic modulus, longitudinal dir, EL	3792 N/mm ² (.55x10 ⁶ psi)	14,962 N/mm ² (2.17x10 ⁶ psi)	12,618 N/mm ² (1.83 x 10 ⁶ psi)
Modulus of rupture		117 N/mm ² (16,900 psi)	
Compression parallel to grain			54 N/mm ² (7,830 psi)
Elastic modulus, transverse (ET/EL)	.015	.050	.050 (est.)
Shear parallel to grain	2.07 N/mm ² (300 psi)		
Shear modulus, (G _{LR} /E) Longitudinal-radial plane	.054		

Based upon the above assumptions and material properties in Table D-2, the bending stiffness of the composite panel can be calculated. For a 25.4 mm wide strip between the grounds the axial stiffnesses of the plywood faces were found to be:

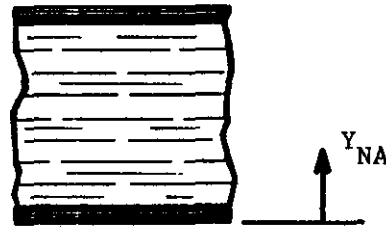
$$\begin{aligned} \text{birch: } (EA)_b &= (14962 \text{ N/mm}^2)(12 \text{ mm})(25.4 \text{ mm})(3/7 + .050 \cdot 4/7) \\ &= 2.085 \times 10^6 \text{ N } (.469 \times 10^6 \text{ lb}) \end{aligned}$$

$$\begin{aligned} \text{maple: } (EA)_m &= 12,618 (3.4)(25.4)(2/5 + .050 \cdot 3/5) \\ &= .4686 \times 10^6 \text{ N } (.105 \times 10^6 \text{ lb}) \end{aligned}$$

Neglecting the contribution of the balsa core to the panel stiffness, the locations of the neutral axis (N.A.) and the bending stiffness (EI) of the panel are:

$$Y_{NA} = \frac{\sum E A y}{\sum E A} = 35.8 \text{ mm} \quad (1.41 \text{ in.})$$

$$\begin{aligned} EI &= \sum E A (y - y_{NA})^2 \\ &= 1.008 \times 10^{10} \text{ Nmm}^2 \quad (3.513 \times 10^6 \text{ lb-in.}^2) \end{aligned}$$



Mass per unit length of the 25.4 mm (1 in.) strip of panel between the grounds must include the mass of the "end grain" balsa pad and the membrane. Measured specific gravity of birch plywood is $\gamma = 0.72$ and this value was used in place of the values given in Table D-2 for birch and maple. For a stainless steel membrane with a thickness of 1.3 mm (.050 in.), the mass per unit length is:

$$\begin{aligned} \text{Panel: } m_p &= 25.4 \text{ mm} \left[(.72 \times 10^{-6} \frac{\text{kg}}{\text{mm}^3})(12 \text{ mm} + 3.4 \text{ mm}) + \right. \\ &\quad \left. .17 \times 10^{-6} \frac{\text{kg}}{\text{mm}^3} (155 \text{ mm}) \right] = 9.509 \times 10^{-4} \frac{\text{kg}}{\text{mm}} (1.379 \times 10^{-4} \text{ lb-sec}^2/\text{in.}^2) \end{aligned}$$

$$\begin{aligned} \text{Pad: } m_{PD} &= 25.4 \text{ mm} (55 \text{ mm}) (.17 \times 10^{-6} \frac{\text{kg}}{\text{mm}^3}) \\ &= 2,375 \times 10^{-4} \frac{\text{kg}}{\text{mm}} (3.445 \times 10^{-5} \text{ lb-sec}^2/\text{in.}^2) \end{aligned}$$

$$\begin{aligned} \text{Membrane: } m_m &= 25.4 \text{ mm} (1.3 \text{ mm}) (7.84 \times 10^{-6} \frac{\text{kg}}{\text{mm}^3}) \\ &= 2.589 \times 10^{-4} \frac{\text{kg}}{\text{mm}} (3.755 \times 10^{-5} \text{ lb-sec}^2/\text{in.}^2) \end{aligned}$$

$$\begin{aligned} \text{Total: } m_T &= (9.509 + 2.375 + 2.589) \times 10^{-4} \\ &= 1.447 \times 10^{-3} \frac{\text{kg}}{\text{mm}} (2.099 \times 10^{-4} \text{ lb sec}^2/\text{in.}^2) \end{aligned}$$

Frequency of the panel can be estimated using the formula for a beam with clamped ends. Den Hartog (95) gives

$$f = \frac{22}{2\pi} \sqrt{\frac{EI}{m_T l^4}}$$

By substituting the known parameters, the frequency and period are

$$f = 1228 \text{ Hz}; T = 0.814 \text{ ms}$$

Because the beam is deep, shear effects may be important. Exact equations are not available for clamped beams with shear; however, the effect of shear deformation can be approximated by

$$T = T \sqrt{\phi}$$

where

$$\phi = 1 + \frac{22EI}{L^2GA}$$

G = modulus of rigidity of the balsa core

$$= (.054)(3792 \text{ N/mm}^2) = 205 \text{ N/mm}^2 (29,700 \text{ psi})$$

A = shear area of balsa core

$$= (25.4)(155) = 3937 \text{ mm}^2 (6.10 \text{ in.}^2)$$

Now

$$\phi = 2.16; T = .814 \sqrt{2.16} = 1.20 \text{ ms}$$

To account for the effect of submersion in LNG Equations (V-8) through (V-10) are used with $a = \infty$. Compute the panel density, ρ_p , from the mass per unit length m_T .

Density of the LNG is

$$\rho_p = \frac{m_T}{(25.4)(170)\text{mm}^2} = .335 \times 10^{-8} \frac{\text{kg}}{\text{mm}^3} \left(3.136 \times 10^{-7} \frac{\text{lb sec}^2}{\text{in.}^4} \right)$$

$$\rho_e = .48 \times 10^{-8} \frac{\text{kg}}{\text{mm}^3} \left(4.49 \times 10^{-7} \frac{\text{lb sec}^2}{\text{in.}^4} \right)$$

Substituting

$$K = \pi h \sqrt{\frac{1}{a^2} + \frac{1}{b^2}} = \pi(170 \text{ mm}) \sqrt{0 + \frac{1}{(487.5 \text{ mm})^2}}$$

$$= 1.096$$

$$\psi = \sqrt{\frac{K}{K + \rho_e/\rho_p}} = .658$$

$$T = 1.20/.658 = 1.82 \text{ ms}$$

For a tank which is 36 m (118 ft) long, the dynamic load factor is read directly from Figure V-2 for the fundamental period of 1.82 ms.

$$\text{DLF} \approx 1.57$$

The maximum stress produced by bending will occur in the maple plywood and is

$$\sigma = \frac{Mc}{EI} \cdot E_M$$

where

$$C = h - Y_{NA}$$

$$E_m = \frac{EA_m}{A} = \frac{EA_m}{(25.4)(3.4)} = 5426 \text{ N/mm}^2 \quad (78,696 \text{ psi})$$

$$M = \text{maximum moment for a clamped beam}$$

$$= \frac{NL^2}{12} = \frac{(b' \cdot P_a \cdot \text{DLF})L^2}{12}$$

$b' = \text{beam width} = 25.4 \text{ mm (1 in.)}$

Solving for the allowable sloshing pressure, P_a , we have

$$P_a = \frac{12 EI \sigma}{b' \cdot DLF \cdot L^2 (h - Y_{NA}) (E_M)} \quad (D-6)$$

For a permissible compressive stress of 54 N/mm^2 in the maple plywood, the allowable sloshing pressure is

$$P_a = 0.957 \text{ N/mm}^2 \text{ (137 psi)}$$

An allowable sloshing pressure for shear strength of the panel will be based upon a constant shear stress through the core. The shear reaction at each end of the 25.4 mm (1 in.) wide beam is

$$V = 1/2(487.5)(25.4)(P_a) \cdot 1.57$$

Using the allowable stress for shear parallel to the grain (a conservative value), the allowable sloshing pressure can be found.

$$\sigma_\delta = 2.07 \text{ N/mm}^2 = \frac{V}{A} = \frac{1/2(487.5)(25.4)P_a(1.57)}{155(25.4)}$$

$$P_a = 0.84 \text{ N/mm}^2 \text{ (122 psi)}$$

Note that the shear and bending strength of the panel are in good balance. The numbers should be somewhat conservative because the shear strength of the face plywood was neglected, the bending strength of the balsa core was neglected and the width between the centerline of the grounds was used for the panel width.

D.3 CONCH Independent Tank

The structural arrangement of the CONCH independent tank is described in Section III.3. One of the weakest parts of the tank is the swash bulkhead. In this analysis, we will predict the allowable sloshing pressure for a section of the bulkhead between Frames 6 and 7 (refer to Figures III-23 and III-24).

A schematic of the section between Frame 6 and 7 is given in Figure D-5. Primary dimensions are in inches as given in the engineering drawings.

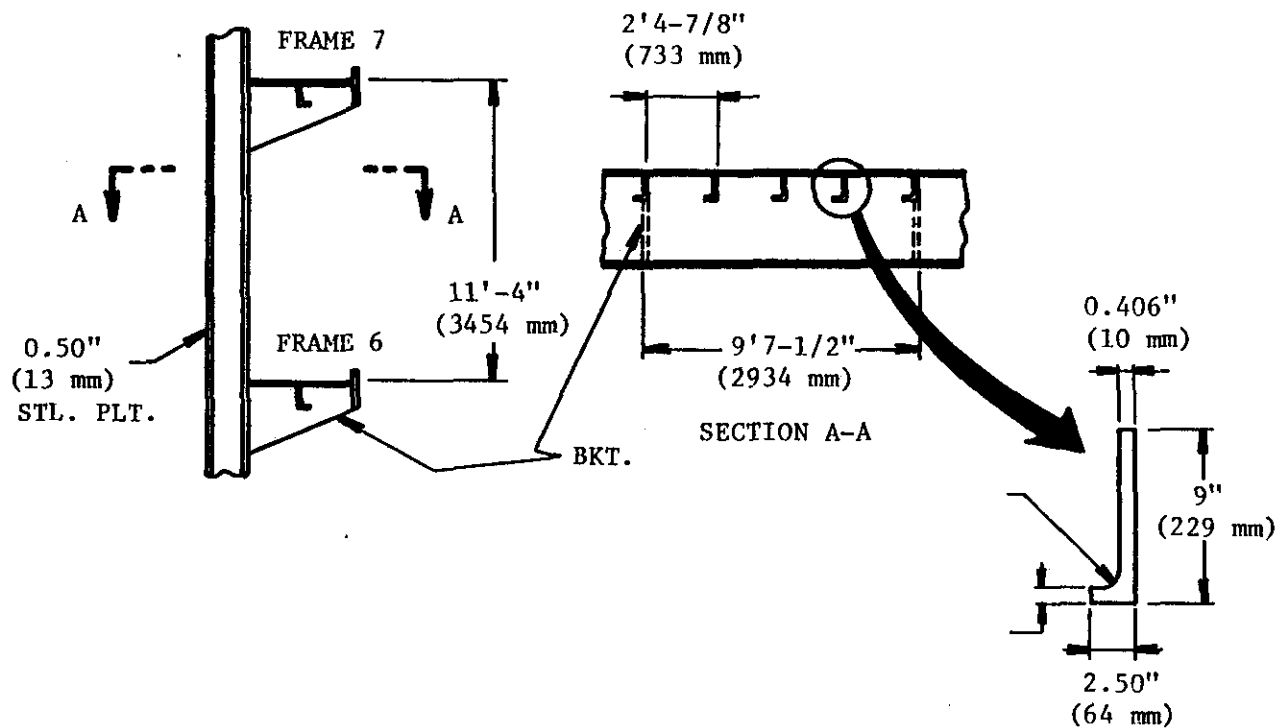


FIGURE D-5

Stiffened Panel

The fundamental frequency of the section of the bulkhead between the frames and between the brackets will be estimated using Equation (V-3). Input parameters for the equation are

$$h = 13 \text{ mm (0.50 in.)}$$

$$E = 71,000 \text{ N/mm}^2 \text{ (10.3 x 10}^6 \text{ psi)}$$

$$\rho = 2.65 \times 10^{-6} \frac{\text{kg}}{\text{mm}^3} (2.49 \times 10^{-4} \text{lb sec}^2/\text{in.}^4)$$

$$I = 61.086 \times 10^6 \text{mm}^4 (146.76 \text{ in.}^4)$$

$$S = 10587 \text{ mm}^2 (16.41 \text{ in.}^2)$$

$$n_s = 3$$

$$p = 733 \text{ mm (28.875 in.)}$$

$$L_s = 3454 \text{ mm (136 in.)}$$

Boundary conditions for the panel can be approximated by clamped boundaries at the frame and simply supported along the stiffener to which the brackets are attached. For these boundary conditions the constants from Table V-2 are

$$A' = 1.5764$$

$$B' = 4.85$$

$$C' = .0833$$

Now substituting into Equation (V-3) we find

$$f = \frac{A'}{L_s^2} \sqrt{\frac{E}{\rho} \left(B' \frac{I}{S} + C' \frac{L_s h^2}{n_s p} \right)} = 121 \text{ Hz}$$

$$T = \frac{1}{f} = 8.25 \text{ ms}$$

The dynamic load factor for the bulkhead will be determined using Figure C-2(b) and the minimum nondimensional rise time T_2 [t_r in Figure C-2(b)] from Table V-1. For a nondimensional time of 0.0005 and a tank length, L , of 15.608 m (51.208 ft) to the swash bulkhead, the rise time t_r is

$$T_2 \sqrt{g/L} = 0.0005$$

$$t_r = T_2 = 0.63 \text{ ms}$$

The ratio of the rise time to the fundamental frequency,

$$t_r/T = \frac{.63}{8.25} = .076$$

is used to enter Figure C-2(a). The dynamic load factor is

$$DLF \approx 2.0$$

Strength of the panel can be approximated by considering the bending of one stiffener and the associated plating between the two frames for a uniform pressure loading acting over the width p (see Section V.2.2.2). The loading per unit length, N , is

$$N = p \cdot DLF \cdot P_a$$

where P_a is the allowable sloshing pressure. Using the standard equation for a uniformly loaded beam with clamped ends and taking the allowable yield stress, σ_y , for 5083 aluminum at -196°C as 158.6 N/mm^2 (23,000 psi), the allowable sloshing pressure is

$$P_a = \frac{12I \sigma_y}{pDLF L_s^2 c} = .034 \text{ N/mm}^2 (5 \text{ psi})$$

where c , the distance from the neutral axis to the extreme fiber, is 193 mm (7.585 in.). This allowable sloshing pressure is quite low and simply indicates that the tops of LNG tanks are designed for relatively low static vapor pressure and small liquid loads and not for dynamic sloshing pressures.

APPENDIX E

IMCO TANK TYPE DEFINITIONS

CHAPTER IV - CARGO CONTAINMENT

4.1 General

Administrations should take appropriate steps to ensure uniformity in the implementation and application of the provisions of this chapter.*

4.2 Definitions

In addition to those in 1.4, the following definitions apply throughout the Code.

4.2.1 Integral tanks

- (a) Integral tanks form a structural part of the ship's hull and are influenced in the same manner and by the same loads which stress the adjacent hull structure.
- (b) The "design vapour pressure" P_0 as defined in 4.2.5 should not normally exceed 0.25 kp/cm^2 . If, however, the hull scantlings are increased accordingly, P_0 may be increased to a higher value but less than 0.7 kp/cm^2 .
- (c) Integral tanks may be used for the products provided that the lowest temperature in any part of the hull structure under no circumstances will fall below -10°C . A lower temperature may be accepted by the Administration subject to special consideration.

4.2.2 Membrane tanks

- (a) Membrane tanks are non-self-supporting tanks which consist of a thin layer (membrane) supported through insulation by the adjacent hull structure. The membrane is designed in such a way that thermal and other expansion or contraction is compensated for without undue stressing of the membrane.
- (b) The design vapour pressure P_0 should not normally exceed 0.25 kp/cm^2 . If, however, the hull scantlings are increased accordingly, and consideration is given, where appropriate, to the strength of the supporting insulation, P_0 may be increased to a higher value but less than 0.7 kp/cm^2 .
- (c) The definition of membrane tanks does not exclude designs such as those in which non-metallic membranes are used or in which membranes are included or incorporated in insulation. Such designs require, however, special consideration by the Administration.

* Reference is made to the published Rules of members and associate members of the International Association of Classification Societies and in particular to IACS Unified Requirements Nos. 92 and 93.

4.2.3 Semi-membrane tanks

- (a) Semi-membrane tanks are non-self-supporting tanks in the loaded condition and consist of a layer, parts of which are supported through insulation by the adjacent hull structure, whereas the rounded parts of this layer connecting the above-mentioned supported parts are designed also to accommodate the thermal and other expansion or contraction.
- (b) The design vapour pressure P_0 should not normally exceed 0.25 kp/cm^2 . If, however, the hull scantlings are increased accordingly, and consideration is given, where appropriate, to the strength of the supporting insulation, P_0 may be increased to a higher value but less than 0.7 kp/cm^2 .

4.2.4 Independent tanks

Independent tanks are self-supporting; they do not form part of the ship's hull and are not essential to the hull strength. The three categories of independent tanks are:

- (a) Independent tanks type A which are designed primarily using Recognized Standards of classical ship-structural analysis procedures. Where such tanks are primarily constructed of plane surfaces (gravity tanks), the design vapour pressure P_0 should be less than 0.7 kp/cm^2 .
- (b) Independent tanks type B which are designed using model tests, refined analytical tools and analysis methods to determine stress levels, fatigue life and crack propagation characteristics. Where such tanks are primarily constructed of plane surfaces (gravity tanks) the design vapour pressure P_0 should be less than 0.7 kp/cm^2 .
- (c) Independent tanks type C (also referred to as pressure vessels) are tanks meeting pressure vessel criteria and having a design vapour pressure not less than:

$$P_0 = 2 + AC(\rho)^{3/2} \left[\text{kp/cm}^2 \right]$$

where

$$A = 0.0185 \left(\frac{\sigma_m}{\Delta\sigma_A} \right)^2$$

with

σ_m = design primary membrane stress

$\Delta\sigma_A$ = allowable dynamic membrane stress (double amplitude at probability level $Q = 10^{-8}$)
 5.5 kp/mm^2 for ferritic/martensitic steel
 2.5 kp/mm^2 for aluminum alloy (5083-0)

C = a characteristic tank dimension to be taken as the greatest of the following:

h ; $0.75b$; or $0.45l$

with

h = height of tank (dimension in ship's vertical direction) (m)

b = width of tank (dimension in ship's transverse direction) (m)

l = length of tank (dimension in ship's longitudinal direction) (m)

ρ = the relative density of the cargo ($\rho = 1$ for fresh water) at the design temperature.

However, the Administration may allocate a tank complying with the criterion of this sub-paragraph to type A or type B, dependent on the configuration of the tank and the arrangement of its supports and attachments.

*U.S. GOVERNMENT PRINTING OFFICE : 1980 O-326-574/6451

SHIP RESEARCH COMMITTEE
Maritime Transportation Research Board
National Academy of Sciences-National Research Council

The Ship Research Committee has technical cognizance of the interagency Ship Structure Committee's research program:

Mr. O. H. Oakley, Chairman, *Consultant, McLean, VA*
Prof. A. H.-S. Ang, *University of Illinois, IL*
Mr. M. D. Burkhart, *Consultant, Clinton, MD*
Dr. J. N. Cordea, *Senior Staff Metallurgist, ARMCO INC., Middletown, OH*
Mr. D. P. Courtsal, *Vice President, DRAVO Corporation, Pittsburgh, PA*
Mr. W. J. Lane, *Consultant, Baltimore, MD*
Mr. A. C. McClure, *Alan C. McClure Associates, Inc., Houston, TX*
Dr. W. R. Porter, *Vice Pres. for Academic Affairs, State Univ. of N.Y.
Maritime College*
Prof. H. E. Sheets, *Director of Engineering, Analysis & Technology, Inc.,
North Stonington, CT*

The Ship Design, Response, and Load Criteria Advisory Group prepared the project prospectus, evaluated the proposals for this project, provided the liaison technical guidance, and reviewed the project reports with the investigator:

Mr. W. J. Lane, Chairman, *Consultant, Baltimore, MD*
Mr. J. W. Boylston, *Manager, Marine Operations, El Paso Marine Company
Solomons, MD*
Prof. J.-N. Yang, *Department of Civil, Mechanical & Environmental Engineering,
George Washington University, Washington, DC*
Mr. L. R. Glostén, *L. R. Glostén Associates, Inc., Seattle, WA*
Mr. P. M. Kimon, *EXXON International Company, Florham Park, NJ*
Dr. O. H. Oakley, Jr., *Project Engineer, GULF R&D Company, Houston, TX*
Mr. J. E. Steele, *Naval Architect, Quakertown, PA*

SHIP STRUCTURE COMMITTEE PUBLICATIONS

These documents are distributed by the National Technical Information Service, Springfield, VA 22314. These documents have been announced in the Clearinghouse Journal U. S. Government Research & Development Reports (USGRDR) under the indicated AD numbers.

- SSC-285, *Critical Evaluation of Low-Energy Ship Collision-Damage Theories and Design Methodologies - Volume II - Evaluation and Recommendations* by P. R. Van Mater, Jr., and J. G. Giannotti. 1979. AD-A070568.
- SSC-286, *Results of the First Five "Data Years" of Extreme Stress Scratch Gauge Data Collection Aboard Sea-Land's SL-7's* by R. A. Fain and E. T. Booth. 1979. AD-A072945.
- SSC-287, *Examination of Service and Stress Data of Three Ships for Development of Hull Girder Load Criteria* by J. F. Dalzell, N. M. Maniar, and M. W. Hsu. 1979. AD-A072910.
- SSC-288, *The Effects of Varying Ship Hull Proportions and Hull Materials on Hull Flexibility Bending and Vibratory Stresses* by P. Y. Chang. 1979. AD-A075477.
- SSC-289, *A Method for Economic Trade-Offs of Alternate Ship Structural Materials* by C. R. Jordan, J. B. Montgomery, R. P. Krumpen, and D. J. Woodley. 1979. AD-A075457.
- SSC-290, *Significance and Control of Lamellar Tearing of Steel Plate in the Shipbuilding Industry* by J. Sommella. 1979. AD-A075473.
- SSC-291, *A Design Procedure for Minimizing Propeller-Induced Vibration in Hull Structural Elements* by O. H. Burnside, D. D. Kana, and F. E. Reed. 1979. AD-A079443.
- SSC-292, *Report on Ship Vibration Symposium '78 - Sheraton National Hotel, Arlington, VA.* by E. Scott Dillon. 1979. AD-A079291.
- SSC-293, *Underwater Nondestructive Testing of Ship Hull Welds* by R. Youshaw and C. Dyer. 1979. AD-A079445.
- SSC-294, *Further Survey of Inservice Performance of Structural Details* by C. R. Jordan and L. T. Knight. 1979.
- SSC-295, *Nondestructive Inspection of Longitudinal Stiffener Butt Welds in Commercial Vessels* by R. A. Youshaw. 1980.
- SSC-296, *Review of Fillet Weld Strength Parameters for Shipbuilding* by C-L Tsai, K. Itoga, A. P. Malliris, W. C. McCabe, and K. Masubuchi. 1980.